Structure-Property Relationships Of Flexible Polyurethane Foams

By
Bryan D. Kaushiva

Dissertation Submitted to the Faculty of
Virginia Polytechnic Institute and State University
In Partial Fulfillment of the Requirements for the Degree of

Doctor of Philosophy
In
Chemical Engineering

Dr. Garth L. Wilkes (Chairman)
Dr. Thomas C. Ward
Dr. Richey M. Davis
Dr. William L. Conger
Dr. Eva Marand

August 16, 1999
Blacksburg, Virginia

Keywords: **flexible polyurethane foam; structure-property relationships; diethanolamine; copolymer polyol; surfactant; fluoropolymers**

Structure-Property Relationships in Flexible Polyurethane Foams

By Bryan D. Kaushiva (Copyright 1999)

Research Committee Chairman: Garth L. Wilkes
Chemical Engineering Department

Abstract

This study examined several structure-property features of flexible polyurethane foams that are important aspects of foam production. AFM and WAXS were used to demonstrate the existence, for the first time in typical polyurethane foam systems, of lamellae-like polyurea structures ca. 0.2 μm long and ca 5-10 nm across. Aggregations of these lamellae-like hard domains may be the polyurea balls typically observed via TEM. Diethanolamine, a widely used cross-linking agent in molded foams, was shown to disrupt ordering in the polyurea hard domains and alter the interconnectivity of hard domains by preventing the formation of lamellae-like structures. These changes were shown to lead to softening of the foam. Copolymer polyol is frequently applied as reinforcing filler in foams. It was found that a common method of adding this component alters the hard segment/soft segment (HS/SS) ratio, thus increasing the load bearing capacity of the foam. It was observed in this report that at constant HS/SS ratio, the copolymer polyol only increased load bearing under humid conditions. It was also shown that the collapse of the cellular structure of a foam prior to the point of urea precipitation alters the aggregation behavior of the hard domains and alters solid-state properties. Surfactant is thus suggested to play a secondary role in the development of the hard domains by maintaining the cellular structure in the foam as the phase separation occurs and at least until the polyurethane foam has more fully organized hard segment domains. It was found that cure temperature could be manipulated to predictably change interdomain spacings and hydrogen bond development in the polymer. Curing above 100°C was found to lower hard segment content for plaques of the same formulation possibly as a result of water and isocyanate vaporization. Apart from polyurethane materials, structure-property relationships were examined in cast blends based on poly(tetrafluoroethylene) (PTFE) and the terpolymer poly(tetrafluoroethylene-co-vinylidene fluoride-co-hexafluoropropylene) (FKM). This revealed that tensile and dynamic moduli could be predictably altered by controlling the degree of FKM cross-linking or by varying PTFE content in the film. Inducing PTFE fibrillation was found to yield higher modulus films without increasing PTFE content.

This dissertation is dedicated to the glory of my Savior,
the Lord Jesus Christ, who welcomes the humble and provides
perfect peace and complete joy to all who draw near to Him.

Acknowledgments

I would like to thank my advisor, Professor G.L. Wilkes for his patient guidance and encouragement throughout my graduate studies at Virginia Tech. I can not imagine a more professional or knowledgeable advisor, and I am grateful for the opportunity to develop as a researcher under his direction.

I would also like to express my thanks to Dr. T.C. Ward, Dr. R.M. Davis, Dr. E. Marand, and Dr. W.L. Conger for their contributions to this work and for taking the time to read this document. It has been a privilege to interact with you, particularly in the classroom. Your courses always inspired me to dig a little deeper than I would have otherwise thought to do.

Special recognition goes to Dow Chemical and its workers, both for sponsoring much of this research and for their collaboration over the past few years. In particular, I'd like to acknowledge Dr. Werner Lidy for his many helpful discussions on the complexities of foam, and I extend special thanks to Bobby O'Neill for making so many of my foam samples. I would also like to thank Ed Rightor and Dana Gier for all their courteous assistance and instruction when I was visiting Freeport, Texas. Finally, I need to thank them and everyone else who helped make the Dow Polyurethane Workshops in Freeport so instructive and interesting, particularly Rene Broos, Chris Christenson, Philippe Knaub, David Laylock, and Ralph Priester.

I also owe a thank you to the now retired Dr. Gerd Rossmy and his former employer, Goldschmidt AG, for their collaboration and support of the surfactant study in chapter 7. I admire your contributions to the field of polyurethanes, and I found our interaction to be challenging and inspiring.

Chemfab Corp. and its people also deserve a word of thanks for their support of the fluoropolymer work in chapter 9. I enjoyed the opportunity to step outside of polyurethanes, and I greatly appreciate your courtesy and many helpful discussions. In particular, I'd like to recognize Chris Comeaux for working so closely with me in the characterization effort and Richard L. Stone for making all those films.

I would like to acknowledge the raucous bunch that it has been my pleasure to share a laboratory with. In particular, Christopher Robertson, Dimitrios Dounis, Robert Greer, Ta-hua Yu, and Watson Srinivasan for teaching me how to use so many of our more finicky instruments. I'd also like to recognize everyone else who has contributed to the many technical and social goings-on that I've enjoyed, so thank you Kurt Jordens, David Shelby, Varun Ratta, Jianye Wen,

Matthew O'Sickey, Matthew Johnson, David Godshall, and Chenghong Li. Amy Revita is also acknowledged for working as an undergraduate researcher and running DMA analysis on so many of the plaque samples.

Steve McCartney gets his own paragraph because he's such a good microscopist. Thanks, Steve, for all your help in learning the AFM and cryo-microtomy and for your patience as I messed up your darkroom and left block-trimmings everywhere. Thanks also for all the TEM that never seemed to end and for the many helpful discussions which often facilitated my thinking through things.

Sandy Simpkins is also acknowledged for her continual patience with our group. Thanks for keeping things organized and helping out in so many ways.

I would like to thank the many people of Chi Alpha for their support and friendship. In particular, I'd like to thank Kimberly Watson for her patience with my being in the lab at all hours and for her continual encouragement. Special thanks also goes to Ryan Krauss for being genuine and for keeping things real.

Finally, and I put them last only to emphasize them most, I want to express my love and thanks to my whole family. To my perennially patient parents, I thank you for your instruction and care through all the years. I thank my older sister, Shanti, and her husband, Brett, for their friendship and support for the past several years. To my little sister, Dana, thanks for not disowning your absentee brother these past few years, and I hope that we can be better friends. Lastly, I need to acknowledge the two men I most wish could be here to see me receive my doctorate: my perfectly opposite grandfathers, Dr. Brahma Kaushiva and Alvie Edison Moore. I learned so much from you, and I know that I owe much of what I am to each of you. You will always be in my memory and in my heart.

Table of Contents

ABSTRACT…….. i

DEDICATION……..ii

ACKNOWLEDGEMENTS……iii

TABLE OF CONTENTS……..v

LIST OF FIGURES……...viii

LIST OF TABLES…….xvi

LIST OF EQUATIONS…….xvi

1. INTRODUCTION …….. 1

2. LITERATURE REVIEW …….. 5

2.1 BASIC CHEMISTRY OF FLEXIBLE POLYURETHANE FOAMS ……... 5

2.1.1 Blow Reaction …….. *5*

2.1.2 Gelation Reaction …… *6*

2.1.3 Isocyanate Group Chemistry ……... *7*

2.1.4 Components of Foam Formulations……. *8*

2.1.4.1 Isocyanates …… 10

2.1.4.2 Polyols……... 12

2.1.4.3 Water …… 17

2.1.4.4 Catalysts…… 17

2.1.4.5 Surfactants …… 19

2.1.4.6 Cross-linking Agents……. 20

2.1.4.7 Auxillary Blowing Agents …… 21

2.1.4.8 Additives …….. 21

2.2 THE FOAMING PROCESS ……..... 22

2.2.1 Bubble Initiation …….. 22

2.2.2 Bubble Growth……..24

2.2.3 Bubble Packing ……25

2.2.4 Cell Opening ……26

2.3 MORPHOLOGY …….. 29

2.4 RESEARCH OBJECTIVES…….. 33

2.5 REFERENCES …… 34

3. INFLUENCE OF DIETHANOLAMINE (DEOA) ON STRUCTURE-PROPERTY BEHAVIOR OF MOLDED FLEXIBLE POLYURETHANE FOAMS…… 35

3.1 CHAPTER SUMMARY……35

3.2 INTRODUCTION…….. 35

3.3 EXPERIMENTAL ……39

3.3.1 *Materials*…….. 39

3.3.2 *Methods*……..…40

3.4 RESULTS AND DISCUSSION……42

3.4.1 *Mechanical Properties*……..44

3.4.2 *Structure and Morphology*……..…...49

3.5 CONCLUSIONS……...57

3.6 ACKNOWLEDGMENTS ……....59

3.7 REFERENCES……..59

4. ALTERATION OF POLYUREA HARD DOMAIN MORPHOLOGY BY DIETHANOLAMINE (DEOA) IN MOLDED FLEXIBLE POLYURETHANE FOAMS..... 60

4.1 CHAPTER SUMMARY..... 60

4.2 INTRODUCTION 60

4.3 EXPERIMENTAL.....63
4.3.1 *Materials*..... 63
4.3.2 *Methods* 64

4.4 RESULTS AND DISCUSSION..... 65

4.5 CONCLUSIONS..... 71

4.6 ACKNOWLEDGMENTS..... 71

4.7 REFERENCES.....72

5. UNIAXIAL ORIENTATION BEHAVIOR AND CONSIDERATION OF THE GEOMETRIC ANISOTROPY OF POLYUREA HARD DOMAIN STRUCTURE IN FLEXIBLE POLYURETHANE FOAMS..... 73

5.1 CHAPTER SUMMARY.....73

5.2 INTRODUCTION..... 73

5.3 EXPERIMENTAL..... ... 76
5.3.1 *Materials*..... 76
5.3.2 *Methods*..... 77

5.4 RESULTS AND DISCUSSION.....77

5.5 CONCLUSIONS..... 81

5.6 ACKNOWLEDGEMENTS..... 81

5.7 REFERENCES..... 81

6. INFLUENCES OF COPOLYMER POLYOL ON STRUCTURAL AND VISCOELASTIC PROPERTIES IN MOLDED FLEXIBLE POLYURETHANE FOAMS.....82

6.1 CHAPTER SUMMARY..... 82

6.2 INTRODUCTION..... 83

6.3 EXPERIMENTAL MATERIALS AND METHODS..... 85
6.3.1 *Materials*..... 85
6.3.2 *Methods*..... 88

6.4 RESULTS AND DISCUSSION..... **91**
6.4.1 *Cellular Structure and Solid Morphology*.....91
6.4.2 *Mechanical and Viscoelastic Properties*.....97

6.5 CONCLUSIONS.....109

6.6 ACKNOWLEDGEMENTS.....110

6.7 REFERENCES.....110

7. SURFACTANT LEVEL INFLUENCES ON STRUCTURE AND PROPERTIES OF FLEXIBLE SLABSTOCK POLYURETHANE FOAMS……111

7.1 CHAPTER SUMMARY……111

7.2 INTRODUCTION……...112

7.3 EXPERIMENTAL……...117
7.3.1 *Materials*…….. 117
7.3.2 *Methods*……...120

7.4 RESULTS AND DISCUSSION……..123

7.5 CONCLUSIONS……..147

7.6 ACKNOWLEDGEMENTS……148

7.7 REFERENCES……148

8. CURE TEMPERATURE INFLUENCES ON STRUCTURE-PROPERTY RELATIONSHIPS IN PLAQUES BASED ON MOLDED FLEXIBLE POLYURETHANE FOAM FORMULATIONS……..150

8.1 CHAPTER SUMMARY…… 150

8.2 INTRODUCTION……... 151

8.3 EXPERIMENTAL…….. 153
8.3.1 *Materials*……..153
8.3.2 *Methods*…….. 155

8.4 RESULTS AND DISCUSSION……. 158

8.5 CONCLUSIONS…… 169

8.6 ACKNOWLEDGEMENTS……... 171

8.7 REFERENCES……... 171

9. STRUCTURE-PROPERTY RELATIONSHIPS OF POLYTETRAFLUOROETHYLENE — POLY(TETRAFLUOROETHYLENE-CO-VINYLIDENE FLUORIDE-CO-HEXAFLUOROPROPYLENE) BLENDS……172

9.1 CHAPTER SUMMARY……. 172

9.2 INTRODUCTION……. 174

9.3 EXPERIMENTAL…….. 177
9.3.1 *Materials*……. 177
9.3.2 *Methods*…….. 180

9.4 RESULTS AND DISCUSSION…….. 183
9.4.1 *Mechanical and Viscoelastic Properties*…….. 183
9.4.2 *Property Dependence on Raw Material Sources*……. 197
9.4.3 *Polymer Morphology*…….. 200
9.4.4 *Fibrillation Reinforcement of the Polymer Film*……. 210

9.5 CONCLUSIONS……. 220

9.6 ACKNOWLEDGEMENTS…… 221

9.7 REFERENCES…… 221

10. SUMMARY CHAPTER ……..**222**

A. APPENDIX - TAPPING MODE ATOMIC FORCE MICROSCOPY……..**226**

A.1 REFERENCES……233

VITA……...234

List of Figures

Figure #	Caption	Page
1.1	Applications of Flexible Polyurethane Foam Technology	2
1.2	Conventional Slabstock Process	3
1.3	Carousel Molding Process	4
2.1	First Step of the Blow Reaction	5
2.2	Second Step of the Blow Reaction	6
2.3	Formation of a Biuret Linkage	6
2.4	The Gelation or Cross-linking Reaction	7
2.5	Allophanate Formation	7
2.6	Resonance Structures of the Isocyanate Group	8
2.7	Isomers of Toluene Diisocyanate (TDI) and the Relative Reaction Rates of the Various Isocyanate Groups at Room Temperature	10
2.8	General Ways for Controlling Isomer Blend in TDI Production	11
2.9	Typical Ring Count Distribution in Crude MDI	12
2.10	Poly(oxydiethylene adipate)	13
2.11	Repeat Units if Copolymers of Ethylene Oxide and Propylene Oxide	13
2.12	Showing a Normal Termination Resulting in a 2° Hydroxyl and a Defect Termination Resulting in a 1° Hydroxyl Functionality.	14
2.13	Side reaction of base catalyzed polypropylene oxide resulting in monofunctional chain.	14
2.14	Effect of Concentration for a Typical Silicone Surfactant on Airflow.	19
2.15	Structure of Diethanolamine	20
2.16	Impact of Polyol Dissolved Gas on Cell Count in a Final Foam	24
2.17	Liquid Arrangement About Developing Polyhedra	26
2.18	Schematic of Phase Separation Behavior in Some Polyurethane Foams	27
2.19	Typical Sequence of Events in Foam Production	29
2.20	TEM Micrographs for Four Slabstock Foams of Increasing Water Content	31
3.1	Scanning electron micrograph of MaD2.0.	43
3.2	Variation of airflow measurements as a function of diethanolamine concentration.	44
3.3	DMA storage moduli at 1 Hz. for non-annealed foams of varying DEOA content.	44

Figure #	Caption	Page
3.4	Load relaxation data at 65% compression for non-annealed foams at: a) 30°C-15 % RH and b) 100°C-75 % RH	45
3.5	Percent load relaxation data at a) 30°C-15 % RH and b) 100°C-75 % RH. This was calculated by comparing the load bearing at 0.1 and 10,000 seconds after compression to 65%.	46
3.6	Percent change after annealing in the initial load bearing at 65% compression for the foams measured at 0.1 seconds after compression	47
3.7	Percent hysteresis at a) 30°C-15 % RH and b) 100°C-75 % RH	48
3.8	Solvent extraction results for foams of varying DEOA content	49
3.9	SAXS profiles for non-annealed foams of varying DEOA content	50
3.10	Influence of DEOA on the SAXS interdomain spacings of annealed and non-annealed materials.	51
3.11	DMA tan delta curve for the 0.0 DEOA pphp non-annealed foam.	52
3.12	Polyol glass transition region from DMA tan delta curves for foams of various DEOA content. a) non-annealed samples and b) annealed samples.	53
3.13	WAXS patterns for foams with a) 0.0 DEOA pphp and b) 2.0 DEOA pphp.	54
3.14	FTIR spectra showing the carbonyl vibration region for a) non-annealed and b) annealed foams	55
3.15	Influence of annealing on the FTIR spectra of a) 0.0 DEOA pphp and b) 2.0 DEOA pphp foams	55
3.16	Ratio of hydrogen bonded carbonyl peak height to the free carbonyl peak height as a function of DEOA content	56
3.17	Schematic representation of polyurea segment packing in a hard domain a) without DEOA and b) with DEOA	58
4.1	AFM phase images of a molded foam without diethanolamine at a) low magnification and b) high magnification.	67
4.2	AFM phase images of a molded foam with diethanolamine a) at low magnification, b) showing the hard domain dispersion at high magnification.	68
4.3	a) SAXS profiles for the foam samples with and without DEOA. b) Three dimensional correlation functions for the foam samples.	70
5.1	WAXS patterns of a) C80-Su1.5 before deformation; b) C80-Su1.5 at 50% elongation; and c) C106-Su1.5 at 50% elongation. White arrows note areas of intensification along the meridian. Axis of deformation is noted on WAXS patterns where relevant.	78
5.2	AFM Phase image of cryo-microtomed cross-section of foam sample C80-Su1.5.	79

Figure #	Caption	Page
5.3	AFM Phase image of cryo-microtomed cross-section of foam sample SSu1.5.	80
6.1	Scanning electron micrographs of foam M1c observed both (A) parallel to the rise direction and (B) perpendicular to the rise direction.	91
6.2	Scanning electron micrograph of foam M1n observed parallel to the rise direction.	92
6.3	Transmission electron micrograph of foam M1c (mag. = 27 kx).	93
6.4	Transmission electron micrograph of foam M1c after 90 % compression at 150°C (mag. = 27 kx). Arrow signifies deformation axis.	93
6.5	Influence of CPP particles on the tanδ peak of the molded foams illustrated using (a) M1c and (b) M1n.	94
6.6	SAXS profiles of molded foams illustrating the influence of the CPP particles: (a) M1c and (b) M1n.	95
6.7	Percent extractables from a DMF extraction of Series 1 and Series 2 foams.	96
6.8	Load-strain behavior illustrating mechanical hysteresis upon loading and unloading for a) M1c and b) M1n.	97
6.9	a) Load-strain behavior for M2F0.0 and M2F13.0 illustrating their mechanical hysteresis behavior upon loading and unloading at 30°C-15%RH b) Average load at 1 second after compression to 65% strain at 30°C-15%RH for the foams of Series 2.	98
6.10	Load-strain behavior for M2F0.0 and M2F13.0 illustrating their hysteresis curves upon loading and unloading at 30°C-100%RH.	99
6.11	Percent Hysteresis for Series 2 foams a) at 30°C-100%RH and b) at 100°C-75%RH.	100
6.12	Load relaxation behavior of M1n as a function of temperature and relative humidity: a) 30°C-35%RH, b) 100°C-35%RH, c) 30°C-98%RH, and d) 100°C-98%RH	101
6.13	Load relaxation behavior of M1c as a function of temperature/relative humidity: (a) 30°C-35%RH, (b) 100°C-35%RH, (c) 30°C-98%RH, and (d) 100°C-98%RH.	102
6.14	a) Load relaxation behavior at 30°C-35%RH for the 4 pphp water content foams as a function of the CPP used: (a) M1c and (b) M1n. 14b) shows percent load loss calculated from loads at 0.1 and 25,000 seconds for Series 2 foams at 30°C-15%RH.	103
6.15	a) Load relaxation behavior at 30°C-98%RH for the 4 pphp water content foams as a function of the CPP used: (a) M1c and (b) M1n. 15 b) shows percent load loss calculated from loads at 0.1 and 10,000 seconds for Series 2 foams at 30°C-100%RH.	104

Figure #	Caption	Page
6.16	Load relaxation behavior at 100°C-35%RH for the 4 pphp water content foams as a function of the CPP used: (a) M1c and (b) M1n	104
6.17	a) Load relaxation behavior at 100°C-98%RH for the 4 pphp water content foams as a function of the CPP used: (a) M1c and (b) M1n. 17 b) shows percent load loss calculated from loads at 0.1 and 10,000 seconds for Series 2 foams at 30°C-100%RH and at 100°C-75%RH	105
6.18	Creep response at 30°C-35%RH as a function of CPP used: (a) M1c and (b) M1n.	106
6.19	Creep response at 100°C-35%RH as a function of CPP used: (a) M1c and (b) M1n.	107
7.1	Structure of Tegostab™ BF 2370 (Goldschmidt AG). Average molecular weight for the copolymer is 8,800. There are no emulsifying ingredients present in the surfactant besides remaining monol residues of the polyether mixture used for the copolymer synthesis.	119
7.2	Scanning electron micrographs of foams in various states: 2a) SSu0.0, 2b) SSu1.5, 2c) Q100-Su0.0, 2d) Q100-Su1.5, 2e) Q120-Su0.0, 2f) Q120-Su1.5, 2g) C80-Su1.5, and 2h) C106-Su1.5. The scale bar shown in 2a) applies to all of the micrographs.	124
7.3	Transmission electron high magnification micrographs for two foams with varying surfactant concentration: 3a) SSu0.0 and 3b) SSu1.5.	126
7.4	Transmission electron medium magnification micrographs of foams in various states: 4a) SSu0.0, 4b) SSu1.5, 4c) Q100-Su0.0, 4d) Q100-Su1.5, 4e) Q120-Su0.0, 4f) Q120-Su1.5, 4g) C80-Su1.5, and 4h) C106-Su1.5	128
7.5	Transmission electron low magnification micrographs of foams in various states: 5a) Q100-Su0.0, 5b) Q100-Su1.5, 5c) Q120-Su0.0, 5d) Q120-Su1.5, 5e) C80-Su1.5, and 5f) C106-Su1.5.	129
7.6	Atomic force microscopy phase images of two quenched materials: 6a) Q100-Su0.0 and 6b) Q100-Su1.5. The z axis scale has been inverted from the machine default such that higher phase offset is induced by softer material. This is only done in these two images to parallel the TEM micrographs of Figures 3-5.	129
7.7	a) Small angle x-ray scattering data for foams of varying composition. 7 b) Three dimensional correlation functions for four slabstock foams of varying surfactant concentration.	131
7.8	a) Small angles x-ray scattering data for two foams quenched from reaction at different times. 8b) Three dimensional correlation functions for four quenched foams of varying surfactant concentration. 8c) Three dimensional correlation functions for two crushed foams of 1.5 surfactant pphp concentration. 8d) Comparison of the mean chord lengths for all the samples.	132

Figure #	Caption	Page
7.9	Correlation of Fourier transform infrared spectroscopy and wide-angle x-ray scattering for polyurethane foams: 9a) transmission mode FTIR spectrum of UPA, 9b) WAXS pattern of UPA, 9c) transmission mode FTIR spectrum of UPSu, 9d) WAXS pattern of UPSu, 9e) attentuated total reflectance mode FTIR spectrum of SHiEO, 9f) WAXS pattern of SHiEO.	135
7.10	Atomic force microscopy phase image of SHiEO.	136
7.11	Fourier transform infrared spectroscopy and wide-angle x-ray scattering of polyurethane foams: 11a) attentuated total reflectance mode FTIR spectrum of SSu0.0 and SSu1.5, 11b) WAXS pattern of SSu1.5, 11c) WAXS pattern of SSu0.0, 11d) attentuated total reflectance mode FTIR spectrum of MD0.0 and MD2.0, 11e) WAXS pattern of MD0.0, and 11f) WAXS pattern of MD2.0.	137
7.12	Atomic force microscopy phase image of SSu1.5, representative of a typical image from the polyurethane foams in this study.	139
7.13	Power spectral density (a Fourier transform analysis) of SSu1.5 illustrating the two scale lengths (ca. 0.5 μm and ca 8 nm) in the distribution of wavelengths that characterize the distribution of domains with similar phase offsets in the surface.	140
7.14	Representative section analysis of the phase image SSu1.5 shown in Figure 7.12.	141
7.15	a) Maximal phase offsets for foams of various surfactant concentration. 15b) Comparative trends between the 1640 cm-1 absorbance from FTIR and the maximal phase offsets of AFM tapping mode. 15c) Maximal phase offsets for foams in various states (fully developed, quenched, or crushed). 15d) Normalized 1640 cm-1 absorbances from FTIR for foams of various states. This demonstrates that the 1640 cm-1 absorbance is consistent for each level of cure but cannot be used to explain the behavior of samples at different states shown in Figure 7.15c.	142
7.16	Tan delta from DMS for: 16a) samples of various surfactant concentrations, 16b) samples with 1.5 surfactant pphp concentration at different states, 16c) all samples that collapsed spontaneously, were quenched, or were crushed.	144
7.17	Storage modulus from DMS for: 17a) samples of various surfactant concentrations, 17b) samples with 1.5 surfactant pphp concentration at different states, 17c) all samples that collapsed spontaneously, were quenched, or were crushed.	146
8.1	Estimate of hard segment content of the plaques showing variation due to cure temperature relative to that observed in the plaque pressed from a fully cured foam.	160
8.2	FTIR Spectra of Plaques without CPP.	161

Figure #	Caption	Page
8.3	Nitrogen Analysis of the Various Samples	162
8.4	Solvent Extraction Results	163
8.5	SAXS profiles of foams and plaques (a) with copolymer polyol and (b) without copolymer polyol.	164
8.6	Influence of annealing treatment on the SAXS profiles of (a) foams and (b) plaques.	164
8.7	Analysis of carbonyl region of FTIR spectra of foams and plaques. (a) Shows influence of annealing upon spectra of foams, and (b) examines ratio of hydrogen bonded polyurea peak height (at ca. 1640cm^{-1}) to free polyurea peak height (at ca. 1710cm^{-1}).	165
8.8	DMA data for plaques containing copolymer polyol (a) storage moduli and (b) tanδ.	167
8.9	DMA data for plaques without copolymer polyol (a) storage moduli and (b) tanδ.	168
8.10	DMA data comparing plaques and foams: (a) storage moduli and (b) tanδ.	168
9.1	Schematic diagram of mold used to study film deformation at various temperatures.	182
9.2	Summary of data from Instron tensile tests at room temperature: a) Young's modulus and b) toughness.	183
9.3	Room temperature stress-strain behavior comparing different levels of PTFE content for materials that are a) greenleaf, b) cured, and c) post-cured.	185
9.4	Room temp. stress-strain behavior comparing degree of cross-linking at each level of PTFE content: a) 0 wt%, b) 20 wt%, c) 40 wt%, d) 60 wt%, and e) 70 wt%.	186
9.5	Thermal variation of the stress-strain behavior for the greenleaf materials. Stress-strain curves for a) 0 wt% PTFE, b) 40 wt% PTFE, and c) 60 wt% PTFE.	187
9.6	Summary of the thermal variation tensile tests: a) modulus and b) toughness.	188
9.7	Comparison of the experimental data with various theories of filled materials.	190
9.8	Influence of PTFE wt% on the Dynamic Mechanical Analysis results: a) storage moduli and b) tanδ curves of greenleaf materials; a) storage moduli and b) tanδ curves of cured materials; and a) storage moduli and b) tanδ curves of post-cured materials	193
9.9	Influence of cross-linking on the DMA results: a) storage moduli and b) tanδ curves of 0 wt% PTFE films; a) storage moduli and b) tanδ curves of 40 wt% PTFE films; and a) storage moduli and b) tanδ curves of 70 wt% PTFE films.	196

Figure #	Caption	Page
9.10	Mechanical property variation due to changes in altering FKM or PTFE component. Comparison of: a) storage moduli and b) tanδ curves of 0 wt% PTFE films of FKM A and FKM B; c) storage moduli and d) tanδ curves of 40 wt% PTFE films based on PTFE 1 / FKM A and PTFE 2 / FKM B; d) storage moduli and e) tanδ curves of 40 wt% PTFE films based on PTFE 1 / FKM A and PTFE 3 / FKM C; and g) storage moduli and h) tanδ curves of 20 wt% PTFE films based on PTFE 1 / FKM A and PTFE 3 / FKM D.	198-199
9.11	Degree of covalent cross-linking characterized by solvent extraction where sol percent represents the weight percent of extractable material.	200
9.12	TEM micrgraphs showing the development of beam damage: a) and b) in as-cast greenleaf films containing 40 wt% PTFE; and c) and d) showing the same area of a 60 wt% PTFE calendered film.	202
9.13	High magnification view of epoxy/film interface for the 40 wt% film. Arrow indicates aggregate of ca. 0.2 μm PTFE particles.	204
9.14	TEM micrographs of as-cast greenleaf films containing a) and b) 20 wt% PTFE; c) 40 wt% PTFE; and d) 60 wt% PTFE. White arrows indicate pull-out artifacts.	205
9.15	Phase images from atomic force microscopy: a) of the polyester carrier side of a 20 wt% PTFE film; and b) of the carrier side of an 80 wt% PTFE film.	206
9.16	WAXS patterns of a) an as-cast 70 wt% PTFE film, b) the 70 wt% film at 103% elongation, and c) paste-extruded and drawn 100% PTFE fiber.	209
9.17	Mechanical properties from tensile testing of the calendered films: a) stress-strain data for the 40 and 60 wt% films comparing machine axis properties to those of the transverse axis and of as-cast films; b) modulus data; and c) toughness data from the tensile experiments.	211
9.18	WAXS patterns of the calendered films: a) the 40 wt% PTFE film and b) the 60 wt% PTFE film where the machine axis is shown as vertical.	212
9.19	Phase images from atomic force microscopy of: the 40 wt% PTFE calendered film and b) the 60 wt% PTFE film where the machine axes in the images are vertical.	212
9.20	TEM micrographs of the calendered 40 wt% PTFE films a) parallel to the machine axis, b) perpendicular to the machine axis, and the film/epoxy interface after beam damage has stabilized at c) low mag. parallel to the machine axis and d) at high mag perpendicular to the machine axis.	213

Figure #	Caption	Page
9.21	TEM micrographs of the calendered 60 wt% PTFE films a) and b) parallel to the machine axis, c) perpendicular to the machine axis, and d) the film/epoxy interface after beam damage has stabilized viewed parallel to the machine.	214
9.22	Phase images from AFM of: a) the 40 wt% PTFE film and b) the 60 wt% PTFE film drawn to ca. 3,130% elongation where the deformation axes are oriented vertically in the images.	215
9.23	TEM micrographs of the drawn PTFE films parallel to the machine axis: a) and b) the 40 wt% film, and c) the 60 wt% film.	216
9.24	TEM micrographs of the drawn PTFE films parallel to the machine axis after beam damage has stabilized: a) the 40 wt% film and b) the 60 wt% film. The as-cast 60 wt% film/epoxy interface is shown in c).	217
9.25	Results of the mechanical testing of the deformed 40 wt% PTFE 2 / FKM B films: a) moduli and b) toughness data.	218
9.26	WAXS patterns of the 40 wt% PTFE 2 / FKM B films deformed for 11 minutes at a) 15°C and b) at 22°C. Direction of “c” axis orientation indicated by white arrows.	219
9.27	Phase images from AFM of the 40 wt% PTFE 2 / FKM B film a) prior to deformation and b) after 11 minute deformation at 15°C	219
A.1	Surface Interaction in Tapping Mode AFM.	227
A.2	Taking a Cross-section of an Image.	229
A.3	Two Surfaces with Equal Roughnesses.	230
A.4	A Surface Comprised of Two Waveforms.	230
A.5	Height Image of Epitaxial Gallium Arsenide.	231
A.6	Power Spectral Density Plot for Epitaxial Gallium Arsenide.	231
A.7	A Synthetic Waveform Having a Wavelength of 100 Nanometers.	232
A.8	Power Spectral Density Plot for the Synthetic Waveform.	232

List of Tables

Table #	Table Title	Page
2.1	Relative Reaction Rates of Common Foam Components with Isocyanate Groups	9
2.2	Typical Components and their Normal Usage in Flexible Polyurethane Foam Formulations	10
3.1	Variation of DEOA and TDI 80 in the Five Samples	40
3.2	Influence of DEOA on Polyol Glass Transition Temperatures	53
6.1	Series 1 Foam Formulation Components (all formulation amounts are given in pphp)	87
6.2	Series 2 Foam Formulation Components (all formulation amounts are given in pphp)	87
6.3	Compression Set Results for the Two Foams of Series 1	108
7.1	Sample Designations and Their Meanings	118
7.2	Some Relevant IR Absorbances of the Carbonyl Chromophore	121
7.3	Apparent Densities of the Samples	125
8.1	Thermal History of the Samples	156
9.1	General Formulation for the Fluoroelastomer/Fluoroplastic Blends	179
9.2	FKM Composition	180

List of Equations

Equation #	Equation Name	Page
2.1	LaPlace Equation	25
9.1	Guth-Smallwood Equation	190
9.2	Kerner Equation	190
9.3	Mooney Equation	190
9.4	Uniaxial Orientation Function for Hexagonal Unit Cell	208
9.5	Relation of $\phi_{100,Z}$ to θ_{100} and ψ_{100}	208
9.6	Bragg's Law	208
A.1	Maganov Relation of Phase Offset to Surface Elasticity	228
A.2	Simplified Relation of Phase Offset to Surface Elasticity	228

1. Introduction

Polyurethanes are a broad class of materials utilized in a wide variety of applications. Products in this family are chemically complex and may contain several different types of bonds, yet all have the polyurethane linkage in common. This linkage is formed from the reaction between the isocyanate functionality of one component with the alcohol group of another component. By controlling the composition of each component, two solid state phases frequently result. This two-phase morphology provides the key to controlling performance of the final product and gives the manufacturer versatility in tuning properties as desired by varying the composition or content of one or the other phases.

One major application of polyurethanes is in the area of flexible foams. As discussed above, through controlling the morphology, manufacturers currently produce some low-density foams that feel as soft as down and other "foams" that are essentially high-strength, bubble-free elastomeric castings. This range of properties has allowed flexible polyurethane foams to attain the sixth position in sales volume relative to all major plastics. In 1995, for instance, nearly 10 billion pounds of flexible foam products were produced.[1] Other applications of this technology can be seen in Figure 1.1.

As widely utilized as flexible polyurethane foams have become, clear scientific understanding of how changes in formulation ultimately lead to properties is still far from complete. This is partly due to the "technological" approach taken in the past in developing processing techniques, but it is also largely due to the complex nature of these materials.[2] Many advances have occurred in the collective knowledge of how morphology develops based on formulation, and this has led to a better understanding of how those various structures lead to properties. However, as will be reviewed in later sections, formulations needed for new applications continue to develop, challenging existing knowledge of structure-property relationships and demanding better explanations. This is particularly true where formulations need to be altered to meet more rigorous performance criteria.

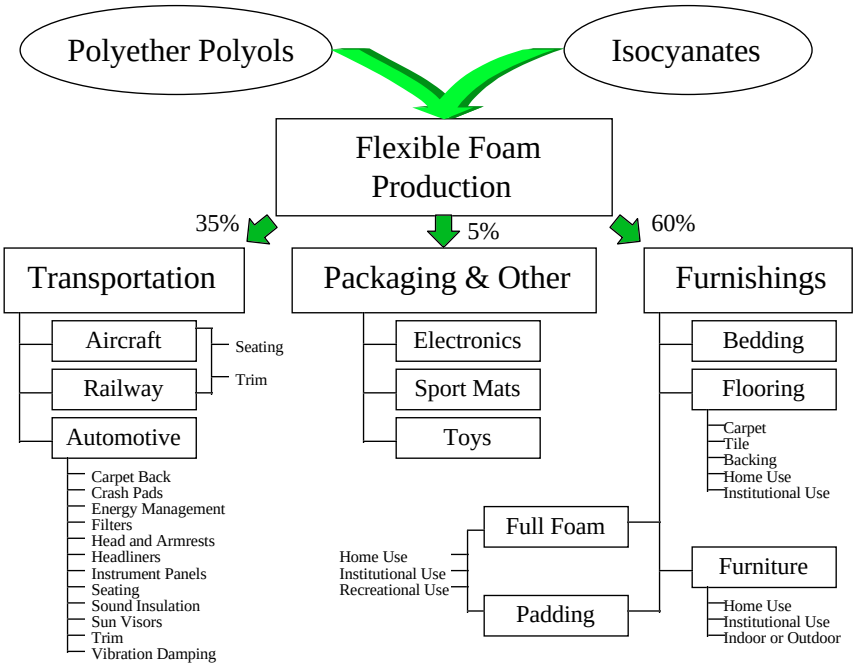

Figure 1.1 - Applications of Flexible Polyurethane Foam Technology[1]

One example of these changes in technology is the move towards molded foam production from slabstock production techniques. A typical slabstock production line is shown in Figure 1.2. In that process, the reactive components are blended in the transverse mixing head and laid out on the conveyor belt. As the conveyor moves, the foaming reactions initiate rapidly and give off carbon dioxide. This evolving CO_2 induces entrained gas bubbles in the liquid mixture to grow large enough to scatter visible light, causing a coloration change termed "creaming" which occurs in the diagram at the "cream line." As the reactions progress further, they cause the liquid to rise into the desired cellular structure, until the cells reach the point where they open. At that point, gas can move freely through the matrix, allowing the foam to settle down, or "sigh back," to its final height. Both the chemistry of the reactions and the processes of developing cellular morphology will be explained in detail in later sections. The important point here is to observe that these slabstock processes are essentially continuous operations, in which production can be optimized by changing the volume of the foam bun produced.

Cutting large slabstock buns into complex shapes like car seats takes time and produces a lot of waste. Both of these can be avoided by producing the foam in a mold of the desired shape, yielding significant savings. This improvement has led to molded processes growing to comprise about one-fourth of the flexible polyurethane foam market. A carousel molding line is

shown in Figure 1.3. The proper charge of reactive components are mixed and placed into a mold as the turntable moves it into place. The mixture reacts and a foam of the mold's shape is produced. It is then removed, and, as the now empty mold completes the circle, the mold is recharged. Thus, in these batchwise processes, the limiting factor to production is residence time in the molds. Therefore, to achieve lower demold times, many changes have been introduced to the formulations, such as the addition of the cross-linking agent diethanolamine. Two purposes of this work, then, are to examine the changes that occur in the morphology of these molded foams as a result of these formulation changes, and to extend known structure-property relationships for flexible polyurethane foams to this newer area of molded materials.

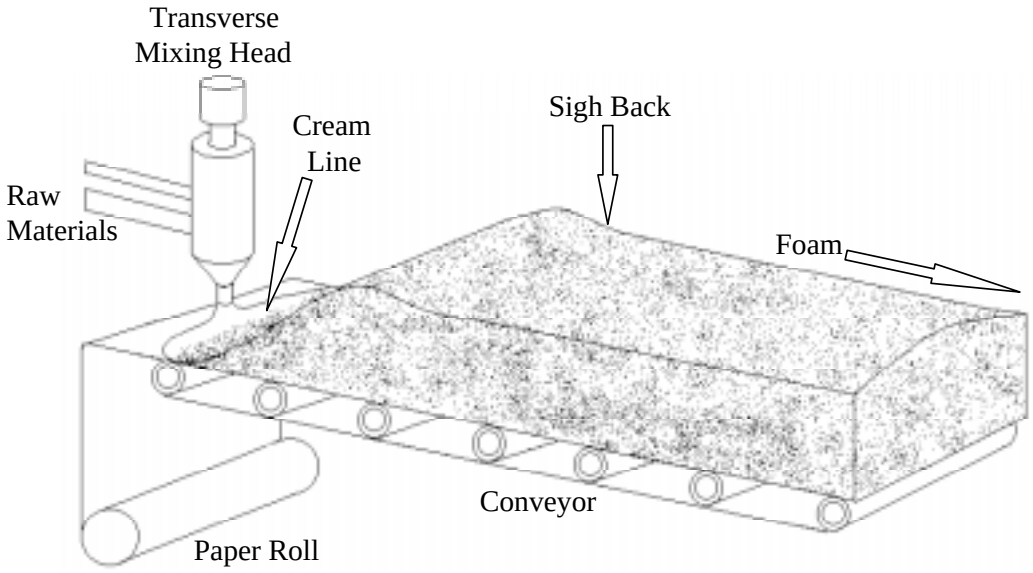

Figure 1.2 - Conventional Slabstock Process[1]

To accomplish these purposes, the format of this dissertation will begin with a literature review which will survey the current understanding of the morphology and viscoelastic properties of flexible polyurethane foams. Because many of the properties which will be examined in later sections depend upon the morphology of the solid state and of the cellular structure, the literature review will place particular emphasis on how foam production leads to the development of the final morphology. Following the literature review, several important variables to the area of flexible polyurethane foams will be explored in succeeding chapters. These chapters are formatted as manuscripts, and they contain additional introductory reviews of different aspects of the literature. Influences on structure-property relationships of

diethanolamine, a cross-linking agent used in molded foams, will be evaluated in Chapter 3. Tapping-mode atomic force microscopy will be used in Chapter 4 to further explore the alterations which diethanolamine makes on the morphology of hard domains. The anisotropic structure of those hard domains will be further elucidated in Chapter 5. Chapter 6 will examine the properties which result from using a reinforcing filler called copolymer polyol, which is widely utilized in molded and slabstock foam production. The dependence of hard domain development upon the presence of cellular structure will be examined by varying the surfactant concentration in the formation in Chapter 7. This will be further studied in Chapter 8, by examining the morphology which results from varying the cure temperature in void-free plaques based on molded foam formulations. Finally, in a major departure from polyurethane foams, Chapter 9 will present a study into the structure-property relationships of blends of polytetrafluoroethylene and the terpolymer poly(tetrafluoroethylene-co-vinylidene fluoride-co-hexafluoropropylene). A review of the objectives and the literature for the fluoropolymer study will be presented in the Chapter 9 introduction.

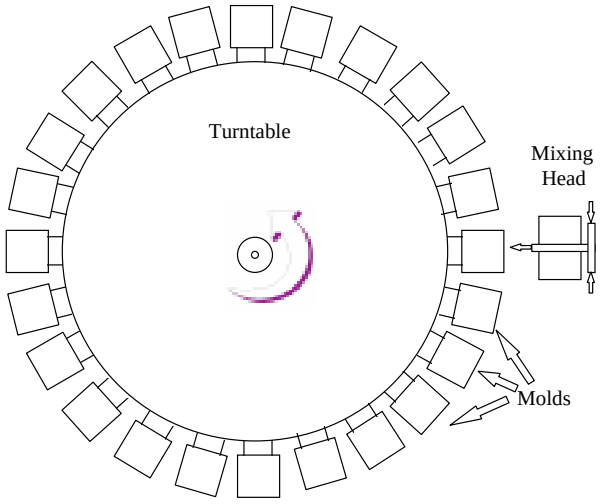

Figure 1.3 - Carousel Molding Process[1]

1.1 References

1. Herrington R; Hock K; Flexible Polyurethane Foams, 2nd Ed.; The Dow Chem Co: (1998)
2. Armistead JP; *Ph. D. Dissertation*; VPI & SU: (1985)

2. Literature Review

2.1 Basic Chemistry of Flexible Polyurethane Foams

There are two main reactions important in the production of flexible polyurethane foams: the blow reaction and the gelation reaction. To the manufacturer, balancing the respective rates of these two reactions provides the open-celled morphology in the foam that is highly important to physical properties. If the gelation, or cross-linking, reaction occurs too quickly, a tight close-celled foam may result. If the blow, or gas-producing, reaction occurs too quickly, the cells may open before the polymer has enough strength to uphold the cellular structure, resulting in collapse of the foam. Thus, as will be discussed in the catalysts section (Section 2.1.4.4), these two reactions must kept in proper balance in order to obtain the desired product.

2.1.1 Blow Reaction

The reaction of water with isocyanates is a two-step process termed the blow reaction because, in addition to a polyurea product, a gas is evolved which plays a large role in blowing the liquid into a foam. Auxiliary blowing agents can also be utilized, and these will be discussed later in Section 2.1.4.7. The initial step of the blow reaction, which occurs through an intermediate, can be seen in Figure 2.1 where a thermally unstable carbamic acid is generated. This carbamic acid then spontaneously decomposes yielding heat, carbon dioxide, and an amine functionality. The carbon dioxide diffuses into existing bubbles already nucleated in the liquid causing expansion of the foam. In addition to that, the heat generated will also play a large role in expanding the gas in the liquid to form the desired cellular morphology.

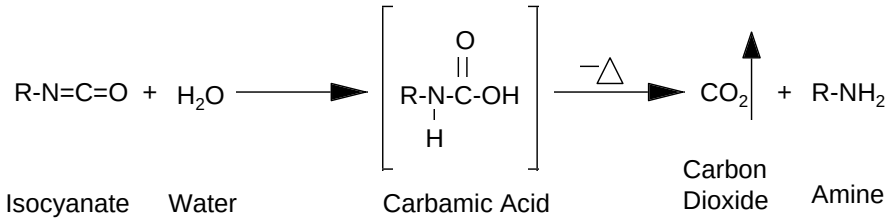

Figure 2.1 - First Step of the Blow Reaction

The amine functionality proceeds to the second step of the blow reaction. As shown in Figure 2.2, it reacts with an additional isocyanate group to form a disubstituted urea linkage. The total heat given off in the reactions of Figure 2.1 and Figure 2.2 is approximately 47

kcal/mol. This second reaction can also be source of covalent cross-links if either the isocyanate has more than two functional groups or if polyfunctional amines (e.g. diethanolamine) have been added to the formulation.

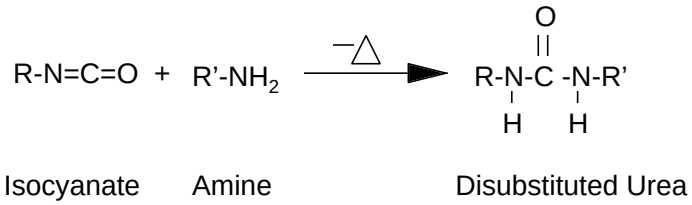

Figure 2.2 - Second Step of the Blow Reaction

There is an additional reaction which could also produce covalent cross-links. The formation of biuret linkages, as shown in Figure 2.3, can occur if one of the hydrogens from the disubstituted urea product reacts with an isocyanate functionality. However, this reaction is reversible and generally does not occur below 100°C,[2] and no evidence exists which suggests that birurets are produced to a significant extent in typical polyurethane foams.[2] It has been suggested that biurets may not be produced partly because of their reversibility but also because of the catalysis of the two desired reactions.[1]

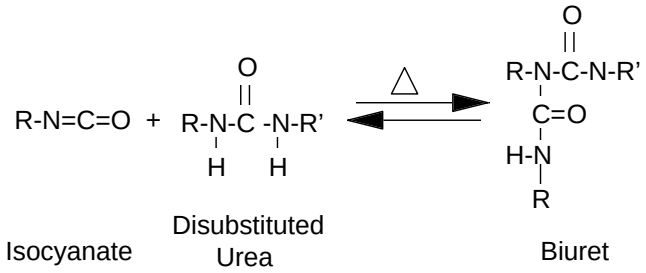

Figure 2.3 - Formation of a Biuret Linkage

2.1.2 Gelation Reaction

The polyurethane linkage is produced by the reaction of an alcohol functionality with an isocyanate group as shown in Figure 2.4. This addition reaction is exothermic with a heat of reaction of approximately 24 kcal/mol of urethane.[1] The nature of the R and R' groups shown in Figure 2.4 can vary depending on the selection of components in the formulation, and these choices will be discussed in the polyol and isocyanate parts of Section 2.1.4. Generally, one of these components is multifunctional so that these reactions lead to a covalent network.

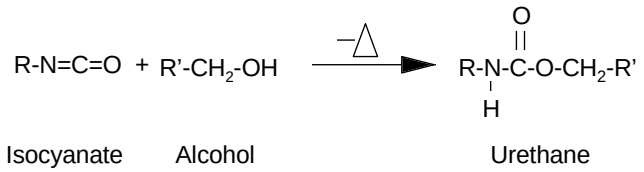

Figure 2.4 - The Gelation or Cross-linking Reaction

A side-reaction that can result from this urethane product is the allophanate forming reaction. This occurs when another isocyanate group reacts with the urethane linkage through the hydrogen on the nitrogen atom as is shown in Figure 2.5. This formation reaction occurs mainly at high temperatures and is reversible. It is uncertain whether this reaction actually occurs in normal foam processes, as the catalysts utilized generally do not promote this reaction.[2] Also, since it only occurs in significant levels above 110°C, the allophanate reaction may reverse as the foam cools following production.[2] If it does occur, it can be seen from Figure 2.5 that it serves as an additional point of cross-linking; however, this side reaction has not been shown to actually occur in typical foam production. [1]

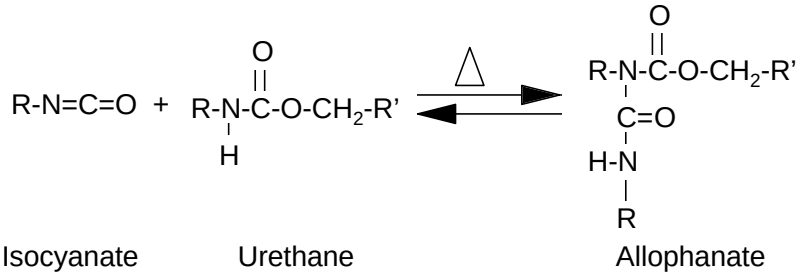

Figure 2.5 - Allophanate Formation

2.1.3 Isocyanate Group Chemistry

It should be obvious from the preceding discussion that the isocyanate functional group is the foundation of polyurethane chemistry. Therefore some details about that particular group are valuable in understanding the overall process. In general, the term “isocyanate” is used to refer to compounds which contain the (-N=C=O) group. Any hydrogen atoms attached to atoms more electronegative than carbon are active for reaction with isocyanates. This high reactivity can be explained by considering the resonance structure for isocyanates shown in Figure 2.6.

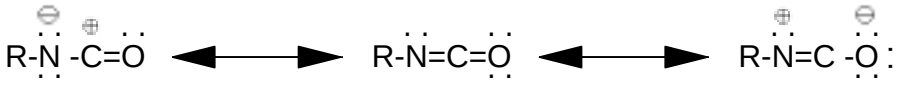

Figure 2.6 - Resonance Structures of the Isocyanate Group[1]

The more electronegative oxygen atom has a net negative charge as it draws the highest electron density. Having the least electronegativity, the carbon atom has a net positive charge, and the nitrogen atom thus has an intermediate net negative charge. Because of this, most of the isocyanate reactions involve a hydrogen-containing nucleophile adding to the electrophilic carbon atom. The hydrogen from the attacking group will then add to the nitrogen atom.[1]

It may also be observed from this discussion that the groups to which the isocyanate moieties are attached play a large role in overall reactivity. Electron withdrawing groups, like many aromatics, will enhance the reactivity of the isocyanate. On the other hand, electron donating groups, like aliphatics, will reduce reactivity. Besides these considerations, it should also be clear that steric hindrance from the neighboring group can hinder the reactivity of the isocyanate molecule.[1]

As was mentioned in the introduction to this chapter, the relative rates of the gelation reaction as compared to the blow reaction are of great importance to the manufacturers of foams. In Table 2.1 there is a listing of common components of interest to polyurethane manufacturers, and their relative rates of reaction with isocyanate groups. Typically, the reactants in the gelation reaction are either secondary or primary hydroxyls, and the reactants in the blow reaction are water and the resulting primary aromatic amine. The range of rates shown in Table 2.1 should indicate the need for using catalysts to achieve the proper balance of the two main reactions.

2.1.4 Components of Foam Formulations

Each application of flexible polyurethane foams has specific performance criteria, so there are many components needed in a typical formulation to ensure that the product will be open-celled and still meet other requirements. For example, fillers may be added to enhance strength, or a lower potency surfactant may be used to provide more cell openness. An example of the types of components that might be involved in a formulation, and some typical concentration ranges that they are used in, is provided in Table 2.2. It should be noted that, by convention, flexible polyurethane foam formulations are calculated as weight fractions based on

total polyol added (termed parts per hundred polyol). Each type of component will be discussed in detail in the following subsections.

Table 2.1 – Relative Reaction Rates of Common Foam Components with Isocyanate Groups[1]

Component with an Active Hydrogen	**Structure**	**Relative Reaction Rate (Uncatalyzed at 25 °C)**
Primary Aliphatic Amine	$R\text{-}NH_2$	100,000
Secondary Aliphatic Amine	$R_2\text{-}NH$	20,000-50,000
Primary Aromatic Amine	$Ar\text{-}NH_2$	200-300
Primary Hydroxyl	$R\text{-}CH_2\text{-}OH$	100
Water	H_2O	100
Carboxylic Acid	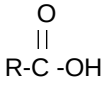	40
Secondary Hydroxyl	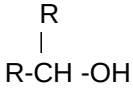	30
Ureas	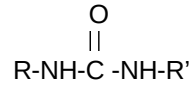	15
Tertiary Hydroxyl	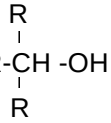	0.5
Urethane	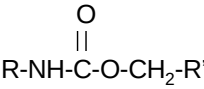	0.3
Amide	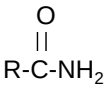	0.1

Table 2.2 - Typical Components and their Normal Usage in Flexible Polyurethane Foam Formulations[1]

Component	Weight Added [Parts Per Hundred Polyol]
Polyol	100
Water	1.5-7.5
Inorganic Fillers	0-150
Silicone Surfactant	0.5-2.5
Amine Catalyst	0.1-1.0
Tin Catalyst	0.0-0.5
Chain Extender	0-10
Cross Linker	0-5
Additive	Variable
Auxiliary Blowing Agent	0-35
Isocyanate	25-85

2.1.4.1 Isocyanates

A broad range of compounds containing isocyanate functional groups are currently used throughout the flexible foam industry. However, toluene diisocyanate (TDI) is, by volume, the most important. This compound can exist in two isomers as shown in Figure 2.7, and both of these isomers are used in these processes. Figure 2.7 also shows their relative reaction rates at room temperature. As the temperature in the reactive mixture approaches 100°C, steric hindrance in the 2,4 isomer is overcome and the two positions react at approximately the same rate.[1]

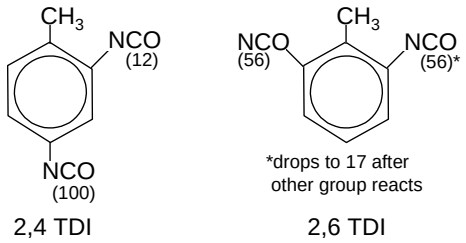

Figure 2.7 - Isomers of Toluene Diisocyanate (TDI) and the Relative Reaction Rates of the Various Isocyanate Groups at Room Temperature. [1]

As shown in Figure 2.8, the isomer produced can to some extent be controlled. An 80/20 2,4/2,6 isomeric blend is obtained from the double nitration of toluene. To get other blend ratios, the mixture is purified after a single nitration. This purification is typically accomplished by crystallization, and it results in pure para-nitrotoluene and pure ortho-nitrotoluene products. The second nitration of para-nitrotoluene leads to pure 2,4-nitrotoluene, and second nitration of ortho-nitrotoluene leads to a 65/35 blend of the 2,4/2,6 isomers. Phosgenation of either of these dinitrotoluenes yields toluene diisocyanate which is then purified by distillation.

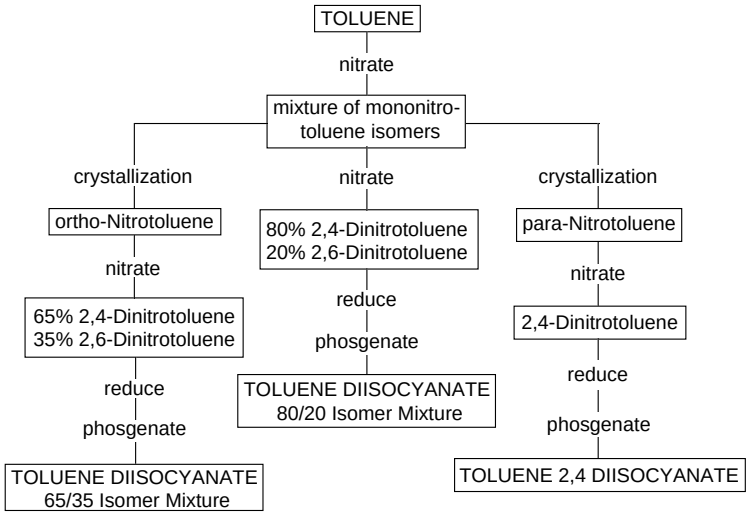

Figure 2.8 - General Ways for Controlling Isomer Blend in TDI Production[1]

Properties of the foam can be drastically altered by changing the isocyanate component. For example, the blend ratio of the isomers can have large effects. Although catalyst adjustment is necessary due to lower reactivity, the 65/35 isomeric blend provides higher load bearing foams. Since hard segments based on the pure 2,6 isomer has the potential to crystallize but the 2,4 isomer product does not, some of these differences may be explained from packing considerations between the hard segments. Properties can also be altered by using modified TDI. End-capping polyol chains with TDI yields isocyanate ended polyether urethane, which is useful for ensuring satisfactory chain extension. This type of modification was more utilized prior to the development of tin catalysts, but they still find application today in the area of adhesives and surface coatings. Another useful modification is produced by altering the functionality of the isocyanate through allophanate or isocyanurate reactions. These adaptations increase the load bearing of cold-cure molded systems, but they can also disrupt hydrogen

bonding within the phase separated hard domains. Details of these and other little used modified TDI components are available in references 1 and 2.

In high resiliency, semiflexible, and microcellular foams, various forms of diphenylmethane diisocyanate (MDI) are also utilized. The reaction of aniline with formaldehyde leads to polymeric amines which are then phosgenated. This results in a mixture of various forms of MDI, and a typical distribution of the forms is shown in Figure 2.9. Pure MDI is the most widely used, and it is obtained by distilling the mixed product. The other fractions are characterized based on viscosity, functionality, and reactivity. This allows foam manufactures to find an appropriate blend of MDI fractions that give the properties they desire. Blends of MDI and TDI are also utilized today. A benefit of these products is that using polymeric MDI and TDI endcapped polyol reduces the vapor hazard of the isocyanate component.[1]

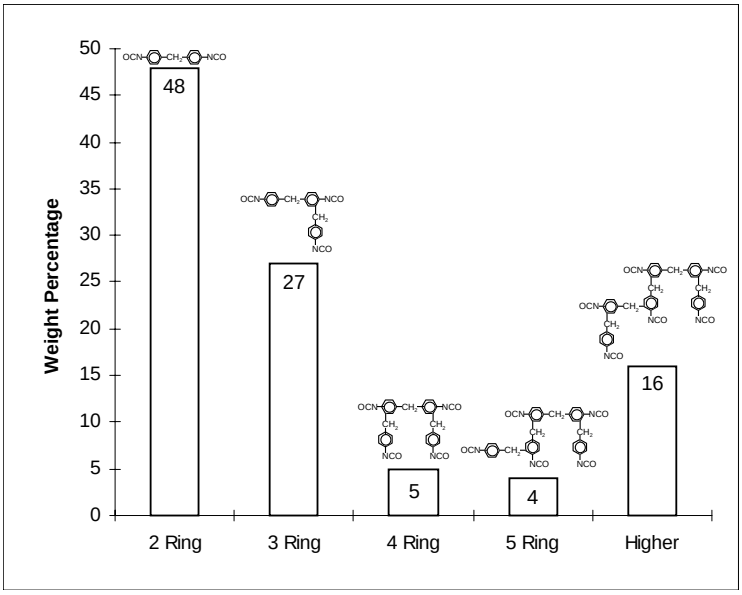

Figure 2.9 - Typical Ring Count Distribution in Crude MDI[1]

2.1.4.2 Polyols

A polyol is generally an alcohol functionalized low molecular weight polymer (ca. 3,000 to 5,000 Daltons), but it can also contain additional isocyanate-reactive groups. This very broad definition is required, because many types of polyol structures are employed to achieved desired combinations of properties and processing requirements. Moreover, composition of the polyols used may vary from supplier to supplier because what performs well in one case may not hold

true everywhere. Therefore, although about ninety percent of polyols utilized today are polyether polyols, it should be kept in mind that their specific composition is frequently tailored to meet very specific requirements.[1]

As mentioned earlier, the properties of the final foam are highly dependent on the composition of the polyol. The reason that ninety percent of polyols are polyether based is because they are cheap, easy to handle, and are more resistant to hydrolysis than polyesters. Polymers based on polyester polyols are stronger than those of polyether polyols; therefore, polyesters are still used for some applications.[1,2,3] An example are the polyols based on poly(diethylene adipates) with either low levels of branching or the linear form shown in Figure 2.10.

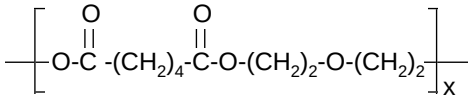

Figure 2.10 - Poly(oxydiethylene adipate)[3]

The most widely utilized polyether polyols are copolymers of propylene oxide and ethylene oxide as shown in Figure 2.11. These are used as copolymers to gain the benefits of each repeat unit. Ethylene oxide polymers are water soluble and their primary hydroxyl groups are highly reactive to isocyanates; however, they have poor hydrolytic stability. Propylene oxide polymers have better resistance to hydrolysis, due to their hydrophobicity. Since many of the other components in a foam formulation are water soluble good mixing can be a problem with pure propylene oxide based polymers, which makes reaction between components more difficult. Thus, by copolymerizing the two monomers, polyether polyols are obtained with reasonable reactivity and mixing characteristics as well as acceptable resistance to hydrolysis.[1,2]

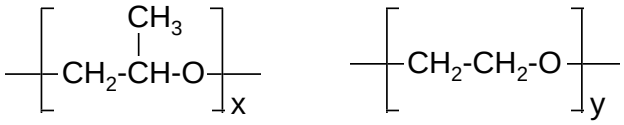

Figure 2.11 - Repeat Units if Copolymers of Ethylene Oxide and Propylene Oxide[2]

One limitation to propylene oxide polymers is that a polyol cannot be made with it which contains only secondary hydroxyl groups. This is due to head-to-head and tail-to-tail defects resulting from asymmetry of the monomer. Such a defect occurring at the end of a chain caps

that polymer with a primary hydroxyl as shown in Figure 2.12. These defects occur in this polymer about once every ten repeat units, resulting in a polymer that falls significantly short of containing only secondary hydroxyls.[1,2] The difference in reactivity between primary and secondary hydroxyl groups means that this shortfall may alter other factors affecting final foam properties such as rate of viscosity build and cell openness.

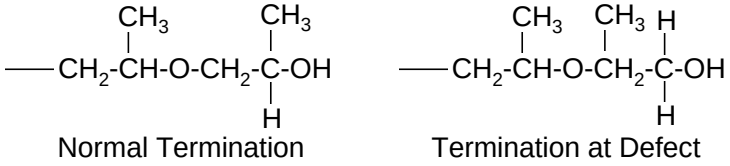

Figure 2.12 - Showing a Normal Termination Resulting in a 2° Hydroxyl and a Defect Termination Resulting in a 1° Hydroxyl Functionality.[2]

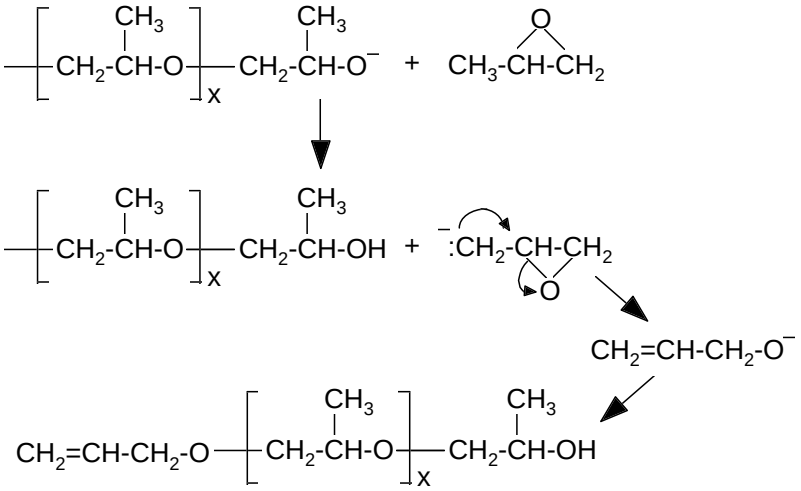

Figure 2.13 - Side reaction of base catalyzed polypropylene oxide resulting in monofunctional chain.[2]

Another more significant limitation of propylene oxide polymers is an undesirable side reaction that results in unsaturated and non-isocyanate reactive endgroups. This occurs in the conventional base catalyzed polymerization, when one chain terminates by stripping a proton from the methyl group of a monomer unit. That monomer unit then polymerizes, but only one end of the chain becomes hydroxyl functionalized. This side reaction is shown above in Figure 2.13. The resulting monofunctional chain would then become a defect (i.e. a dangling chain) in the cross-linked network of a polyurethane foam. The reaction rate of this side reaction increases rapidly with temperature or, at constant temperature, with molecular weight. Since the amount of unsaturated chains must be as low as possible, this process puts constraints on the molecular weight range of useful pure propylene oxide polymers. It is noted that this chain transfer process does not occur with the ethylene oxide monomer, and so random

copolymerization of the two significantly reduces the number of chains with this unsaturation.[1,2] New catalyst technology has been recently commercialized which limits the chain transfer process so that producing high molecular weight PPO based polyol with very low degrees of unsaturation is now possible.[4] These new polyols have been demonstrated to provide advantages in specialized elastomer applications;[4] however, only limited amounts of the ongoing proprietary research on their usefulness to foam applications has been released into the general literature. The mechanical tests in recent publications suggest that lower monol content polyols yield foams with lower compression sets and hysteresis loss and with higher tear and tensile strengths.[5,6] The lower monol contents foams were also suggested to provide advantages by increasing the damping of undesirable vibrations and providing lower resiliency (i.e. ball rebound) measurements.[5,6]

The polyol variables mainly utilized in tuning the properties of the final polymer are polyol functionality, oxypropylene/oxyethylene ratio, placement of oxyethylene in the backbone, and endcapping of the chains. Functionality is generally controlled through the choice of the initiator. Water and ethylene glycol both lead to diol chains, and glycerine leads to triol chains. However, the average functionality is always lower than the theoretical one due to the side reaction shown in Figure 2.13. Sucrose (functionality of eight) is another common initiator typically used in combination with others to better control average functionality. Other initiators are used, but these are the most common.[1]

The other three variables mentioned above are controlled by the method used to copolymerize the oxypropylene and oxyethylene. Today, there are three main techniques utilized. The simplest involves endcapping a purely oxypropylene polyol with an oxyethylene group, resulting in a primary hydroxyl functionality. As primary hydroxyls are roughly three times more reactive than secondary hydroxyls, these endcaps provide the increased reaction rate desired in many molded applications. However, this technique is not widely used in industry.[1,2]

Largely due to the unsaturation generating side reaction of propylene oxide, oxypropylene to oxyethylene blends in the range of 80/20 are more popular alternatives. These are produced with either of the other two copolymerization techniques. One approach is to blend the initiator with the desired proportions of ethylene oxide and propylene oxide. Although differences exist in their respective reactivities, this results in a copolymer that is essentially random.[1] The other method utilized is to sequentially add propylene oxide and ethylene oxide to

the reactor, which results in a block copolymer where the block sizes are approximately controlled by the amount added in each step with respect to the initiator concentration.[1,2]

To increase the load-bearing of open-celled foams, polyols can be modified with fillers. This is most frequently accomplished by forming the filler particles in the base polyol through free radical or step addition polymerization techniques. The growing filler particles must be prevented from aggregating, and this is the usually accomplished by grafting with either the base polyol or a stabilizer molecule. Commercially, the high viscosity of the modified polyol and the efficiency of the stabilization mechanism used limits how much filler can be used in a foam formulation.[1,2]

The most common modified systems used today are based on chain growth polymerization initiated by a free radical generated, usually, from an azo compound such as 2,2'-azo-bis-isobutyrnitrile. Also, to help control the molecular weight of the polymer formed, chain transfer agents are frequently used to terminate one chain and initiate another. Originally, these "polymer polyols" were based solely on acrylonitrile. However, due to low flame resistance, a yellowing of the foam, high viscosities, and an undesirably odor, copolymerizing the acrylonitrile with styrene in a 40:60 ratio has become popular. This product is thus termed a "co-polymer polyol" or CPP.[1,2]

Recently, the use of organic peroxide catalysts, such as tertiary alkyl peroxy esters, have been claimed to provide advantages in allowing higher monomer concentrations to be used without agglomeration of the filler. This higher degree of stabilization is suggested to be achieved via promoting the grafting process of the vinyl polymer onto the base polyether chain. Unfortunately, the styrene monomer has a negative effect on the grafting reaction, so another stabilization method is frequently utilized. This involves using a macromolecule functionalized with a vinyl moiety which then co-polymerizes with the SAN. This results in a comb topology wherein the SAN forms the backbone and the stabilizer molecules form the teeth. Thus, as the SAN phase separates, the stabilizer naturally extends out into the base polyol and the SAN forms at the center of the spheroid. This process results in final particles between 0.3-0.5 μm.. The CPP products made in this fashion are used with solids levels between 10-40% and viscosities between 2500-4000 centipoise. [1,2]

While these CPP are the most commonly used, other systems are sometimes utilized. One of the more popular are Poly Harnstoff Dispersion (PHD) polyols. These were developed as

alternatives to the polymer polyol systems, and they are synthesized in high molecular weight polyether triols. The PHD is a dispersion of polyurea based on the reaction of a polyamine with a aromatic diisocyanate (usually TDI). A secondary reaction between the isocyanate and the base polyol form a urethane linkage that helps to stabilize the growing polyurea particle. Hydroxyl functionalized alkanolamines or linear polyethers with amine end groups are also sometimes added to further stabilize the dispersion. These polyurea particles usually reach a size of about 1 μm and are used in concentrations of 5 to 20 % by weight of polyol. Other reinforcement types being used today also include polyurethane particles and epoxy based fillers.[1,2]

2.1.4.3 Water

Water is added to these formulations to react with the isocyanate as discussed in Section 2.1.1. This reaction ultimately produces polyurea, carbon dioxide and heat. This carbon dioxide diffuses to existing gas bubbles in the polyol and so expands the mixture into a foam. Control of the amount of air contained in the polyol raw material is one way that manufacturers control the number of nucleation sites in the reacting mixture. These initially small bubbles quickly grow through either gaining gas from the diffusing carbon dioxide or by coalescing with other bubbles.

2.1.4.4 Catalysts

Because flexible polyurethane foams are the product of two competing reactions, a proper balance is required between the two reaction rates to obtain a good open-celled morphology of the desired apparent density. If the gelation reaction proceeds too slowly, there will not be sufficient viscosity in the polymer when the cells open to maintain the cellular structure resulting in collapse. Another consequence of slow gelation can be an inadequate entrapment of the evolving carbon dioxide resulting in a boiling effect rather than bubble expansion. On the other hand, if the gelation reaction proceeds too quickly, the viscosity will rise too fast and slow down rate of bubble expansion, which may prevent the cells from opening at all.

The most commonly used type of catalyst are the tertiary amines. These catalysts are generally thought of as blowing catalysts but they do provide some enhancement of the gelation reaction. The extra electron pair on the nitrogen atom provides a strong nucleophile which is capable of attacking the carbon of the isocyanate group. Steric hindrance and electronic effects

of the substituent groups are the two main tools used to adjust the relative catalytic activity in the various tertiary amines. In some foam systems, combinations of amines are used to balance the gelation and blow reactions. [1,2]

The gelation reaction is also promoted through the use of organometallic catalysts, of which the tin based catalysts are the most popular. These compounds behave as Lewis acids and are generally thought to associate with the basic sites of the isocyanate and polyol groups. One common hypothesis is that this interaction enhances the Lewis acidic nature of the carbon in the isocyanate group, making it more reactive towards the oxygen of the polyol hydroxyl functionality. Another hypothesis suggests that the organometallic compound actually complexes with the strongest Lewis bases in the system—the tertiary amines. This new complex is postulated to associate with a polyol molecule forming a tin alkoxide and promoting its reaction with isocyanate groups. This reaction generates a urethane linkage and regenerates the catalytic complex.[1,2]

More thorough discussions of these catalytic mechanisms are available in references 1 and 2. It is important to point out that the use of these catalysts varies widely according to desired performance in a specific manufacturing processes. For example, molded foam production tends to use higher levels of both kinds of catalysts to achieve the highest rates of polymerization and cure possible. Other factors that must be taken into consideration are the reactivity of the polyols being used and the solubility of the catalysts in water. Moreover, even after careful literature reviews and pilot scale testing, the exact amount of catalyst used must often be tuned to each system once applied to production scale.

One newer type of catalyst being examined for use in foams is the delayed action catalyst. This type is being developed in response to the growing demand for better in-mold flowability and faster cure times. The concept is to use chemicals with low activity at room temperature but which become activated as the foaming reactions heat up the system. Tertiary amine salts in a solvent such as low molecular weight glycol or water are the most frequently utilized catalysts of this type. Often these catalysts are added in combination with organic acids such as carbonic, formic, and acetic acids. A disadvantage to these catalysts is that they produce phase incompatibility and metal corrosion problems when used in combination with standard tertiary amine catalysts.[1]

2.1.4.5 Surfactants

Non-ionic surfactants are ubiquitous in the foam industry because production of a good open celled morphology is nearly impossible without them. Some of the functions they perform are reducing surface tension, emulsifying incompatible ingredients, promoting bubble nucleation, stabilizing the rising foam, and reducing the defoaming effect. Of these, the most crucial to foam production is stabilization of the cell walls. Without any surfactant, the foam will collapse completely and behave like a boiling thick liquid. Therefore, in every foam formulation, there is a minimal surfactant concentration necessary for producing an acceptable foam. Below this level, a range of structural defects may occur such as collapse, densification, or splitting. Above that level, there is a processing window within which the surfactant concentration can be utilized to tune the precise moment of cell opening. However, over-stabilization of the cell windows may prevent rupture from occurring, resulting in reduced airflow. Cell openness is very important to the mechanical properties of the foam. At high levels of closed windows, this lack of airflow can induce the foam to shrink as it cools. These ideas are summarized in Figure 2.14 where airflow through a 1" thick foam sample is plotted versus surfactant concentration.[1,2]

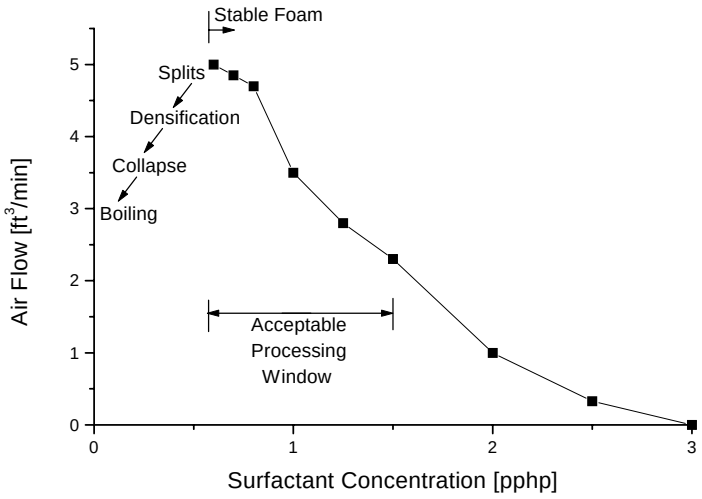

Figure 2.14 Effect of Concentration for a Typical Silicone Surfactant on Airflow[1]

The most common surfactants in use today are polysiloxane-polyoxyalkylene block copolymers. The silicone block aids in lowering bulk surface tension. The polyoxyalkylene (or

polyether polyol) block promotes solubilization of the surfactant into the bulk polyol, aiding in elmusifying the formulation components.[1,2]

To meet the precise needs of a specific foam system, many molecular parameters may be in adjusted within the surfactant. The length and composition can be altered for either the siloxane or the polyether polyol blocks. Also, the molecular topology can be altered. AB, ABA, comb-like, or branched structures can be utilized as needed, as the number of polyether polyol blocks are tuned. Finding the proper balance between the two blocks is an important part of finding the correct surfactant for a specific formulation.[1,2]

One good example of this tuning occurs in the molded foam systems. Here, higher molecular weight, more reactive polyols are utilized in combination with an increased amount of catalyst (as compared to slabstock systems). This leads to a much faster viscosity build in the developing foam, and, if typical slabstock surfactants were utilized, the foams would have too many closed cells. Therefore, the surfactants for molded applications have deliberately reduced emulsification efficiency so that the cells may open. The challenge in providing enough stabilization but not too much is shown in that, even with such molecular tuning, manufactures in the molded area still find it necessary to mechanically crush the foams with rollers to force open more cells.[1,2,7]

2.1.4.6 Cross-linking Agents

In polyurethane systems, cross-linking agents are typically short-chain molecules containing amine or hydroxyl functional groups and having a functionality greater than three. They can be added to these systems to provide increased load bearing or initial foam stability. By far, the most common cross-linking agent is diethanolamine (DEOA), and its structure is shown in Figure 2.15. This cross-linking agent will be discussed in some detail in Chapter 3.

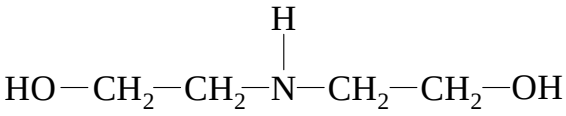

Figure 2.15 Structure of Diethanolamine

These cross-linkers are most frequently applied in molded foam formulations. As discussed in the last section, high molecular weight polyols and faster reaction rates in those systems build viscosity so fast that use of typical foam surfactants over stabilizes the cell walls, preventing many cells from opening. To allow cell opening to occur, lower potency surfactants

must be utilized. However, these surfactants are not potent enough to fully stabilize the foam, and so cross-linking agents are added to provide an added degree of dimensional stability.

2.1.4.7 Auxiliary Blowing Agents

While the water-isocyanate reaction provides the primary blowing mechanism for flexible polyurethane foams, some products require the use of auxiliary blowing agents to achieve desired levels of apparent density or softness. These blowing agents are low boiling solvents which are inert in the chemical reactions already described. As the highly exothermic foaming reactions proceed, the temperature in the mixtures reach or exceed 130°C within two minutes. This large temperature rise is enough to vaporize the low boiling solvents, providing additional gas to expand the foam. The vaporization of these additional fluids does absorb a lot of the heat needed to expand the gas into the cellular structure; therefore, these formulations generally employ higher catalyst levels to promote increased levels of heat generation.[1,2]

In terms of processing, the auxiliary blowing agent of choice is still chlorofluorocarbon 11 (CFC 11); however, environmental concerns regarding ozone depletion have made its use untenable. One alternative to CFC 11 is to use halogenated chlorinated fluorocarbons (HCFC-123 and HCFC-141) which are reported to have lower ozone depleting potentials. However, large-scale production of these agents is difficult and these, too, are being phased out due to environmental concerns. Therefore, finding alternatives is a high priority for foam manufacturers. Technology currently exists for using methylene chloride and acetone, but each of these includes their own hazards. The methylene chloride processes currently available also require adding delayed action catalysts to the formulations to obtain the desired products. The use of liquid carbon dioxide is growing in popularity now that many of the process-related problems in using that agent are being solved. These agents are only a few of those being researched, and many others are also currently being evaluated.[1,2,8]

2.1.4.8 Additives

In order to achieve specific properties, it is sometimes necessary to include an additive. Some additives are used to make the product more appealing to consumers. For example colorants (e.g. metal oxides, carbon black, or azo/diazo dyes) may be added to conceal product yellowing or achieve a design specification. Other additives are included to improve product performance such as flame retardants, antistatic agents, bacteriostats, or UV stabilizers to prevent

yellowing of the foam. Finally, some additives may be necessary in special applications. For example, plasticizers to reduce in-mold viscosity, cell-openers to enhance the cell wall rupture mechanisms, and compatibilzers to enhance emulsification beyond what the standard surfactant systems can achieve. None of these additives form a major part of this research and therefore will not be discussed in detail. More thorough reviews are available in references 1 and 2.

2.2 The Foaming Process

Part of the complexity of these systems is that the development of cellular structure and of polymer solid state morphology occur simultaneously and may to some extent be co-dependent. This complicates the processing because, unlike polyurethane elastomers, it is not enough to have a good polymer solid—it must be arranged in an open celled structure of the proper density. Likewise, it is not enough to have generated an open celled foam if the polymer does not have the correct mechanical or chemical properties. Furthermore, the rising of the foam can lead to anisotropy of the cellular structure in slabstock systems, leading to differences in load bearing properties perpendicular and parallel to the rise direction. Since macroscopic mechanical properties convolute contributions from every length scale, it is necessary to understand how they relate to one another.[1,2,9]

The process of taking a liquid and producing a dry, mechanically sound foam passes through four basic recognizable steps. These steps are bubble initiation, bubble growth, bubble packing, and cell opening. At every step, something can go wrong leading to unacceptable product. This may occur as complete collapse of the growing foam, the foam splitting apart, or even the wrong size cells developing in the product. The ease with which good foam may be ruined may be concluded by considering that each step in the foam process yields a large increase of surface area and therefore a large jump in the free energy of the system. Therefore it is necessary to carefully control many parameters throughout the process to grow a quality foam.

2.2.1 Bubble Initiation

The cell density in a foam not only has direct effects on its physical properties, but it has also been shown that larger numbers of cells per volume result in a more viscous and stable foam. To handle this important parameter, it is therefore it is important to understand and control the nucleation mechanism in the foam. Prior to being laid onto a slabstock conveyor or

shot into a mold, the reactive mixture is basically a continuous liquid phase. Gas bubbles in the foam may grow as gas diffuses to them, and that gas may originate from five main sources:

1) gas evolved by the foam reactions,
2) gas entrained in the liquid during blending,
3) gas dissolved in the liquid reactants,
4) auxiliary blowing agents vaporizing,
5) and gas evolved by thermal decomposition of additives or components.[1]

Kanner and Decker[10] have shown that carbon dioxide evolving from the reactions (source one) does not occur in these systems. Self-nucleation was shown to be absent over a broad range of conditions, including many that are more favorable to nucleation than those which actually exist on foam production lines. They showed that bubbles are only introduced by physically blending air into the mixture, and that this entrainment produces more than enough bubbles to account for all the cells present in a polyurethane foam. Their work also showed that new, smaller bubbles do not appear at any time during the foaming process as would be expected if self-nucleation of carbon dioxide occurs. Other workers have presented a thermodynamic treatment which has shown that bubble nucleation in polyurethane foams requires more energy (455 Joules per gram of carbon dioxide bubbles based on an estimated 1×10^{-5} cm diameter) than is available by any mechanism other than mechanical entrainment when considering the number of bubbles produced in the typical foam.[1]

This knowledge has led many manufacturers to intentionally bleed air into their mixing heads. A typical air injection rate for slabstock manufacturing is 0.5 scf/hr per 100 pounds per minute of mixture throughput. However, there is one other important parameter to consider. Research has shown that if there is insufficient dissolved gas in the components prior to mixing (source three), poor or inconsistent foams will result. This may occur if a formulation component is used *too soon* after it is made. For example, the equilibrium amount of air that most polyether polyols will absorb is 6-10 volume percent; however, it can take 10 days of tank storage before these levels are reached. To emphasize the large impact that dissolved gas in a polyol can have, the results of a study on cell count in a final foam are shown in Figure 2.16.[1,2]

Because of the importance of cell count on final foam properties, manufacturers attempt to control the amount of entrained and dissolved gas entering the system. Too much dissolved or entrained gas can easily lead to problems in the cellular structure. Therefore, the nucleation

density is controlled by using raw materials that are of a consistent dissolved gas level (i.e. time in tank storage) and then intentionally add air via entrainment to obtain the desired cell counts.

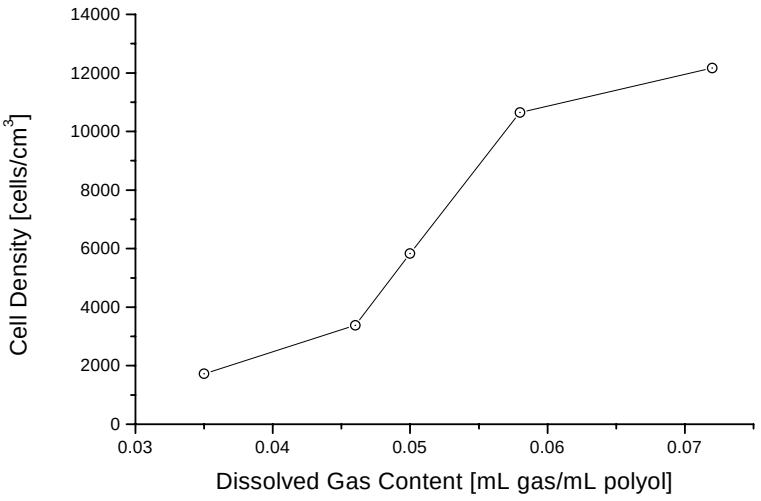

Figure 2.16 Impact of Polyol Dissolved Gas on Cell Count in a Final Foam[1]

2.2.2 Bubble Growth

As discussed in the previous section, dissolved gas in the liquid phase may result from several sources. Once the liquid is saturated with gas, additional gas evolved in the system will phase separate. As discussed, nucleation of molecules into a new phase has not been observed to occur, which indicates that the primary outlet for gas molecules from the liquid is into already existing bubbles. Thus, bubble growth is promoted from diffusion of gas into the bubbles and expansion of the gas phases due to the increasing temperature of the foam.[1,2]

The other important mechanism of bubble growth is a consequence of the free surface energy in curved gas-liquid interfaces. This is related by the well known LaPlace relation shown in Equation 2.1 where ΔP is the excess of pressure in the bubble relative to the liquid that surrounds it, γ is the surface tension of the liquid, and R_c is the critical radius of the bubble. A result of Equation 2.1 is that smaller bubbles are at higher pressure than larger bubbles. All real foams begin with a distribution of bubble sizes, but diffusion from the smaller bubbles into the larger ones sets in quickly. It has been observed that as reaction time increases, the average bubble size for a polydisperse system increases, but the total number of bubbles decreases. [1,2]

$$\Delta P = \frac{2\gamma}{R_c} \qquad \textbf{[Equation 2.1]}$$

Clearly, coalescence of bubbles is not the only mechanism of bubble growth or every attempt to produce a foam would result in a single large cell. This is especially unlikely in view of the increasing viscosity of the polyol phase as the gelation reaction proceeds. On the other hand, this information does provide some useful knowledge. If the surface tension of the liquid can be reduced, then the pressure driving force to coalesce will be reduced—leading to a more stable foam composed of smaller average cell sizes. Overall, it is considered that evolution of carbon dioxide, heating from the exothermic reactions, and coalescence all work together to contribute to the rate of bubble growth.[1,2]

2.2.3 Bubble Packing

As the bubble growth proceeds, the gas phase will eventually exceed 74 volume percent of the foam. This is the point when the bubbles being to spatially interfere with one another, becoming distorted from perfect spheres. Researchers have attempted to approximate the final polyhedral shapes of the cells, but due to the polydispersity of cell sizes these attempts are most useful only as idealized models. Even Lord Kelvin's fourteen-faced tetrakaidecahedron, which does fill the space without gaps, is inadequate for modeling foam behavior. Those attempting to model the mechanical behavior of these foams via computer simulation have moved to different methods of digitizing the cellular structure of actual foams.[1,2]

More useful to this research is to consider the development of the polyhedron. As the bubbles begin to impede each other's growth, the liquid phase is forced to distribute itself around and between the developing polyhedra. As shown in Figure 2.17, the liquid resides in lamellae and plateau borders in between the bubbles. It is vital to notice that the plateau borders are not flat but rather that they have curved gas/liquid interfaces. This results, according to Equation 2.1, in a pressure drop across the interface. This means that liquid in the lamellae, which are relatively large and flat, are at higher pressure than liquid in the plateau borders. The net impact of this is that a suction force exists which pulls or drains liquid out of the lamellae. Therefore it is considered that a combination of this suction, drainage due to gravity, and continued bubble growth all lead to a continuous thinning of the lamellae between the bubbles.[1,2,9]

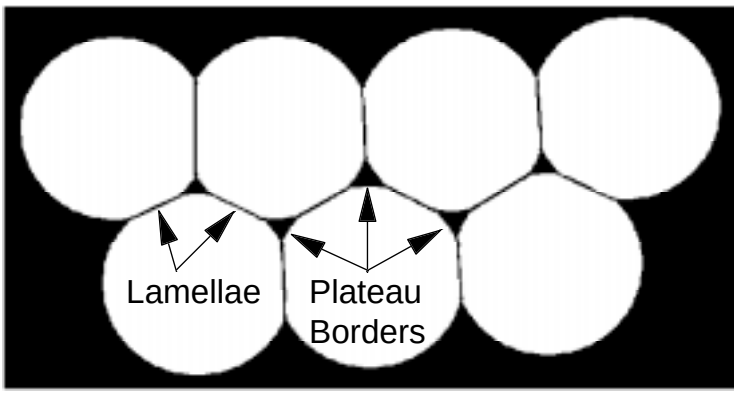

Figure 2.17 Liquid Arrangement About Developing Polyhedra[1]

It is unfortunate that this stage of the foam process is the least understood and, therefore, the least controllable. Being able to vary cellular structure independently of the polymer chemistry might provide some advantages. However, experimental difficulties have so far prevented much revelation concerning the intimate details of this stage. What is important is understanding the forces that are in action on the polymer liquid as the reactions are proceeding. The fluid is by no means static but must be involved in some flow as it drains into the plateau borders.

2.2.4 Cell Opening

It should also be clear from the picture so far presented, that stabilization of these ever thinning lamellae is highly important to maintaining the foam structure. Once the bubbles rupture, all the stress of maintaining the cellular morphology rests on what were the plateau borders. At that point, the gelation reaction must have proceeded far enough to give some integrity and strength to the polymer. Otherwise, the foam collapses.

Many theories exist regarding the stabilization mechanism and what finally results in the opening of the cells. However, common to every theory is the idea that a lamellae (or cell window) will eventually rupture at some localized thinning in the window. A localized thinning implies that some small region has an expanded surface area, which reduces the local concentration of surfactant. This could result in a higher than equilibrium surface tension. If that energy state is higher than the energy necessary to generate a new surface through rupture of the lamellae, then the window might open. On the other hand, effects like surface elasticity or film elasticity may actually work to pull the film back to a uniform thickness. [1,2]

The one cause of cell opening with experimental evidence to back it up is that of the precipitation of urea into hard domains. This precipitation will be discussed further in the morphology section, but it is necessary to mention it here. Rossmy and coworkers found that high polymer molecular weight was not present at the time of cell opening and that the amount of urethane linkages present was only negligible. However, just prior to cell opening, they observed via FTIR that hydrogen bonded urea absorptions became very strong. This indicates that the phase separation of the polyurea into hard domains somehow triggers the event of cell opening. That relationship is not well understood. It may be that the existence of these particulate reduces the film elasticity effects which had prevented the lamellae from rupturing. In slabstock systems, the polyurea phase separates into two sized domains: the well known microdomains observed by SAXS, and larger macrodomains or aggregates which can be observed via TEM. These macrodomains are often termed "polyurea balls." This phase separation behavior, illustrated in Figure 2.18, is very different from that typically observed in polyurethane elastomers. Based on this solid state morphology, another hypothesis suggest that, in slabstock foams, some precipitates reach a size where they may themselves rupture the windows or destabilize their surfaces.[1,11]

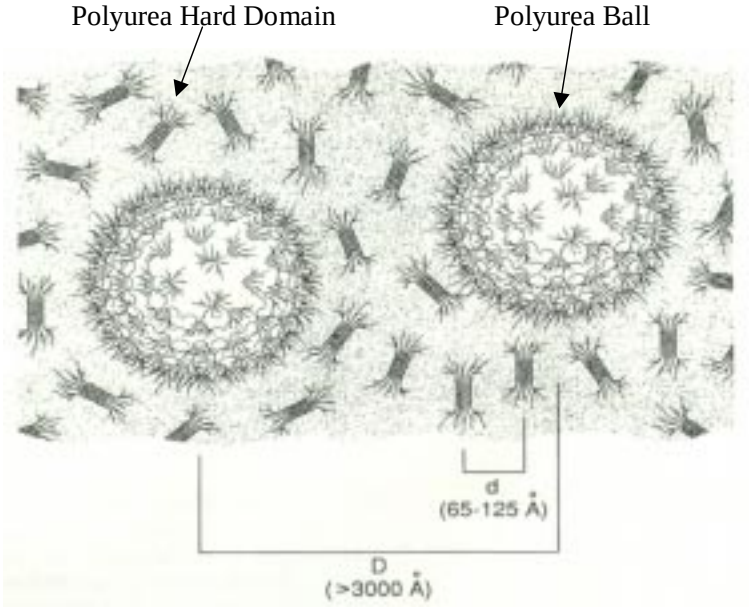

Figure 2.18 Schematic of Phase Separation Behavior in Some Polyurethane Foams[1]

One point that was observed by Rossmy and coworkers,[12] and has recently been observed again by other researchers,[13] is that silicone surfactants can delay the time to cell opening. The type and concentration of surfactant can alter the rate of foam expansion and it can also influence

the time of cell opening. This indirectly implies that the surfactant may, through some mechanism, influence the time of urea precipitation. This suggests that it may also affect the structure of the resulting precipitates.[14] That effect has not been thoroughly examined, and it is one question which this proposed research seeks to address.

In molded systems, the mechanism of cell opening is complicated by higher reactivity ingredients and higher molecular weight polyols. The combination of these yields foams that tend to have more closed cells. Because polyols for molded systems have a higher degree of ethylene oxide endcapping, the polyurea is more soluble in the polyol phase. A consequence of this is that only microdomains form in molded foams (i.e. no polyurea balls). Based on this, one theory which explains this cell non-opening is that a lack of macrodomains removes one mechanism of window rupturing.[1]

Acting on that theory, foam producers try to induce the foam to open by adding another mechanism. This generally means using an additive. Some common additives used for this purpose are fillers (i.e. CPPs or PHD polyols), TDI/polymeric MDI blends, special polyols, and fumed silica. However, none of these additives has achieved universal success in all molded formulations. Therefore, another common approach is to mechanically induce cell opening. This is typically achieved by crushing the foam pad through narrow-gapped rollers or by some pressure release treatments.[1]

At this point it should be obvious that many factors interdependently yield the ideal open celled foam. One key concept is that the foam should open at an ideal time, coincident for many of these factors, and this is summarized in the time line provided in Figure 2.19. When things go awry from this timeline, the product quality suffers. For example, too fast a viscosity build can prevent cell opening from occurring and from the foam to fully rise. It is preferred that the cells open just after the viscosity vs. time curve has reached the dramatically increasing portion of its exponential curve. Likewise there are ideal operating windows for catalyst concentration, polyol functionality, and polyol reactivity all of which should be optimized for a given formulation to produce the desired cellular structure.[1]

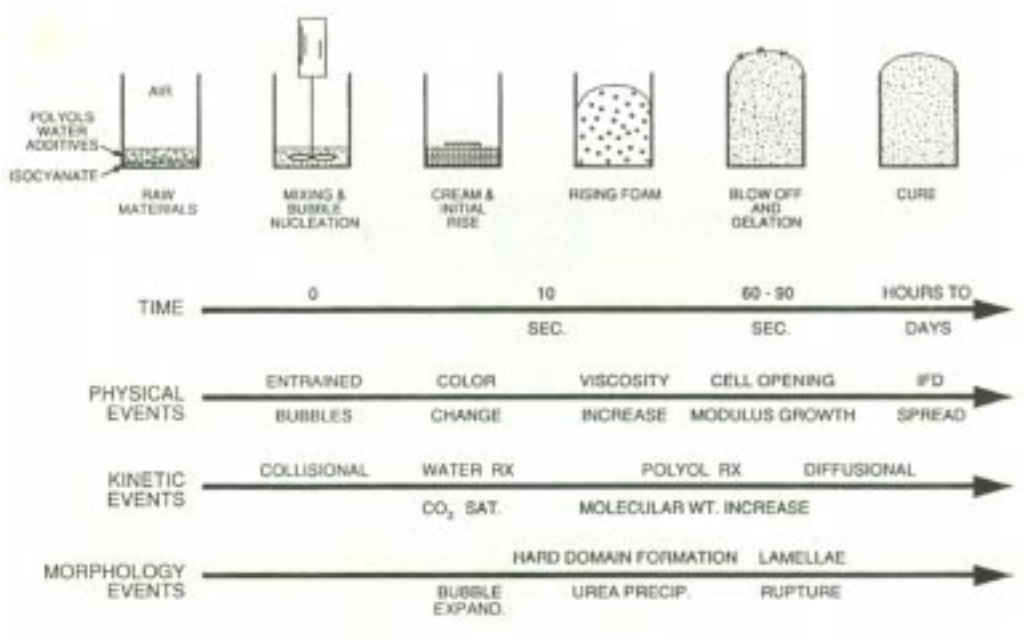

Figure 2.19 Typical Sequence of Events in Foam Production[1]

2.3 Morphology

The cellular structure of foams does have significant effects on mechanical properties, and further clarifying these is the subject of ongoing research. However, the morphology of the polymer making up that foam is also of great importance. As a result much research has explored how alterations of certain parameters can lead to clear mechanical effects.[15, 16, 17]

As the foam reactions proceed, they do not have equal kinetics. A large body of work shows that the water-isocyanate reaction initiates and proceeds the fastest.[1,11,18,19] This is particularly true in slabstock systems, where the polyols mainly have secondary hydroxyl groups. The faster water-isocyanate reaction leads to the development of polyurea molecules that are often termed “hard segments” and continue to grow in length and eventually become insoluble in the polyol phase. Hard segment molecular weights have been shown in molded and slabstock foams to have a distribution between 2 and 14 repeat units for 3 water pphp formulations with a peak at ca. 4-6 repeat units.[22] This growth leads to the precipitation of the polyurea into “hard domains” as mentioned earlier. These hard domains are not, generally, covalently bound together but derive their cohesive strength from physical associations. However, since most hard segments will eventually be bound into the polyol phase via the gelation reaction, it is considered that the properties of these polymers depend on a network of covalent and a physical cross-links.

In typical slabstock systems, these physical associations are the very strong bidentate hydrogen bonds which occur between carbonyl groups and the hydrogen atoms of urea linkages in adjacent hard segments. It is generally understood that disruption of the physical associations, for example by temperature or humidity, can lead to a softening of the foam by plasticizing the hard domains. This was most clearly demonstrated by Dounis and coworkers,[20] where humidity was cycled between 10 and 98% R.H. at during a creep experiment on a foam. This experiment showed increased creep rates during all dehumidification cycles, providing a much higher level of creep overall as compared to experiments performed at constant humidity. This strongly suggests that removal of water from the foam leaves behind some plasticized hard domains which exhibit higher than normal rates of deformation.

In other systems, additives may disrupt this packing, but they do not disrupt they formation of microphase hard domains. This was demonstrated in work by Moreland et al[21] in which a softening agent, LiCl, was added to the formulations of some slabstock foams. This material was shown via WAXS to disrupt the ordering of the hard domains. It was also shown via SAXS to alter the spatial arrangement those hard domains and the breadth of the distribution of interdomain spacings. These changes in structure thus provided an explanation for the faster rates of compressive load decay and creep that were observed in the LiCl containing foams.

However, the morphology of these systems should not be oversimplified. As discussed previously, there exists in some of these foams another structure which is less well understood. At high enough water concentration for a specific polyol system (with stoichiometric isocyanate feeds), aggregations of polyurea may form which are much larger than the microdomains. Whereas the microdomains are approximately 30-60 Å in size with interdomain spacings of ca. 70-120 Å, these macrodomains are more spherical and ca. 3000 Å in diameter. This morphology is schematically represented in Figure 2.18, and its water concentration dependence can be seen in the TEM micrographs of Figure 2.20.

One mechanism suggested for the formation of the macrodomains is that they are agglomerations of hard domains. This implies that the phase separation occurs in two stages: the first where the hard segments aggregate into hard domains, and the second where hard domains are close enough together to flocculate into the larger structure. Such a mechanism would require the diffusion of a great many microdomains, and it seems unlikely in the presence of the rapidly increasing viscosity of the system.

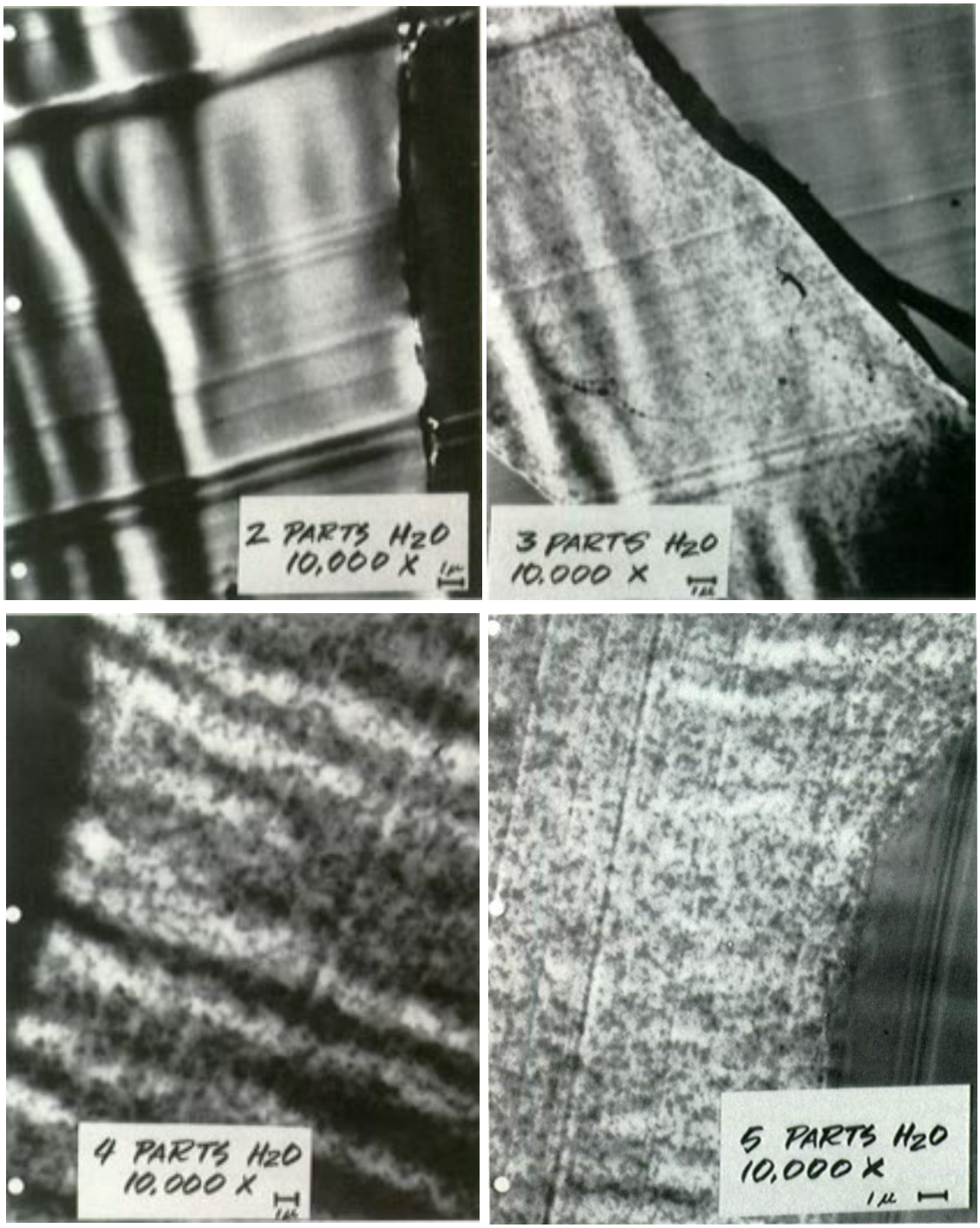

Figure 2.20 TEM Micrographs for Four Slabstock Foams of Increasing Water Content[1]

Another mechanism proposes that the higher water concentrations may exceed the water solubility in the liquid mixture, and some water droplets may form in the polyol. These areas with locally higher concentrations of water than others would naturally give rise to higher oligomer concentration, and that would result in allow the hard segments to aggregate into the

larger structures in one step. This hypothesis implies that better emulsification of the original blend would eliminate the formation of these large aggregates, and yet this has never been observed to be true.

These macrophases are not observed in typical molded foams.[1,17,22,23] Interestingly, both hypotheses adequately explain why. One suggestion is that the more reactive polyols and the presence of a cross-linker produces more competition for the water-isocyanate reaction. This results in a higher viscosity build which would prevent the second stage formation of polyurea balls of the first hypothesis. On the other hand, it is believed that the cross-linking agents of molded foams become incorporated within the hard segments which would alter their solubility characteristics. Also, the primary hydroxyl polyols promote solubility of the water. These two factors could work together to prevent the formation of the necessary water droplets, the suggested prerequisite of the second hypothesis.

Not only is it unclear how these macrophases form, it is also unclear what they actually are. Recently, workers in the field of x-ray microscopy have begun to explore this question.[24] This technique allows the determination of composition in structures down to about 55 nm. By examining thin sections of a foam, it has been determined that the polyurea balls contain ca. 10% polyol in their centers and increase in polyol content closer to the surface. This type of structure suggests the polyurea balls are aggregates and did not form from water droplets in the polyol. However, analysis of these large precipitates has only begun, and it is far to early to draw concrete conclusions.

It is also not established how these macrophases contribute to the overall mechanical properties of the foam. Work by Moreland et al[25] revealed that uniaxially extending a plaque made from a slabstock foam led to unanticipated behavior. It is commonly held that the hard domains are anisotropic in dimensions and that they are longer parallel to the hard segments and narrower perpendicular to the molecules. This is how they are drawn in Figure 2.18. However, Moreland and coworkers showed via linear dichroism that the hard segments in foam plaques actually initially orient transverse to the stretch direction. Similar behavior was observed in polyurea-urethane elastomers up to ca. 50% elongation, after which the hard segments began to orient parallel to the deformation axis. This type of behavior indicates that, in foams, hard segments are part of a structure that is anistropic but opposite to what had previously been thought. Since the dimensions of a typical hard segment are known (ca. 6 repeat units for a 3

water pphp foam[23]), this suggests that a larger structure is playing a role that what current models can explain.

2.4 Research Objectives

Considering the above discussion of common formulation components and the morphology which develops from them, it should be obvious that structure-property behavior in these materials is complex. Some structures, like the larger polyurea aggregates are little understood. Other formulation components have clear effects, but mechanisms of those changes are unclear. Therefore, in order to make the largest possible contribution to this field, a multiple technique approach will be used in the examination of several different variables. The objectives of this dissertation are:

1) to elucidate the influence of the commercially predominant cross-linking agent, diethanolamine (DEOA), on the structure-property relationships of molded flexible polyurethane foams,
2) to probe polyurea hard domain morphology and study its relationship to the larger polyurea aggregates,
3) to examine the importance of copolymer polyols to the viscoelastic properties of molded flexible polyurethane foams,
4) to determine the effects of surfactant on the phase separated morphology of slabstock flexible polyurethane foams and the resulting viscoelastic properties,
5) and to evaluate the significance of cure temperatures and post-cure annealing treatments in the formation of the microphase separated morphology of polyurethane foams and plaques.

The research objectives of the fluoropolymer study will be examined separately in Chapter 9.

2.5 References

1. Herrington R; Hock K; Flexible Polyurethane Foams, 2nd Ed.; The Dow Chem Co (1998)
2. Woods G; Flexible Polyurethane Foams, Chemistry and Technology; Appl Sci Pub Ltd; Essex, England: (1982)
3. Moreland JC; *Ph. D. Dissertation*; VPI & SU: (1991)
4. Seneker SD; Barksby N; Lawrey BD; *Proc of the SPI Polyurethanes Conf*: (1998) 195-206
5. Crocco GL; Kinkelaar MR; Neal BL; *Polyurethanes World Congress '97*: (1997) 428-434
6. Toyota Y; Hasegawa N; Wada H; Horie A; Hatano S; Sasake T; Oki S; *Polyurethanes World Congress '97*: (1997) 421-427
7. Kollmeier HJ, Burkhart G, Klietsch J; Lammerting H; *SPI Polyurethanes Conf*: (1988) 261
8. Vandichel J-CNE; Appleyard P; *J Cell Plast*: **27** (1991) 279-294
9. Hilyard NC; Cunningham A; Low Density Cellular Plastics, Physical Basis of Behavior; Chapman & Hall, London, UK: (1994) 1-19
10. Kanner B; Decker TG; *J Cell Plast*: **5** (1969) 32-39
11. Macosko CW; Artavia LD; Low Density Cellular Plastics, Physical Basis of Behavior, edited by Hilyard NC; Cunningham A; Chapman & Hall, London, UK: (1994) 33-51
12. Rossmy GR; Kollmeier HJ; Lidy W; Schator H; Wiemann M; *J Cell Plast:* **13** (1977) 26
13. Yasunaga K; Neff RA; Zhang XD; Macosko CW; *J Cell Plast*: **32** (1996) 428-448
14. Rossmy G; *Progr Colloid Poly Sci*: **111** (1998) 17-26
15. Moreland JC; Wilkes GL; Turner RB; *J Appl Poly Sci*: **52** (1994) 549-568
16. Moreland JC; Wilkes GL; Turner RB; *J Appl Poly Sci*: **52** (1994) 569-576
17. Dounis DV; Wilkes GL; *Proc of Polyurethane 1995*: (1995) 353-361
18. Rossmy GR; Kollmeier HJ; Lidy W; Schator H; Wiemann M; *J Cel. Plast*: **17** (1981) 319
19. Elwell MJ; Ryan AJ; Grunbauer HJM; Van Lieshout HC; *Macromolecules*: **29** (1996) 2960
20. Dounis DV; Moreland JC; Wilkes GL; Dillard DA; Turner RB; *J Appl Poly Sci*: **50** (1993) 293
21. Moreland JC; Wilkes GL; Turner RB; Rightor EG; *J Appl Poly Sci*: **52** (1994) 1459-1476
22. Lidy WA; Rightor E; Thanh HP; Cadolle D; *Polyurethanes Expo '96*: (1996) 119-135
23. Lidy WA; Rightor E; Heaney M; Davis B; Latham L; Barnes G; *Polyurethanes World Congress '97*: (1997) 95-117
24. Ade H; Smith AP; Cameron S; Cieslinski R; Mitchell G; Hsiao B; Rightor E; *Polymer*: **36** (1995) 1843-1848
25. Moreland JC; Wilkes GL; Turner RB; *J Appl Poly Sci*: **43** (1991) 801-815

3 Influence of Diethanolamine (DEOA) on Structure-Property Behavior of Molded Flexible Polyurethane Foams

3.1 Chapter Summary

In this study, the viscoelastic and morphological properties of molded foams were investigated to determine the influence of varying the concentration of diethanolamine (DEOA), a commercially utilized cross-linking agent. FTIR and WAXS analyses showed that DEOA had a disrupting affect on the bidentate hydrogen bonding within the hard domains of the polymer. DMS revealed that DEOA softens the foam above the T_g of the soft segment but only causes minor changes in degree of microphase separation. Annealing treatments were shown to remove the DEOA influence on microphase separation as well as some of the softening effect. FTIR was used to show that bidentate hydrogen bonding is enhanced through the annealing of DEOA foams.

3.2 Introduction

Polyurethane foam is widely utilized in many applications including thermal insulation, furniture, packaging, and novelty applications. Often these uses demand altering the large initial foam "bun" into complex shapes, and it has proven more economical in many cases to produce foams by casting the reactive mixture into molds of the desired form rather than by the traditional slabstock method. This eliminates the time and waste involved in trimming and shaping large buns of foam. Furthermore, molded foams can be made to meet a broad range of property specifications via including inserts for support, varying zones of hardness, or with liners or skins of fabric or plastic. Therefore, while slabstock operations dominates the volume of flexible foam produced, the technique of molded foam production is gaining popularity.

Changing from slabstock to molded foam processing involves switching modes of production from a continuous method to a semi-batchwise operation in which each mold is essentially a reactor. Molded operations usually involve many individual molds being rotated through the production cycle from being charged with reactants to product removal and preparation for another charging. Since the volume of the batch is fixed by the mold size, and

since the number of molds is essentially fixed by the size of the process, decreasing residence time in the molds (or demold times) is an effective way to increase production.[1]

Flexible polyurethane foams are based on two well known reactions. The "blow" reaction sequence typically involves the reaction of water with toluene diisocyanate to yield an amine, carbon dioxide and heat. The evolved gas and the reaction exotherm help to expand the fluid into a cellular structure, and the amine undergoes reaction with another isocyanate group to yield a urea linkage. Toluene diisocyante is typically used in an 80/20 blend of the 2,4 and 2,6 isomers, but other isomeric blends and other isocyanates are sometimes utilized. Generally, the blow reaction initiates first and proceeds at a faster rate yielding an essentially linear polyurea "hard" segment of four to six repeat units.

The second major reaction occurs between the isocyanate groups and the hydroxyl functionalities of the polyether polyol. Because the polyol usually has a functionality between two and three, this process leads to a three dimensional covalent network. At some point, the concentration of hard segments being generated by the blow reaction will surpass a system-dependent solubility limit leading to a microphase separation of the urea-based hard segments which produces precipitates of the polyurea. Each of these precipitates or "hard domains" is another pseudo or physical cross-linking point that is instead dependent upon strong intermolecular interactions (i.e. hydrogen bonding) for its cohesive strength.

To achieve lower demold times, the formulation of a molded foam varies significantly from that of a traditional slabstock. The polyols used for each are different in three ways. First, the polyol of a molded foam tends to be end-capped with polyethylene-oxide for increased reaction rates. Second, the polyol molecular weight is generally higher than what is used in slabstocks (ca. 5000 MW in molded compared to ca. 3000 MW in slabstock) thus yielding faster viscosity builds as the gelation reaction proceeds. Finally, filler particles are sometimes added to formulations to increase load bearing properties. The predominant filler currently used is termed "copolymer polyol" (CPP), and it is a particulate dispersion produced via the free-radical copolymerization of styrene and acrylonitrile in a polyether polyol. Since the reaction of either the styrene or the acrylonitrile free radicals with the polyol is not favored, the dispersion is stabilized by also copolymerizing the SAN with polyether polyol molecules functionalized with a vinyl moiety. This process produces a stable dispersion of SAN particulate that are typically

ca. 0.3-0.5 μm in size. The influence of CPP on the structure-property relationships in molded foams is addressed in another work by the authors.[2]

Because the filler particulate aids in cell opening, the CPP component does play a particularly important role in facilitating this work. In another study from this laboratory on molded foams without CPP, workers reported in reference 3 that the increased rate of cross-linking provided by DEOA prevents more cells from opening than occurs without DEOA.[3] This was observed as a significant decrease in airflow through a foam sample. The samples from that study showed that compressive load bearing increased as DEOA concentration increased in the formulation; however, because all levels of structure contribute to the macroscopic properties of foams, it was not possible to absolutely distinguish whether the observed increase in load bearing was due to the higher content of closed cells or due to the presence of the cross-linking agent, DEOA.[3] Filler particles such as those of the CPP are known to have destabilizing effects on the cell windows as they become thinner, thus offsetting the stabilizing effect of the DEOA. Therefore, to obtain a set of foams which have the same airflow characteristics but vary in their DEOA content, CPP was included in the formulations reported here.

Another major difference between molded and slabstock formulations is the presence of the cross-linking agent diethanolamine (DEOA). Typically, this component is fed at concentrations between 1.0-2.0 parts per hundred parts polyol (pphp). Because of its low molecular weight, this is a small weight fraction; however, in total number of functionalities added, at these levels the DEOA is of approximately equal importance as the polyol and water. Using typical feed proportions from a formulation as a basis for calculation makes this clear. For example, 100 grams of a 5,000 MW polyether polyol with a functionality of 2.4 would only provide ca. 0.048 moles of hydroxyl groups for reaction; however, only 2 grams of DEOA provides 0.057 moles of reactive groups. This component is added to increase the degree of covalent cross-linking in the foam, thus more quickly adding the dimensional stability required for the foam to be pulled out of the mold and therefore decreases demold times.

Simultaneously, however, DEOA has a single amine and two alcohol functionalities, and, since they respectively produce urea and urethane linkages upon reaction with isocyanate, it can be seen that DEOA might play a significant role in the development and organization of the polyurea hard domains. Typical flexible polyurethane foams are phase separated systems composed of the polyol (“soft”) matrix with polyurea hard domains interspersed throughout.

These hard domains organize in a specific way due to hydrogen-bonding, sometimes termed "para-crystalline" ordering, and variation of their size and concentration has been shown to have profound influence on the overall properties of the foam. In the molded foams studied here, it is therefore anticipated that the DEOA will have its impact by changing the makeup and molecular packing of the hard domains and thereby influencing overall properties.

Several other components in the formulation must be discussed when considering a molded foam. While TDI is widely utilized in both slabstock and molded foam formulations, the concentration of isocyanate in a foam has significant influences on its final properties. A foam that has a stoichiometric ratio of TDI to other components is said to have an isocyanate index of 100. It has been shown that producing foams with less than a stoichiometric feed, ca. 85-90 for example, significantly reduces the level of covalent cross-linking in system, resulting in a substantial softening of the foam.[4] For example, at 30°C-35%R.H., the 85 index foam exhibited a 43% lower load bearing than the 100 index foam.[4] Foams produced above stoichiometric feed, ca. 105-110 for example, typically produces harder foams, exhibiting load bearings ca. 21% higher than the 100 index foam.[4] This increase in load bearing with the higher index foams has been attributed to a faster viscosity rise resulting in less phase separation of the hard segments from the polyol.[4] To avoid such variation, therefore, the concentration of TDI in this study has been increased as DEOA is added to maintain a stoichiometric feed ratio (100 index).

Since catalysts in foam formulations are blended to balance the gelation and blowing reactions so that the foam has the right properties, changing the reactivity of the polyol components and the presence of DEOA requires alteration of the catalyst blend. Surfactant concentration has also been modified relative to a slabstock formulation to provide for cells of the desired size for seating applications (ca. 1 mm diameter) that open at the appropriate time. Both the catalyst and the surfactant concentrations have been maintained at constant levels for all the samples studied here.

The thermal history of these foams is the final variable to be considered. A typical molded foam is produced by injecting a reactive mixture into a ca. 68°C mold. The mixture expands to fill the mold within a minute and the foam is left to cure for ca. 4-5 minutes. The foam bun is then removed from the mold and mechanically crushed twice between rollers to further aid cell opening. Once the reactive blend is injected into the mold, the mixture heats itself to ca. 140°C within 120 seconds of injection and then ambiently cools after the crushing

steps. Molded foam buns are typically only ca. four to six inches thick and cool within hours. Slabstock buns are usually several feet thick and cool much more slowly over several days. Remaining at higher temperatures for so much longer could allow slabstock foams to cure further and possibly achieve a higher degree of phase separation than the molded foams. A rapid viscosity rise due to cooling might prevent similar phase separation in molded systems than occurs in slabstocks and ultimately reduce the overall level of hard domain ordering in the foam. As the organization of the hard domains is crucial to mechanical properties, the usefulness of an annealing step to the production of the foams was therefore also addressed in the present work by annealing some samples for 2 hours at 130°C.

In light of this discussion, it is clear that DEOA may have a significant impact on the composition of the hard segments by co-reacting with the isocyanate simultaneously with the water and polyol. Such alteration in the structure of the hard segments could have dramatic effects on the way that they order within the hard domains, and variation of that packing is known to strongly alter the mechanical properties of a foam. From this discussion and the earlier results from this laboratory,[3] it is clear that the relationships between formulation, structure, and properties are not completely understood. Therefore, since DEOA is so widely utilized commercially, this work seeks to further elucidate such relationships and to further clarify the results of our earlier study.

3.3 Experimental

3.3.1 Materials

Five foam samples of flexible water-blown polyurethane foams were made with varying DEOA concentrations by workers using a Hi-Tech RCM 30 foam machine at Dow Chemical in Freeport, Texas. This operation consists of two hydraulic pistons to dispense the liquid components to the mixing head. The formulation components described below were prepared in two storage tanks, A and B. The A side consisted of the isocyanate. The B side consisted of the polyols, water, surfactants, and catalysts. An aluminum mold having dimensions of 15”x15”x4.5” was used which was heated to 68 °C prior to injection of the reactive mixture.

These foams were based on 62.86 parts of an experimental ethylene oxide endcapped polyether polyol produced by Dow Chemical which was based on a glycerine/sucrose mixed initiator and had a functionality ca. 2.4 and a molecular weight of 5000. The foams were also based on 37.14 parts of Voranol® 4935 (Dow Chemical), a copolymer polyol containing 35

weight percent styrene/acrylonitrile random copolymer (60/40 styrene/acrylonitrile) particles. These particles were ca. 0.5-1.3 μm diameter. Five different concentrations of DEOA were used: 0.0 parts per hundred polyol (pphp), 0.85 pphp, 1.275 pphp, 1.7 pphp, and 2.0 pphp. Total water in each foam was 3.82 pphp. Three catalysts were used: 0.15 pphp of Dabco® 33LV (Air Products and Chemicals) which is 33% triethylene diamine in dipropylene glycol; 0.08 pphp of Dabco® BL11 (Air Products and Chemicals) which is 70% bis(N,N dimethylaminoethyl) ether in dipropylene glycol; and 0.6 pphp of Niax® A4 (Union Carbide) which is a catalyst blend primarily promoting the gelation reaction but tends to increase the blow reaction rate as well. Two surfactants were utilized to obtain the desired cell structure: 0.5 pphp of DC5043 and 0.5 pphp of DC5169. The 80/20 2,4/2,6 isomeric blend of toluene diisocyanate was used at a stoichiometric feed rate. Therefore, to maintain stoichiometry, the TDI was decreased in portion to the decrease of DEOA for each sample as shown in Table 1.

Table 3.1 - Variation of DEOA and TDI 80 in the Five Samples

Sample Names	DEOA Added	Total TDI 80 Added
McD2.0 / MaD2.0	2.35 (2.0) pphp	46.45 pphp
McD1.7 / MaD1.7	2.0 (1.7) pphp	45.2 pphp
McD1.3 / MaD1.3	1.5 (1.275) pphp	43.42 pphp
McD0.9 / MaD0.9	1.0 (0.85) pphp	41.64 pphp
McD0.0 / MaD0.0	0.0 pphp	40.1 pphp

3.3.2 Methods

Dynamic mechanical analysis (DMA) was carried out using a Seiko model 210 in the tensile mode. The samples were heated from -120 °C to 350 °C at a rate of 0.5 °C/min. from which the storage modulus (E') and tan δ data were collected at a frequency of 1 Hz. Bar shaped samples were cut from the foam with die-punches and had dimensions of approximately 5 x 5 x 15 mm with a grip-to-grip distance of 10 mm. Well below the T_g of the soft segment (at ca. -100°C), the storage moduli were then normalized to 3 x 10^9 Pa to remove the effect of varying density which is only a function of cellular structure.[5]

Mechanical properties were investigated through compressive load relaxation. Samples, having dimensions of 3.5" x 3.5" x 1", were cut from the foam bun using a band saw equipped with a smooth "wavy edge" saw blade to eliminate tearing. Each sample was first dried under vacuum and at 40 °C for 3.5 hr. in order to equilibrate each sample to an equal level of moisture content. The samples were then placed in an environmental chamber preset at the testing

conditions for ca. 60 min. The latter involved compressing a foam square at 300 mm/min using a 2" diameter indentor to 65% compressive strain three times and maintaining compression after the third time. The load relaxation was then tracked. This was performed on an Instron model 4400R with a 25 lb_f load cell produced by Transducer Techniques model MDB-25. The environment chamber produced by Russells Technical Products used a Watlow 922 microprocessor for environmental control. Tests were performed at low humidity and low temperature (30°C-15%RH), low humidity and high temperature (100°C-15%RH), and at high humidity and high temperature (100°C-70%RH).

Small angle X-ray scattering (SAXS) was utilized to evaluate the presence of microphase separation. This was performed with a Phillips model PW1729 generator operating at 40 kV and 20 ma and a slit collimated (0.03 x 5 mm) Kratky camera with nickel filtered CuKα radiation having a wavelength of 1.542 Å. The detector utilized was a Braun OED 50 position-sensitive platinum wire detector. Scattering data were corrected for parasitic scattering and normalized using a Lupolen standard. The beam path length was not corrected for density as in Chapter 7 because apparent density for these samples did not vary significantly; therefore, these samples will only be compared with each other to examine for trends. The foam samples were cut approximately 8 mm thick and compressed to approximately 2 mm. This data was analyzed using the TOPAS program developed by Dr. Stribeck at the University of Hamburg. Dr. Stribeck has graciously posted TOPAS for free downloading on the world wide web at http://www.chemie.uni-hamburg.de/tmc/stribeck/index.html.

The cellular structure of the foams was evaluated and compared using scanning electron microscopy (SEM). Thin slices (3 - 4 mm) of foam were adhered to aluminum stubs using silver paint and allowed to dry. A thin layer of gold was then applied to the surface of the foam using a SPI model 13131 sputter coater. Micrographs were taken using a Stereoscan 100 SEM (Cambridge Instruments, Ltd.) operating at 20 kV and at a magnification of approximately 30x.

To explore the ordering within the hard domains, the technique of wide angle X-ray scattering (WAXS) was applied via a Phillips model PW1720 generator with a Warhus camera. Nickel filtered CuK radiation was used with a wavelength of 1.542 Å and pinhole collimation with a diameter of 0.020 inches. Foam samples varied in density; therefore, they were cut to thicknesses which would expose ca. 3.2 mg of material to the beam and then were compressed to a ca. 2 mm thickness. Sample to film distance was 7.7 cm and exposure times were ca. 10 hours.

Fourier transform infrared (FTIR) was also used to evaluate hydrogen bonding in the hard domains.[6] FTIR Spectra were collected on a Nicolet 510 Spectrometer utilizing a Spectra-Tech ATR attachment model 0012-405 using a horizontal ZnSe crystal. Spectra were analyzed using Omnic 3.0 software, and all scans were normalized by the corrected peak height at 2970 cm^{-1} which corresponds to a CH_3 absorbance. For quantitative analysis, the ratio of the absorbance of the 1640-1650 cm^{-1} peak to the 1710 cm^{-1} peak was used. This provides a measure of the ratio of hydrogen bonded polyurea carbonyl groups to polyurea carbonyl groups which have not formed hydrogen bonds, and it serves as an internal calibration for each spectrum. Using this ratio allows the level of hydrogen bonding in one sample to be compared with another one with good precision (ca. 3% error).

Extraction experiments were carried out on selected samples to compare the level of cross-linking (gel fraction). Samples were submerged in a succession of DMF solutions of LiCl. Lithium chloride solutions are used to increase the rate of extraction for these materials by disrupting the level of hydrogen bonding, thus facilitating the evaluation of the amount of extractable material in a given sample. The succession consisted of two submersions at 10 wt % LiCl, one at 6 wt %, one at 3 wt %, followed by three submersions at 0 wt %. The period of each submersion was four to five days. The samples were then repeatedly evacuated at 40 °C for two weeks followed by two days at 80 °C. Samples were weighed throughout the drying process until a stable weight was achieved. The level of weight lost via extraction provides an index of the sol fraction while the remaining extracted matrix represents the gel fraction.

3.4 Results and Discussion

Since macroscopic tests on foams convolute the properties of the solid polymer with the character of the cellular structure, it is important in systematic comparisons to evaluate how much either are being changed. For example, scanning electron micrographs of the foam, such as that of MaD2.0 shown in Figure 3.1, allow for comparison of the size of the cells and of the number of closed cell windows observed. However, examining these samples via SEM revealed no difference in either of those characteristics; therefore, micrographs of the other samples are not presented here.

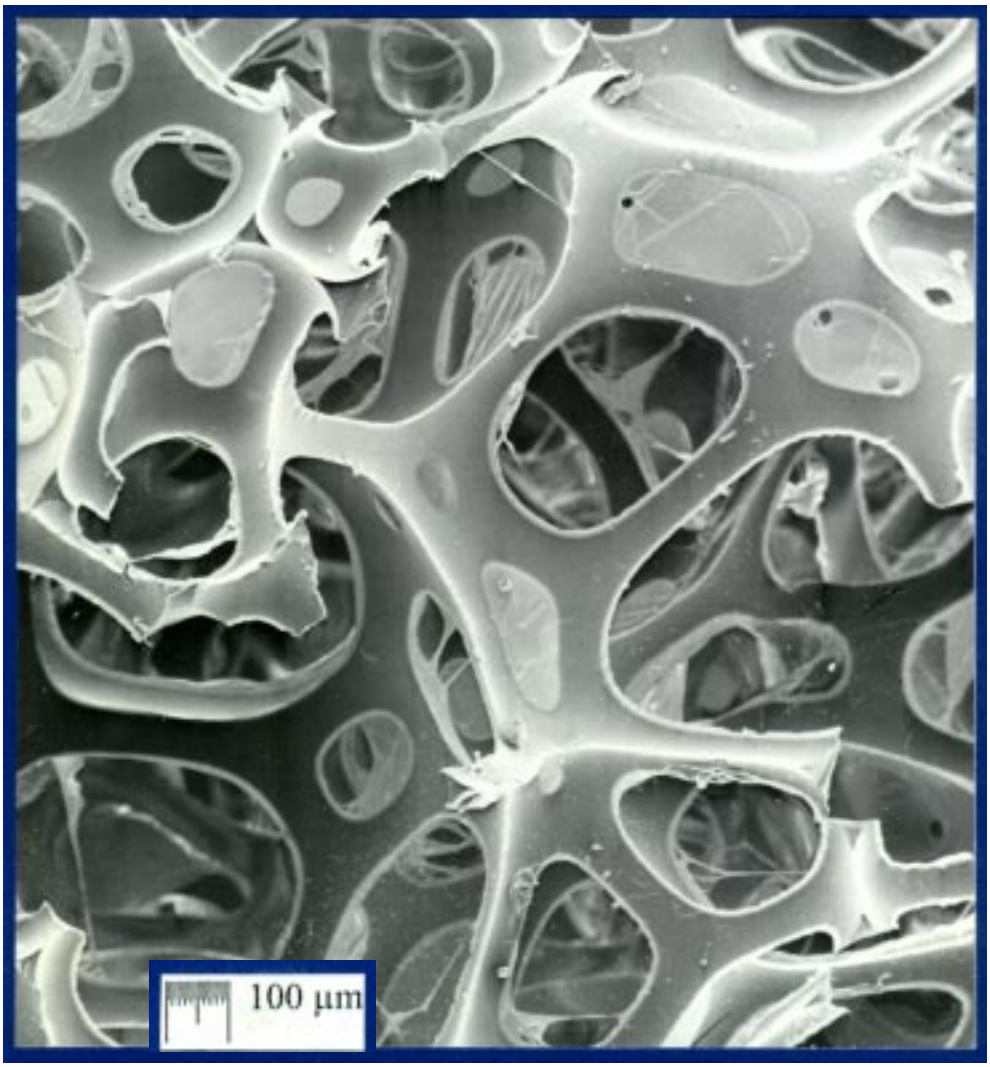

Figure 3.1 Scanning electron micrograph of MaD2.0

Airflow measurements were used to more qualitatively evaluate cell openness, and that data can be seen in Figure 3.2. In contrast to the data reported earlier from this laboratory,[3] our new results clearly show that these samples have essentially the same degree of openness in their cellular structure. Another measure of the cellular structure is the core density, and all of these samples had an apparent density of 1.86 ± 0.04 lbs/ft^3. Without observing differences between the apparent densities, the air flow measurements, and the SEM examinations, it is inferred that the cellular structures of the samples in this study are sufficiently equivalent to allow any major variations of the other foam properties to be attributed to differences in the polymer itself.

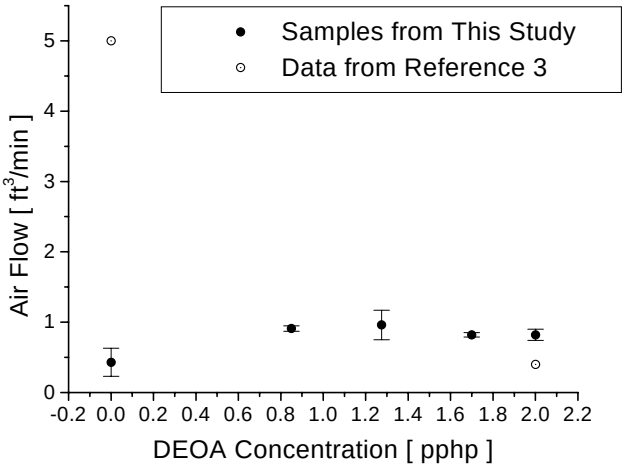

Figure 3.2 Variation of airflow measurements as a function of diethanolamine concentration.

3.4.1 Mechanical Properties

The mechanical properties of these samples were investigated through tensile DMA and compressive load relaxation studies. The DMA storage moduli for the non-annealed samples are shown in Figure 3.3. This data reveals that in the rubbery region, even the addition of small amounts of DEOA to the foam results in significant softening. It also shows that there is a softening at ca. 125°C which corresponds to the glass transition of the SAN reinforcing filler particles.[2] The annealed samples showed identical trends of softening with increasing DEOA concentration, so those storage moduli are not presented.

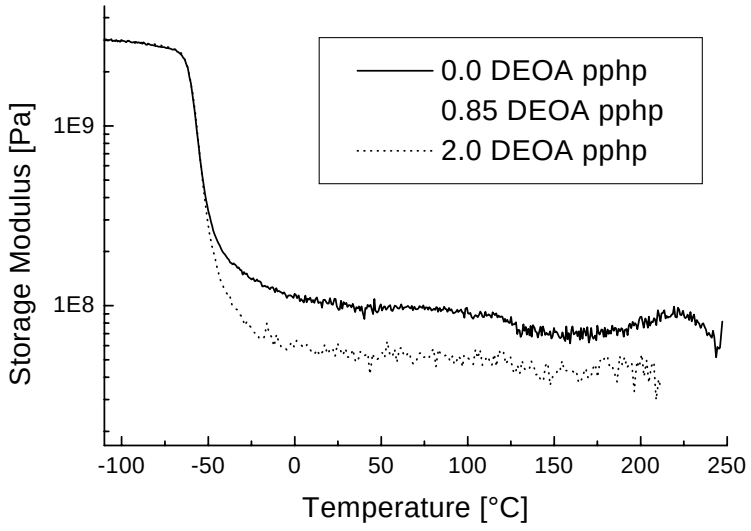

Figure 3.3 DMA storage moduli at 1 Hz. for non-annealed foams of varying DEOA content.

The 65% compressive load relaxation studies were performed at low temperature and low humidity, where hydrogen bonds would be expected to be strongest, and at high temperature and high humidity where hydrogen bonds would be most disrupted. The results of these tests are shown in Figure 3.4a and 3.4b. At low temperature and low humidity (Figure 3.4a), the non-annealed foams are observed to have significantly lower load bearing with increasing DEOA content. For example, the initial compressive load on the non-annealed foam with 0.0 DEOA pphp is ca. 6.5 kg_f but with 2.0 DEOA pphp it is ca. 2 kg_f. This trend was also observed in the foams at high temperature and high humidity (Figure 3.4b), wherein the foams at 0.0 DEOA pphp are approximately twice as hard as the foams at 2.0 DEOA pphp. The shape of the load relaxation curve at 100°C is different than at 30°C due to being in thermal proximity to the glass transition of the SAN reinforcing filler.[2, 7] The annealed foams revealed an identical trend of significant softening with increasing DEOA content at both environmental conditions, so those load relaxation curves are not presented. This dramatic softening influence of DEOA is the opposite of what was observed in our earlier study[3], and it points on the importance of considering the cellular structure in systematic work on foams. Because a restricted airflow in a foam would result in a higher compressive load bearing, it is suggested that the trend of DEOA increasing foam hardness observed in the earlier work[3] is due to the higher closed cell content of the foams and not changes in the polymer itself.

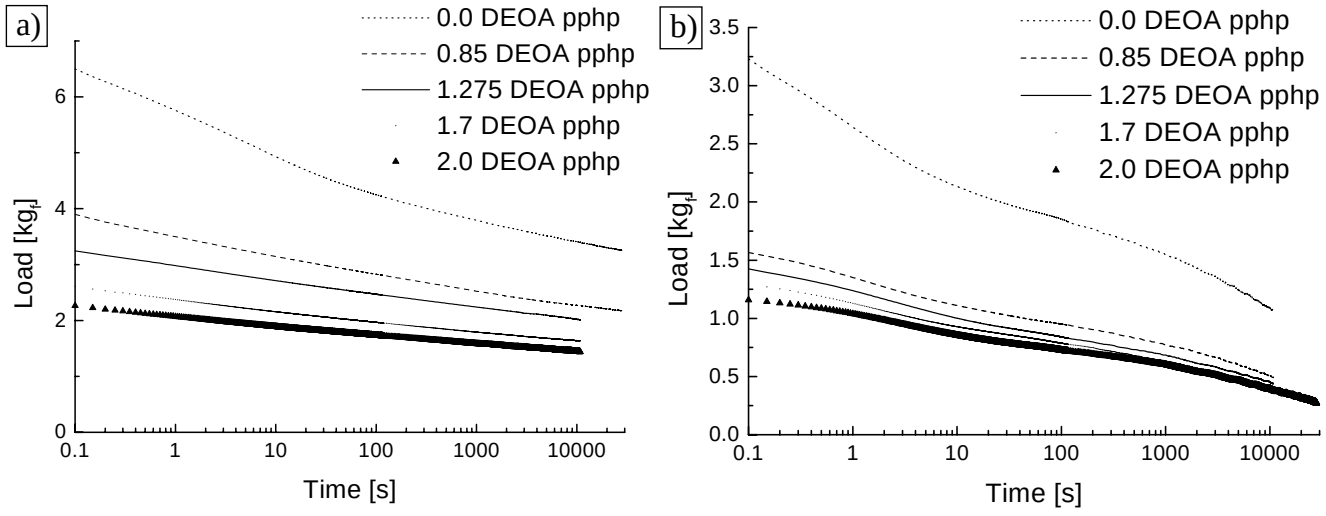

Figure 3.4 Load relaxation data at 65% compression for non-annealed foams at: a) 30°C-15 % RH and b) 100°C-75 % RH

Observing the softening effect of DEOA is the major trend to consider from the compressive load relaxation work, but there are some minor points to also note. For example, the annealing does not appear to influence the overall rate of relaxation, but DEOA does. This is shown in Figure 3.5a which reveals that, although the annealed foam data overlays the non-annealed foams, increasing DEOA content in a foam significantly reduces its total 3 hour load relaxation at 30°C-15 %RH. At 0.0 DEOA pphp, the foams exhibit ca. 45% load relaxation whereas, at 2.0 DEOA pphp, they relax ca. 30%. However, as shown in Figure 3.5b, at 100°C-75 %RH, the data reveals no variation of the percent relaxation with respect to DEOA content. This strongly suggests that, whatever influence the DEOA has in reducing the percent load loss, it is undetectable or removed in the high temperature/high humidity environment. This is suggestive that the DEOA may be influencing the hydrogen bonding properties of the polymer and more specifically of the hard segments.

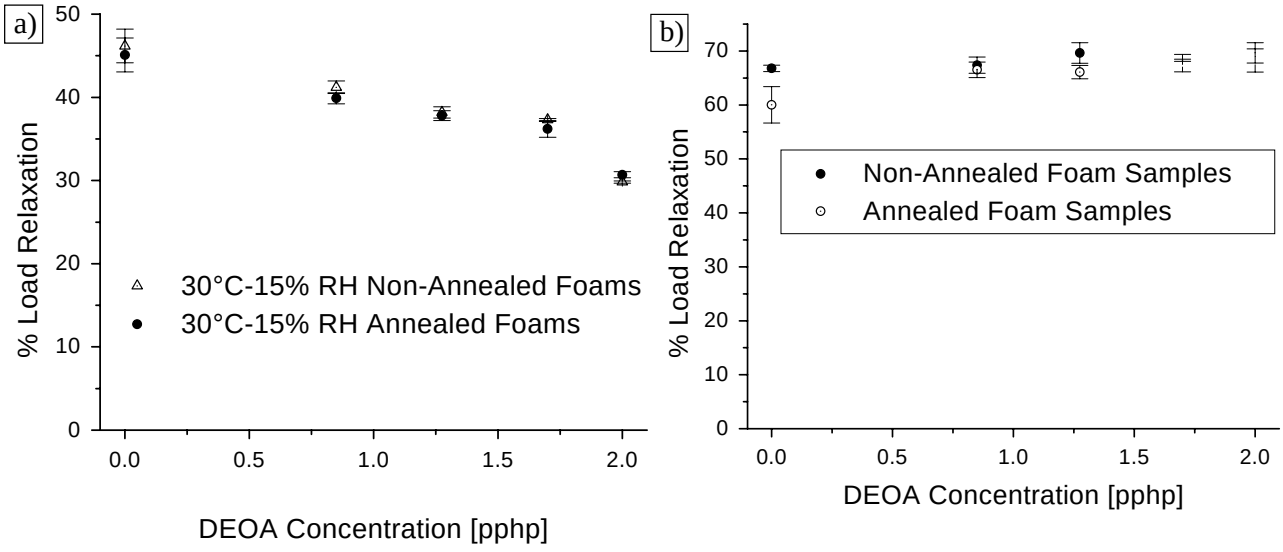

Figure 3.5 Percent load relaxation data at a) 30°C-15 % RH and b) 100°C-75 % RH. This was calculated by comparing the load bearing at 0.1 and 10,000 seconds after compression to 65%.

Another observation from the load relaxation work is that the annealing of the foams does not alter that softening trend, but it does have some effect on the load bearing at each DEOA concentration. As shown in Figure 3.6, at 30°C-15 %RH the annealing has very little effect on the foams below ca. 1.3 DEOA pphp, but above that DEOA content the load bearing is improved by as much as ca. 15% in the 2.0 DEOA pphp foams. This reveals that the annealing

is improving the load bearing but only in foams with higher levels of DEOA. A similar trend is seen in the 100°C-75 %RH results, where at no DEOA the annealing seems to have no influence, but, at higher concentrations, the annealing does appear to increase the load bearing. Thus the annealing seems to be significant in improving foam properties only in the higher DEOA concentrations that were examined here.

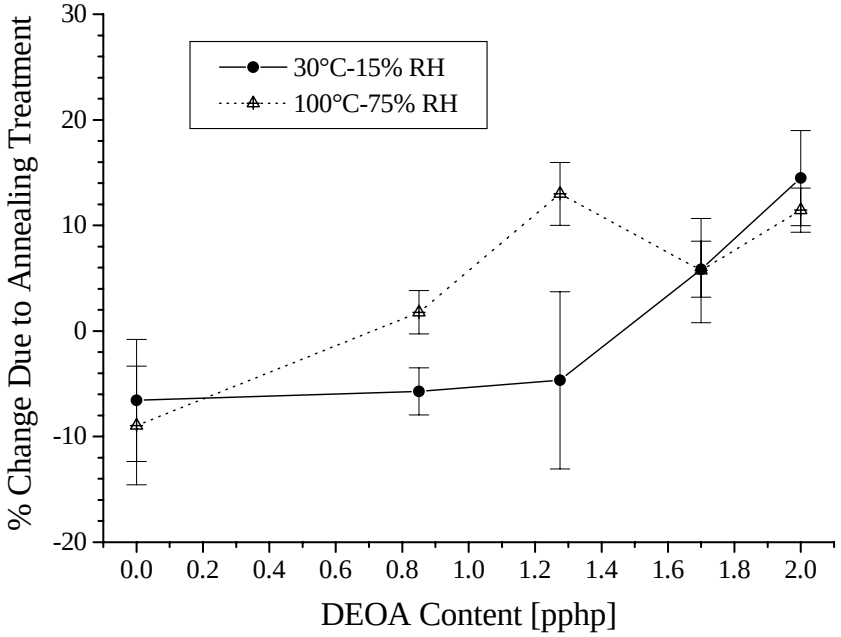

Figure 3.6 Percent change after annealing in the initial load bearing at 65% compression for the foams measured at 0.1 seconds after compression

In addition to these observations, the percent hysteresis also comes from the load relaxation work, and it is calculated as the percent difference in the area below the loading and unloading curves of the second 65% compression. At 30°C-15 %RH, as Figure 3.7a reveals, the amount of energy dissipated during a compression cycle decreases systematically with higher DEOA concentrations. This suggests that DEOA reduces the dependence of these materials on the hydrogen bonding for their properties. It is interesting that up to 1 DEOA pphp, the annealing treatment seems to have little discernible effect, yet above that concentration the annealing marginally increases the hysteresis of the foams. As shown in Figure 3.7b, this subtlety is lost at 100°C-75 %RH, a condition where much hydrogen bonding lability exists in the foam. No significant difference can be observed between the annealed and non-annealed

materials, but the consistent decrease of hysteresis with increasing DEOA content remains. This decrease from ca. 35% at 0.0 DEOA pphp to ca. 25% at 2.0 DEOA pphp should emphasize that the DEOA is clearly changing the viscoelastic properties of the foam. Since hysteresis in these materials is frequently associated with hydrogen bonding, Figures 3.7a and 3.7b suggest that DEOA is reducing the extent to which the foam depends upon these cohesive physical bonds for its mechanical properties.

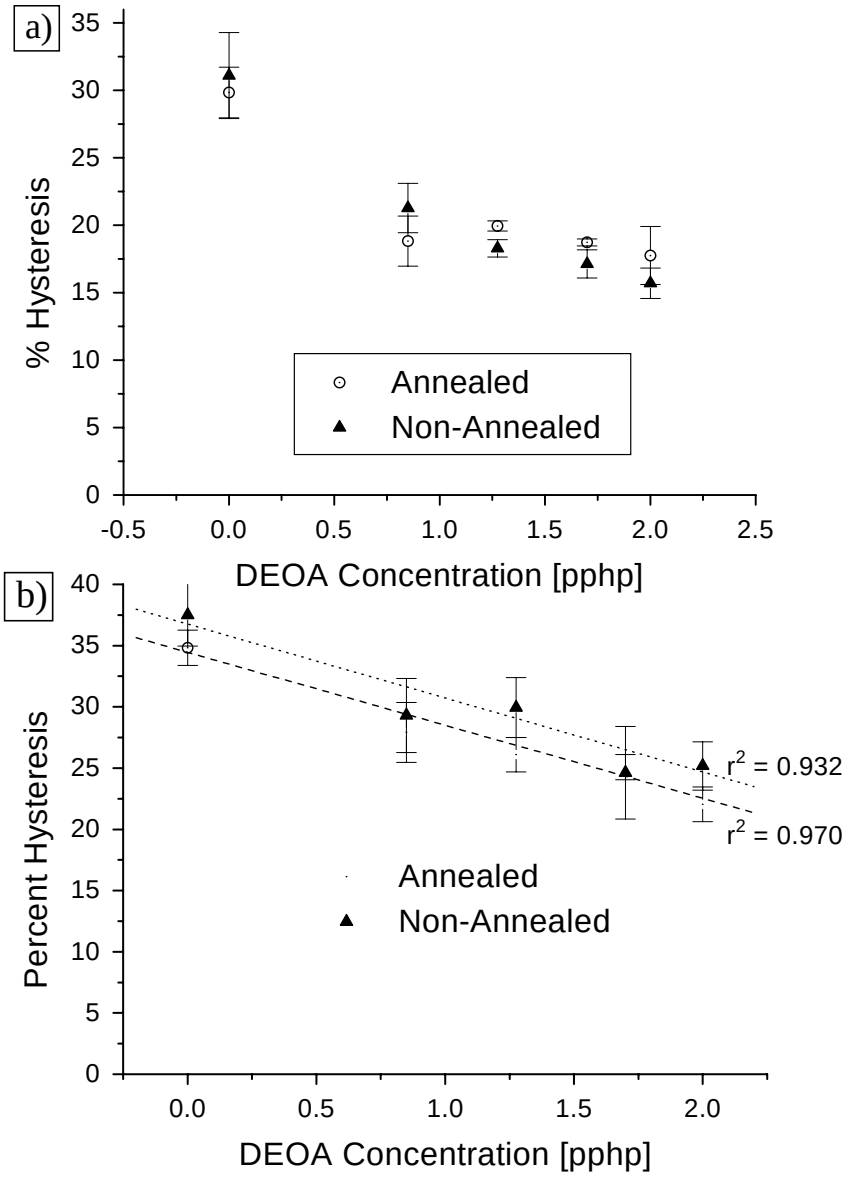

Figure 3.7 Percent hysteresis at a) 30°C-15 % RH and b) 100°C-75 % RH

3.4.2 Structure and Morphology

The above analysis of the mechanical properties of these foams has presented an intriguing question. The theory of rubber elasticity states that higher levels of covalent cross-linking should increase the modulus or stiffness of the polymer. Yet this study has so far demonstrated that, if influences of the cellular structure are removed, 2.0 diethanolamine pphp reduces the load bearing (i.e. stiffness) of the foam by nearly 50%. This dichotomy is further established by the fact that DEOA can be proven to increase the level of covalent cross-linking by using solvent extraction to probe how much material was covalently bound into the three dimensional network. As Figure 3.8 reveals, the weight fraction of extractables is substantially decreased as DEOA content is increased, decreasing from ca. 13 wt% at 0 DEOA pphp to ca 4.5 wt % at 2 DEOA pphp. This is interpreted to mean that the DEOA does significantly increase the amount of material becoming bound into the covalent network. Figure 3.8 also reveals that the level of extractables is not substantially changed by the annealing step. Clearly, then, the DEOA is increasing the level of covalent cross-linking and so the question of how softening results from the addition of DEOA must be answered from another change in the polymer.

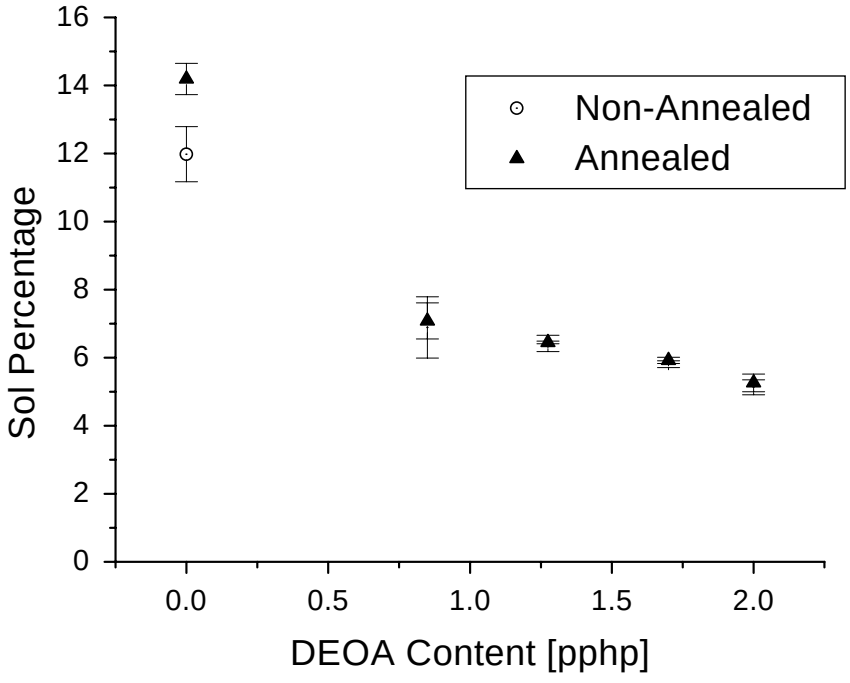

Figure 3.8 Solvent extraction results for foams of varying DEOA content

The properties of flexible polyurethane foams are well known to be largely dependent on their microphase separated morphology to the extent that alterations in that phase separation can have dramatic effects. This is discussed at length in references 8 and 9. SAXS is one technique which has been frequently used to examine the microphase separation of these materials. The shoulder in the SAXS profiles of Figure 3.9 show that even the highest concentrations of DEOA studied did not prevent these systems from phase separating. On the contrary, the profiles of Figure 3.9 show that increasing DEOA content systematically increases the observed scattering intensities of the foam samples. This might occur through either an enhancement of the phase separation or through an increase in the hard segment content of the foam. Considering the increase in TDI fed, it is suggested that the latter is more probable.

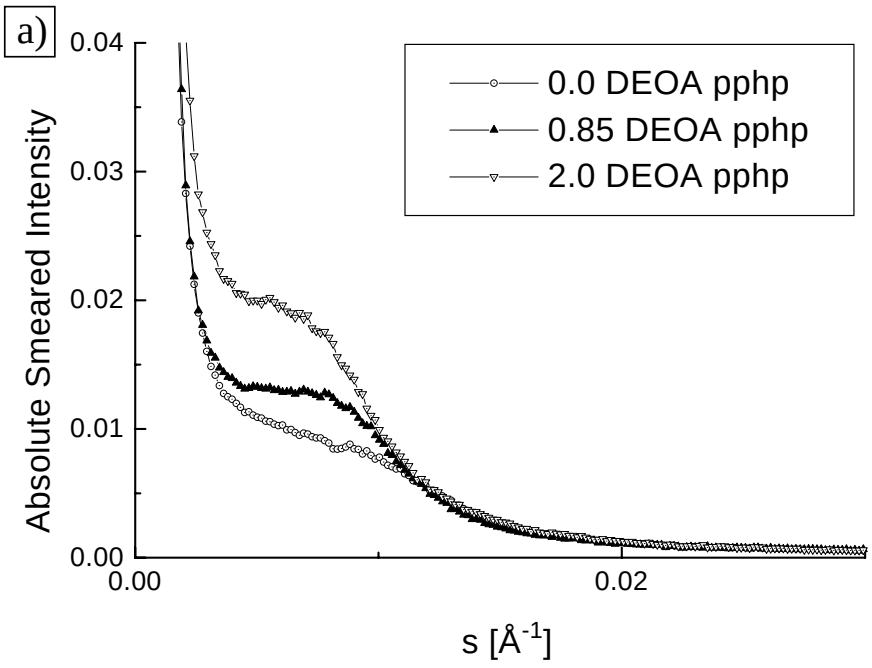

Figure 3.9 SAXS profiles for non-annealed foams of varying DEOA content

The profiles do show distinct movement to lower angles (i.e. longer interdomain spacings) with increasing DEOA concentration. This was examined further using the three dimensional correlation function analysis described in reference 10. That analysis provides a way to better estimate the interdomain spacing which underlies the scattering profile, and the results of this are shown in Figure 3.10 where it can be seen that the spacing between hard domains systematically increases from ca. 10 nm at 0.0 DEOA pphp to ca. 13 nm at 2.0 DEOA

pphp. It also shows that annealing may have a subtle influence on the interdomain spacings, but only at DEOA feed concentrations above 1 pphp. Two separate but conceptually valid hypotheses would explain this increase in spacing. If the DEOA and whatever reacts with it reside completely in the polyol phase and the hard domains are essentially unchanged, the resulting increase in polyol phase volume fraction might distribute the hard domains further apart. On the other hand, the interdomain spacing relates the most probable distance from the center of one domain to the center of the next. Therefore, if the DEOA and its co-reactants reside more so in the hard domains, then the increase of hard domain volume would result in their centers being further from each other. This latter explanation may be supported by the increasing intensities observed in Figure 3.9. The SAXS thus provides strong evidence that the microphase separation is being altered somehow by including DEOA in the formulation; however, information from another technique is required to provide a satisfying interpretation of that change.

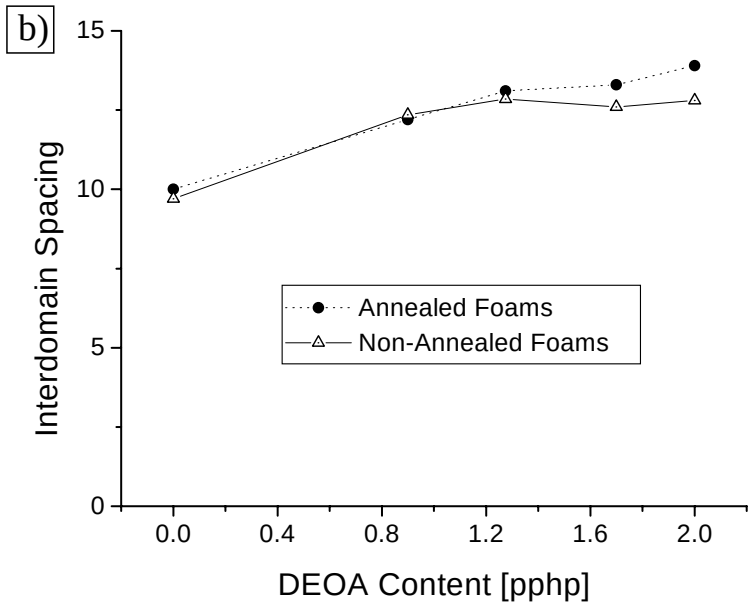

Figure 3.10 Influence of DEOA on the SAXS interdomain spacings of annealed and non-annealed materials

Examination of the polyol glass transition is one way to evaluate whether the DEOA and whatever reacts with it resides in the soft or hard phases of the polymer. The very flexible polyether polyol chains are usually observed to have very low glass transitions (ca. -55°C by DMA at 1 Hz.), and so relatively small amounts of hard segment material becoming mixed with

it can restrict chain mobility and result in higher glass transition values. Using this technique to evaluate polyol purity has been established by other workers.[11] A typical DMA tan delta curve may be observed in Figure 3.11. This shows the dominant relaxation is that of the polyol at ca. -55 °C and that a minor relaxation peak occurs at ca. 125°C which is attributable to the stryene-co-acrylontrile reinforcing filler.[2]

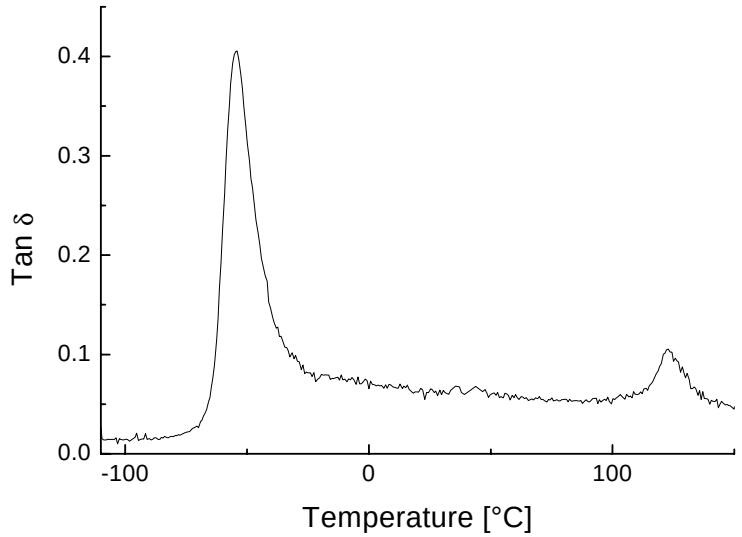

Figure 3.11 DMA tan delta curve for the 0.0 DEOA pphp non-annealed foam.

Complete understanding of the DEOA influence on the polyol glass transition requires consideration of the results in both a numerical and graphical form. As Table 3.2 shows, the non-annealed materials show that without DEOA, the polymer attains a level of phase separation that exhibits a polyol glass transition peak at -54.0 ± 0.3 °C. However, as DEOA content is increased the location of the tan delta peak shifts to ca. -52.4 ± 0.3 °C. After annealing, however, all the samples, regardless of DEOA content, have their tan delta peaks centered on -54 °C. This suggests that whatever level of phase separation is attained by the 0.0 DEOA pphp foam is regained by the foams with DEOA after the annealing step. The reality of this somewhat subtle difference is demonstrated in Figures 3.12a and 3.12b which examine the polyol glass transition region. Figure 3.12a shows that the onset of the glass transition for all of the non-annealed foams begins at about the same temperature (ca. -65°C). However, the peaks of these relaxations move systematically higher with increasing DEOA content. Furthermore, the tail of the relaxation extends to higher and higher temperatures as the DEOA concentration is

increased, which suggests the distribution of chain mobility in the polyol is broadening. This is established by Figure 3.12b, which shows that all the foams which were annealed have their glass transitions centered upon the same temperature. Furthermore, as the DEOA level is increased, Figure 3.12b clearly shows that the tan delta peak is broadening and increasing in height. This data suggests that the DEOA initially affects the level of phase separation obtained in the polymer, but that this influence is removed via annealing. Furthermore, because the polyol is reaching the same level of mobility in the annealed foams regardless of DEOA content, *it is suggested that the DEOA and its co-reactants largely reside within the hard domains*. However, the annealing does not change the wider distribution of molecular mobility shown by the broader tan delta peaks and this suggests more permanent alterations changes in microphase separated morphology.

Table 3.2 - Influence of DEOA on Polyol Glass Transition Temperature

DEOA Content [pphp]	Non-Annealed Tanδ Peak	Annealed Tanδ Peak
0.0	-54.0 ± 0.1 °C	-54.1 ± 0.3 °C
0.85	-53.2 ± 0.3 °C	-53.8 ± 0.7 °C
1.275	-52.7 ± 0.2 °C	-54.3 ± 0.1 °C
1.7	-52.3 ± 0.4 °C	
2.0	-52.4 ± 0.3 °C	-54.2 ± 0.5 °C

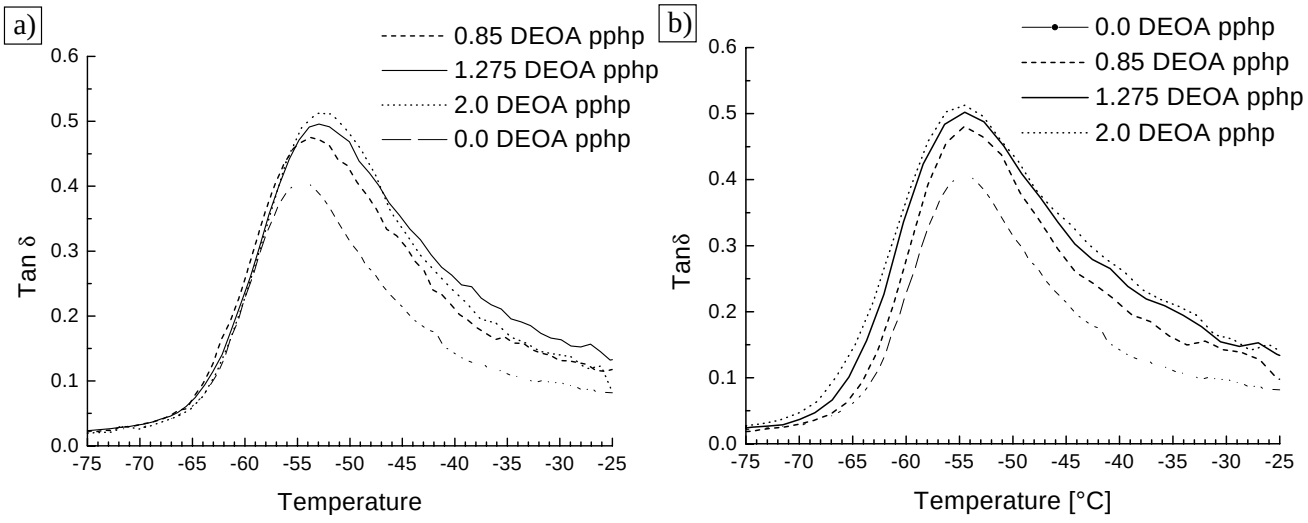

Figure 3.12 Polyol glass transition region from DMA tan delta curves for foams of various DEOA content. a) non-annealed samples and b) annealed samples

WAXS and FTIR are two complementary techniques which can be used to evaluate structure and ordering in the hard domains of flexible polyurethane foams.[9] As shown in Figure 3.13a, the WAXS pattern of the 0.0 DEOA pphp foam exhibits a 4.7 Å reflection overlying an amorphous halo. As shown in reference 9, this indicates that bidentate hydrogen bonding is present and that the hard domains possess internal order of a somewhat para-crystalline nature. However, as Figure 3.13b shows, this reflection is no longer visible at 2.0 DEOA pphp, revealing that the no short range periodic spacing exists within the hard domains when DEOA is present. Because the 4.7 Å reflection could not be brought back after annealing and additional heat treatments, it is concluded that this disorder is due to alterations in the covalent structure of the hard segments themselves. Furthermore, because this occurred at even the lowest levels of DEOA content studied (0.85 pphp), it is suggested that the DEOA reacts early in the sequence of foam reactions incorporating itself internally in the hard segments and ultimately the polyurea hard domains as well.

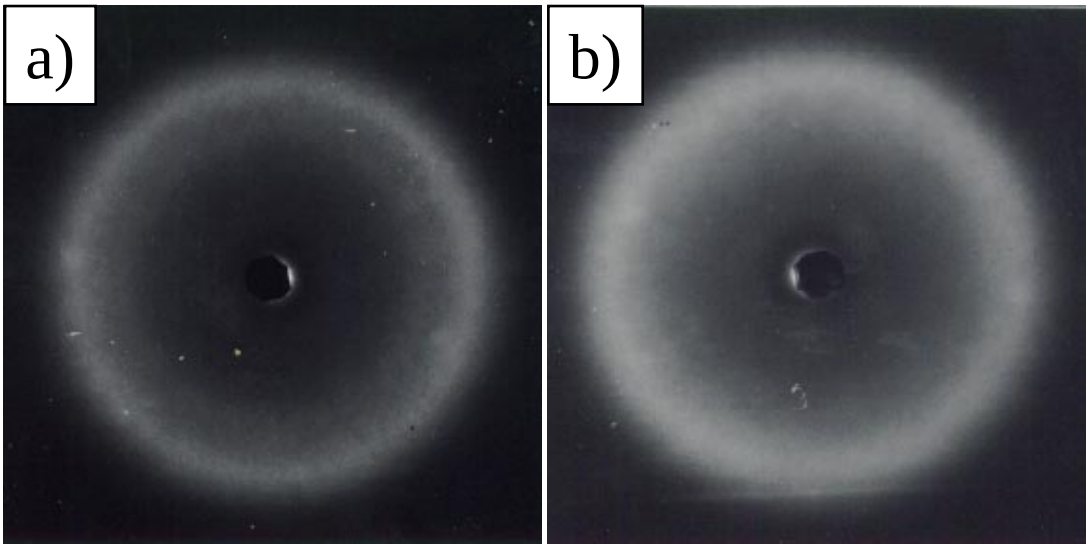

Figure 3.13 WAXS patterns for foams with a) 0.0 DEOA pphp and b) 2.0 DEOA pphp

The hypotheses proposed above are supported by FTIR results. As shown in Figure 3.14a, the overall character of the carbonyl region is dramatically altered even at the lowest levels of DEOA used here. All spectra have been normalized for these qualitative comparisons using the CH_2 peak at 2969 cm^{-1}. The outstanding peak at ca. 1640 cm^{-1} indicates the presence of bidentate hydrogen bonding. By comparing the height of that peak with the vibration at 1710 cm^{-1}, which arises from carbonyl groups that are not hydrogen bonded, it can be observed that

without DEOA, hydrogen bonding is much more prevalent. With DEOA, the bidentate vibration appears to be of the same significance as the free carbonyl vibration. However, with annealing, the situation changes as shown in Figure 3.14b. It can be observed that hydrogen bonding is significant after annealing for all the samples as judged by the height of the 1710 cm^{-1} absorbance. What is important to notice, however, is that, even after annealing, no foam with DEOA in it regained an aborbance at ca. 1640 cm^{-1}, but rather they only exhibit weaker peaks at ca. 1645 cm^{-1}. This is significant because it indicates that those peaks have become more convoluted with the monodentate hydrogen bonding vibrations in the region of 1650-1660 cm^{-1}. This indicates that although some level of hydrogen bonding is obtained through the annealing step, the covalent alterations that DEOA makes on the chemical structure of the hard segments may preclude a return to true bidentate hydrogen bonding.

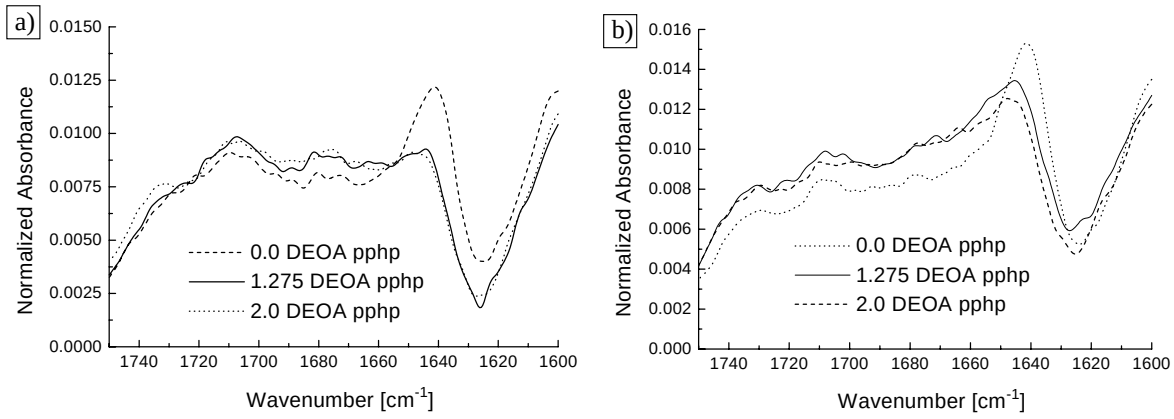

Figure 3.14 FTIR spectra showing the carbonyl vibration region for a) non-annealed and b) annealed foams

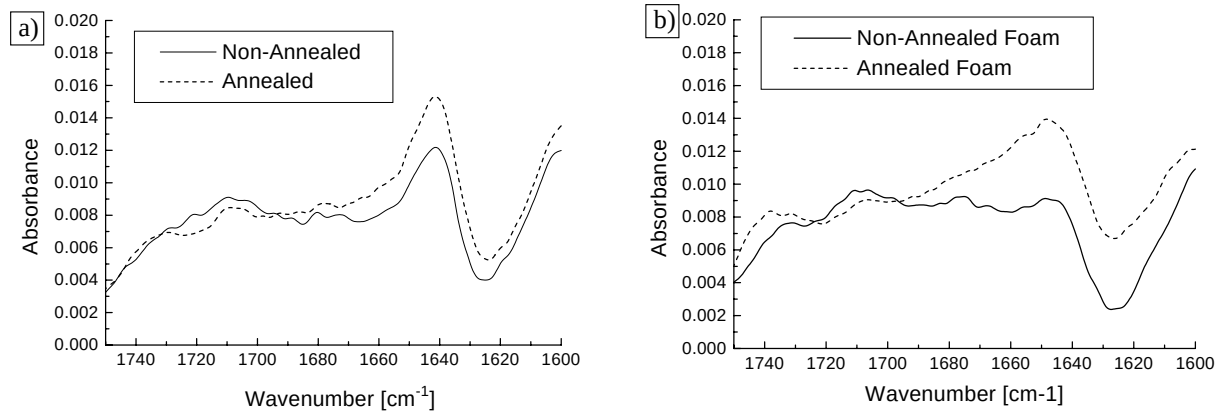

Figure 3.15 Influence of annealing on the FTIR spectra of a) 0.0 DEOA pphp and b) 2.0 DEOA pphp foams

The FTIR also brings an explanation to why foams with higher levels of DEOA show the most influence during the annealing step. As Figure 3.15a shows, the character of the carbonyl region is not altered for a foam without DEOA. The 1640 cm^{-1} peak is still predominant in comparison to the free carbonyl vibration. However, for the foam with 2.0 DEOA pphp, Figure 3.15b illustrates that its carbonyl spectra is dramatically altered. The annealing step brings significant monodentate hydrogen bonding into a material which formerly had levels that were approximately comparable to the amount of non-associated carbonyl groups. This can be made more quantitative by taking a ratio of the peak height at 1645-1640 cm^{-1} to the peak height at 1710 cm^{-1}. Two major observations can be made from the data that this provides in Figure 3.16. First, as DEOA is increased in a foam, whether or not it is annealed, the level of hydrogen bonded carbonyl groups systematically decreases. This is concluded to be the source of the decreasing hysteresis observed in Figures 3.7a and 3.7b. Another observation is that the annealing makes a more significant difference to the hydrogen bonding in the material at and above 1.3 DEOA pphp than it does below that level. The similarities in this regard between Figure 3.16 and Figure 3.7a cannot be a coincidence. It is therefore concluded that annealing treatment does somewhat improve the phase separation of the polymer as shown by DMA, but that the largest affects on the mechanical properties are made by increasing the level of hydrogen bonding in the system.

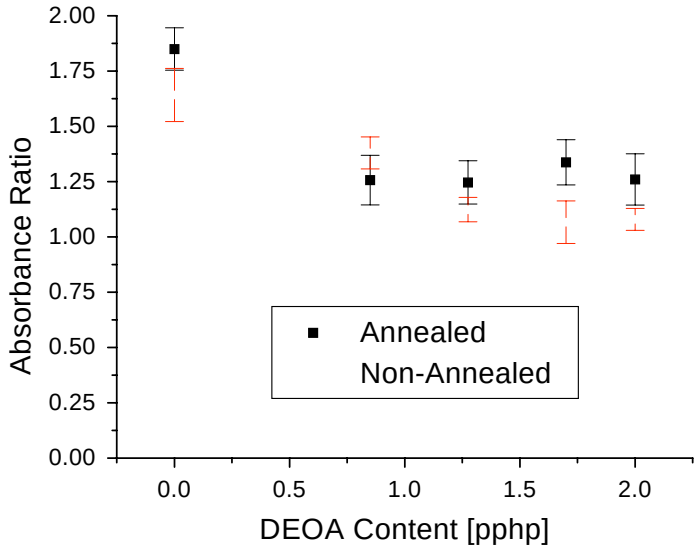

Figure 3.16 Ratio of hydrogen bonded carbonyl peak height to the free carbonyl peak height as a function of DEOA content

3.5 Conclusions

These results have shown that the use of DEOA in the formulation of molded flexible polyurethane foams has clear and related effects on morphology and properties. The DEOA was shown to reside largely in the hard domains and to alter their "para-crystalline" ordering. This results in lower rubbery moduli and lower overall load bearing properties. Without DEOA, each hard domain in the foam serves as a point of cross-linking but relies completely upon physical associations for its cohesive strength. When DEOA is added, it becomes incorporated in the hard segments and ultimately the hard domains as well, so that each hard domain now also contains some covalent cross-links. Since the DEOA resides largely in those domains, the overall number of cross-linking points are not increased in the polymer. *Thus the softening occurs because the DEOA alters the chemical structure of the hard segments, reducing their ability to form the bidentate hydrogen bond which typically increases foam stiffness.*

This idea is presented as a very simplified schematic diagram in Figures 3.17a and 3.17b. As Figure 3.17a shows, without DEOA it is fairly easy to conceive of ways for the hard segments to pack so that polyurea carbonyl groups are able to associate with both hydrogens of an adjacent polyurea. This well ordered packing provides a structure which yields the 4.7 Å reflection in WAXS.[9] Figure 3.17b attempts to illustrate that adding DEOA alters two main features of the hard segment. Most clearly, it reduces the number of polyurea groups and increases the number of polyurethane linkages in the hard segment. Even where a polyurea link has been generated from the amine of the DEOA, only a single hydrogen is available for association with any adjacent carbonyl groups. This change reduces the likelihood for forming the strong bidentate hydrogen bonding between hard segments, and the loss of short range ordering in the hard domains results in the WAXS pattern exhibiting no detectable reflections. These over simplified schematics thus convey the idea that DEOA disrupts a manner of molecular packing in the hard domains that typically leads to strong associations.

This increase of the covalent nature (but not the cross-link density) of the network was also seen to result in lower mechanical hysteresis. Additionally, DEOA alters the initial degree of phase separation which results in subtle increases in T_g before annealing. However, the near-equilibrium degree of phase separation was shown to be uninfluenced by the addition of DEOA as shown by the annealing steps. Finally, it was also observed that foams containing the highest DEOA concentrations have the most to gain in terms of properties from an annealing step.

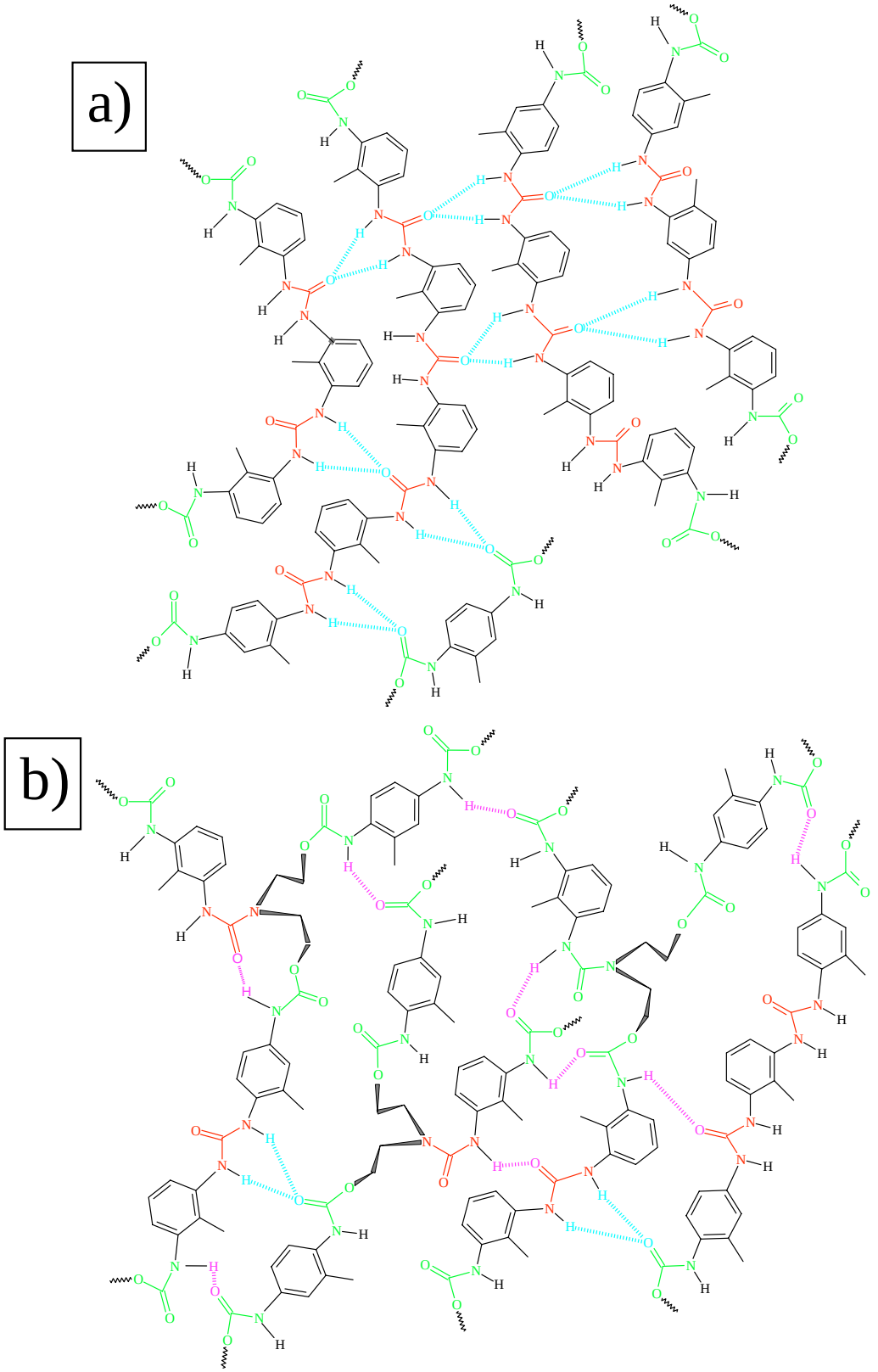

Figure 3.17 Schematic representation of polyurea segment packing in a hard domain a) without DEOA and b) with DEOA

3.6 Acknowledgments

The authors gratefully acknowledge the Dow Chemical Company for their financial support of this work.

3.7 References

[1] Herrington R; Hock K; Flexible Polyurethane Foams, 2nd Ed.; The Dow Chem Co: (1998)
[2] Kaushiva BD; Dounis DV; Wilkes, GL; *J Appl Polym Sci*: in press
[3] Dounis DV; Wilkes GL; *J Appl Polym Sci*: **65** (1997) 525
[4] Dounis DV; Wilkes GL; *J Appl Polym Sci*: **66** (1997) 2395
[5] Turner RB; Spell HL; Wilkes GL; *Proc of the SPI 28th Annual Technica/Marketing Meeting Conf*: (1984) 244
[6] McClusky JV; Priester Jr RD; O'Neill RE; Willkomm WR; Heaney MD; Capel MA; *J Cell Plast*: **30** (1994) 338
[7] Aklonis JJ; MacKnight WJ; Introduction to Polymer Viscoelasticity; John Wiley & Sons, Inc, New York: (1983) 44
[8] Dounis DV; Wilkes GL; *Proc of the Polyurethanes 1995 Conf*: (1995) 353
[9] Kaushiva BD; McCartney SR; Rossmy GR; Wilkes GL; *Polymer*: in press
[10] Tyagi D; McGrath JE; Wilkes GL; *Polym and Eng Sci*: **26** (1986) 1371
[11] Lidy WA; Rightor E; Thanh HP; Cadolle D; *Polyurethanes Expo '96*: (1996) 119-135

4 Alteration of Polyurea Hard Domain Morphology by Diethanolamine (DEOA) in Molded Flexible Polyurethane Foams

4.1 Chapter Summary

In this study, the morphology of polyurea hard domains in flexible polyurethane molded foams was investigated to evaluate the influence of diethanolamine (DEOA), a commercially utilized cross-linking agent. Tapping Mode AFM was utilized to reveal that DEOA dramatically alters the morphology of the solid state. Without DEOA, the solid state phase separation leads to the formation of lamellae-like polyurea domains ca. 50-100 nm long by 5 nm wide, and these lamellae frequently aggregate to form larger precipitates ca. 30-50 nm in diameter. These larger aggregations appear to be evenly distributed in the material. However, when DEOA is added to the formulation, the hard domains become smaller and more geometrically isotropic, ca. 5 nm in diameter. Furthermore, in the DEOA containing material, the hard domains do not appear to form the larger 50 nm aggregates but instead remain distributed at ca. 10 nm apart. The addition of DEOA thus reduced the level of hard domain interconnectivity, an effect which is strongly hypothesized to explain in part the corresponding reduction in modulus (i.e. stiffness) that is commonly observed when DEOA is added to such foam formulations. The morphological alterations observed using AFM were also found to correlate well with the DEOA induced changes in the small angle X-ray scattering profiles of these samples.

4.2 Introduction

As flexible polyurethane foams have been introduced for many new applications, it has proven more economical in some cases to produce foams by casting the reactive mixture into molds of the desired form rather than by the traditional slabstock method. As discussed elsewhere, this production technique eliminates much time and waste in trimming, and it widens the range of obtainable properties[1]. To take advantage of these possible benefits and to meet the demands of processing with molds, many changes have been made in the formulations of flexible polyurethane foams.[1,2]

These formulations are optimized to obtain the lowest mold residence times possible while still achieving the desired performance in tests such as compressive load bearing and

resiliency. Among these alterations is the addition of cross-linking agents for improved stability of the cellular structure. Increasing the rate of covalent cross-linking allows other changes to be made to the formulation which reduce the time that the foam requires to achieve enough dimensional stability for it to be removed from the mold. These changes are enumerated in a recent publication by the authors.[3] As formulations are altered with a view toward macroscopic mechanical performance, the optimization generally focuses much attention on the cellular structure of the foam with measurements such as airflow, cell count, and apparent density.

Despite this emphasis on millimeter scale morphology, structure occurs at many scale lengths in flexible foams, and it is important to consider how they convolute together to yield the properties exhibited in macroscopic mechanical tests. This convolution was clearly demonstrated by two recent studies from this laboratory on the influence of a commercially used cross-linking agent, diethanolamine (DEOA). In one study,[4] DEOA was shown to increase the compressive load bearing (i.e. stiffness) as a result of increasing the amount of closed cells in the foam. This constricted the air from flowing through the cellular matrix resulting in an apparently stiffer foam bun. In a subsequent work,[3] the variation of airflow was removed by controlling the millimeter scale structure, and it was shown that DEOA actually reduces the compressive load bearing (i.e. stiffness) by nearly half as a result of the DEOA altering the structure and distribution of the polyurea hard domains (ca. 10 nm structure). Taken together, these two studies help to underline the fact that every level of structure in a flexible foam contributes significantly to its properties.

The complex morphology of the solid state arises from the microphase separation that occurs during the production of the foam. Flexible polyurethane foams are based on two well known reactions. The “blow” reaction sequence typically involves the reaction of water with toluene diisocyanate to yield an amine, carbon dioxide and heat. The evolved gas and the reaction exotherm help to expand the fluid into a cellular structure, and the amine undergoes reaction with another isocyanate group to yield a urea linkage. Toluene diisocyante is typically used in an 80/20 blend of the 2,4 and 2,6 isomers, but other isomeric blends and other isocyanates are sometimes utilized. Generally, the blow reaction initiates first and proceeds at a faster rate yielding an essentially linear polyurea “hard” segment of four to six repeat units.

The second major reaction occurs between the isocyanate groups and the hydroxyl functionalities of the polyether polyol, and it generates a urethane linkage. Because the polyol

usually has a functionality between two and three, this process leads to a three dimensional covalent network. At some point, the concentration of hard segments being generated by the blow reaction will surpass a system-dependent solubility limit leading to a microphase separation of the urea-based hard segments which produces precipitates of the polyurea. Each of these precipitates or "hard domains" is another pseudo or physical cross-linking point that is instead dependent upon strong intermolecular interactions (i.e. hydrogen bonding) for its cohesive strength. These strong interactions cause the hard domains to internally organize in a specific way, sometimes termed "para-crystalline" ordering, and variation of their size and concentration has been shown to have profound influence on the overall properties of the foam. In slabstock foams with ca. 29 wt% hard segment material in the formulation, recent work from our own laboratory has shown that this ordering can lead to the formation of lamellae-like hard domains ca. 10 nm wide by 50-300 nm long.[5]

An additional structure is also frequently observed in slabstock foam systems. At high water feed concentration with a stoichiometrically higher feed of isocyanate, the urea precipitates can aggregate further to form what have been termed "urea balls" or urea-rich aggregates.[1,6] These larger aggregates (ca. 200-500 nm in diameter) are frequently observed in conventional slabstock flexible foam formulations of high water concentration; however, these structures are not typically observed in molded or high-resiliency (HR) foams of the same water feed concentration.[1,2,7] This difference results from the chemistry of the typical components (most significantly the polyol component) used in each. Other recent work has suggested that the polyurea balls in slabstock systems are actually aggregations of lamellae-like hard domains.[5] The typical slabstock formulation used for that study, having 4 parts water per hundred polyol and an isocyanate index of 105, suggested that even at relatively low volume percent (estimated to be 24 vol. % hard segment material) the development of geometrically anisotropic hard domains may lead to significant amounts of connectivity and dramatically alter the properties of the solid state.[5,8]

A large amount of interconnectivity between the hard domains may lead to a much higher modulus (i.e. stiffness) than a polymer with a dispersed hard domain morphology would attain. Moreover, alterations in that interconnectivity might be observed as a significant softening. It was shown in the earlier study[3] that DEOA substantially softens the foam by disrupting the "para-crystalline" ordering of the hard domains.[9] This disruption occurs as the DEOA changes

the hard segment structure precluding the development of local ordering. However, it is unclear whether the softening occurred solely due to the changes in the packing of the hard segments within the hard domains (ca. 10 nm structure), or whether these alterations of the hard segment composition altered the larger scale morphology (ca.50-500 nm) that might lead to interconnectivity. Since the properties of these foams depend so strongly upon the morphology of the solid-state, and since DEOA is so widely utilized commercially, this work seeks to further elucidate the influence which that component has upon hard domain morphology.

4.3 Experimental

4.3.1 Materials

Two foam samples of flexible water-blown polyurethane foams were made with varying DEOA concentrations by workers using a Hi-Tech RCM 30 foam machine at Dow Chemical in Freeport, Texas. This operation consists of two hydraulic pistons to dispense the liquid components to the mixing head. The formulation components described below were prepared in two storage tanks, A and B. The A side consisted of the isocyanate. The B side consisted of the polyols, water, surfactants, and catalysts. An aluminum mold having dimensions of 15”x15”x4.5” was used and the mold was at room temperature when the reactive mixture was injected.

These foams were based on 72.25 parts of an experimental ethylene oxide endcapped polyether polyol produced by Dow Chemical which was based on a glycerine/sucrose mixed initiator and had a functionality ca. 2.4 and a molecular weight of 5000. The foams were also based on 27.75 parts of Voranol® 4703 (Dow Chemical), a 5000 molecular weight polyether triol. No copolymer polyol (a common reinforcing filler for molded foams) was used for these formulations. One foam was made with 1.275 DEOA parts per hundred polyol (pphp), and one was made without any DEOA. Total water in each foam was 3.82 pphp. Three catalysts were used: 0.22 pphp of Dabco® 33LV (Air Products and Chemicals) which is 33% triethylene diamine in dipropylene glycol; 0.08 pphp of Dabco® BL11 (Air Products and Chemicals) which is 70% bis(N,N dimethylaminoethyl) ether in dipropylene glycol; and 0.6 pphp of Niax® A4 (Union Carbide) which is a catalyst blend primarily promoting the gelation reaction but tends to increase the blow reaction rate as well. Two surfactants were utilized for the foam with DEOA to obtain the desired cell structure: 0.5 pphp of DC5043 and 0.5 pphp of DC5169. The foam

without DEOA required further stabilization and the surfactant blend was: 0.43 DC5043 pphp, 0.43 DC5169 pphp, and 0.15 BF2370 pphp. The 80/20 2,4/2,6 isomeric blend of toluene diisocyanate was used at a stoichiometric feed rate. Therefore, to maintain stoichiometry, the TDI was decreased in proportion to the decrease of DEOA. For the foam with DEOA, 45.39 TDI pphp were fed, and for the foam without DEOA, 42.27 TDI pphp were fed.

Because the density of pure polyurea was required for the estimation of hard segment volume, a pure polyurea powder was produced by dissolving the 80/20 2,4/2,6 isomeric blend of toluene diisocyanate in acetone and slowly feeding in an excess of water while vigorously mixing. The acetone was then evaporated and the resulting powder was dried in a vacuum oven. One powder sample was produced with a calculated number average of 10 repeat units, and another was produced with an average of 30 repeat units. These powders were highly crystalline as shown by the WAXS pattern in reference 9. To facilitate the estimation of density, the resulting powders were separated according to particle size, where one group was of ca. 1-3 mm in size and the other was of ca. 0.1 mm in size.

4.3.2 Methods

Atomic force microscopy (AFM) in tapping mode was utilized to study nanoscopic level structure. These experiments were performed on a Digital Instruments Scanning Probe Dimension 3000 Microscope using a Nanoscope IIIa controller and Nanosensors TESP (Tapping Etched Silicon Probe) type single beam cantilevers. These cantilevers had nominal lengths of ca. 125 μm, force constants of approximately 35 ± 7 N/m, and were used at oscillation frequencies at ca. 290 kHz. The samples were mounted and cured in epoxy (for 12 hours at 60°C) as for transmission electron microscopy, and cross-sections were cryo-microtomed smooth and then examined by AFM. The procedure used for flexible polyurethane foams is described further in reference 9.

Swelling experiments were performed to examine to study epoxy interaction with the polyurethane materials. One slabstock foam was studied, and SSu1.5 from Chapters 5 and 7. This foam was formed into voidless films (ca. 1 mil thick) by compressing it under ca. 15,000 lbs_f for two hours at 130°C. One plaque, PFI-110 from Chapter 8, was also examined, and it was formulated to be similar to the molded foams of this chapter. The initial widths (ca. 2 mm) of these samples were estimated with calipers and also from SEM micrographs of the non-sputter-coated samples. They were then cured in epoxy at 60°C overnight as all TEM and AFM foam

samples are in this dissertation. Upon removal from the curing oven the following day, caliper measurements were made of the samples in the epoxy. Once the samples were carefully removed from the epoxy, their dimensions were also reexamined via SEM. No swelling could be detected in any of the samples.

Density measurements on the polyurea powders were performed using a Denver Instruments Co. analytical balance model A-200DS and a Micrometrics Accupyc 1330 pycnometer. Argon was the expansion gas used for the pycnometer. Because the polyurea was in powder form, it was important to evaluate whether the pycnometer was correctly estimating the volume occupied by the sample. If the powder was too tightly packed, an over estimate of the volume would occur resulting in dependence of the density measurement on particle size. Two samples of different particle sizes were therefore used for each molecular weight polyurea powder, but no such variation was found.

Small angle X-ray scattering (SAXS) was utilized to provide quantitative characterization of the microphase separation for comparison with the AFM micrographs. Nickel filtered CuKα radiation having a wavelength of 1.542 Å was produced with a Philips model PW1729 generator operating at 40 kV and 20 ma. A slit collimated (0.03 x 5 mm) Kratky camera with a Braun OED 50 position-sensitive platinum wire detector was utilized for the scattering experiment. Because the apparent density of these foam samples did not vary with DEOA content, the beam path length was not corrected to account for the voids in the sample. Any error thus introduced to the absolute intensity of the SAXS profile is not expected to alter the relative comparisons for which this data was utilized.

4.4 Results and Discussion

The properties of flexible polyurethane foams are well known to be largely dependent on their microphase separated morphology to the extent that alterations in that phase separation can have dramatic effects. This is discussed at length in references 2 and 9. However, many techniques have proven to be limited in the analysis of these materials by either the scale lengths that they study or their attainable resolution. For example, SAXS has proven to be valuable for studying the microphase separation, but it is not useful for evaluating phase separations on the scale of 500 nm.[9] TEM is another useful technique but obtaining adequate contrast for imaging in these materials at ca. 50 nm has proven to be difficult.[10] Phase imaging with tapping mode AFM, on the other hand, has been shown to be useful over a broad range of length scales

because it relies upon stiffness variation in the local surface rather than upon electron density differences. Furthermore, TEM utilizes 2-D projections of the thin sections and has the potential to convolute "z-axis" information, whereas AFM provides clear imaging of the morphology in the plane of the other two axes. These differences enabled AFM to be used in other work to show for the first time how the microphase separation as shown by SAXS relates to the macrophase separation typically observed via TEM.[5,9] As discussed earlier, this occurs through the formation of lamellae-like hard domains which have the potential to aggregate to form larger structures.

As can be seen in Figure 4.1a, the molded foam without DEOA exhibits an even dispersion of aggregates (ca. 50 nm in size). In typical phase images from tapping mode AFM, higher offsets are usually generated by interactions of the tip with materials of higher dynamic modulus; therefore, in Figure 4.1a the *lighter phases are richer in polyurea* and the *darker phases correspond to the polyol phase*. As discussed in the methods section, epoxy was not found to swell samples of these polymers, so it may be concluded that the lighter phases observed are polyurea and not epoxy which might have penetrated the sample. The polyurea aggregates of Figure 4.1a are smaller than what is typically observed in slabstock systems,[9] and this is attributed to the high content of ethylene oxide endcapping in the polyol used. Using polyols with higher concentrations of primary hydroxyl groups is known to improve the solubility of the hard segments in the polyol. Even at the low magnification of Figure 4.1a, the aggregates appear to be geometrically anisotropic, and this is shown to be true in the higher magnification micrograph of Figure 4.1b. As was shown in reference 5, it appears that the hard domains are actually lath-like, with dimensions of ca. 5 nm wide by 50-100 nm long. Moreover, Figure 4.1b suggests that what appeared at low magnification to be polyurea aggregates are the association of several of these lamellae-like polyurea hard domains. Figure 4.1b also seems to attest to a high degree of interconnectivity between the larger polyurea aggregates. These micrographs suggest that the lamellae-like structures previously only observed in slabstock systems may also occur in molded foams when DEOA is not utilized. This suggests that the formation of lath-like structure is more dependent on the structure of the TDI-water based hard segment than upon the polyol system utilized.

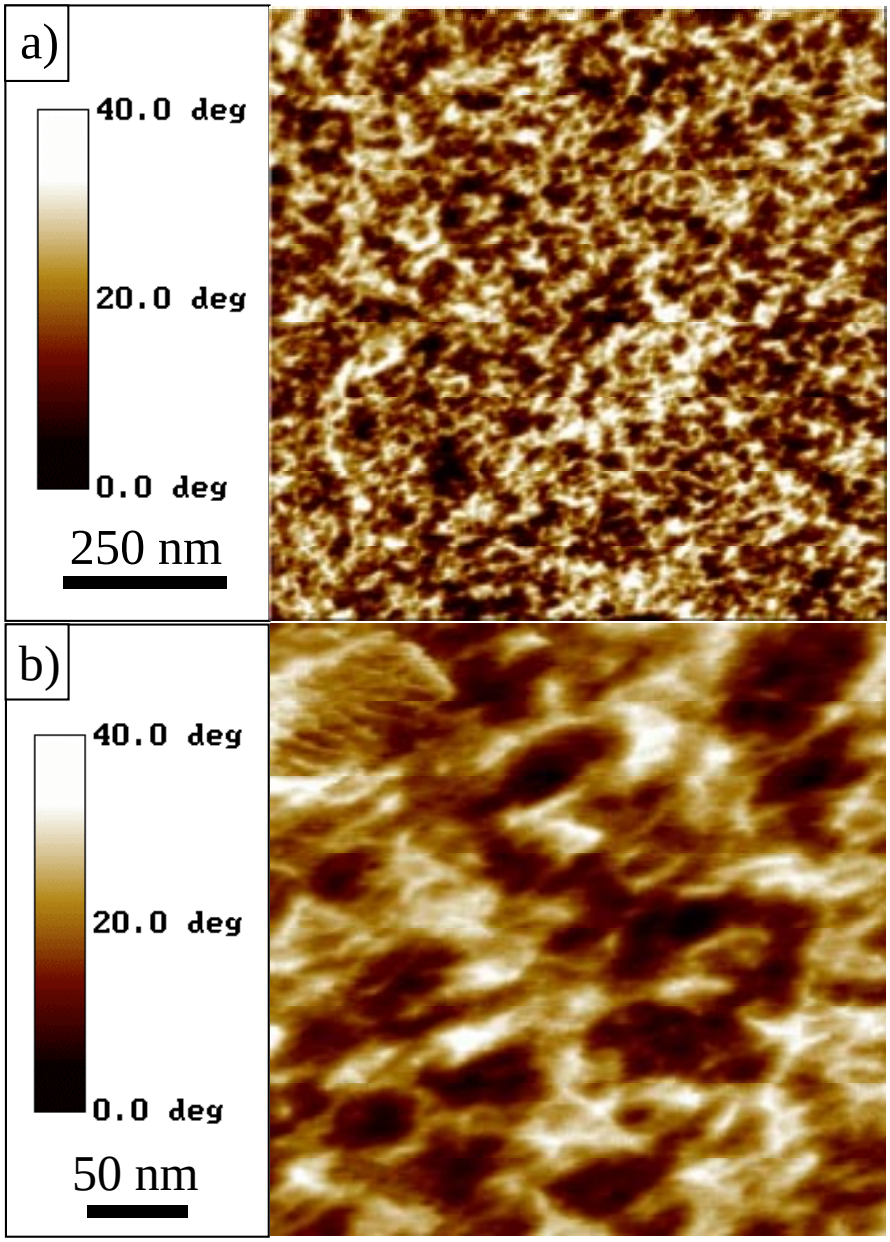

Figure 4.1 AFM phase images of a molded foam without diethanolamine at a) low magnification and b) high magnification

Once DEOA is added, however, the morphology of the solid state is dramatically altered. As Figure 4.2a reveals, the hard domains appear to be much smaller and very evenly distributed throughout the surface. No aggregates (ca. 50 nm) were observed in these samples, and the lower level of structure, that of the polyurea hard domains, can also be seen to be different. As observed by comparing Figures 4.1a to 4.2a, the hard domains appear to be smaller (ca 5 nm) and more geometrically isotropic in the foam with DEOA. This conclusion is borne out by comparing Figures 4.1b and 4.2b. The hard domains in Figure 4.2b are not the lath-like

structures of Figure 4.1b, and they have not aggregated as much as in Figure 4.1b. Although a few anisotropic structures are observed in Figure 4.2b, they are not as large and do not appear to occur as frequently. Figure 4.2b also suggests a much lower degree of interconnectivity between the hard domains.

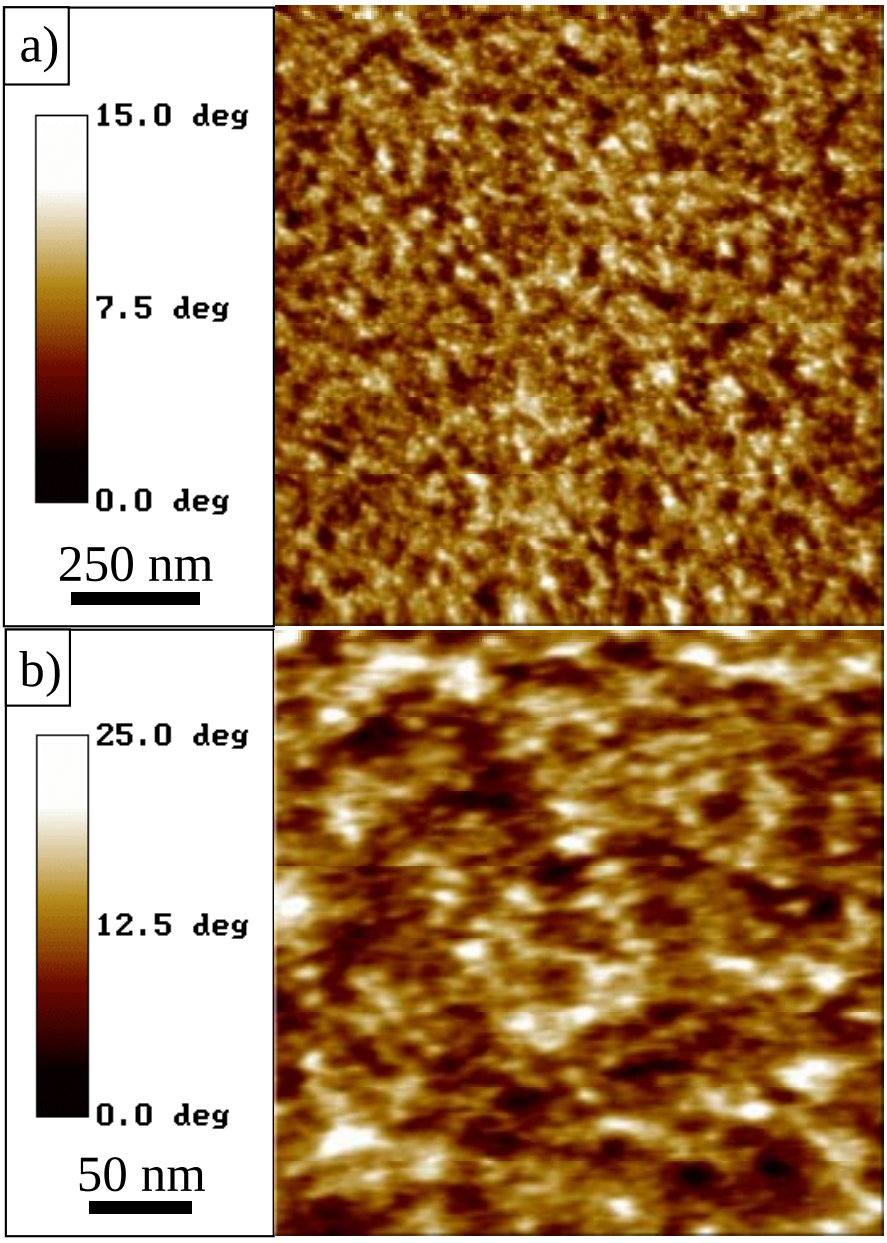

Figure 4.2 AFM phase images of a molded foam with diethanolamine a) at low magnification, b) showing the hard domain dispersion at high magnification

It is worth considering the significance of having no larger structures in the DEOA containing foams. Aggregations have been observed via TEM by other workers in materials with higher DEOA and TDI feeds [7], but they were found to occur irregularly in the sample in

comparison to the aggregates of slabstock systems. It has been therefore hypothesized that aggregates occur in DEOA containing systems as a result of difficulties in keeping the liquid reactive mixture homogeneous while the foam is forming.[7] In slabstock foam, polyurea aggregates tend to form evenly throughout the material[2] as a result of association between lath-like polyurea hard domains which occur everywhere in the material.[5] In molded foams, when enough DEOA is added, the reactive mixture can phase separate even before the polyurea hard segments precipitate into hard domains. It is observed here that the sample without DEOA, which has a lower hard segment content (27 wt. %), forms aggregates evenly throughout the matrix; however, the DEOA containing sample (29 wt % hard segment content) does not. This suggests that DEOA distinctly alters the mechanism of aggregate formation. Without the DEOA, the evenly distributed aggregates appear to form as the association of lamellae-like hard domains. However, considering the data of the other study,[7] it is suggested that a hard segment solubility limit in the polyol system must be surpassed to induce a phase separation leading to the formation of irregularly spaced aggregates. These samples were clearly below that limit and therefore exhibited no polyurea aggregation.

An interesting correlation to consider is that the SAXS of similar materials revealed that adding DEOA alters the interdomain spacing from ca. 9 nm without DEOA to ca. 12 nm with DEOA.[3] Figure 4.3 shows that, for these foams, the interdomain spacing was 9.5 without DEOA and 12.7 nm with DEOA. Considering the morphology observed in Figure 4.1b, this suggests that without DEOA, the SAXS spacing may be an indicator of the most probable distance between lamellae-like structures *within the polyurea aggregates*. This is hypothesized because it observed in Figure 4.1b that the spacing between the hard domains outside of the aggregates is ca. 30-50 nm which is much too large to explain the shoulder in the typical SAXS profile.[3] Moreover, where it could be measured within the aggregates of Figure 4.1b, the distance between the lamellae was ca. 10 nm. On the other hand, Figure 4.2b shows that with DEOA a ca. 13 nm spacing frequently occurs as the distance between the geometrically isotropic ca. 5 nm hard domains which are distributed evenly across the sample. *This may indicate that the ultimate result of the composition change that occurs with DEOA addition is a reduction in the association between hard domains.* The interdomain associations are weakened and so the hard domains themselves become more evenly dispersed and further apart, thus the reduced hard domain interconnectivity results in a polymer that exhibits a lower modulus (i.e. stiffness).

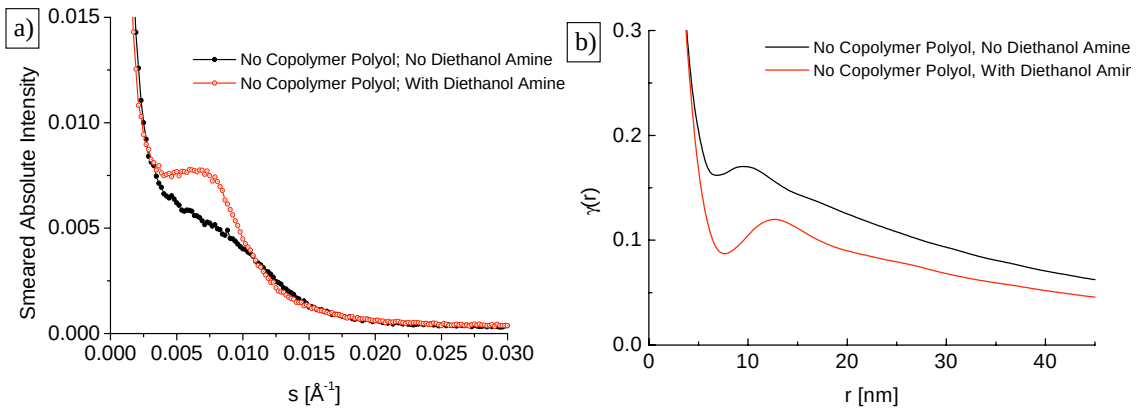

Figure 4.3 a) SAXS profiles for the foam samples with and without DEOA b) Three dimensional correlation functions for the foam samples

It can also be observed that the shoulder in the SAXS profile of Figure 4.3a becomes much sharper when DEOA is added to the formulation. This suggests a more even periodic microstructure such as is observed in Figure 4.2b in comparison to Figure 4.1b. The less distinct shoulder of the SAXS profile without DEOA is similar to what is commonly observed in slabstock foams, and it suggests a broader distribution of interdomain distances and/or hard domain sizes throughout the sample. This corresponds well to Figure 4.1b, wherein urea-rich domains (i.e. aggregates) are separated by ca. 30-50 nm urea-poor regions, and the aggregates themselves contain several lamellae which are spaced at ca. 10 nm.

As with an earlier AFM study on slabstock foams,[3] the micrographs presented suggest a higher volume percent of hard segment material than would be expected from the formulation. To estimate the volume fractions, the densities of the respective phases in the foam are required, but the range of volume percents possible can be estimated by using the densities of the pure components. For that purpose, the densities of the polyurea powders described earlier were evaluated with a pycnometer. It was found that the pure polyurea had a density of 1.3 ± 0.002 g/cm^3 which was independent of both the particle size and the calculated molecular weight of the polyurea hard segment. The polyols used had densities of 1.0 g/cm^3. The foam without DEOA, having 27 weight percent hard segment material, would have a hard segment volume percent between 22 and 27%, depending on how organized the hard domains are relative to the packing that occurs in pure polyurea powder. Assuming that all of the DEOA becomes incorporated into the hard domains,[3] the foam with DEOA, which has 29 weight percent hard segment material, would result in hard segment volume percents between 23 and 29 %. The micrographs, such as

Figure 1a, suggest volume percents higher than that range, and this is suggested to mainly result from the well known difficulties associated with using 2-D micrographs to evaluate volume fractions. Additionally, three other factors in these materials might contribute further to this. Primarily, the intermixing of hard and soft material even in the larger aggregates makes characterization of domain sizes more challenging. Secondly, secondary interactions at the interface of every hard domain could lead to stiffening of the polyol which would result in higher phase offsets, thus increasing the apparent size of the hard domains in the micrograph. Finally, material below the surface as deep as ca. 100 Å can induce offset in the tip, so some hard domain material just below the microtomed surface may appear in the image thus over representing the hard domains of the microtomed plane.

4.5 Conclusions

These results have shown that the use of DEOA in the formulation of molded flexible polyurethane foams has clear effects on the morphology of the solid state. The DEOA was shown to disrupt the formation of long (ca. 100 nm) lamellae-like polyurea hard domains. It also disrupts the formation of an consistent distribution of polyurea aggregates (ca. 50 nm in diameter) and instead yields a finer dispersion of isotropic ca. 5 nm hard domains. It is hypothesized that this change reduces the strength of the interconnection between hard domains, leading ultimately to a solid state with a lower modulus (i.e. stiffness).

4.6 Acknowledgments

The authors gratefully acknowledge the Dow Chemical Company for their financial support of this work and for supplying the necessary samples. We also would like to thank Dr. Herve Marand in the Chemistry Department of V.P.I. & S.U. for the use of the pycnometer in his laboratory. Christopher Robertson is also acknowledged for his assistance in the performance of the density measurements.

4.7 References

1. Herrington R; Hock K; Flexible Polyurethane Foams, 2nd Ed.; The Dow Chem Co: (1998)
2. Dounis DV; Wilkes GL; *Proc of the Polyurethanes 1995 Conf*: (1995) 353
3. Kaushiva BD; Wilkes GL; *J Appl Polym Sci*: (1999) in press
4. Dounis DV; Wilkes GL; *J Appl Polym Sci*: **65** (1997) 525
5. Kaushiva BD; Wilkes GL; *Polym Comm*: (1999) in press
6. Armistead JP; Wilkes GL; Turner RB; *J Appl Polym Sci*: **35** (1988) 601
7. Lidy WA; Rightor E; Heaney M; Davis B; Latham L; Barnes G; *Proc. of the Polyurethanes World Congress '97*: (1997) 95
8. Abouzahr S; Wilkes GL; Ophir Z; *Polymer*: **32** (1982) 1077
9. Kaushiva BD; McCartney SR; Rossmy GR; Wilkes GL; *Polymer*: (1999) in press
10. Neff R; Adedeji A; Macosko CW; Ryan AJ; *J Polym Sci B: Polym Phys*: **36** (1998) 573

5 Uniaxial Orientation Behavior and Consideration of the Geometric Anisotropy of Polyurea Hard Domain Structure in Flexible Polyurethane Foams

5.1 Chapter Summary

Atomic Force Microscopy (AFM) and Wide Angle X-ray Scattering (WAXS) were used to examine the morphology of hard domains in flexible polyurethane foams and plaques based on slabstock formulations. In plaque samples that were uniaxially deformed to 50% elongation, WAXS was utilized to demonstrate transverse hard segment orientation relative to the axis of deformation. AFM was utilized to directly observe the morphology of the foams and plaques. Micrographs from this technique present, for the first time in polyurethane foam systems, lamellae-like structures ca. 0.2 μm long and ca 10 nm across. These structures are believed to be precipitates of polyurea hard segments and are considered to be responsible for the orientation behavior presented.

5.2 Introduction

Flexible polyurethane foams are currently utilized in a broad range of applications in such areas as furniture, packaging, and transportation. Although polymer composition varies with each different product, this chemically complex family is united by utilizing a urethane linkage to covalently bond hard segments with soft segments. This linkage is typically formed from the reaction between the isocyanate functionality of one component with the hydroxyl group of another component. By controlling the composition of each component, two solid state phases are expected. This two-phase morphology provides the key to controlling performance of the final product and gives the manufacturer versatility in tuning properties as desired by varying the composition or content of one or the other phases.

One phase of typical water-blown foam systems is based upon the reaction of water with a diisocyanate such as toluene diisocyanate (TDI). This reaction initially produces a carbamic acid which then decomposes yielding heat, carbon dioxide, and an amine functionality.[1] The heat and carbon dioxide contribute to the expansion of the gas-liquid phase separation in the reactive mixture and so play important roles in the development of the foam's cellular structure. On the other hand, a disubstituted urea product results from the reaction of the amine with other

isocyanate groups. A "hard segment" results from several isocyanate groups covalently bonding through the urea linkages, and solid-state phase separation in typical systems arises from the precipitation of these segments into "hard domains." A more detailed discussion of the morphology and composition of these polyurea based hard domains may be found in reference 11.

An additional structure is also sometimes observed in these foam systems. At high water feed concentration with a stoichiometrically higher feed of isocyanate, the urea precipitates can aggregate further to form what have been termed "urea balls" or urea-rich aggregates.[1,2] These larger aggregates are frequently observed in conventional slabstock flexible foam formulations of high water concentration; however, these structures are not typically observed in molded or high-resiliency (HR) foams of the same water feed concentration.[1,3,4] This difference results from the chemistry of the typical components used in each. Whereas both molded (HR) and slabstock flexible foams most commonly utilize TDI (fed at an 80/20 2,4/2,6 isomer ratio), the polyol used for each is one major formulation difference. The higher primary hydroxyl content in molded foam polyols provides a much faster reaction rate and therefore requires a different blend of catalysts as well as lower potency surfactants to obtain an open celled foam. Also, increasing the EO content of the polyol dramatically alters the miscibility of water and other reaction components. Furthermore, it is believed that variation of the EO/PO ratio also has profound effects on the solubility of the hard segments in the polyol matrix of the final foam. It is therefore deduced that the larger aggregates (urea balls) may form as either the hard segments or the urea precipitates or some combination of both reach a molecular weight or a concentration that surpasses a solubility limit which varies depending on the chemical system being utilized.[1,2]

In examining how these materials behave during mechanical deformation by using FTIR linear dichroism techniques, workers[5] have shown initial hard segment orientation transverse to the direction of elongation in flexible slabstock foams followed by transformation to parallel orientation parallel to the stretch direction at higher uniaxial deformations. This somewhat surprising orientation behavior, also consistently well noted in segmented polyurethane elastomers,[6,7,8,9] has been explained by suggesting that hard domains are associating with one another to form lamellar-like structures which then dissociate under shear yielding and rupturing at the higher elongations, thereby causing the transformation of the smaller hard segment bundles to show orientation from partially perpendicular to partially parallel to the deformation

axis.[5-9] Considering the interdomain distances typically observed via small-angle x-ray scattering (7-11 nm), this orientation behavior suggests that these spacings may not result from a dispersion of small, geometrically isotropic hard domains. It instead indicates that such spacings may be the distances between lamellar-like formations, and that much larger lateral dimensions of the lamellae exist. However, well defined lamellar-like structure on any larger scale in polyurethane foams has not been unambiguously observed via microscopy. Recent work by Neff et al[10] has attempted to utilize TEM to probe the scale lengths below that of the polyurea aggregates which are ca. 50-200 nm. By degrading the samples with the electron beam, image contrast was enhanced enough for the micrographs to suggest the presence of evenly distributed anisotropic structures on the order of 1 nm across with lengths ca. 4-6 nm.[10] Given the beam damage, and thus the pronounced local chemical changes, required to induce the formation of an observable structure, the question remains whether such structures occur in a polyurethane foam under typical conditions. Also, the chemistry and space filling considerations suggest that the observed domains might contain only a few hard segments oriented parallel to the long axis of the polyurea precipitate. Therefore, hard domain structure on that level would not explain the orientation behavior observed, and it does not provide an explanation for how the microphase separation (as observed via SAXS, ca. 7-11 nm) relates to the macrophase separation (typically observed via TEM, ca. 50-200 nm). This discussion brings up the question of how well dispersed the hard domains actually are in polyurethane foams.[11] One would, however, expect that the level of hard domain dispersement or its inverse, domain connectivity, would depend on the relative composition or volume fractions of the respective hard and soft segment components. In fact, an earlier report from this same laboratory addressed this issue for segmented urethane elastomers.[12] Of interest is whether such domain connectivity exists in urethane foams and what is the nature of the morphological texture of the respective hard segment regions. This report will attempt to address this topic.

Given the wide use of polyurethane foams and elastomers, and the dependence of their properties on these hard domains, it can be seen that it would be valuable to understand their morphology. In particular, it would be of great importance to understand how the hard domains relate to the larger urea ball structures. In a recent publication, the authors have presented strong evidence that the WAXS 4.7 Å reflection frequently observed in these materials results from ordered packing of hard segments via bidentate hydrogen bonding which is commonly detected

via FTIR.[11] This local packing provides a Bragg spacing that is perpendicular to the long axis of the hard segments, and that spacing yields the observed WAXS reflection. A postulate to be tested in this study is that if such a link exists, the orientation behavior previously observed through linear dichroism should also be detectable with WAXS. This would be observed as the 4.7 Å reflection becoming more concentrated in the meridional regions of a uniaxially deformed sample. This study will therefore utilize samples characterized in another work to further elucidate the hard domain morphology between the scale lengths of SAXS and TEM.

5.3 Experimental Materials and Methods

5.3.1 Materials

Samples of flexible water-blown polyurethane foams were made with conventional slabstock formulations.[1] These samples were based on 100 parts of ™Voranol CP 3322 (Dow Chemical), a triol containing 88% propyleneoxide and 12% ethyleneoxide with terminal secondary OH-groups. The foams also used 4 parts of water and TDI 80 (an 80/20 mixture of the 2,4/2,6 isomers) fed at an isocyanate index of 105. Dimethylethanolamine was used as a catalyst for the water-isocyanate reaction at a concentration of 0.2 parts per hundred polyol (pphp). Stannus octoate was used as a polyol-isocyanate reaction catalyst also at 0.2 pphp. The surfactant used was ™TEGOSTAB BF 2370 (Goldschmidt), and it was fed at a concentration of 1.5 pphp. BF2370 is a siloxane-polyether block copolymer with an average molecular weight of 8,800. The precise structure of BF 2370 is given in reference 11.

One foam was made that was allowed to fully develop with an additional 15 minute cure at 140°C to remove tackiness. This sample is named "SSu1.5." Two foams of the same formulation were also mechanically compressed to examine possible influences that the removal of cellular structure may have on the development of microphase separation in the solid state. One of these was crushed at 80 seconds to match the time at which a 0.0 surfactant pphp foam spontaneously collapsed. The other foam was crushed at 106 seconds, the rise time to final height for that foam formulation. For these samples, small quantities of material were taken from the reacting foam and then quenched or crushed. This was done to assure that the entire sample had a uniform thermal and morphological history characteristic of their respective times of quenching or crushing. The crushed samples shall be referred to as "C80-Su1.5" and "C106-Su1.5"

5.3.2 Methods

To explore the ordering of the hard domains, the WAXS technique was applied using a Philips model PW1720 generator equipped with a Warhus camera. Nickel filtered CuK radiation was used with a wavelength of 1.542 Å and pinhole collimation with a diameter of 0.020 inches. Samples were mounted in a uniaxial extension device designed to fit in the camera and expose the gauge section of the sample to the x-ray beam. Sample time was ca. 3 hours.

Atomic force microscopy (AFM) in tapping mode was also used to study nanoscopic level structure. These experiments were performed on a Digital Instruments Scanning Probe Microscope using Nanosensors TESP (Tapping Etched Silicon Probe) type single beam cantilevers. These cantilevers had nominal lengths of ca. 125 μm, force constants of approximately 35 ± 7 N/m, and were used at oscillation frequencies at ca. 290 kHz. The samples mounted and cured in epoxy for TEM at 60°C were cryo-microtomed smooth and then examined by AFM. The procedure used for flexible polyurethane foams is described further in reference 11.

5.4 Results and Discussion

As stated earlier, in reference 11 the authors presented evidence that ordered packing within the polyurea hard domains, which occurs as bidentate hydrogen bonding observed via FTIR, is the source of the 4.7 Å reflection observed via WAXS. As already discussed, FTIR linear dichroic evaluations of foams and elastomers have well demonstrated that the hard domains initially orient transverse to the extension direction.[5-9] Such behavior is believed to be only truly explained by the presence of lamellar-like hard domains in the polymer. Furthermore, there must be enough such domains in the material to dominate the FTIR linear dichroic measurements of orientation.

Figure 5.1 presents three WAXS patterns of the slabstock formulation samples which were crushed into plaques, C80-Su1.5 and C106-Su1.5. The deformation axis of the samples is always kept vertical. In Figure 5.1a, a typical WAXS pattern of an undeformed polyurethane foam material may be seen from sample C80-Su1.5, wherein a 4.7 Å reflection is observed with no azimuthal intensity dependence. This single maximum overlays an amorphous halo seen as a diffuse ring. Such uniformity is indicative of samples with no orientation. Figure 5.1b, however, shows the same sample extended at room temperature to only 50 % elongation. It may be observed in that pattern that there is an intensification of the 4.7 Å reflection around the

meridional centerline. However, on the equatorial axis, the reflection has lost enough intensity that it is difficult to differentiate it from the underlying amorphous halo. This is evidence of transverse orientation of the hard segments in the polymer, providing strong support of behavior observed via FTIR linear dichroism. This behavior is also seen in Figure 5.1c from sample C106-Su1.5 also extended to 50% elongation. Given the large morphological differences between these two samples, discussed at length in reference 11, this suggests that the formation of lamellae occurs widely in typical slabstock polyurethane foam polymers.

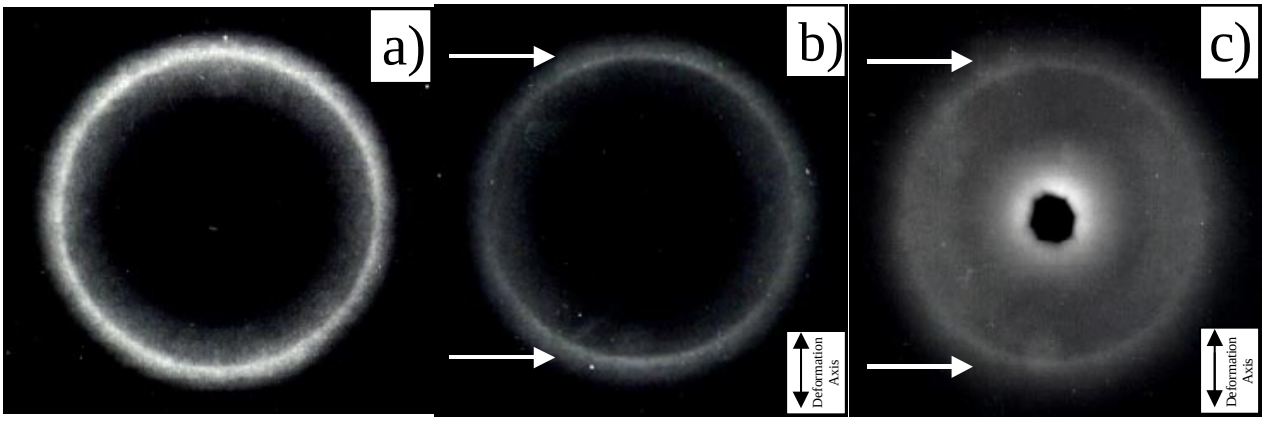

Figure 5.1 WAXS patterns of a) C80-Su1.5 before deformation; b) C80-Su1.5 at 50% elongation; and c) C106-Su1.5 at 50% elongation. White arrows note areas of intensification along the meridian. Axis of deformation is noted on WAXS patterns where relevant.

To find further information regarding the morphology of the hard domains, the technique of tapping mode AFM was applied. A phase image of the sample C80-Su1.5 is shown in Figure 5.2. This is a higher magnification view than any published in reference 11. The most important observation to make is that the higher phase offset features on this surface, which correspond to the polyurea hard domains, are not at all spherical in shape. Instead, it can be observed that thin lath-like aggregations are pervasive throughout the material. *It should be noted that the apparent orientation of the lath-like structures observed in Figure 5.2 was a local phenomenon, and that larger scale phase images and planar axis WAXS patterns revealed no distinct large scale planar orientation which might be induced by squeezing the sample into a plaque.* Where it could be measured in Figure 5.2, these lath-like structures had dimensions of ca. 18 nm across and range in length to as large as ca. 0.3-0.5 microns, and they were spaced ca. 30 nm from center to center. Interdomain distances from SAXS are typically 7-11 nm, and it is suggested that

the discrepancy largely arises because these measurements where made on domains away from the larger aggregates. It can be observed in Figures 5.2 and 5.3 that the laths are smaller and closer together within the large aggregations where consistent measurements are difficult to make. Also, if the laths are not normal to the cutting plane for the microtome, estimations of their size will contain error. Finally, it should also be noted that C80-Su1.5 was shown in reference 11 to have an atypical distribution of its aggregates. In TEM, 2-D projections of the thin sections reveal dark aggregates that are usually interpreted as polyurea rich domains; however, AFM does not convolute "z-axis" information but provides clear imaging of the morphology in the plane of the other two axes. Figure 5.2 clearly exhibits the formation of lath-like structure, and it suggests that large aggregations of polyurea hard segments may be clusters of these lath-like hard domains.

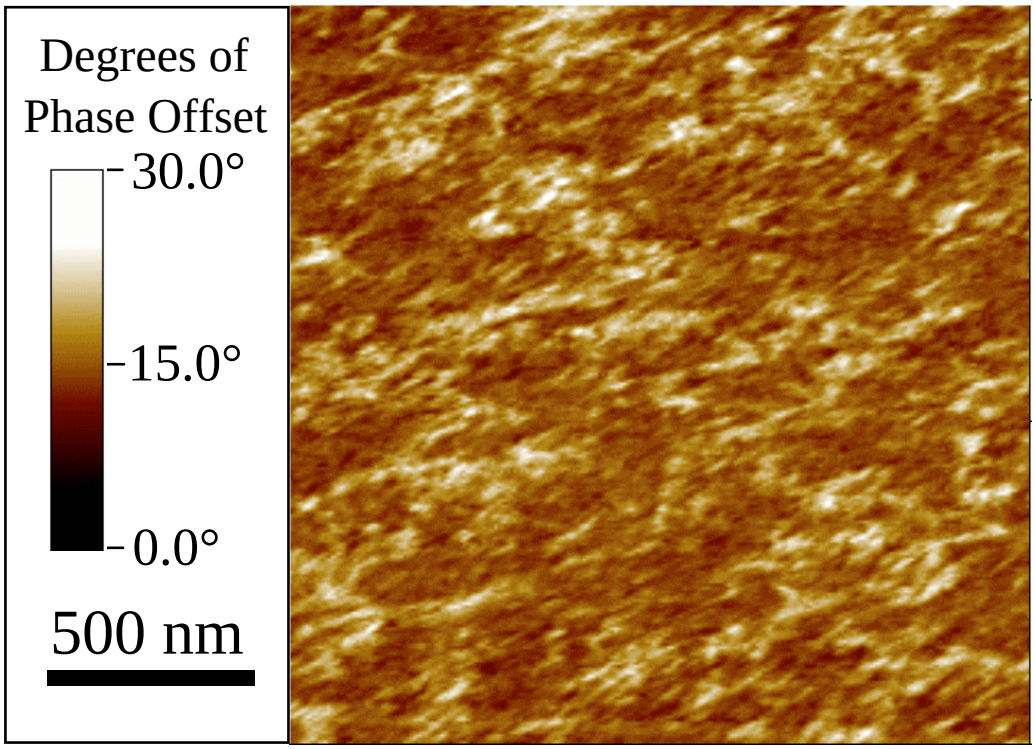

Figure 5.2 AFM Phase image of cryo-microtomed cross-section of foam sample C80-Su1.5

Figure 5.3 is another phase image from AFM of *a typical slabstock foam*, SSu1.5. It is observed in Figure 5.3 that the polyurea aggregations are larger and more evenly distributed across the surface, and this more even distribution relative to C80-Su1.5 is consistent with what was shown in reference 11. Upon closer inspection, however, it can be seen that similar if somewhat shorter lath-like domains can be observed throughout the image. At some places,

these lamellae-like structures even appear to bridge between larger polyurea aggregations. This suggests a higher level of connectivity than would be expected considering that these materials contained only 29 weight percent hard segment material (24 volume percent). It is hypothesized that this connectivity would lead to considerable stiffening of the polymer. It can be observed, especially in Figure 5.3, that more hard segment material appears to be present than just 24 volume percent, and this appearance is suggested to be the result of three main factors. Primarily the hard and soft domains are somewhat intermixed so that even the larger aggregates can be seen to contain some amount of polyol. This makes visual estimation of volume fractions difficult. Secondly, higher phase offset is induced by any stiff material, and it is likely that some polyol is stiffened through secondary interactions at the interface of every hard domain. This is supported by the observation of many domains in the image which induced intermediate phase offsets. Finally, material below the surface as deep as ca. 100 Å can induce offset in the tip, so some hard domain material just below the microtomed surface may appear in the image thus over representing the hard domains of the microtomed plane.

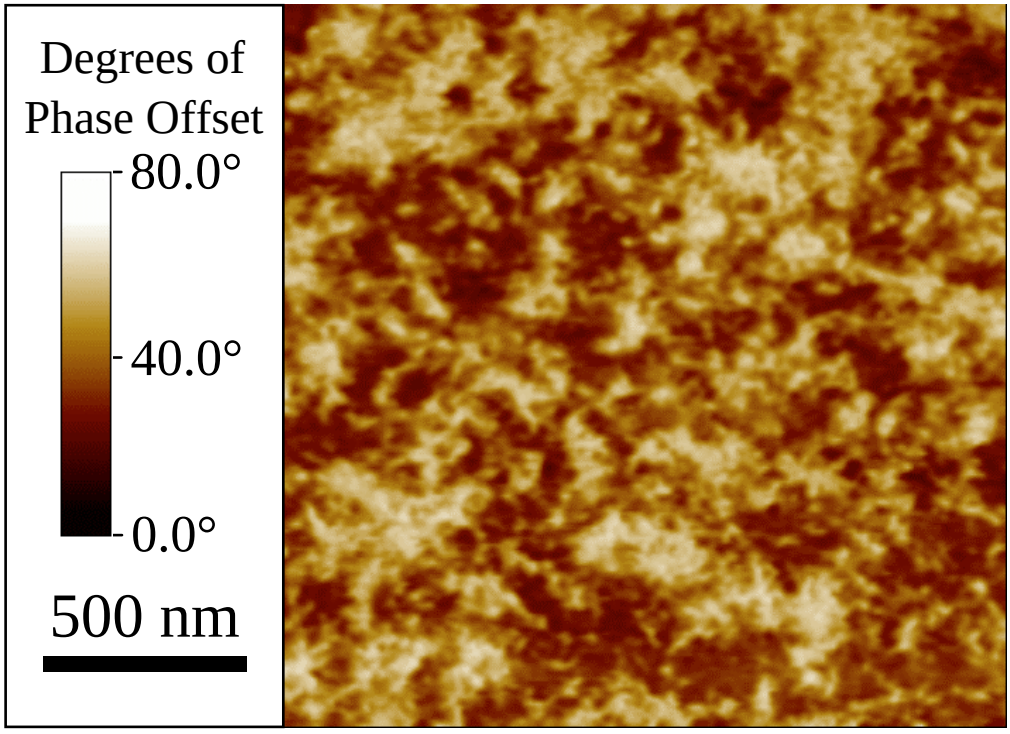

Figure 5.3 AFM Phase image of cryo-microtomed cross-section of foam sample SSu1.5

5.5 Conclusions

This study has shown that the polyurea hard domains do develop lamellar-like structure in typical slabstock flexible polyurethane foam systems. It is suggested that these lath-like structures develop as the polyurea hard segments precipitate into hard domains. Furthermore, it also appears from this examination that polyurea balls (macrophase aggregations) are clusters of these lamellae. This indicates that the polyurea balls may either form as developing lamellae spatially interfere with each other or as several lamellae grow out from a single nucleation site. Current work is examining the thermal stability of these lamellae and their orientation. Also materials based on a molded foam formulation will be used to examine whether the anisotropic hard domain morphology is ubiquitous in these materials or just isolated to systems wherein polyurea balls typically occur.

5.6 Acknowledgements

This work has been financially supported by the Dow Chemical Company and Goldschmidt AG, and their support is gratefully acknowledged. We also thank Helmut Schator of Goldschmidt AG for directing the slabstock foaming experiments at Goldschmidt AG. Finally, we acknowledge the contributions and many helpful discussions of Dr. Gerd Rossmy.

5.7 References

[1] Herrington R; Hock K; Flexible Polyurethane Foams; Dow Chem Co, Midland, MI: 1991
[2] Armistead JP; Wilkes GL; Turner RB; *J Appl Polym Sci*: **35** (1988) 601
[3] Dounis DV; Wilkes GL; *Proc. of Polyurethane 1995*: (1995) 353
[4] Lidy WA; Rightor E; Heaney M; Davis B; Latham L; Barnes G; *Proc of Polyurethanes World Congress '97*: (1997) 95
[5] Moreland JC; Wilkes GL; Turner RB; *J Appl Polym Sci*: **43** (1991) 801
[6] Siesler HW; *Pure Appl Chem* **57** (1985) 1603
[7] Wang CB; Cooper SL; *Macromolecules*: **16** (1983) 775
[8] Hoffman K; Bonart R; *Makromol Chem*: **184** (1983) 1529
[9] Kimura I; Ishihara H; Ono H; Yoshihara N; Nomura S; Kawai H; *Macromolecules*: **7** (1974)355
[10] Neff R; Adedeji A; Macosko CW; Ryan AJ; *J Polym Sci B: Polym Phys*: **36** (1998) 573
[11] Kaushiva BD; McCartney SR; Rossmy GR; Wilkes GL; *Polymer*: in press
[12] Abouzahr S; Ophir Z; Wilkes GL; *Polymer*: **23** (1982) 1077

6 Influences of Copolymer Polyol on Structural and Viscoelastic Properties in Molded Flexible Polyurethane Foams

6.1 Chapter Summary

In this study, the viscoelastic and morphological properties of molded foams were investigated to determine the influence of the presence or absence of reinforcing particulate copolymer polyols (CPP). The molded foams were based on toluene diisocyanate (TDI) and glycerol initiated ethylene-oxide endcapped polypropylene-oxide and, in most samples, some amount of copolymer polyol. Two series of foams were studied. In Series 1, as CPP is added to the formulation, the amount of TDI fed is kept constant. This results in a constant amount of hard segment content as the filler in the system displaces, by weight, the polyether polyol in the foam, and it increases the hard segment to soft segment ratio (HS/SS). In Series 2, the amount of hard segment material is proportionally decreased as CPP is added resulting in a constant HS/SS ratio. Structural investigations of the foams displayed rather similar textures. The cellular structures of a copolymer polyol (CPP) containing foam was very similar to a foam lacking the copolymer polyols. Transmission electron microscopy revealed that the CPP particles were well dispersed and that they possessed significant rigidity even at high temperature and under high compression. While all of the foams were microphase-separated, they varied slightly in that the copolymer polyol containing foams exhibited higher weight fractions of extractables in both Series 1 and Series 2. This suggests that not all of the CPP material is covalently bonded into the polyol matrix. It was found that temperatures above ambient as well as humidity "plasticized" the viscoelastic behavior of all the molded foams evaluated. It was also found that the copolymer polyol particles, as added to the molded foams of Series 1, increased load bearing capabilities but had a negative effect on the stress relaxation, creep and compression set properties. In particular the viscoelastic properties of the CPP containing foam were distinctly more time-dependent than those of the foam lacking these particles. However, the Series 2 foams show that most of these effects are a result of the increased HS/SS ratio and not a result of the CPP particulate. *It was shown that adding CPP while maintaining a constant HS/SS ratio improves percent load loss and load bearing under high humidity conditions, two important*

properties in flexible polyurethane foams. Finally, it was shown that at high temperatures (ca. 100°C) an additional relaxation mechanism occurs which cannot be attributed to changes in the HS/SS ratio, but must be a result of the CPP components themselves. This additional mechanism results in higher rates of load relaxation and creep in foams containing CPP at high temperatures for foams of both series.

6.2 Introduction

Polyurethane foams are used in a broad range of applications primarily in the areas of insulation, packaging and load-bearing such as cushioning. Molded foams, a relatively newer technology, are foams in which the formulation mix is either poured into a heated mold that is then closed or injected into a closed mold. Approximately one-fourth of all polyurethane foams produced commercially are molded foams as opposed to slabstock foams. The majority of molded foams are used in transportation seating and trim parts. However, they are also used in packaging, furniture, and novelty items. The biggest advantage is that the foam is molded into the intricate shape desired and, hence, the need for cutting is eliminated. Also, molded foams can be produced with inserts for reinforcement, multiple zones of hardness or with a liner such as a plastic or fabric skin all of which reduce labor costs of final product assembly.

Molded foams do not differ from conventional slabstock foams in just that they are produced in molds rather than in a semicontinuous process but, in fact, are considerably more chemically complex. Generally, higher molecular-weight, more reactive polyols are used in molded foams for reasons of increased productivity. Along with a higher reactivity formulation, factors such as size of individual shot, release agents, mold temperature gradients and curing times also contribute to the complication. Furthermore, the polyols can be and often are modified with fillers to produce open-cell foams of higher hardness.[1,2,3]

Polymeric “fillers” for foams are typically synthesized via either free radical or step addition polymerization. To prevent flocculation, the particles are stabilized through a grafting process where either the base polyol or an added stabilizer molecule copolymerizes with the added monomer leading to what are commonly designated as “copolymer polyols” or “CPP” particles. The most common filler or dispersion in polyether polyols is produced through chain-growth polymerization where free radicals are generated from an initiator molecule, typically an

azo compound. The dispersions, originally based on acrylonitrile as the sole monomer, were first used for the production of "cold-molded" high resiliency foams with increased hardness and strength. Due to deficiencies in certain properties such as lower flame resistance as well as a yellow appearance, styrene-acrylonitrile (SAN) mixtures are now used in place of acrylonitrile alone.[4] In this case, more efficient stabilizer species are required since copolymerization of the styrene and acrylonitrile is more favorable than either of the those with the base polyol.[1] Here, polymerization begins with a graft-polyol where the backbone is the SAN copolymer chain and the grafted species are the stabilizer molecules of the graft. As monomer and initiator are added, the "comb-like" polymers associate in a spherical structure where the insoluble copolymer portion, SAN, lies inside and the stabilizer chains extend outward. It is hypothesized that once these particles have phase separated to form micellar structures, polymerization occurs mainly inside these particles. During this stage, the particles grow from their initial size of 0.01-0.05 μm to a final size of 0.3-0.5 μm. High resiliency molded and sometimes slabstock foams are made with polyols having 10-40% solids and viscosities of 2500-4000 CP using this "macromer" process.

Although not as common, other fillers or dispersions are utilized in the production of polyurethane foams. For example, dispersions of polyurea particles known as the polyharnstoff dispersion (PHD) is one commercial protocol.[5,6] The particles are prepared through step growth polymerization of a diamine with a diisocyanate which are dispersed in a polyether polyol. These polyurea oligomers quickly phase separate from the continuous phase as their molecular weight increases but are "naturally" grafted to the base polyurea through reaction of the diisocyanate to the polyol. The filler is thus less grafted to the polyether polyol than in the case of SAN polyols since the amine-diisocyanate reaction is favored, which also leads to a broader size distribution of filler particles in the PHD dispersion. PHD polyols typically contain 20-30% solids and have viscosities of 3000-3500 cp. Along with polyurea particles, others such as polyurethane particles formed by the in-situ reaction of an isocyanate with an alkanolamine and new epoxy fillers can also be utilized.[1]

Besides the obvious cellular structure of polyurethane foams, the network structure within the polymer material also influences physical properties. The network structure in a typical molded polyurethane foam is comprised of both chemical and physical "cross-links" as

well as the copolymer dispersions. The chemical cross-links arise from the use of a hydroxyl polyol of functionality greater than two while the physical "cross-links" arise from the phase separated hard segment domains (urea segments). Although both types of "cross-links" enhance the foam's physical properties, the physical "cross-links" are labile at high temperatures and high humidity thus dramatically altering the foam's properties.[1] Since these are realistic conditions for CPP containing foams as well, the response of the CPP particles to these conditions is also of great importance. This is especially true in view of the fact that, to the authors' knowledge, work focusing on the properties of copolymer polyols is extremely limited in the literature and that foams containing CPP materials are used under many different conditions.

In view of the complexities just discussed, the need exists for a greater fundamental understanding of the relationships between the structure/morphology and physical properties of those polyurethane foams which are reinforced by a particulate phase. This paper will address that issue by examining two series of foams. Series 1 will examine the case where a fraction of polyol is simply displaced with CPP without otherwise changing the foam. This series will be used to evaluate properties and to study the influence of CPP on the structure of the foam. In Series 2, the composition of the foams will be varied as CPP is added to maintain a constant hard segment to soft segment ratio throughout the series. These foams will be used to isolate the influence of CPP on properties separate from the HS/SS ratio.

6.3 Experimental Materials and Methods

6.3.1 Materials

Two series of samples of flexible water-blown molded polyurethane foams were made with a Hi-Tech RCM 30 foam machine at Dow Chemical in Freeport, Texas. This operation consists of two hydraulic pistons to dispense the liquid components to the mixing head. The formulation components presented in Table 1 were prepared in two storage tanks, A and B. The A side consisted of the isocyanate. The B side consisted of the polyols, water, surfactants, and catalysts. The CPP particles were dispersed in the polyol for the foams containing these particles. An aluminum mold having dimensions of 15"x15"x4.5" was used. This mold was heated to 140°F (60°C) at which point the foam mixture was dispensed into the mold. For Series 1, the mold was also placed in an oven at 250 °F (121 °C) for 2.5 min. after which the foam pad

was removed and mechanically crushed by passing it three times through steel rollers while decreasing the gap. For Series 2, the mold was preheated to 68°C, and the pads were left to cure in the mold (at ca. 140 °C) for four minutes after which they were removed from the mold and mechanically crushed twice by passing them through steel rollers with a one inch gap. It should be emphasized that properties of a foam sample will only be compared with foams within the same series except for the case of solvent extraction. Therefore the relatively small differences between the manufacturing techniques of the two series should not be of great concern.

The nomenclature of the Series 1 samples presented in Table 6.1 is as follows: "M1" denotes a molded foam sample from Series 1, the third character denotes whether the copolymer polyol was used - "n" refers to no CPP utilized, "c" refers to the presence of a CPP phase. Recall that as a result of the addition of copolymer polyols (CPP) this foam had a reduced soft segment content while the hard segment content (TDI + H_20) is relatively unchanged. This dramatically alters the ratio of hard segment (HS) material to soft segment (SS) material. Series 1 reflects the manner in which CPP components are typically added industrially, where the water and TDI to be added is calculated based on the total weight of the polyol component including the filler weight. It is also noted that M1c contained 17.5 wt % SAN material in its polyol.

To study the influence of CPP addition in foams with a constant ratio (by weight) of hard segment content to soft segment content, the Series 2 foams were produced. The goal of this series was to separate the effect of altering the HS/SS ratio from the effect of introducing CPP. The nomenclature for the Series 2 samples presented in Table 6.2 is as follows: "M2" denotes a molded foam sample from Series 2, the next character, "F," indicates that the filler content is the variable and it is followed by the weight percent of the SAN material in the polyol of that foam (0.0, 3.3, 6.5, 9.8, or 13.0 parts per hundred polyol or pphp). It should be noted in Table 6.2 that, although the diethanolamine, H_2O, and TDI content are all being proportionally reduced to maintain a constant HS/SS ratio, the isocyanate index is maintained at 100 for all of the samples.

Table 6.1 Series 1 Foam Formulation Components (all formulation amounts are given in pphp)

Component	Details	Sample M1c	Sample M1n
Voranol 4703	5000 mol. Wt. ethylene-oxide capped triol, Dow Chemical	50	100
Voranol 4935	copolymer polyol of Voranol 4703, styrene and acrylonitrile which react into the network	50	0
H_2O		4	4
Diethanolamine	cross-linking agent	1.6	1.6
Y-10515	surfactant	1.08	0.5
DC-5244	surfactant	0.54	0.5
DC-5169	surfactant	0.0	0.5
DABCO 33LV	catalyst	0.43	0.34
NIAX A107	catalyst	0.32	0.26
NIAX A4	catalyst	0.32	0.26
TDI	80/20 blend of 2,4 and 2,6 toluene diisocyanate	47.68	48.4
Density [lb/ft^3]		1.9	2.0

Table 6.2 Series 2 Foam Formulation Components (all formulation amounts are given in pphp)

Component	M2F0.0	M2F3.25	M2F6.5	M2F9.75	M2F13.0
5000 MW polyol	72.25	69.00	65.75	62.50	62.86
Voranol 4703	27.75	21.72	15.68	9.64	0.0
Voranol 4935	0.0	9.29	18.56	27.86	37.14
DC-5043	0.5	0.5	0.5	0.5	0.5
DC-5169	0.5	0.5	0.5	0.5	0.5
DABCO 33LV	0.15	0.15	0.15	0.15	0.15
NIAX A11	0.08	0.08	0.08	0.08	0.08
NIAX A4	0.6	0.6	0.6	0.6	0.6
Diethanolamine	0.23	0.22	0.21	0.20	0.19
Total Water	3.82	3.70	3.57	3.45	3.32
TDI 80	44.75	43.73	42.28	40.84	39.37

6.3.2 Methods

The cellular structure of the foams was evaluated and compared using scanning electron microscopy (SEM). Thin slices (3 - 4 mm) of foam were adhered to aluminum stubs using silver paint and allowed to dry. A thin layer of gold was then applied to the surface of the foam using a SPI model 13131 sputter coater. Micrographs were taken using a Stereoscan 100 SEM (Cambridge Instruments, Ltd.) operating at 20 kv and at a magnification of approximately 30x.

The precipitated particulates were observed using transmission electron microscopy (TEM). Thin samples were cut in a similar manner to those for SEM. From these samples, very thin sections were cryogenically microtomed using a diamond knife on a Reincart Junct model FC40 ultramicrotome operating at -90 °C. Ethanol was used to collect the sections onto 600 mesh copper grids. Some micrographs were taken using a Zeiss 10CA transmission electron microscope equipped with a LaB_6 electron gun operating at an accelerating voltage of 80 kv. Others were taken using a scanning transmission electron microscope (STEM) operating at an accelerating voltage of 80 kv.

Dynamic mechanical analysis (DMA) was carried out using a Seiko model 210 in the tension mode. The samples were heated from -100 °C to 140 °C at a rate of 1 °C/min. from which the storage modulus (E') and tan δ data were collected at a frequency of 1 Hz. The sample dimensions were approximately 6.8 x 6.8 x 25 mm with a grip-to-grip distance of 10 mm.

Phase separation was evaluated using small angle X-ray scattering (SAXS) scans which were obtained with a Phillips model PW1729 generator operating at 40 kv and 20 ma. The smeared intensity data were collected using a Kratky camera, with nickel filtered CuKα radiation having a wavelength of 1.542 Å passing through a slit collimator (0.03 x 5 mm). The detector used is a Braun OED 50 position-sensitive platinum wire detector. The raw data were corrected for parasitic scattering and normalized using a Lupolen standard. The foam samples were cut approximately 10 mm thick and compressed to approximately 3 mm.

Extraction experiments were carried out on selected samples to compare the level of cross-linking (gel fraction). Series 1 samples (<0.15 g) were submerged in DMF of approximately 10x the foam volume for a period of 48 hours and then taken out and dried under vacuum at 40 °C for approximately 24 hours after which the temperature was raised to 80 °C for an additional 48 hours. The samples were then weighed again. Series 2 samples were

submerged in a succession of DMF solutions of LiCl. Lithium chloride solutions are used to increase the rate of extraction for these materials by disrupting the level of hydrogen bonding, thus facilitating the evaluation of the amount of extractable material in a given sample. The succession consisted of two submersions at 10 wt % LiCl, one at 6 wt %, one at 3 wt %, followed by three submersions at 0 wt %. The period of each submersion was four to five days. The samples were then repeatedly evacuated at 40 °C for two weeks followed by two days at 80 °C. Samples were weighed throughout the drying process until a stable weight was achieved. The level of weight lost via extraction provides an index of the sol fraction while the remaining extracted matrix represents the gel fraction.

Compression load-strain measurements were conducted using the identical experimental setup used in the load relaxation measurements (described later). The 3.5" x 3.5" x 1" samples were first dried under vacuum and at 40 °C for 3.5 hr. and placed in an environmental chamber at 30 °C-35%R.H. for ca. 60 min. The samples were then compressed at 350 mm/min. to 75% strain and released. This was done to compare the level of hysteresis as a function of CPP content used in the formulation. By numerical integration, the energies upon loading and unloading were calculated and subsequently the fractional hysteresis determined by the relation $1 - E_u/E_l$, where E_u is the energy upon unloading and E_l is the energy upon loading.

Load relaxation experiments were performed using a similar procedure as that used and described by Moreland which was originally designed to mimic the ASTM procedure used for IFD testing.[9] Samples, having dimensions of 3.5" x 3.5" x 1", were cut from the foam bun using a band saw equipped with a smooth "wavy edge" saw blade to eliminate tearing. Each sample was first dried under vacuum and at 40 °C for 3.5 hr. in order to equilibrate each sample to an equal level of moisture content. The samples were then placed in an environmental chamber preset at the testing conditions for ca. 60 min. The environmental chamber was purchased from Russells Technical Products and was equipped with a Watlow 922 microprocessor which controls temperature in the range of 20 °C to 300 °C and humidity in the range of 0 to 100 %. The chamber was fit into the Instron frame equipped with a model MDB-10 compression load cell manufactured by Transducer Techniques. Using a 2" indentor, initially at rest, the samples were twice compressed to 70% and released at a rate of 350 mm/min. After five minutes the

samples were compressed to 65% strain at which point the load was immediately monitored via computer. At 65% compression, relaxation is believed to occur predominately within the solid polymer independent of cellular structure since the onset of "densification" is observed here.

Compression creep experiments were carried out using a device consisting of a twin shaft assembly with a freely moving carriage manufactured by Thompson Inc. Attached to this carriage is an arm which extends into the environmental chamber and is capped with a 2" indentor. This indentor is initially set in contact with the top surface of the foam that is resting on a plate. Also attached to this carriage is the capillary of a linear voltage displacement transducer (LVDT) used to monitor any displacement in the thickness of the foams. The analog voltage signal is sent to a computer equipped with an A/D card converting it to a digital signal which is then converted to strain via a calibration procedure. Also attached to the carriage is a pulley system that enables the user to vary the applied load from approximately 100 g to 5 kg. Conditioning of the samples was carried out in a similar manner to the samples used in the load relaxation measurements. First, the samples were dried and then given a one hour conditioning in the environmental chamber. Following that, the arm with the indentor was allowed to freely drop compressing the foam while the strain was monitored.

The procedure used for the compression set experiments was a non-ASTM procedure but was designed to reflect the load relaxation measurements. The samples were cut into dimensions of 2" x 2" x 1" and dried under vacuum for approximately 3.5 hr. They were then placed in the environmental chamber at the designated environmental conditions for ca. one hour and then, in this same experiment, they were compressed to 65% for 3 hr. The samples were then removed and placed in an oven equilibrated at 40°C for 30 min. after which thickness measurements were made. Recovery measurements were carried out on the samples which displayed the greatest amount of compression set (100 °C-98% R.H.). After about one month of room temperature storage, these samples were placed in an oven at 100 °C for one hr. The thickness of the foams was again measured and recorded.

6.4 Results and Discussion

6.4.1 Cellular Structure and Solid Morphology

In order to understand the observed mechanical behavior, the microstructure and cellular structure of the foams were investigated beginning with the cellular structure. Recall that the two foams of Series 1 differed in that M1n possessed no CPP particles while foam M1c contained the CPP particulate phase. The general cellular structure of the molded foams was evaluated using scanning electron microscopy (SEM). These comparisons were made to document any differences since the cellular structure of polyurethane foams significantly influences the physical properties of these foams. Figures 6.1a and 6.1b show micrographs of one of the molded polyurethane foams, M1c. The two micrographs were taken in two orthogonal directions, (a) parallel to the thickness direction of the molded cushion and (b) perpendicular to the same direction. Comparing the two micrographs indicates that the distinct geometric anisotropy which exists in slabstock foams[9] does not exist for molded foams. As expected, the cells have nearly the same shape in both micrographs.

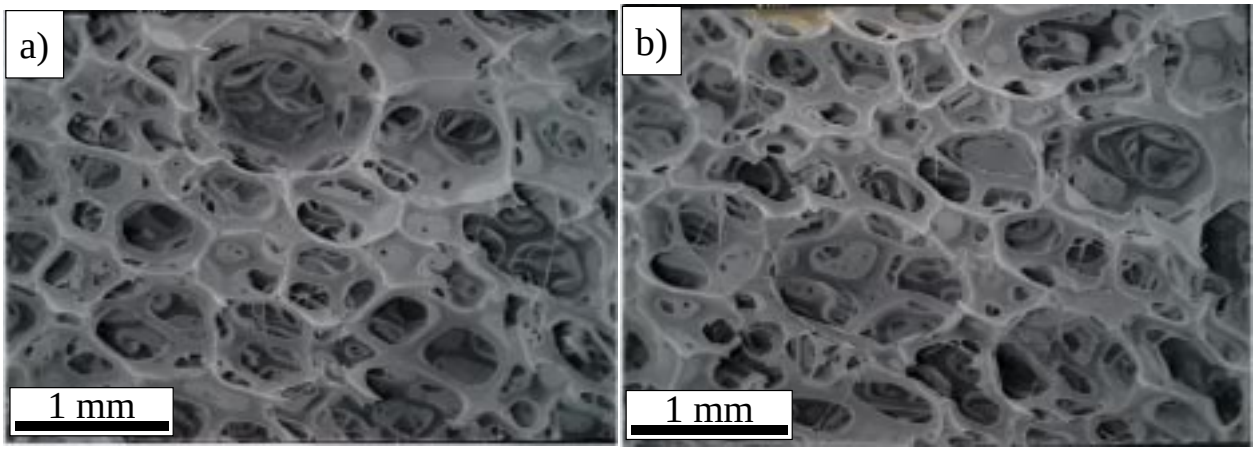

Figure 6.1 Scanning electron micrographs of foam M1c observed both (A) parallel to the rise direction and (B) perpendicular to the rise direction.

A micrograph of M1n is shown in Figure 6.2 so that potential effects of the CPP phase can be investigated. Although copolymer polyols have been reported to aid in cell opening, comparing the micrograph of M1n taken parallel to the thickness direction to that of M1c, shown in Fig. 6.1a, reveals that both foams have relatively the same amount of closed cells. This was also supported by airflow measurements which measured at 1 ft^3/min for both foams. Recall that

these micrographs were taken parallel to the thickness direction and also note that the magnification is approximately the same at 30x. In fact, the only subtle difference observed is that the cells of foam M1c appear somewhat smaller in size than those of M1n. Hence, the CPP containing foam appears to have slightly smaller cells which can be a result of a higher density of cells early in the process when they are nucleated or that less bubble coalescence occurred.

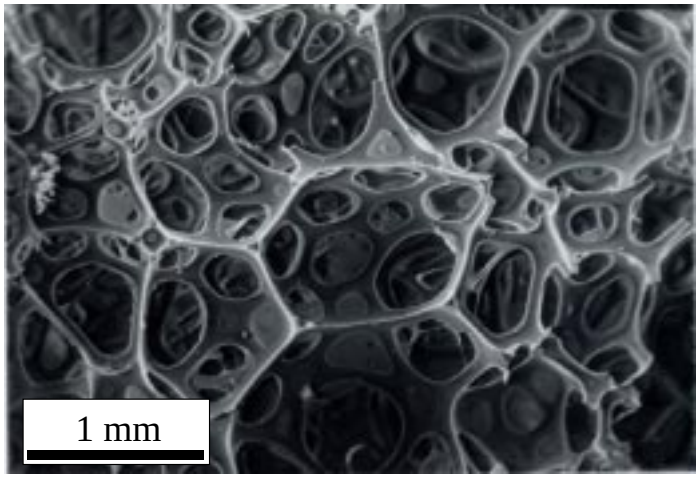

Figure 6.2 Scanning electron micrograph of foam M1n observed parallel to the rise direction.

In order for the effectiveness of the CPP phase to be maximized, it must be well dispersed. To prevent flocculation, as stated earlier, some type of steric stabilization is required which is accomplished during polymerization by a "grafting" process thus allowing the dispersions to copolymerize with the base polyol. To evaluate the effectiveness of this stabilization and the final CPP dispersity, transmission electron microscopy (TEM) investigations were performed. Figure 6.3 is a TEM of foam M1c and reveals a well dispersed particle structure which appears somewhat spherical. The particles range in size from ca. 0.25 to 0.6 μm. The CPP colloidal dispersions illustrate that the stabilization appears to have prevented flocculation.

Foam M1c was subjected to a 90% compression at 150 °C (above the T_g of the CPP) to determine the ease of potential deformability of the CPP particles. The foams were first conditioned at 150°C for one hour, then compressed to 90% for three hours. The load was then removed and the samples were allowed to cool at ambient conditions. Such extreme treatment was chosen in light of earlier experiments at less harsh conditions leading to no observable difference in size or geometry of the particles. The resultant particle structure is shown in Fig.

6.4 which reveals that this treatment promoted slight particle deformation perpendicular to the compression axis as expected, and they now appear somewhat ellipsoidal instead of spherical. In view of the unlikelihood of these materials being exposed to such high thermal conditions in ”real” applications, it was concluded that under realistic temperature and humidity conditions that these materials would be subjected to, the particles are structurally rigid upon high loading.

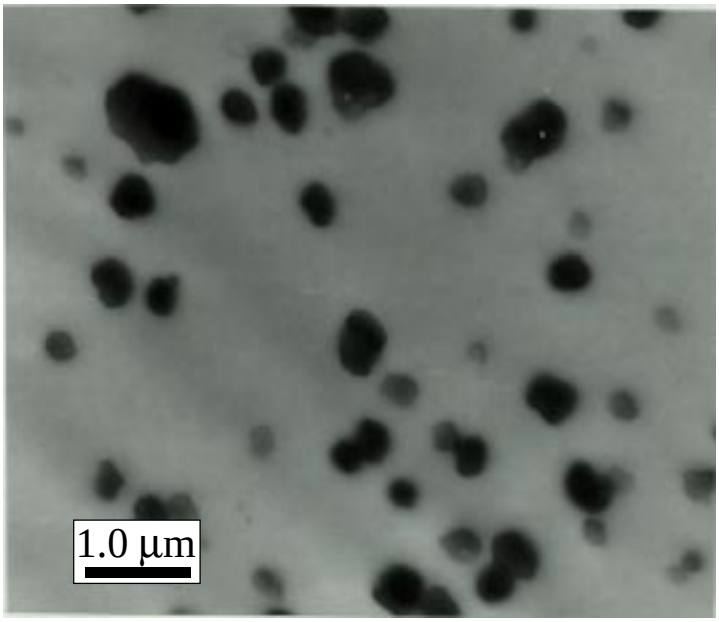

Figure 6.3 Transmission electron micrograph of foam M1c (mag. = 27 kx)

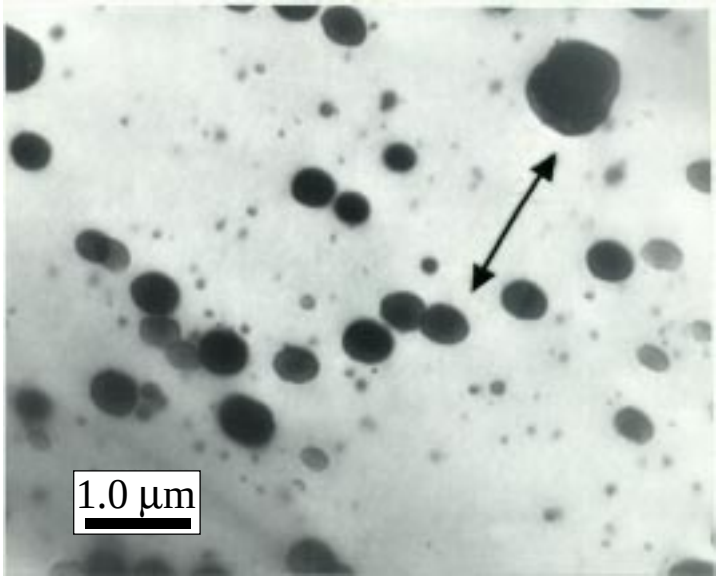

Figure 6.4 Transmission electron micrograph of foam M1c after 90 % compression at 150°C (mag. = 27 kx). Arrow signifies deformation axis.

Since the morphology of the M1c foam is multiphase in nature, i.e., predominately discrete hard segment (HS) microphase domains as well as CPP particles embedded in a rather continuous soft segment phase, the foam properties are strongly dependent on the extent and perfection of these phases. Hence, the microphase separation was investigated as well as the influence of the CPP particles.

The soft segment glass transition temperature, T_g, was determined using DMS, specifically from the peak of the tan delta curve. The tan delta curves (at 1 Hertz) of both foams are shown in Fig. 6.5 which exhibit a strong sharp peak at ca. -58°C which corresponds well with typical literature values for the soft segment T_g and has been supported by differential scanning calorimetry (at 10 °C/min) by the same authors. Also observed in Fig. 5 was a small second tan δ peak at ca. 125 °C displayed only by the CPP containing foam, M1c, shown in curve b—the origin being the T_g of the CPP particulates. Based on the soft segment T_g determined by DMS and DSC, it appeared that the microphase separation of the HS domains was not significantly influenced by the variables in this study. However, the broadening of the tan δ curve for M1c may indicate a broader size distribution of the phase separated hard segment domains. The higher magnitude of tan δ displayed by the foam lacking the CPP particles is clearly attributed to the higher soft segment fraction possessed by this sample.

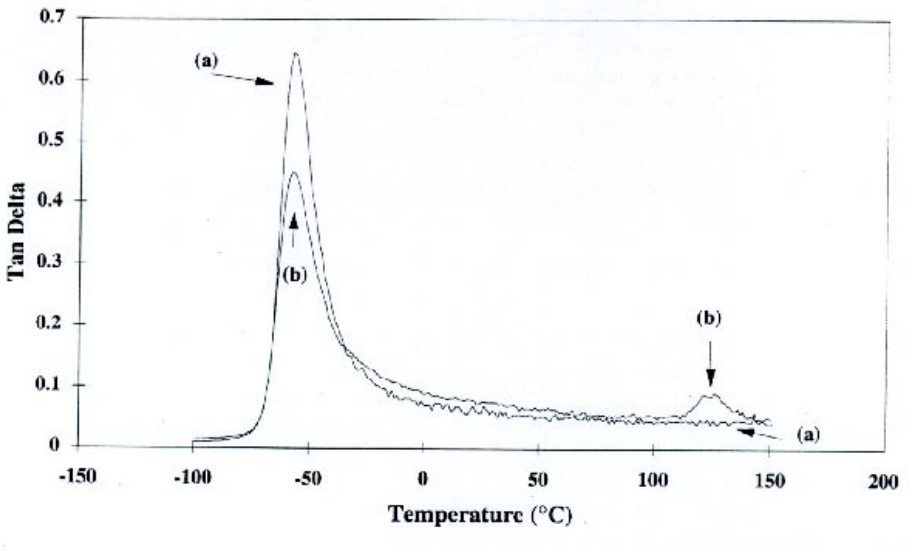

Figure 6.5 Influence of CPP particles on the Tan Delta peak of the molded foams illustrated using (a) M1c and (b) M1n

Small angle x-ray scattering (SAXS) was undertaken to qualitatively evaluate the microphase separation and the influence of the copolymer polyol phase on this behavior. The SAXS profiles for the two molded foams varying in the CPP particle content are presented in Fig. 6.6, which is a plot of the normalized smeared intensity as a function of the angular variable, $s=2\sin\theta/\lambda$ where θ is one half of the radial scattering angle and λ is the wavelength. The average interdomain spacing or Bragg spacing was estimated from the shoulder in the scattering profile. The calculated d-spacing are in the range of 17-19 nm from both M1n and M1c. Figure 6 also reveals that the CPP containing foams displayed a higher scattering intensity over the foams lacking the CPP particles. Since the water/TDI content remains constant, the HS content is also constant and yet the intensity is influenced which is believed to be attributed to the different volume fractions of soft phase as well as the presence of the CPP phase. Specifically, the volume fraction of the soft phase is now lower relative to the hard segment volume fraction since some of the soft segment volume is now occupied by the CPP particulates. Due to the relatively large size of the CPP particles, they do not distinctly display their signature on the SAXS profile in the measurable range.

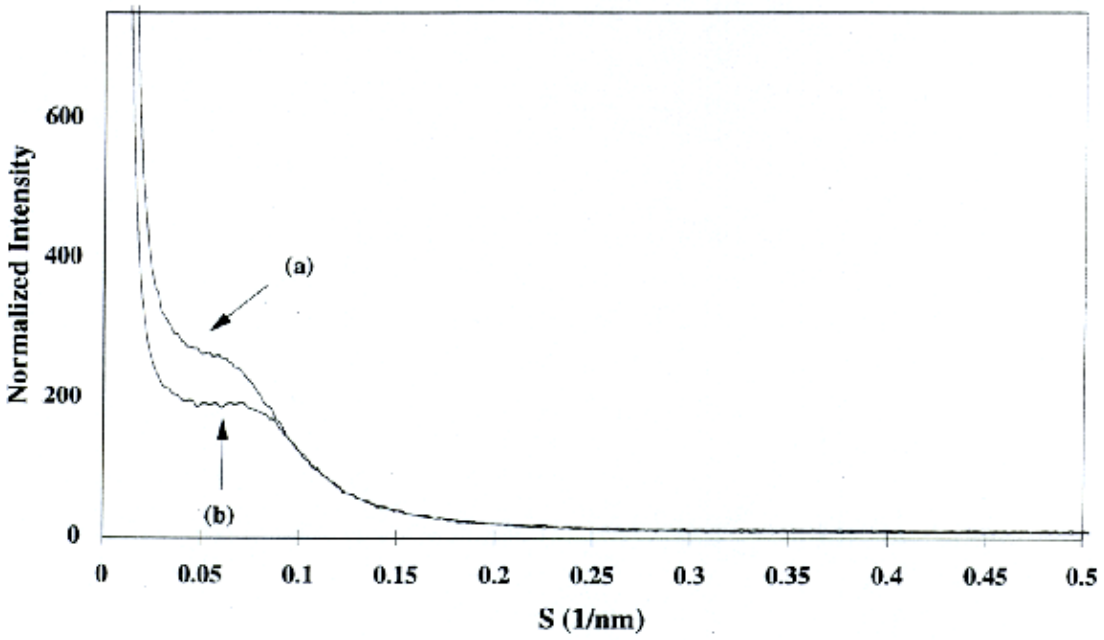

Figure 6.6 SAXS profiles of molded foams illustrating the influence of the CPP particles: (a) M1c and (b) M1n

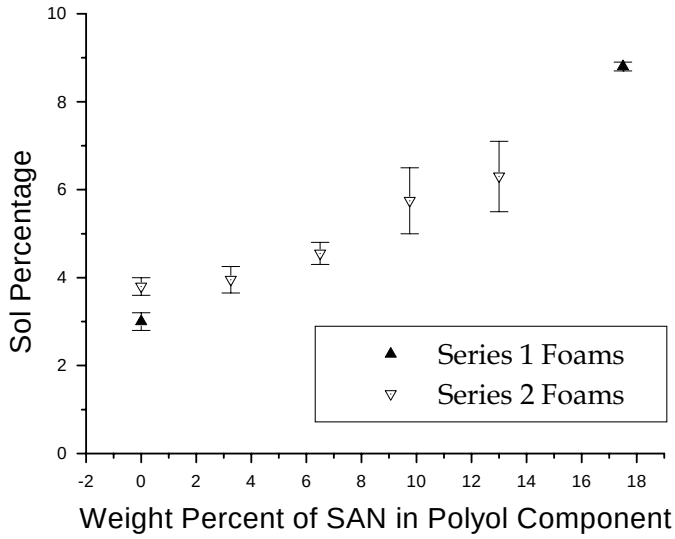

Figure 6.7 Percent extractables from a DMF extraction of Series 1 and Series 2 foams.

The foam's covalent network character was evaluated using extraction studies in dimethyl formamide (DMF). The results, presented in Figure 6.7, indicate that the examined foams are quite extensively cross-linked and that less than 9 wt.% can be extracted using DMF. It can also be seen that the CPP containing foam displayed a greater amount of extractables than the foam lacking the CPP dispersion. In fact, the foam that incorporated CPPs lead to almost three times the amount of extractables over the foam free of CPPs. For example, the sol fraction of foam M1c was ca. 9% where that of foam M1n was significantly lower at 3%. As mentioned in the discussion of the SAXS and DMS data, the ratio of hard segment volume fraction to that of the soft segment is different for the two foams of Series 1; therefore, it might be argued that the additional material being extracted from M1c is hard segment material. To resolve that question, Figure 6.7 also shows the results of an extraction experiment performed on Series 2, in which the amount of CPP is increased while the hard segment/soft segment ratio is maintained constant. It can be observed in Figure 6.7 that the amount of extractables systematically increase from ca. 4.6 wt.% extracted in M2F0.0 to ca. 7.2 wt % in sample M2F13.0. The results from these experiments suggest that the CPPs may not be as extensively reacted into the network as originally expected and that secondary bonding to the surrounding soft segments may also play a significant role in bonding the particles to the rest of the foam. This implies that, while the stabilizer does prevent flocculation of the particles, it may be less effective in grafting the particles to the soft segment matrix. In other words, the links of these particulates to the soft

phase may distinctly depend on physical means such as hydrogen bonding. Further discussion of this conjecture will be presented in a later section (viscoelastic section) where the time-dependent properties of the CPP containing foams displayed much stronger sensitivity to temperature over those lacking CPP particles.

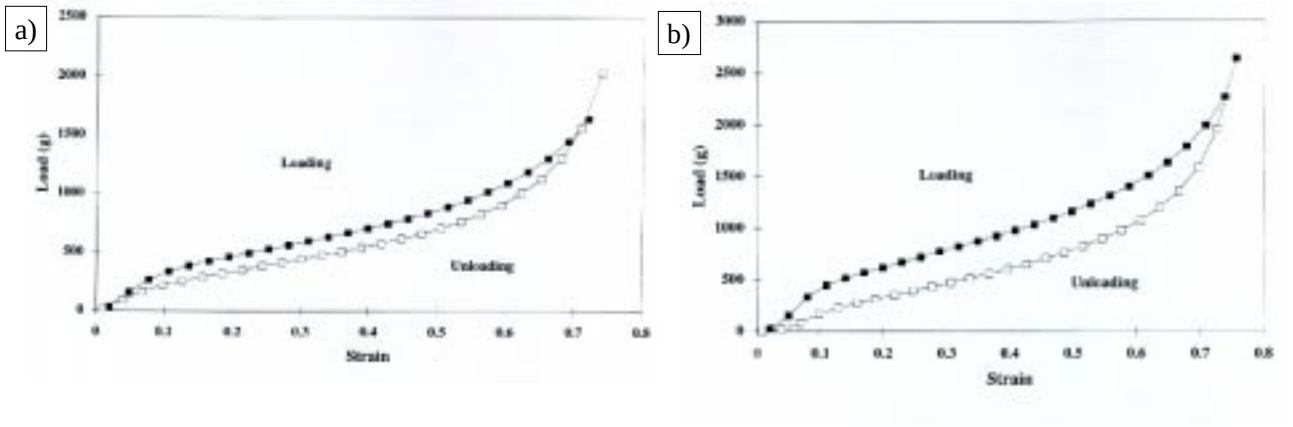

Figure 6.8 Load-strain behavior illustrating mechanical hysteresis upon loading and unloading for a) M1c and b) M1n.

6.4.2 Mechanical and Viscoelastic Properties

The compression loading-unloading response of the two molded foams of Series 1 was evaluated in terms of the formulation difference between them. The compression load-strain behavior of foam M1n is shown in Fig. 6.8a. As can be seen, the curves can be divided into three deformation regions as has been well described by Gibson and Ashby: the linear bending region, the elastic buckling region, and the densification region.[10] The first region occurs in the first 10% strain and is representative of elastic bending of the cell struts. The second region represents buckling of the cell struts where the strain increases with small changes in load. The final densification region begins at ca. 65% strain which, in part, is also the basis for selecting 65% strain as the level of compression chosen for the load relaxation measurements. Here the cells completely collapse and opposing cell walls come into contact. The fact that the loading and unloading curves are not superimposed confirms that these foams exhibit mechanical hysteresis. Mechanical hysteresis is usually attributed to irreversible changes such as disentanglement of chains or plastic deformation, crazing, crack initiation, bond breaking, and even morphological changes such as crystallization and/or other viscoelastic processes.[11]

In polyurethane elastomers, hysteresis also originates from the disruption and deformation of domains primarily through hydrogen bond disruption.[11] Figure 6.8 shows that the foams were compressed to a maximum strain of 76% which was chosen in view of the physical limitation of the load cell. The transitions from one region to the other occurred at a strain of ca. 0.1 and 0.65 respectively. The loads at these strain values were 265 g and 1300 g respectively. Figure 6.8b illustrates the loading-unloading behavior for M1c. The differences between the foams lie in the load values and the amount of hysteresis.

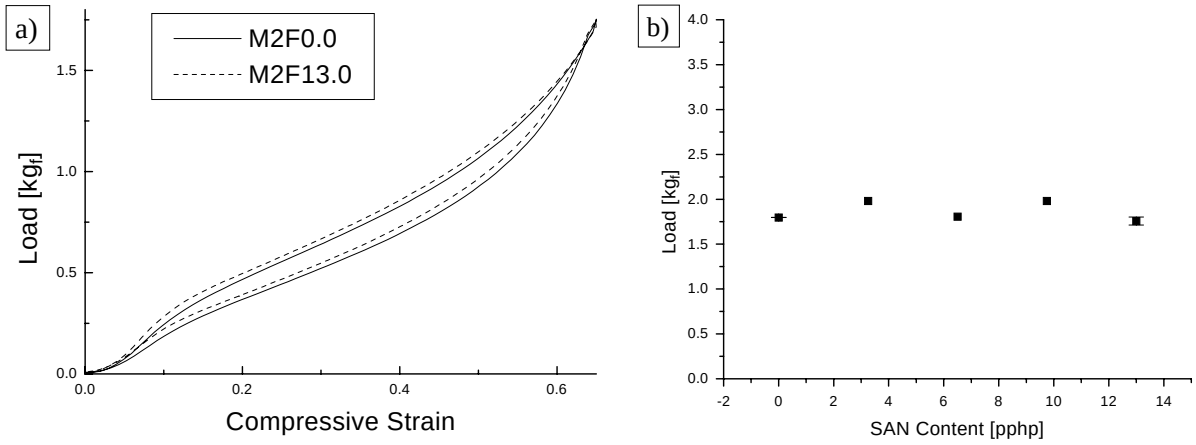

Figure 6.9 a) Load-strain behavior for M2F0.0 and M2F13.0 illustrating their mechanical hysteresis behavior upon loading and unloading at 30°C-15%RH b) Average load at 1 second after compression to 65% strain at 30°C-15%RH for the foams of Series 2.

In general, the inclusion of CPPs in the Series 1 formulation increased the load at any given strain level under this test protocol. The measured loads at a given extension were 25% to 35% higher for the CPP containing foams. For example, at a strain level of 0.4, comparing the loading curves of M1n to M1c, reveals that M1c displayed a load of 960 g while M1n only displayed a load of 710 g. The trend was similar at other strain levels as well, e.g. at a deformation level of 0.7, the loads were 1950 g for M1c and 1500 g for M1n. It can be concluded that, if the HS/SS ratio is not controlled, the incorporation of this rigid filler into the formulation does indeed increase the foam "hardness" based on the increase in displayed loads at any level of deformation. In Series 2, the HS/SS ratio is maintained constant, and the increase of load bearing with CPP is marginal at best under normal conditions as shown in Figure 6.9a. For example, at a strain level of 0.5, M2F0.0 displayed a load of 660 g and M2F13.0 displayed a load

of 620 g. Furthermore, at the higher strain levels, the influence of CPP is undetectable as is shown in Figure 6.9b, where the average load displayed after 1 second of compression at 0.65 strain is ca. 1750 g for every SAN concentration tested. This pattern for load bearing at high strain held true for all conditions that Series 2 was tested with (30°C-15%RH, 100°C-15%RH, 30°C-75%RH, 100°C-75%RH). The most notable feature of adding CPP while maintaining a constant HS/SS ratio can be seen in Figure 6.10, where the CPP containing foam maintains a much higher load at moderate strains than the foam without CPP. For example, at 0.5 strain M2F13.0 displays a load of 560 g and M2F0.0 displayed only a 420 g load. The results shown in Figure 6.10 clearly indicates that replacing hard segment material by weight from the formulation with CPP reduces the negative effects that humidity usually has on polyurethane foams. This would be expected as the relatively hydrophobic SAN particles which comprise the CPP filler would not be softened by water absorption in the way that the hydrophilic hard segment domains are.

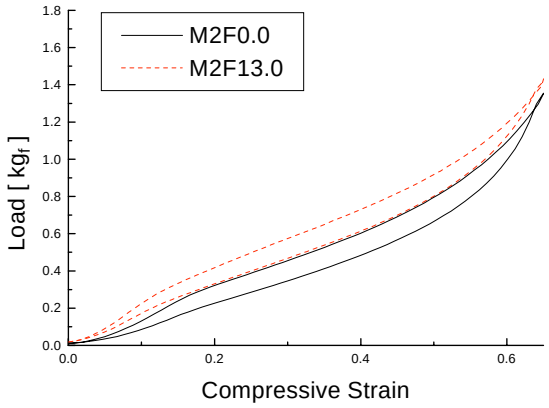

Figure 6.10 Load-strain behavior for M2F0.0 and M2F13.0 illustrating their hysteresis curves upon loading and unloading at 30°C-100%RH

While the CPP containing foams generally displayed higher loads for a given strain during loading, the amount of hysteresis was also greater in Series 1. For example, comparing M1n (Fig. 6.8a) to M1c (Fig. 6.8b) shows that the amount of hysteresis (percent) is greater for M1c, 31% as compared to 16 %. Thus, as compared to the CPP-free foams, the CPP containing foams exhibit greater differences between the loading and unloading curves of the compression/decompression cycle, suggestive of greater load relaxation when the CPP is added

in the manner of Series 1. However, to conclude whether this is an influence of the CPP itself or of the higher HS/SS ratio, the results from Series 2 must also be examined. As shown in Figure 6.11a, all concentrations of filler displayed the same amount of hysteresis (ca. 15 %) even at the harshest humidity condition. *This indicates that at normal usage conditions increased hysteresis with the addition of CPP is actually an effect of having more hard segment material present relative to the soft segment material*. At the highest temperature studied, 100°C, an increase in hysteresis is observed as is shown in Figure 6.11b. For example, M2F0.0 had a hysteresis of 13% and M2F13.0 had a much higher one of 22%. This indicates that in this range of temperature an additional relaxation is occurring which does not occur in foams without CPP. This additional relaxation is possibly a softening effect in the CPP particles, resulting in additional load bearing loss in foams with CPP. It is noted that the DMS results showing a SAN T_g of ca. 125°C occur on a different time scale, and that, under these compression conditions, 100°C may be high enough to induce softening.

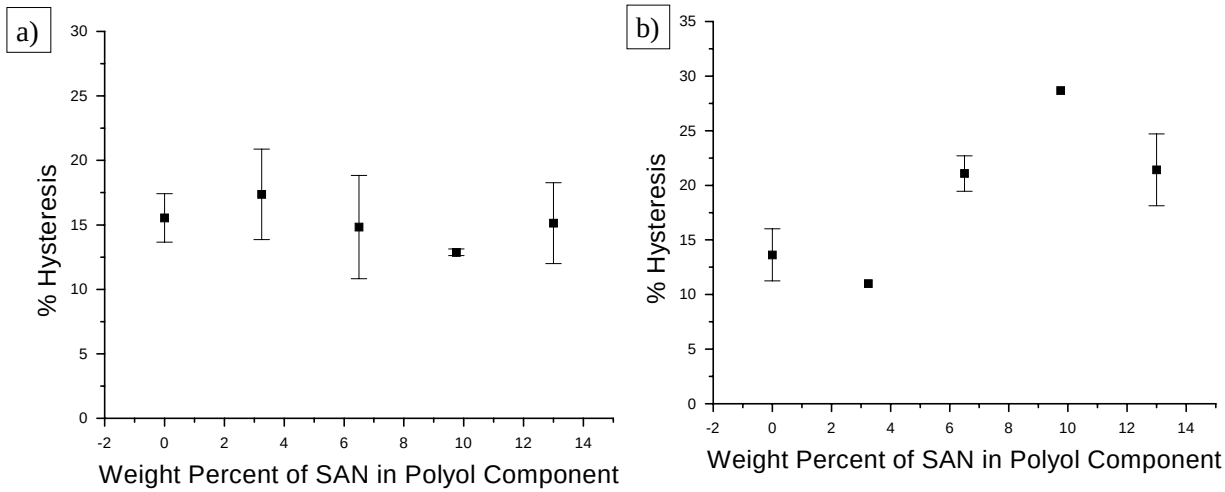

Figure 6.11 Percent Hysteresis for Series 2 foams a) at 30°C-100%RH and b) at 100°C-75%RH

The influences of temperature and humidity on the viscoelastic behavior of the flexible molded polyurethane foams with and without CPPs were evaluated using load relaxation, creep and compression set. In addition to being a good indication of the load bearing capabilities of the foams and the recoverability, the viscoelastic properties are sensitive to the network of the foam arising from the hard segment domains, CPP particles and covalent cross-links.

As described earlier, the compression load relaxation behavior was performed at a constant 65% strain and under different temperature/humidity conditions. The load relaxation behavior as a function of temperature and humidity for M1n (no CPP) is shown in Fig. 6.10. An increase in temperature and/or humidity resulted in a shift of the relaxation curves to lower loads and an increase in the percent decay. As temperature increased from 30 °C to 100 °C under the low humidity condition of 35%, the initial load decreased 28% from 1597g at 30°C-35% RH to 1156g at 100°C-35% RH. Likewise, at the constant high humidity condition of 98% RH, the loads were 1135g at 30°C, and 1049g at 100°C respectively, clearly showing the effect of an increased temperature on relaxation. The percent decay dramatically increased as well from 27% at 30°C-35% RH to 51% at 100°C-98%RH. The results shown in Fig. 6.12 indicate that both temperature and humidity significantly "plasticize" the exhibited mechanical behavior. The decrease in load and increase in percent decay is primarily due to hydrogen bond disruption by the high temperature and/or high humidity therefore increasing the amount of chain slippage that occurs. This suggests that hydrogen bonding (predominately occurring within the hard segment domains) significantly enhances the foam properties, and when disrupted by temperature and/or humidity, these properties are severely altered. In addition, the increased soft segment mobility with temperature contributes to the increased percent decays and decreased initial loads. The nonlinearity observed at high temperatures, especially at 100°C, suggests that the relaxation mechanism is enhanced or possibly an additional mechanism may be occurring. It is well known that temperature can disrupt hydrogen bonding, but certainly humidity can also have a dramatic effect.

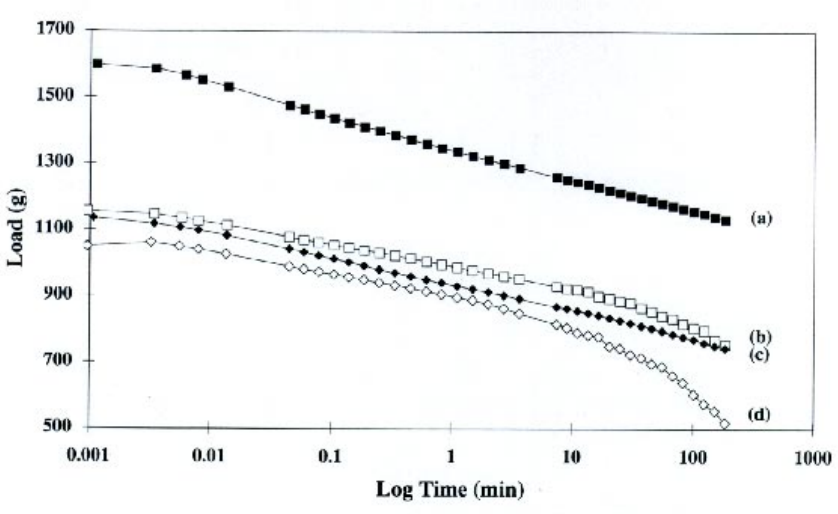

Figure 6.12:
Load relaxation behavior of M1n as a function of temperature and relative humidity:
(a) 30°C-35%RH,
(b) 100°C-35%RH,
(c) 30°C-98%RH, and
(d) 100°C-98%RH

The load relaxation behavior for M1c, as a function of temperature and humidity, is shown in Fig. 6.13 where the load is plotted versus log time. As can be seen, an increase in temperature systematically shifted the relaxation curves to lower loads, similar to M1n. The initial load decreased from 2019g at 30°C-35%RH to 1271g at 100°C-35%RH while the percent decay in the three hour period increased form 36% to 54%. In general, an increase in temperature resulted in a softening of the foam. This figure also elucidates that high humidity has a similar effect to high temperatures at a low humidity. At a constant temperature, an increase in humidity from 35%RH to 98%RH had a similar effect as an increase in temperature from 30°C to 100°C at 35%RH.

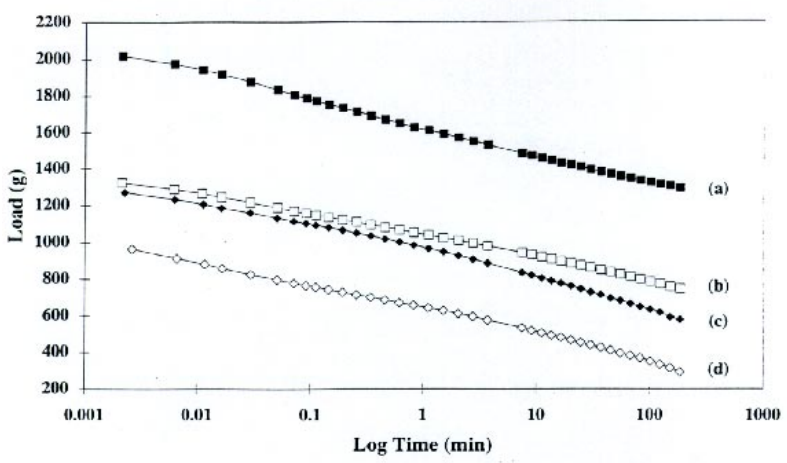

Figure 6.13 Load relaxation behavior of M1c as a function of temperature/relative humidity: (a) 30°C-35%RH, (b) 100°C-35%RH, (c) 30°C-98%RH, and (d) 100°C-98%RH

Figure 6.14a shows the behavior of foams M1n and M1c carried out at 30°C-35%RH. As expected, foam M1c with 12.5% CPP solids displayed higher loads than M1n. The initial load was 1597g for M1n and 2019g for M1c again demonstrating that the foam hardness did indeed increase with the incorporation of CPP particles as expected. However, the slopes of the curves of the CPP containing foams are higher than that of M1n as well as are the percent decays. The percent decays were 27% and 35% for M1n and M1c, respectively in this three hour deformation period. This suggests that while the copolymer polyols do increase the foam hardness of Series 1 foams, they enhance the level of relaxation leading to more time-dependent viscoelastic properties. However, as was shown in the discussion of the hysteresis behavior, *this increase in relaxation is due to the higher HS/SS ratio that occurs upon CPP addition in Series 1.* In

contrast, Figure 6.14b shows the percent load losses for the constant HS/SS ratio foams of Series 2, and it can be clearly seen that at 30°C-15%RH the *CPP concentration does not significantly increase or decrease the rate of load relaxation.*

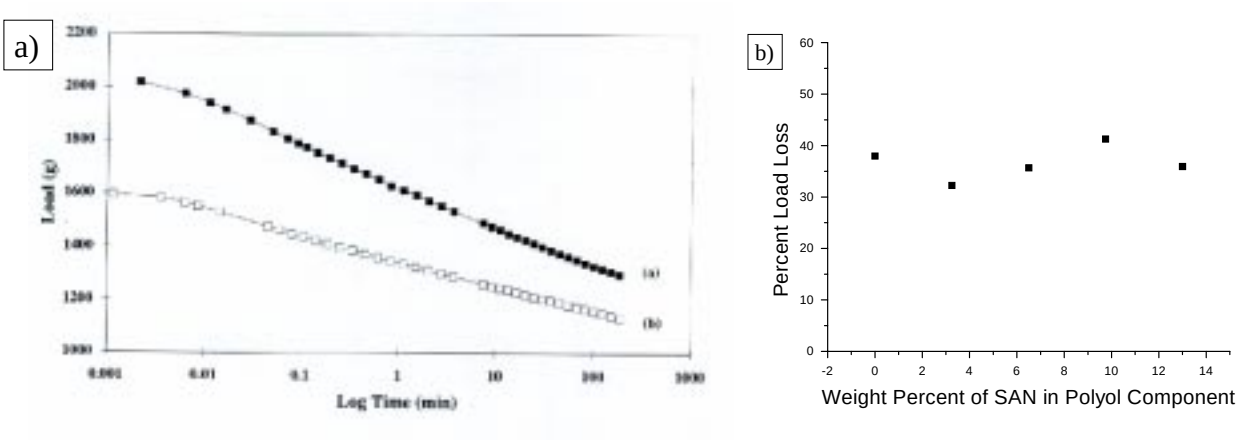

Figure 6.14 a) Load relaxation behavior at 30°C-35%RH for the 4 pphp water content foams as a function of the CPP used: (a) M1c and (b) M1n. 14 b) shows percent load loss calculated from loads at 0.1 and 25,000 seconds for Series 2 foams at 30°C-15%RH

Similar behavior was observed for Series 1 at 30°C-98%RH as shown in Fig. 6.15a. Once more, while the initial load was higher for M1c over M1n, 1325g compared to 1135g, the percent decay was also higher, 43% compared to 34%. Furthermore, the curves appear to "cross-over" right at the three hour point. On the other hand, dramatically different behavior was observed for Series 2, as is shown in Fig. 6.15b. Here, the percent load loss systematically decreases as the CPP component is increased, from 48% for M2F0.0 to 38% for M2F13.0. This emphasizes that the increased rates of relaxation observed in Series 1 result from the increase of the HS/SS ratio as the CPP component is added. In Series 2, as the hard segment material is displaced by the less hydrophilic CPP component, the overall load loss due to humidity plasticization decreases.

The influence of the CPP particles in terms of viscoelastic decay was very distinctly enhanced at 100°C-35%RH as illustrated in Fig. 6.16. Here, the curves crossed where the CPP containing materials displayed higher initial loads but lower final loads at the end of the three hour experiment! For example, foam M1n exhibited an initial load of 1156g, of which 35% decayed in three hours. In contrast, foam M1c displayed an initial load of 1271g, which decayed to 54% of its initial value in three hours—much more than that of M1n. This behavior also

suggests that at these very high temperatures, an additional relaxation mechanism is occurring in the CPP component leading to a greater overall rate of load relaxation.

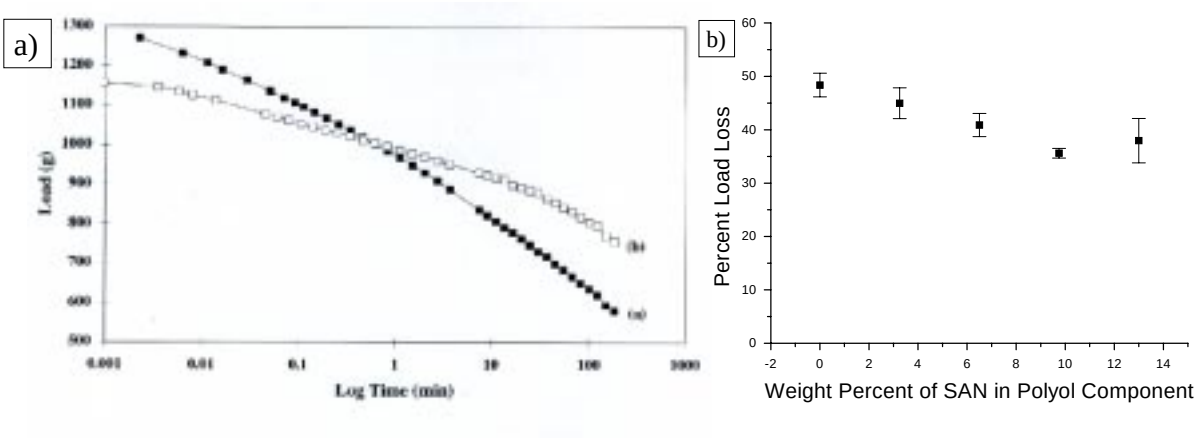

Figure 6.15 a) Load relaxation behavior at 30°C-98%RH for the 4 pphp water content foams as a function of the CPP used: (a) M1c and (b) M1n. 15 b) shows percent load loss calculated from loads at 0.1 and 10,000 seconds for Series 2 foams at 30°C-100%RH

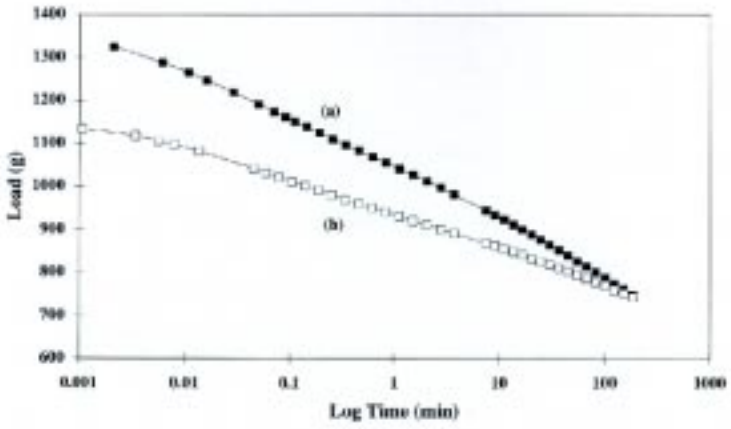

Figure 6.16 Load relaxation behavior at 100°C-35%RH for the 4 pphp water content foams as a function of the CPP used: (a) M1c and (b) M1n

Figure 6.17a illustrates the load relaxation behavior of foams M1n and M1c at the most stringent conditions 100°C-98%RH. Here the initial loads were essentially the same but the percent decays were dramatically different. The initial loads were 1049g and 965g for M1n and M1c—within the experimental scatter based upon multiple runs. However, the percent decays were 51% and 70%, respectively. Consistently, the percent decay was again greater for the CPP containing foam relative to the CPP-free foam. The reason for this is emphasized in Series 2 by overlaying the results at 100°C-75%RH and 30°C-100%RH as is done in Figure 6.17b. There it

can clearly be seen that the improvement in percent load loss through the addition of CPP is completely negated at high temperatures. Furthermore, since the two results for sample M2F0.0 are indiscrete, these effects cannot be the influence of hydrogen-bonding within the hard domains but must result from some effect of the CPP component.

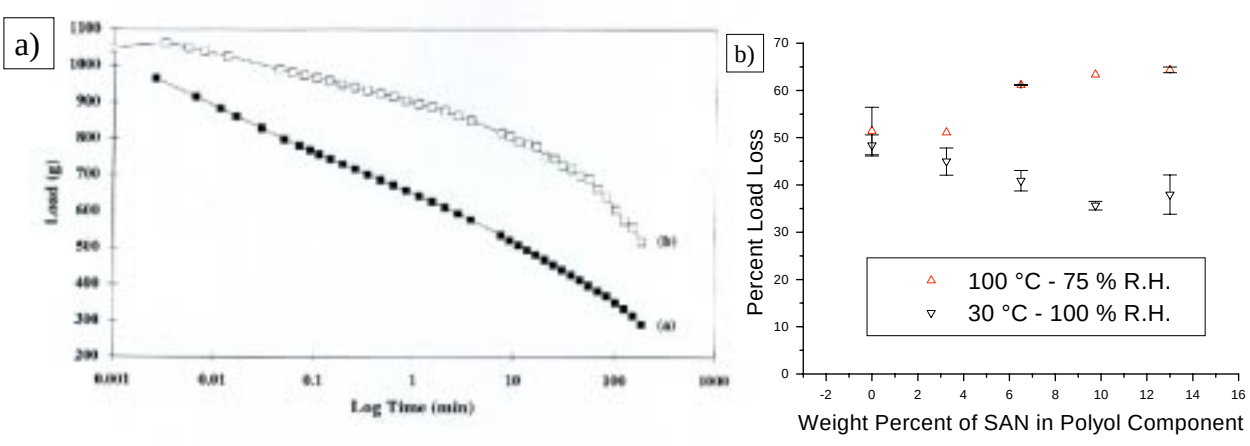

Figure 6.17 a) Load relaxation behavior at 100°C-98%RH for the 4 pphp water content foams as a function of the CPP used: (a) M1c and (b) M1n. 17 b) shows percent load loss calculated from loads at 0.1 and 10,000 seconds for Series 2 foams at 30°C-100%RH and at 100°C-75%RH

In summary of the above load relaxation results, the initial loads increased ca. 10% to 30% with the incorporation of CPPs in Series 1 but the percent decays also increased ca. 30% to 50%. In Series 2, the initial loads, particularly at high strains, are only moderately improved by the addition of CPP, but the relaxation rate under high humidity conditions is reduced. *Overall, these results show that the dramatic increase in initial loads and greater load relaxation for Series 1 is the result of increases in the HS/SS ratio as CPP is added.* Furthermore, it appears that at high temperatures the mechanism of relaxation is different for the foam containing CPPs than for the foam that does not. This may indicate some softening ca. 100°C within the SAN particles allowing them relax under load. As already discussed, this may be due to working in the vicinity of SAN T_g. In other words, the time scales of compression experiments may be different enough from DMS measurements to allow the SAN particles to soften 25°C below the SAN tan δ peak. On the other hand, as the rigid CPP particles can act as stress concentrators leading to increased levels of localized stress, and these test results may indicate that at high temperatures the grafted polyol is being separated from the surface of the filler. Such a

separation could occur through a dissociation of any physical bonds between the CPP and the matrix. The different behavior and thus different mechanisms exhibited by the CPP containing foams correlates well with the compression load strain measurements. Restating, the CPP containing foams in Series 1 demonstrated higher loads (initially), greater hysteresis, and greater relaxation in a three hour period than the foams lacking CPP particles, resulting from the higher HS/SS ratio of CPP foams in Series 1. Furthermore, the fact that either high temperatures or high humidities "plasticized" these CPP containing materials suggests that perhaps the accepted belief that the CPPs are tightly covalently grafted to the foam matrix may not be true.

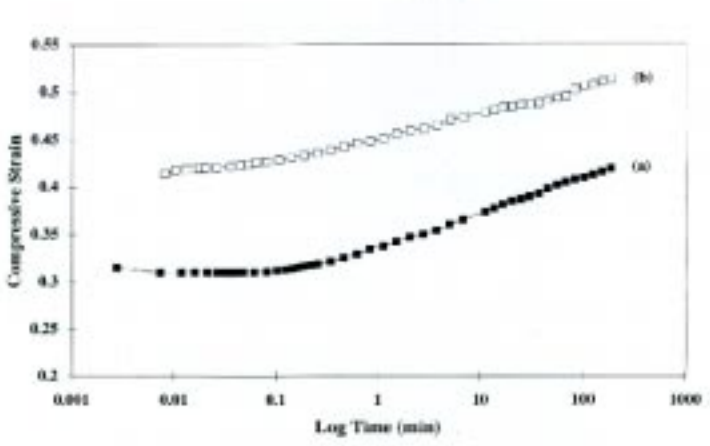

Figure 6.18 Creep response at 30°C-35%RH as a function of CPP used: (a) M1c and (b) M1n

In addition to load relaxation, the change in the thickness of the foam samples under a constant load in compression was also of interest since it directly measures the foam shape under load and closely simulates realistic application conditions. This measurement was also used to complement the load relaxation findings since both tests reflect viscoelastic behavior. The two molded foams samples were compressed under a constant load (800g) and investigated using the same environmental conditions applied in the load relaxation measurements. The creep response of foams M1n and M1c, measured at 30°C-35%RH, is displayed in Fig. 6.18. Foam M1c clearly displayed an induction period of ca. 6 sec. long while M1n displayed no induction time. In addition, since the strains were lower, foam M1c exhibited stiffer behavior than M1n. The initial strain for foams M1n was 0.41 while for M1c, it was 0.32. However, while the use of CPPs did indeed improve initial foam "hardness" and even generated an induction period, they did not decrease the creep strains, i.e., the amount of creep that occurs during the three hour period. In

fact, the final values were slightly greater for the CPP containing foams of both series. For example, the creep strains were 0.10 and 0.11 for M1n and M1c, respectively. This emphasizes again that the increase in the HS/SS ratio as CPP is added results in more hard segment material which can relax at low temperatures.

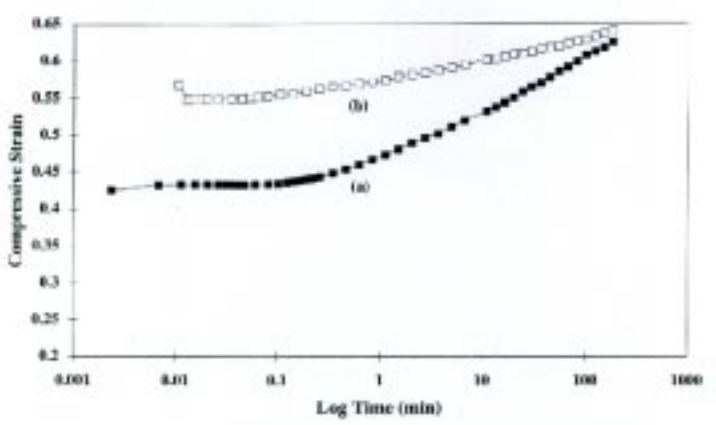

Figure 6.19 Creep response at 100°C-35%RH as a function of CPP used: (a) M1c and (b) M1n

At 100°C-35%RH, the differences between the foams were accented even further specifically in creep strain behavior. Shown in Fig. 6.19 is the creep response of the two molded foams at this high temperature low humidity condition. The initial strains were again lower for the foams with CPPs, but the strain levels of these CPP containing materials surpassed those lacking CPPs. Here, the initial strains were 0.55 and 0.43 for foams M1n and M1c, respectively. *As can be seen, the creep strain values for the CPP containing foams of Series 1 were almost twice as much as those without the CPP particles for the three hour period.* From extrapolation of the curves, the 4 pphp water content foams appear to be heading toward crossover shortly after completion of the three hour experiment. Although the exact reason for the higher creep strains displayed by foam M1c over M1n is not fully understood, this is a clear parallel to the behavior observed in the load relaxation studies. It is suggested that the additional high temperature relaxation observed earlier is the source of the higher rate of creep in M1c.

The results at 98%RH were very similar to those at 35% RH and the trends displayed were the same as those displayed in the load relaxation measurements and are thus not shown. All of the results from the above experiments further confirm the findings of the load relaxation measurements of Series 1 where the incorporation of CPPs increased the foam stiffness by

producing lower strains. While this was a major goal (increase in ILD), the increase in the time dependent strain that accompanied this was definitely unexpected. Not only were the strain levels greater, but at elevated temperatures or humidities, the creep strain levels of the CPP containing foam surpassed those of the foam lacking CPPs. However, the use of Series 2 provided a basis for stating that these higher creep rates induced by humidity are the result of altering the HS/SS ratio, whereas the higher rates observed at the highest temperatures studied also include the influence of an additional relaxation mechanism.

Table 6.3 Compression Set Results for the Two Foams of Series 1

Condition	M1c	M1n
30°C-35%RH	2.5 ± 0.1	1.7 ± 0.2
30°C-98%RH	9.5 ± 1.5	4.0 ± 0.5
100°C-35%RH	59.0 ± 0.3	10.7 ± 0.5
100°C-98%RH	64.3 ± 0.1	63.0 ± 0.1

The viscoelastic experiments were concluded with compression set measurements. Compression set is not only a direct measure of the thickness loss and recoverability of the foam, but is also sensitive to the foam's morphology and network structure. As with the previous viscoelastic measurements, this property was evaluated in terms of the specific formulation variables as well as the environmental conditions. While the influence of CPPs on the compression set behavior is minor in most conditions, they did display a major influence at 100°C-35%RH where the materials with CPPs displayed higher compression sets. Comparing foam M1n to M1c reveals that the compression set of M1c was greater than that of M1n at all conditions but especially at 100°C-35%RH as exhibited in Table 6.3. This is taken as strong further evidence that some addition high temperature relaxation mechanism is significant where CPP is present. As previously mentioned, this may be the result of softening within the CPP itself. Also, hydrogen bond disruption may be occurring with increases in temperature or humidity with bonds specifically existing at the interface between the CPP particles and the surrounding soft segment which otherwise would not exist in the foams lacking the particulates.

6.5 Conclusions

Two series of molded foams were produced to study the effects of incorporating a reinforcing particulate copolymer polyol. These series differed in that in Series 1, the CPP was added in the manner that it is industrially which results in a decreased soft segment content relative to the amount of hard segment material in the foam. The Series 2 foams were therefore made by increasing SAN content while maintaining a constant HS/SS ratio. The effects of adding CPP particulates were then systematically studied. The important aspects addressed were the structure, morphology and viscoelastic properties. First, the influence of the CPPs on the cellular structure of the foams were evaluated with SEM. CPP particulate content did not appear to significantly influence the cellular structure. TEM micrographs displayed evidence of the CPP particulates being distributed in a continuous matrix phase. Both Series 1 molded foams displayed microphase separation as observed using SAXS where the scattering peaks corresponded to a Bragg spacing of ca. 170 Å which varied only slightly depending on the CPP content. In DMA, the CPP-containing foam displayed a second maximum in the tan delta curve clearly attributed to the T_g of the SAN particles in addition to the primary peak attributed to the T_g of the soft phase. In evaluating the covalent network solvent extractions in DMF indicated a higher amount of extractable material in the CPP-containing foams of both series. Overall, the difference in the general cellular structure and microphase hard segment texture between the two foams seemed rather minor.

The viscoelastic properties varied significantly especially when the test temperature and/or humidity was increased. Comparing the load relaxation behavior, under elevated temperature or humidity conditions the relaxation curves of all molded foams resulted in lower loads and greater load decays. Humidity also had a dramatic softening effect on the relaxation behavior of the foams inducing a similar “plasticization” effect. As expected, the foam containing the CPP reinforcing particulates generally displayed greater stiffness at moderate strains. However, at high strains, it was shown that the initial load bearing is unaltered by the addition of CPP if the HS/SS ratio is kept constant. With respect to the load-strain measurements, the CPP containing foam of Series 1 exhibited greater hysteresis than the corresponding foam lacking the particulates. However, Series 2 demonstrated that this was an effect of increasing the HS/SS ratio and not of the CPP particulate themselves. The viscoelastic

properties of the Series 1 foam containing the CPP dispersion were also more time dependent than the foam free of these particulates; however, this was also shown to be an influence of the increased HS/SS ratio. The percent load losses of Series 2 also showed that under high humidity and low temperatures adding CPP actually significantly improves the load loss of the foam. The surprising result from Series 2 was to show that at 100°C the CPP component exhibits an additional relaxation mechanism resulting in dramatically higher load losses than foams without CPP. The particles are believed to act as stress concentrators therefore any softening of the particles themselves or the bonds between them and the soft matrix could result in increasing the relaxation decay. At elevated temperatures and/or humidities, it is possible that hydrogen bond disruption existing at the interface is disrupted which leads to further chain slippage. However, it is also possible that the additional relaxation occurs due to softening of the CPP material itself.

6.6 Acknowledgements

This work has been financially supported by the Dow Chemical Company. Their support is gratefully acknowledged. Stephen McCartney is also thanked for his contributions to the microscopy in this study.

6.7 References

1. Herrington R; Hock K; Flexible Polyurethane Foams; Dow Chem Co, Midland, MI: (1991)
2. Barrett KET; Dispersion Polymerization in Organic Media, John Wiley and Sons, Inc, London: (1975)
3. Napper DH; Polymer Stabilization of Colloidal Particles; Academic Press, London: (1983)
4. Critchfield FE; Koleske JV; Priest DC; *Rubber Chem Tech*: **45** (1972) 1467-1487
5. Spitler KG; Lindsey JJ; *J Cell Plast*: **17** (1981) 43
6. Vehlewald P; Kustoff, **73**(8), 439 (1983)
7. Woods, G. Flexible Polyurethane Foams: Chemistry and Technology, Applied Sci. Publishers, LTD, New Jersey (1982)
8. Hilyard NC; Mechanics of Cellular Plastics; Macmillian Pub Co, Inc, New York: (1982)
9. Moreland JC; *Ph.D. Thesis*; VPI&SU, Chem Eng Dept, Blacksburg, Virginia: (1991)
10. Gibson LJ; Ashby MF; Cellular Solids; Pergamon Press, New York: (1988)
11. Campbell GA; *J Appl Polym Sci*: **24** (1979) 709-723

7 Surfactant Level Influences on Structure and Properties of Flexible Slabstock Polyurethane Foams

7.1 Chapter Summary

A series of flexible polyurethane slabstock foam samples were prepared with varying surfactant concentration. Several samples were also prepared by quenching small pieces into liquid nitrogen during the foaming process. The morphology of these materials was characterized at many length scales via scanning electron microscopy (SEM), transmission electron microscopy (TEM), wide-angle and small-angle X-ray scattering (WAXS and SAXS), tapping-mode atomic force microscopy (AFM), and Fourier transform infrared spectroscopy (FTIR). AFM was also utilized to probe trends in the mechanical stiffness of hard domains in the polyurethane foam. Differential scanning calorimetry (DSC) and dynamic mechanical analysis (DMA) were applied to examine the thermal and viscoelastic properties of these foams. It was shown in this study that collapse of the cellular structure of a foam prior to the point of urea precipitation alters the aggregation behavior of the hard domains and influences their ultimate properties. Samples without surfactant that were quenched in liquid nitrogen exhibited urea-rich aggregations on the order of 2-4 microns with similarly sized urea-poor regions. Equivalent samples with surfactant showed no such aggregations, suggesting that surfactant does play a principal role in the way that urea precipitates in these materials. DMA and DSC revealed that all samples of any surfactant concentration which spontaneously collapsed or were quenched or crushed prior to completely curing had a polyol glass transition 3-5 degrees higher and somewhat broader than any foam sample which maintained its cellular structure until cured. This is interpreted to mean that the polyol matrix of the collapsed, crushed, or quenched materials is not as pure as the cellular samples, indicating that the presence of the cellular morphology plays a significant role in the microphase separation behavior of the solid-state at the molecular level. This hypothesis is supported by the results of WAXS, FTIR, SAXS, and AFM. The WAXS results demonstrate that at no surfactant concentration is the ordering, or hydrogen bonding, within the hard domains being significantly altered; however, in the lower

range of the concentrations studied here, the FTIR results show that the surfactant level in the formulation does play a significant role on the amount of bidentate hydrogen bonded hard domains that locally organize. Furthermore, as shown by SAXS, the surfactant concentration influences the mean chord length across the hard domains. These changes in structure and domain size distribution lead to the properties investigated via AFM, where the relative hardness of the hard domains was noted to initially increase as the surfactant concentration increases and then levels off above a certain concentration. The surfactant is thus suggested to play a secondary role in the development of the hard domains by maintaining the cellular structure in the foam as the phase separation occurs and at least until the polyurethane foam has more fully organized hard segment domains.

7.2 Introduction

The two-phase morphology of the solid state is of great importance to overall properties in polyurethane foams. In typical water-blown systems, the reaction of water with diisocyanate produces a carbamic acid which decomposes yielding heat, carbon dioxide, and an amine functionality.[1] The heat and carbon dioxide contribute to the expansion of the gas-liquid phase separation in the reactive mixture and so play imprint roles in the development of the foam's cellular structure. On the other hand, a disubstituted urea product results from the reaction of the amine with other isocyanate groups. A "hard segment" results from several isocyanate groups covalently bonding through the urea linkages, and solid-state phase separation in typical systems arises from the precipitation of these segments into "hard domains." In conventional flexible slabstock foams, the polyol phase has a very low T_g (ca. -50°C) and so is often termed "soft." The soft polyol is generally thought to be the continuous phase in these systems, and it is considered to be the matrix in which the hard domains are distributed. However, as will be discussed more fully later, some studies in mechanical deformation and hard segment orientation have suggested that there may be some degree of association or connectivity between hard domains than cannot be explained from the fully dispersed hard domain model. Ideally, hard segments are covalently bound to the polyether polyol during the reaction of the polyol with isocyanate groups which lead to urethane linkages at their terminal points; however, it is known that in real systems there is a distribution of urea segment lengths and that some hard segments are incompletely bound to the polyol matrix.[2]

An additional structure is also sometimes observed in these systems. At high water feed concentration with a stoichiometrically higher feed of isocyanate, the urea precipitates can aggregate further to form what have been termed "urea balls" or urea-rich aggregates.[1,3] These larger aggregates are frequently observed in conventional slabstock flexible foam formulations of high water concentration; however, these structures are not typically observed in molded or high-resiliency (HR) foams of the same water feed concentration.[1,4,5] This difference results from the chemistry of the typical components used in each. Whereas both molded (HR) and slabstock flexible foams most commonly utilize toluene diisocyanate or TDI (fed at an 80/20 2,4/2,6 isomer ratio), the polyol used for each is one major formulation difference. Typical slabstock polyols have molecular weights between 3,000 and 4,000 Daltons; molded polyols tend to have higher molecular weights in the range of 4,000 to 6,000 Daltons.[1] Both systems utilize polyether triols; however, the ethylene oxide (EO) to propylene oxide (PO) ratio of each is generally very different. Slabstock foams tend to use lower EO content and have secondary OH endgroups. To achieve faster reaction rates, molded systems most frequently have much higher ethylene oxide content, and they use polyols with primary OH content in the range of 65 to 90%.[1] The faster reaction rate requires a different blend of catalysts as well as lower potency surfactants to obtain an open celled foam. Also, increasing the EO content of the polyol dramatically alters the miscibility of water and other reaction components; furthermore, it is believed that variation of the EO/PO ratio also has profound effects on the solubility of the hard segments in the polyol matrix of the final foam.[1] It is therefore deduced that the larger aggregates (urea balls) may form as either the hard segments or the urea precipitates or some combination of both reach a size or a concentration that surpasses a solubility limit which varies depending on the chemical system being utilized.[1,3]

Because the polyol usually has a functionality between two and three, these systems promote a covalent network. However, the development of hydrogen bonding of the hard segments as they precipitate also forms a network based on physical associations. The mechanical nature of that network is highly dependent on the shape of the polyurea precipitates. For instance, in a system of dispersed spheroids, each of these urea based domains would behave as a physical cross-link; however, if the precipitates develop in a more lamellar-like fashion, a co-continuous network might form instead. In summary, these systems are composed of at least two solid state phases and two types of "cross-links," chemical and physical. A more specific

review of these structures is available in references 4 and 6. It should be made clear that hydrogen bonds provide the physical cross-links with cohesive strength, but they are not themselves the cross-links. This hydrogen bonding between hard segments leads to a partially ordered or to a possibly "para-crystalline" texture which will be discussed more later in this paper. It should also be stated that the hydrogen bonding in a hard domain or urea precipitate is believed to be of the same type as that found in the hard domain aggregates or urea balls. Initial x-ray microscopy work by Ade and coworkers[7] on diphenylmethane diisocyanate (MDI) based foams has shown that these urea balls are not entirely urea but do contain some polyol. As yet unpublished work by Ade[8] on TDI based foams, more similar to typical slabstock formulations like those used in this study, has shown that these large aggregates still consist mainly of urea linked TDI but also contain ca. 5-10% polyol in the center with increasing amounts away from the center of the urea ball. This strongly indicates that the large aggregates are not entirely urea based hard segment material but may be thought of as aggregations of precipitates.

In examining how these materials behave during mechanical deformation, workers[9] have shown hard segment orientation transverse to the direction of elongation in flexible slabstock foams followed by additional orientation parallel to the stretch direction. This somewhat surprising behavior, also noted first in polyurethane elastomers, can best be explained by suggesting that hard domains are associating with one another to form lamellar-like structures which then dissociate under shear, yielding and rupturing upon further elongation.[9,10] This behavior suggests structure on a larger scale than the interdomain distances typically observed via small-angle x-ray scattering (7-11 nm). This indicates that such spacings may be the distances between lamellar-like formations, and that much larger lateral dimensions of the lamellae exist. However, no well defined lamellar-like structure in polyurethane foams has ever been distinctly and unambiguously observed via microscopy.[6] This discussion brings up the question of how well dispersed the hard domains actually are in polyurethane foams. Connectivity between them or associations on a scale larger than the size of hard domains could well lead to the behavior observed in reference 9. It should be obvious from this discussion that, whether in more localized urea-based hard segment domains or in larger urea aggregates, association via hydrogen bonding provides ordering that is of great importance to understanding the properties of these polymers.

Previous studies have demonstrated that many factors can influence the hard domain ordering, and that these can have large impacts on the properties of flexible polyurethane foams.[4-13] Humidity and temperature have both been shown to increase the rate of stress relaxation and compressive load relaxation.[4,11] These variables have also been shown to have an influence on compressive creep behavior.[12,13] It has also been demonstrated that cyclic humidity conditions increase the amount of compressive creep relative to samples held at a constant humidity.[13] These studies were performed over a few hours in the thermal range between room temperature and 100°C, generally too low for polymer decomposition on those time scales. It is therefore widely accepted that the thermal dependence is a result of the weakening of the hydrogen bond associations of the hard segments. This hypothesis is supported by the parallel humidity dependence because the polyol is largely hydrophobic and the urea domains are more hydrophilic.[13] These observations indicate the strength of the dependence of foam properties on the hard domains.

If foam properties are so dependent on the hard domains, it might be anticipated that variables which influence the concentration, composition, distribution, or ordering of the hard domains would thus become important to the final foam. These effects have in fact been demonstrated by many studies.[14-17] Hard segment content can be varied in foams by stoichiometrically increasing water and isocyanate in the feed while maintaining the amount of polyol added. In work by Turner et al, thus increasing hard segment content at constant soft segment content was shown to significantly increase the rubbery modulus of the foam.[14] This confirms that changing hard segment concentration can dramatically alter viscoelastic properties as would be expected. The importance of hard domain composition in foams has been shown by a study that incorporated the cross-linking agent diethanolamine (DEOA) into the foam formulation.[15] DEOA had the effect of altering the composition of the hard segments, and thereby dramatically changing their hydrogen bonding associations. This change in composition increased lability in the hard domains, making them more susceptible to water and thermal "plasticization." Additionally, the use of lithium chloride as a property modifier has been shown to soften the foam by disrupting hard domain ordering as noted by WAXS and altering their distribution in the matrix as revealed by SAXS and by solid-state NMR.[16,17]

The above cases only relate the importance of hard domains to the overall properties of a foam. However, it has also been determined that the precipitation of urea is an important event

in the development of foam structure.[18, 19] Foams without surfactant have been observed to be stable up to the point of urea precipitation—after which point they collapse.[20] More recent work on molded foam formulations using (MDI) rather than TDI have shown that, although urethane and urea linkages form immediately in the reactive mixture, the precipitation of urea groups occurs later, an event which leads to cell opening.[21] This precipitation behavior is thus vital to understanding the formation of a mechanically sound, open-celled foam.

Polysiloxane-polyether block copolymers of various topologies are used as surfactants in foams to stabilize the developing cell structure. In most formulations, stabilization is needed until gelation occurs through chemical cross-linking from the reaction of polyol with isocyanate, and this stabilization can prevent urea precipitation from collapsing the foam upon cell opening. As precipitation of hard segments into hard domains occurs, they organize via hydrogen bonding forming physical cross-links; moreover, it has been observed that this phenomenon parallels dramatic increases in the modulus of the material.[21]

The importance of stabilizing the dispersion of the urea precipitates is underscored by the earlier work of Rossmy and coworkers[20] *wherein foams were made with only surfactant, catalysts, water, and isocyanate (i.e. no polyol)*. In that work, three surfactants were used based on the same polysiloxane blocks but with polyether blocks varying in molecular weight and ethylene oxide/propylene oxide ratio. The first surfactant, using a polyether component of only propylene oxide with a molecular weight of 1,800, was incapable of maintaining the dispersion without the presence of polyol cross-linking, and with this surfactant the foam collapsed immediately following cell opening. The second surfactant used a polyether component of 45 weight percent ethylene oxide and a molecular weight of 1,500, and this second foam also collapsed following cell opening. By contrast, the third surfactant, which also did not have the benefit of polyol covalent cross-linking, did maintain the dispersion and form a stable, open-celled foam. This last surfactant utilized a polyether block of 45 weight percent ethylene oxide and a molecular weight of 2,000. These studies thus indicate that some formulation dependent combination of surfactant stabilization and covalent cross-linking is necessary to prevent urea precipitates from aggregating to sizes that promote collapse of the foam. This shows that, whereas organized urea precipitates provide the necessary modulus for good mechanical properties, *the dispersion of those precipitates throughout the polymer matrix promoted by surfactant stabilization or covalent cross-linking is necessary in maintaining an open celled*

foam structure. This work also points out the crucial role that ethylene oxide can play in polyurea stabilization whether it is used in surfactants or for endcapping polyols as is done in many molded foam formulations.

Recently, Yasunaga and coworkers[22] have further explored the event of cell opening in flexible slabstock foams. One result of that study confirmed the conclusions of Elwell et al[21] in that storage modulus development in foams follows the events of urea precipitation and cell opening. This further establishes the hypothesis that the organization of the hard domains is the driving factor in increasing mechanical properties. However, it also speaks to the importance of understanding the initial event of urea precipitation. Yasunaga and coworkers[22] also confirmed the earlier study of Rossmy and coworkers[18] in that increasing the surfactant concentration slows the rate of foam expansion and lengthens the time to cell-opening. *The implication of this is that surfactant concentration has an influence on the precipitation of the urea and therefore may have an influence on the microphase behavior of the final polymer material comprising the foam, possibly by altering the shape, size, or the distribution of the urea precipitates.*

Given the voluminous use of polyurethane foams and the dependence of their properties on these hard domains, it can be seen that it would be valuable to better understand their structural development and properties. As discussed above, although the surfactant is known to influence the rate of foam development and is hypothesized to influence urea precipitation behavior, this relationship is not well understood. Therefore, rather than study how the topology and composition of a surfactant influences foam stabilization, this study seeks to understand how surfactant influences microphase morphology by choosing one widely used surfactant[1,6] and studying how varying its concentration in a series of slabstock foams alters solid state phase behavior.

7.3 Experimental Materials and Methods

7.3.1 Materials

Several foam samples of flexible water-blown polyurethane foams were made with varying surfactant concentrations. These foams were based on 100 parts of Voranol® CP 3322 (Dow Chemical), a triol containing 88% propyleneoxide and 12% ethyleneoxide with terminal secondary OH-groups. The foams also used 4 parts of water and TDI 80 (an 80/20 mixture of the 2,4/2,6 isomers) fed at an isocyanate index of 105. Dimethylethanolamine was used as a catalyst for the water-isocyanate reaction at a concentration of 0.2 parts per hundred polyol

(pphp). Stannus octoate was used as a polyol-isocyanate reaction catalyst also at 0.2 pphp. A widely used surfactant for slabstock foams, TEGOSTAB® BF 2370 (Goldschmidt), was selected for this study, and it was varied as shown in Table 7.1. The nomenclature in Table 7.1 is completely explained at the end of this section.) The structure of this surfactant is shown in Figure 7.1. (Six foams were made that were allowed to fully develop with an additional 15 minute cure at 140°C to remove tackiness.

Table 7.1 - Sample Designations and Their Meanings

Sample Name	Comments
SSu0.0	Slabstock Foam, 0.0 Surfactant pphp
SSu0.3	Slabstock Foam, 0.3 Surfactant pphp
SSu0.75	Slabstock Foam, 0.75 Surfactant pphp
SSu1.5	Slabstock Foam, 1.5 Surfactant pphp
SSu10.0	Slabstock Foam, 10.0 Surfactant pphp
SSu20.0	Slabstock Foam, 20.0 Surfactant pphp
Q100-Su0.0	Quenched at 100 s, 0.0 Surf. pphp
Q100-Su1.5	Quenched at 100 s, 1.5 Surf. pphp
Q120-Su0.0	Quenched at 120 s, 0.0 Surf. pphp
Q120-Su1.5	Quenched at 120 s, 1.5 Surf pphp
C80-Su1.5	Mechanically Crushed at 80 s, 1.5 Surf. pphp
C106-Su1.5	Mechanically Crushed at 106 s, 1.5 Surf pphp
SHiEO	High Ethylene Oxide Content Slabstock
UPA	Urea Powder (TDI/H_2O) made in acetone
UPSu	Urea Powder (TDI/H_2O) made in surfactant
MD0.0	Molded Foam with 0.0 DEOA pphp
MD2.0	Molded Foam with 2.0 DEOA pphp

To explore the development of polymer morphology, four foams were quenched in liquid nitrogen at specific times during the foam reaction, two at 100 seconds and two at 120 seconds. Blow-off time for these formulations generally occurred at 110 seconds, so these quench times were picked to bracket that event. Two surfactant containing foams were also mechanically compressed to examine possible influences that the removal of cellular structure may have on the development of microphase separation in the solid state. One of these was crushed at 80 seconds, the time at which the 0.0 surfactant pphp foam spontaneously collapsed. The other foam was crushed at 106 seconds, the rise time to final height for that foam formulation. For all six of these samples, small quantities of material were taken from the reacting foam and then quenched or crushed. This was done to assure that the entire sample had a uniform thermal and morphological history characteristic of their respective times of quenching or crushing.

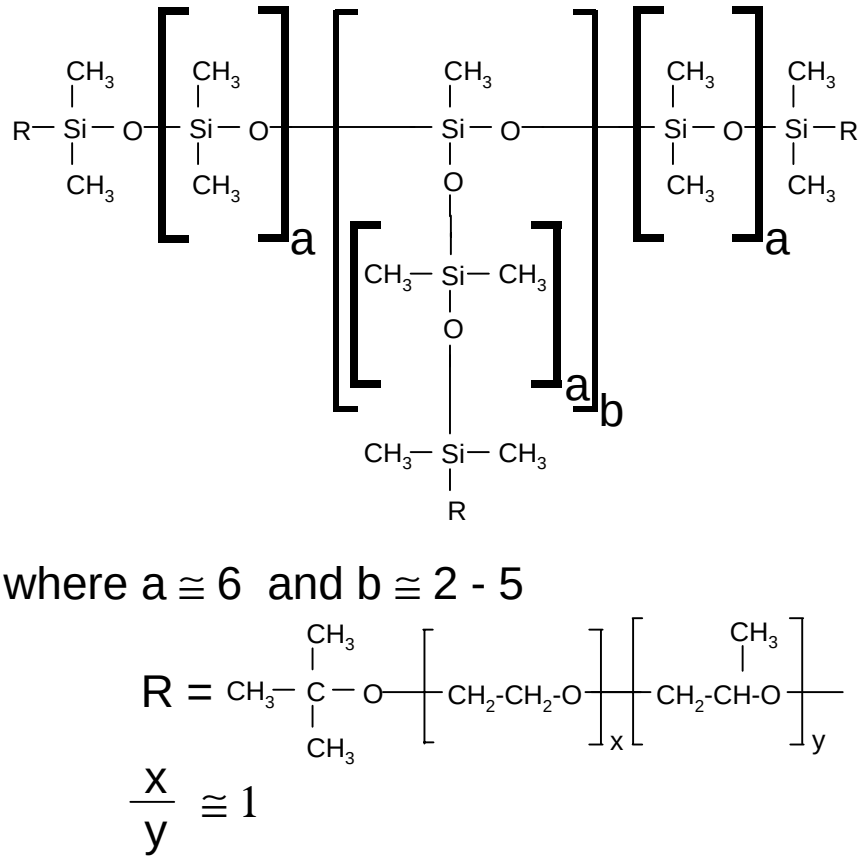

Figure 7.1 Structure of Tegostab® BF 2370 (Goldschmidt AG). Average molecular weight for the copolymer is 8,800. There are no emulsifying ingredients present in the surfactant besides remaining monol residues of the polyether mixture used for the copolymer synthesis.

For general comparisons, one additional foam was prepared specifically to reduce urea particle precipitation into hard domains. This formula was based on 75 parts of polyol ™Desmophen 7040 with an ethylene oxide content of 75% and 25 parts of polyol ™Desmophen 7160 with an ethylene oxide content of 12%. This formula used 2.0 surfactant pphp, 3.8 water pphp, and 0.3 amine catalyst (™Dabco) pphp. This formula also used a TDI 80 at an isocyanate index of 95. Finally, two polyurea based powders were produced. One was made by dissolving TDI 80 in acetone and slowly feeding in an excess of water to produce polyurea segments with a calculated number average of 10 repeat units. The acetone was evaporated and the powder was then dried in a vacuum oven. The other powder was produced by using the same formula as the slabstock foams but replacing all of the polyol with ™TEGOSTAB BF 2370 (Goldschmidt).[23]

The nomenclature for these samples is as follows. Generally, the first letter of a sample name indicates the type of sample and the manner in which it was made. The next set of letters indicate what the variable was for that sample. For instance, SSu0.0 is a slabstock foam in which the surfactant concentration was 0.0 pphp. Possible first letters include: "S" for a slabstock foam, "M" for a molded foam (two molded foams were utilized for comparative WAXS and FTIR analyses), "C" for a foam that was crushed, "Q" for a foam that was quenched in liquid nitrogen, and "UP" for a polyurea powder. Numbers are included for the letter of the variable that they follow. As used above, it gives the concentration of surfactant in a sample. In Q100-Su0.0 or C80-Su0.0, the 100 or 80 corresponds to the time in seconds after the foam reactions were initiated that the samples were quenched or crushed, respectively. Finally, there are three exceptions to this nomenclature. SHiEO is the slabstock foam made with the high ethylene oxide content polyol discussed. UPA and UPSu are polyurea powders made in pure acetone and pure surfactant, respectively.

7.3.2 Methods

Dynamic mechanical analysis (DMA) was carried out using a Seiko model 210 in the tension mode. The samples were heated from -120 °C to 350 °C at a rate of 0.5 °C/min. from which the storage modulus (E') and tan δ data were collected at a frequency of 1 Hz. Samples were cut from the foam with die-punches and had dimensions of approximately 5 x 5 x 15 mm with a grip-to-grip distance of 10 mm. Storage moduli are normalized to 3×10^9 Pa to remove the effect of varying density which is only a function of cellular structure.[14] Differential scanning calorimetry (DSC) was performed on a Seiko model. Scanning at 10°C/min from -120 to 350 °C. This was performed for comparison with the tan δ data from the DMA.

Small angle X-ray scattering (SAXS) was utilized to evaluate the presence of microphase separation. This was performed with a Phillips model PW1729 generator operating at 40 kv and 20 ma and a slit collimated (0.03 x 5 mm) Kratky camera with nickel filtered CuKα radiation having a wavelength of 1.542 Å. The detector utilized was a Braun OED 50 position-sensitive platinum wire detector. Scattering data were corrected for parasitic scattering and normalized using a Lupolen standard. Because apparent density varied, the beam path length for the non-quenched and non-crushed foam samples ("S" series in Table 1) was also corrected based on density relative to the apparent density of sample C80-Su1.5. The foam samples were cut

approximately 8 mm thick and compressed to approximately 2 mm. This data was analyzed using the TOPAS program developed by Dr. Stribeck at the University of Hamburg. Dr. Stribeck has graciously posted TOPAS for free downloading on the world wide web at http://www.chemie.uni-hamburg.de/tmc/stribeck/index.html.

To explore the ordering of the hard domains, the technique of wide angle X-ray scattering (WAXS) was applied via a Phillips model PW1720 generator with a Warhus camera. Nickel filtered CuK radiation was used with a wavelength of 1.542 Å and pinhole collimation with a diameter of 0.020 inches. These samples varied widely in apparent density; therefore, using their apparent density and the 0.020 inch beam diameter as a basis for the calculation, samples were cut to thicknesses which would expose ca. 3.2 mg of material to the beam. Foam samples were compressed to a ca. 2 mm thicknesses, but the collapsed materials did not need this compression. Sample to film distance was 7.7 cm and exposure times were ca. 10 hours.

Fourier transform infrared (FTIR) was also used to evaluate hydrogen bonding in the hard domains as shown in Table 7.2.[24] FTIR Spectra were collected on a Nicolet 510 Spectrometer using a Spectra-Tech ATR attachment. The ATR cell utilized a horizontal ZnSe crystal. Spectra were analyzed using Omnic 3.0 software, and all scans were normalized by the corrected peak height at 2970 cm^{-1} which corresponds to a CH_3 absorbance.[18]

Table 7.2 - Some Relevant IR Absorbances of the Carbonyl Chromophore

Group Containing Carbonyl	Wavenumber (cm^{-1})
Free Urethane	1730
Free Urea	1715
Hydrogen bonded Urethane	1705-1700
Monodentate Urea	1700-1650
Bidentate Urea	1640

Characterization of the cellular structure of the foam was performed with scanning electron microscopy (SEM). Thin foam slices, ca. 5 mm, were mounted to aluminum stubs using copper tape. These samples were then sputter coated with gold to ca. 15 nm thicknesses. Micrographs were taken using a Cambridge Stereoscan model 200 operating at 10 kv and at magnifications of ca. 100x.

Transmission electron microscopy (TEM) was used to observe the precipitated urea particulate. Small samples were cut from the foams and then embedded in epoxy which cured at 60 °C overnight. Thin sections (ca. 80 nm) were then cryogenically microtomed using a

diamond knife on a Reichert-Jung Cryo-ultramicrotome Ultracut E with a model FC-4D cryo-attachment operating at -90 °C. Ethanol was used to collect the sections onto 600 mesh copper grids. Micrographs were taken using a Philips 420T scanning transmission electron microscope (STEM) operating at an accelerating voltage of 80 kv. Micrographs were taken at three levels of magnification, corresponding on the negatives to 37,500x, 10,500x, and 3,300x.

Atomic force microscopy (AFM) in tapping mode was also used to study nanoscopic level structure. These experiments were performed on a Digital Instruments Scanning Probe Microscope using Nanosensors TESP (Tapping Etched Silicon Probe) type single beam cantilevers. These cantilevers had nominal lengths of ca. 125 μm, force constants of approximately 35 ± 7 N/m, and were used at oscillation frequencies at ca. 290 kHz. The samples mounted in epoxy for TEM were cryo-microtomed smooth and then examined by AFM. The phase image of AFM is generated by recording the phase shift that occurs between the drive oscillation on the cantilever and the oscillation of the cantilever tip. The phase shift of a cantilever oscillating in free air would be close to zero. As the oscillating tip contacts the surface its phase shift is relative to the interactions occurring between tip and sample. Phase shift becomes more positive when interacting with harder materials, and estimations from the Hertz theory lead to the relation that phase shift scales with the dynamic modulus of the sample.[25] It should also be pointed out that once AFM phase images using scales above 1 or 2 microns are saved much information on the scale lengths of the hard domains (ca. 7-11 nm) is lost. Thus, to obtain and later analyze the high resolution information needed regarding the phase offset, phase images measuring 2 microns by 2 microns were collected for quantitative analysis. Further details of phase imaging with tapping mode AFM are available online at http://www.digital.com/AppNotes/Phase/PhaseMain.html.

A series of AFM experiments were used wherein the force applied to the surface was controlled by holding two variables constant. The amplitude of the cantilever's free air oscillation was maintained at 5.05 V. However, as the tip oscillates, its amplitude while striking the surface is lower than that value and was maintained at 60 percent of the value of the free air amplitude. Control of these two factors should maintain constant the energy of the cantilever as well as the force being applied to the surface. By randomly sampling the surfaces, by using new tips, and by scanning surfaces multiple times, reproducible levels of maximum phase offset were observed. These values are used in this work to follow trends regarding the *relative hardness* of

the hard domains. This effect has been recently been qualitatively shown in triblock copolymers and polyurethane elastomers by McLean and Sauer.[26] Furthermore, this technique was first demonstrated by application to flexible polyurethane foams by the authors in a previous publication.[27] This work will also seek to further quantify these efforts.

7.4 Results and Discussion

To understand the influence of surfactant on properties, its effect upon morphology must also be understood. It is well known that without surfactant, the cellular structure collapses before the gelation reaction can stabilize the foam.[1] This can be observed in Figures 7.2a-7.2h where eight SEM micrographs show the typical pattern of cellular structure observed.

Figure 7.2a reveals that the morphology of SSu0.0 might be characterized as large gas pockets held within wide, voidless polymeric regions. Figure 7.2b shows that SSu1.5 has the cellular structure expected in a slabstock foam with cell diameters greater than 1 mm. This cellular morphology was observed at all surfactant concentrations examined greater than zero. Figures 7.2c and 7.2d compare the structure of the quenched foams, Q100-Su0.0 and Q100-Su1.5. It is observed that, even in these incompletely reacted foams, the difference made by the presence of the surfactant is apparent. Q100-Su0.0 shows a very smooth surface compared to Q100-Su1.5 which exhibits smaller (<1 mm diameters) but recognizable cells “frozen” in their nascent state. The micrographs of samples Q120-Su0.0 and Q120-Su1.5 are presented in Figures 7.2e and 7.2f, and it can be seen that they exhibit similar behavior to samples Q100-Su0.0 and Q100-Su1.5, respectively. Figure 7.2g reveals that sample C80-Su1.5 resembles the morphology of samples Q100-Su0.0 and Q120-Su0.0 in that it is not composed of cells but of a continuous polymer matrix with some gas bubbles spread throughout it. It is noted, however, that this sample has many more gas pockets than any of the Figures 7.2c through 7.2f. However, the small amount of gas present in sample C80-Su1.5 is demonstrated by the apparent densities of the samples listed in Table 7.3. It is shown there that this crushed sample has half as much gas as the other collapsed specimens.

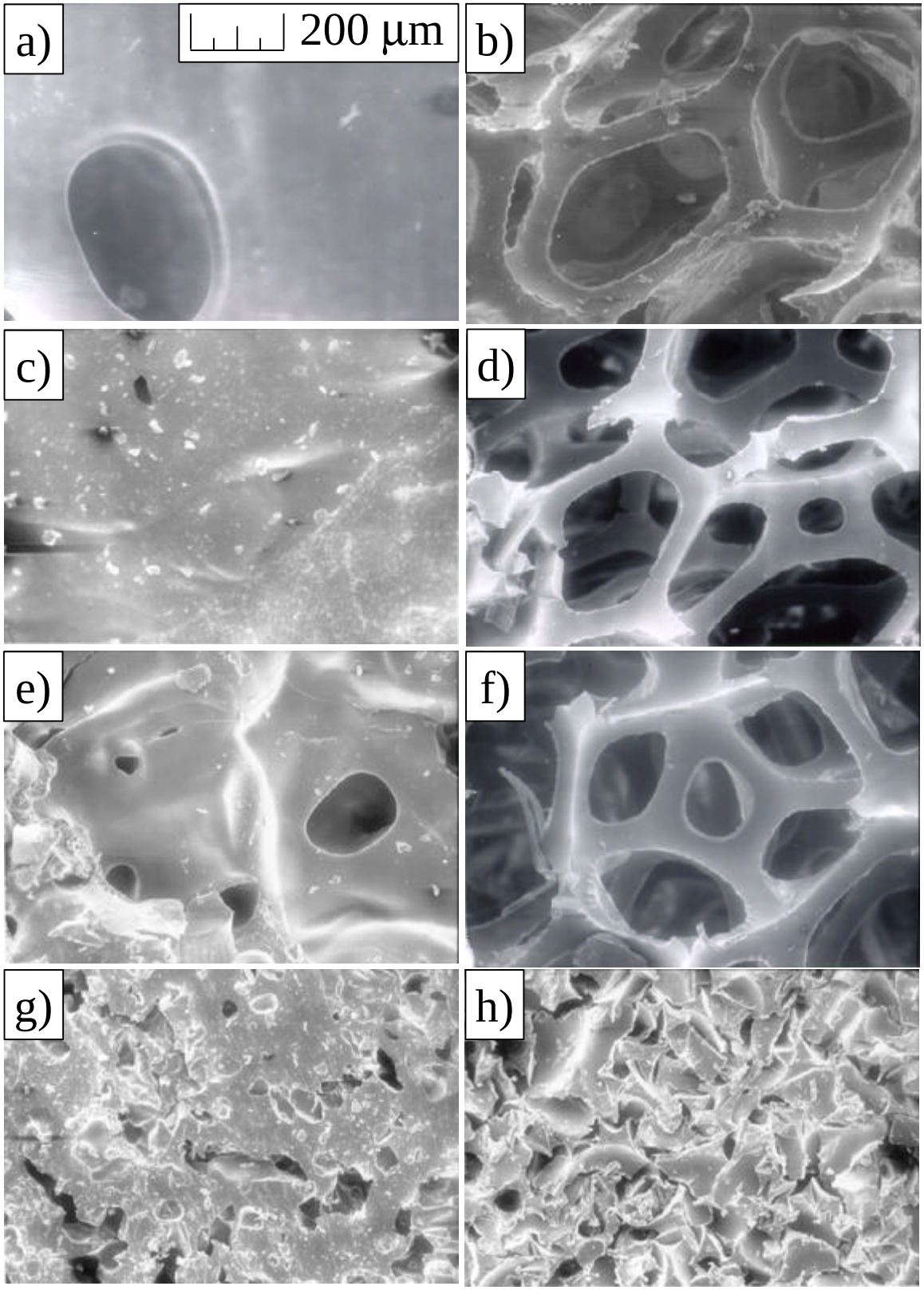

Figure 7.2 Scanning electron micrographs of foams in various states: 2a) SSu0.0, 2b) SSu1.5, 2c) Q100-Su0.0, 2d) Q100-Su1.5, 2e) Q120-Su0.0, 2f) Q120-Su1.5, 2g) C80-Su1.5, and 2h) C106-Su1.5. The scale bar shown in 2a) applies to all of the micrographs.

Table 7.3 – Apparent Densities of the Samples

Sample Name	Apparent Density [g/cm^3]
SSu0.0	0.1810
SSu0.3	0.0260
SSu0.75	0.0234
SSu1.5	0.0245
SSu10.0	0.0226
SSu20.0	0.0265
Q100-Su0.0	0.3978
Q100-Su1.5	0.3225
Q120-Su0.0	0.0332
Q120-Su1.5	0.0590
C80-Su1.5	0.7446
C106-Su1.5	0.3536
SHiEO	0.0232

Figure 7.2h reveals that C106-Su1.5 has very different morphology. This crushed foam is composed of pieces of the cellular structure observed in Figures 7.2d or 7.2f squeezed together. It seems that just after cell opening at 106 seconds, the foam has achieved enough dimensional stability to prevent congealing to the extent seen in Figure 7.2g. This sample and sample C80-Su1.5 will then be used to evaluate the importance of the presence of the cellular structure to the organization of the hard domains at the point of urea precipitation. Furthermore, these micrographs illustrate that, without surfactant, the reactive mixture has relatively little surface area of an gas-liquid interface in comparison to mixes with surfactant. It also shows that with surfactant the larger surface area may be altered by crushing or quenching but it is still clearly present.

TEM was used to evaluate the solid morphology within the cell wall material itself. This technique has been used in other studies[6] to examine larger scale precipitation behavior of the urea which shows up as dark regions in the micrographs. At the highest magnifications used, the two micrographs of Figure 7.3 examine the size of the urea rich aggregations. Figure 7.3a shows that in SSu0.0 the precipitates begin around 100 nm in diameter and get larger. Figure 7.3b reveals, however, that in SSu1.5 precipitates begin around 100 nm in diameter and get smaller. While these are subtle size differences, they are representative and, furthermore, this subtle difference will be supported by other results. Furthermore, this may be one sign of alterations in the distribution of urea precipitates in the matrix. It may indicate that what connectivity may be

developing occurs via associations between the larger urea balls and not of a lamellar-like structure—at least at this scale length.

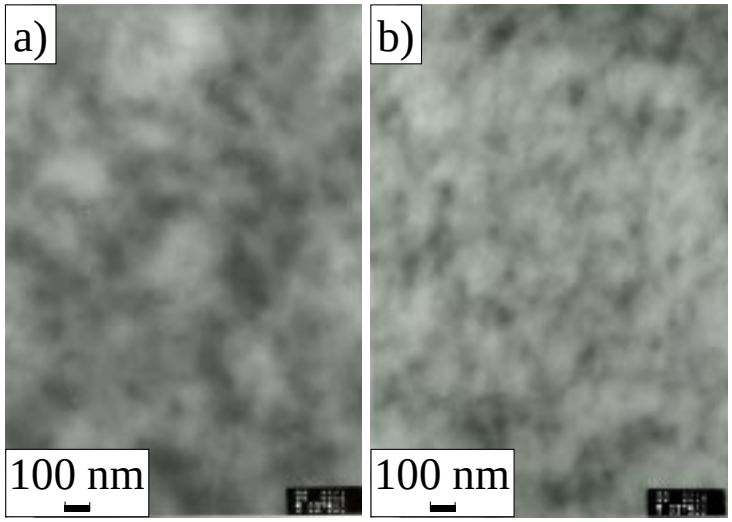

Figure 7.3 Transmission electron high magnification micrographs for two foams with varying surfactant concentration: 3a) SSu0.0 and 3b) SSu1.5

Also interesting is the comparison of phase behavior at a moderate magnification. Figure 7.4 exhibits eight micrographs, two of fully formed foams, four of quenched samples, and two of the crushed samples. It should be noted that the darker stripes observed in Figures 7.4b and 7.4d are due to variation in the thickness of the section and not to any change in morphological character. Figures 7.4a and 7.4b show SSu0.0 and SSu1.5, respectively, and illustrate the typical behavior of slabstock foam samples. Both of those two micrographs reveal a uniform dispersion of the aggregates observed in Figure 7.3. It also shows no noticeable differences *at this scale* between samples with and without surfactant. However, Figures 7.4c and 7.4d show that, at the same magnification, dramatically different behavior can be observed in the quenched samples. Sample Q100-SSu0.0 shown in Figure 7.4c reveals large areas with little urea precipitation and other large regions with much aggregation occurring. Sample Q100-SSu1.5 shown in Figure 7.4d reveals that this does not occur in foams with surfactant, providing further evidence that surfactant does have a stabilizing influence on urea precipitates. Figure 7.4e shows that sample Q120-Su0.0 has aggregates that are more dispersed. This indicates that the additional 20 seconds of reaction time provided this sample with more stability in preventing large scale aggregation due to a higher degree of covalent bonding than sample Q100-Su0.0 had. Figure 7.4f illustrates that sample Q120-Su1.5 had a similar morphology to sample Q100-Su1.5, indicating that with surfactant present, the time of quench made much less of an impact. It is

worth emphasizing that the morphology observed in the micrographs of the quenched materials is not supposed to characterize the morphology of the high temperature reactive state. Rather, they characterize the aggregation behavior of the hard segments at that level of covalent cross-linking, concentration of surfactant, and with or without the presence of the cellular structure.

The most intriguing parts of Figure 7.4 are in Figure 7.4g and 7.4h. These two micrographs are of the two foams that were mechanically crushed. Figure 7.4g shows that in sample C80-Su1.5 the same morphology was developed as in sample Q100-Su0.0. This indicates that surfactant alone is not enough to prevent large scale aggregation from occurring. Observing that sample C106-Su1.5 does not exhibit this aggregation but does exhibit a dispersed morphology indicates that being in the collapsed state at the time of urea precipitation plays a large role in the final morphology of the polymer.

Figure 7.5 seeks to examine this better by presenting six micrographs of the quenched and crushed samples at the lowest level of magnification used. Figure 7.5a shows that the large scale aggregation behavior of sample Q100-Su0.0 was characteristic of the entire polymer sample. It also shows that these aggregates cover spaces of several microns. This is dramatically different than the very even distribution seen in Figures 7.5b, 7.5d or 7.5f (samples Q100-Su1.5, Q120-Su1.5, and C106-Su1.5 respectively). Figure 7.5c reveals that in sample Q120-Su0.0, although the precipitates are more disperse than sample Q100-Su0.0, some large aggregation can still be seen. Finally, in Figure 7.5e it is observed that sample C80-Su1.5 does have a very similar morphology to sample Q100-Su0.0, and that this morphology is characteristic of the whole. Before making final conclusions about the TEM data, two AFM phase images are also presented in Figures 7.6a and 7.6b to attest to the validity of that technique for use in foam research. Figure 7.6a (Q100-Su0.0) and Figure 7.6b (Q100-Su1.5) are shown in similar scale for easy comparison to TEM micrographs of Figures 7.4c and 7.4d. *Also, the scales of the AFM phase images in Figure 7.6 have been inverted so that the harder material has lower offset and appears darker just as the urea-rich regions appear dark in the TEM. This was done only to these two images in order to parallel the TEM images for convenience; however, in the rest of this paper all AFM phase images will use the normal scale for the instrument wherein higher phase offset indicates harder material and appears whiter.*

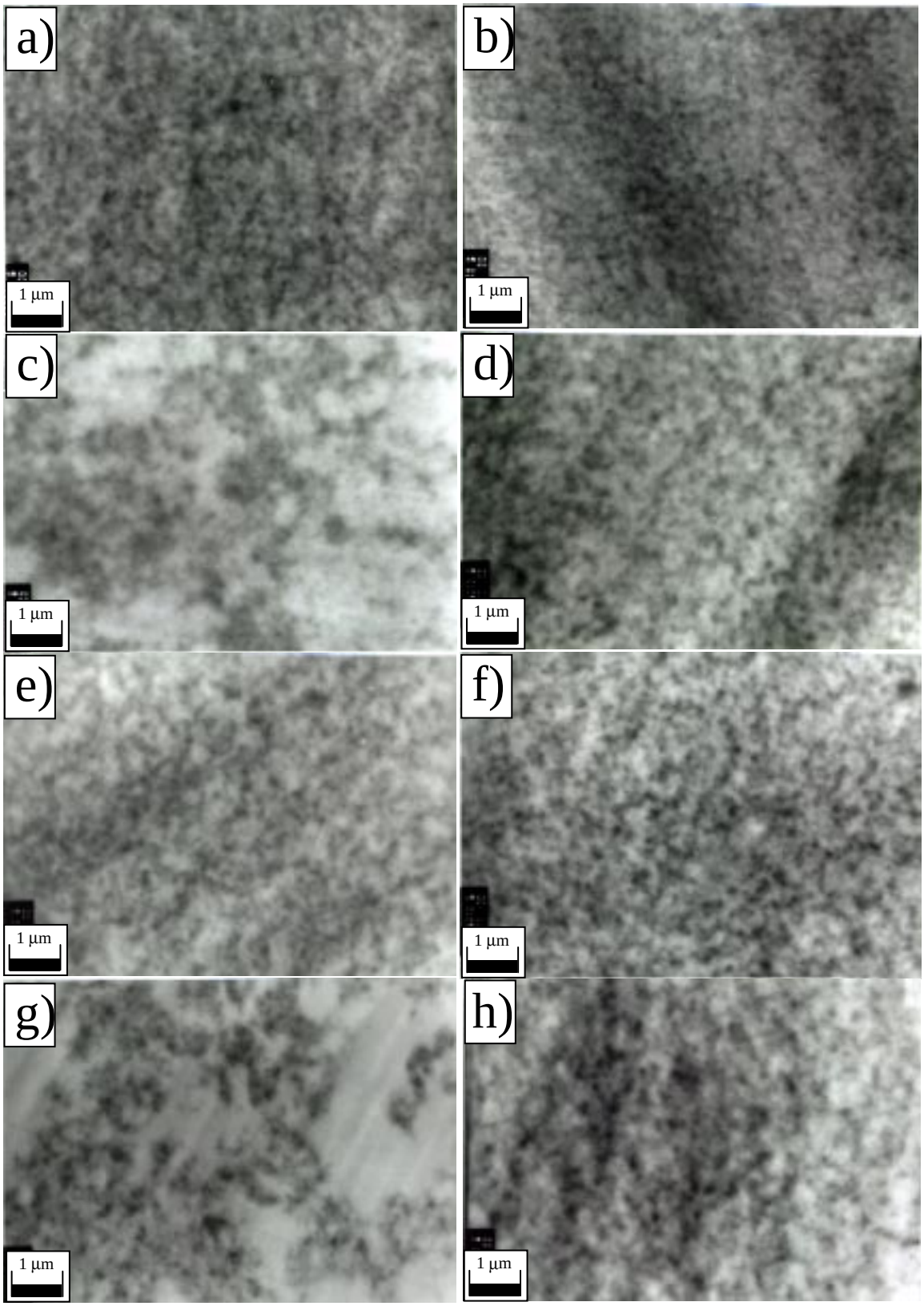

Figure 7.4 Transmission electron medium magnification micrographs of foams in various states: 4a) SSu0.0, 4b) SSu1.5, 4c) Q100-Su0.0, 4d) Q100-Su1.5, 4e) Q120-Su0.0, 4f) Q120-Su1.5, 4g) C80-Su1.5, and 4h) C106-Su1.5

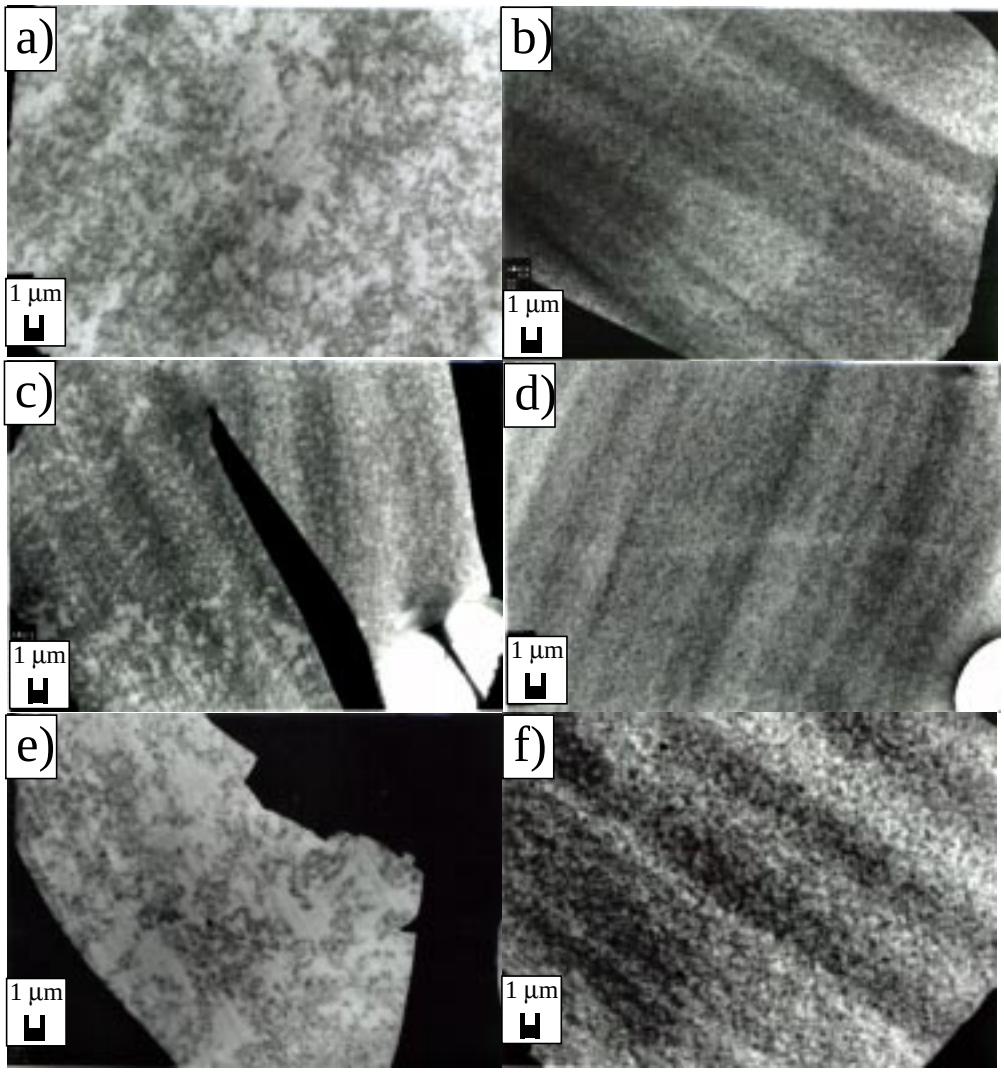

Figure 7.5 Transmission electron low magnifation micrographs of foams in various states: 5a) Q100-Su0.0, 5b) Q100-Su1.5, 5c) Q120-Su0.0, 5d) Q120-Su1.5, 5e) C80-Su1.5, and 5f) C106-Su1.5

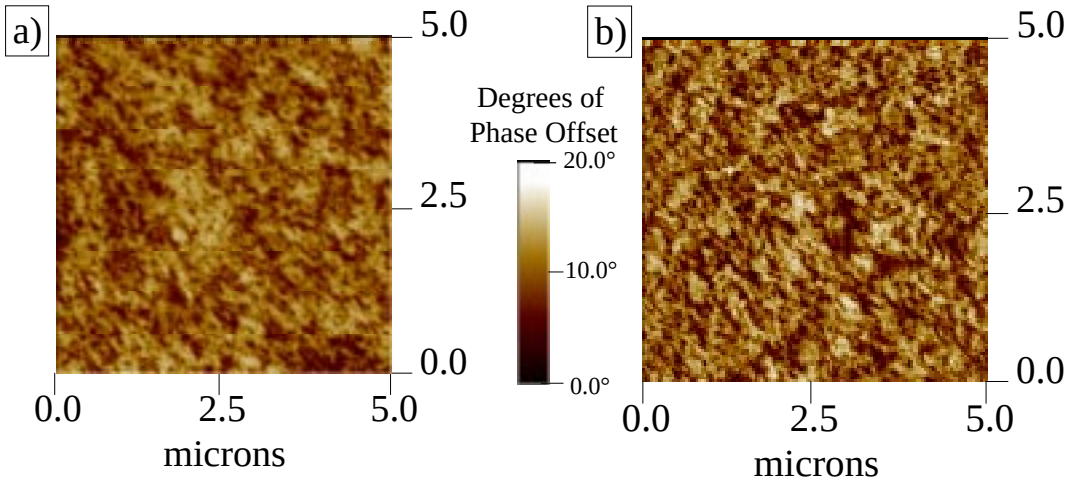

Figure 7.6 Atomic force microscopy phase images of two quenched materials: 6a) Q100-Su0.0 and 6b) Q100-Su1.5. The z axis scale has been inverted from the machine default such that higher phase offset is induced by softer material. This is only done in these two images to parallel the TEM micrographs of Figures 3-5.

Altogether, the TEM micrographs presented show an interesting pattern. They reveal that when the reactive mixture is allowed to go to completion at high temperature (ca. 140 °C), an evenly dispersed morphology is achieved over the whole range of surfactant concentrations studied. Without the stabilizing effect of the surfactant, however, aggregation does occur when quenched prior to reaction completion. Comparison of Figures 7.4c and 7.4e (or 7.5a and 7.5c) also shows that allowing the reaction to proceed an additional 20 seconds stabilizes the urea further so that the precipitates of sample Q120-Su0.0 are smaller. This is attributed to further completion of the gelation reaction. With surfactant this behavior is not observed, and the precipitates are observed to be dispersed regardless of the progress of the reactions. This is taken as direct evidence of the ability of surfactant to influence urea precipitation; however, the mechanism of that influence needs further elucidation. This is why samples C80-Su1.5 and C106-Su1.5 are so important. *These show that the observed behavior is not strictly a direct function of the surfactant but also of the presence of the cellular morphology.* All three samples shown in Figure 7.5 that exhibit large scale aggregation behavior were in the collapsed state when the urea precipitated. All three samples of Figure 7.5 that show a dispersed morphology still had a cellular morphology at the point of urea precipitation. Why then is there not large-scale aggregation observed in the micrographs of SSu0.0 (Figure 7.4a)? It is recalled that sample SSu0.0 is the only sample that collapsed which had a thermal history more similar to a normal foam despite losing some heat in the expulsion of gas upon collapse. This indicates the importance of maintaining a high temperature until the gelation reaction adds enough stability to the system to prevent large scale aggregation from being induced by dramatic cooling. Such cooling may occur either by quench or by squeezing into a thin film between two unheated metal plates. It can be said from all of these micrographs that, without cellular structure, high temperature is necessary to maintain the dispersion of urea precipitate; however, with cellular structure at the point of urea precipitation, thermal history is less important to the phase separation behavior at these scales. This raises the question of what influence does quenching or cooling or spontaneously collapsing have on even lower scale morphology, and this will be examined next.

SAXS has been widely used in polyurethane foam research[28] to follow phase separation behavior; however, the laws of scattering and the wavelengths of x-rays only allow this technique to examine scales smaller than what is needed here for a complete analysis of phase

behavior. This technique thus explores phase separation behavior on length scales between TEM and WAXS. Figures 7.7a-7.7e show some representative SAXS data and the results of the correlation function analyses. One thing that this revealed is that all of the foams, including SHiEO, are microphase separated. It can also be observed in Figure 7.7a that the scattering intensity of SSu0.0 is much lower than that of the other completely reacted samples. This is suggestive of less microphase separation in the collapsed material. Taking the Fourier transform of the scattering curves in the proper manner[29] can lead to the three dimensional correlation functions shown in Figure 7.7b. This is essentially a plot of the probability that a rod of length "r" has both of its ends in a domain of similar electron density.[29] Figure 7.7b clearly shows that every completely reacted foam exhibits an interdomain spacing of 7.6 nm. Thus revealing that the surfactant concentration does not have a detectable influence on the interdomain spacing of the completely reacted foams.

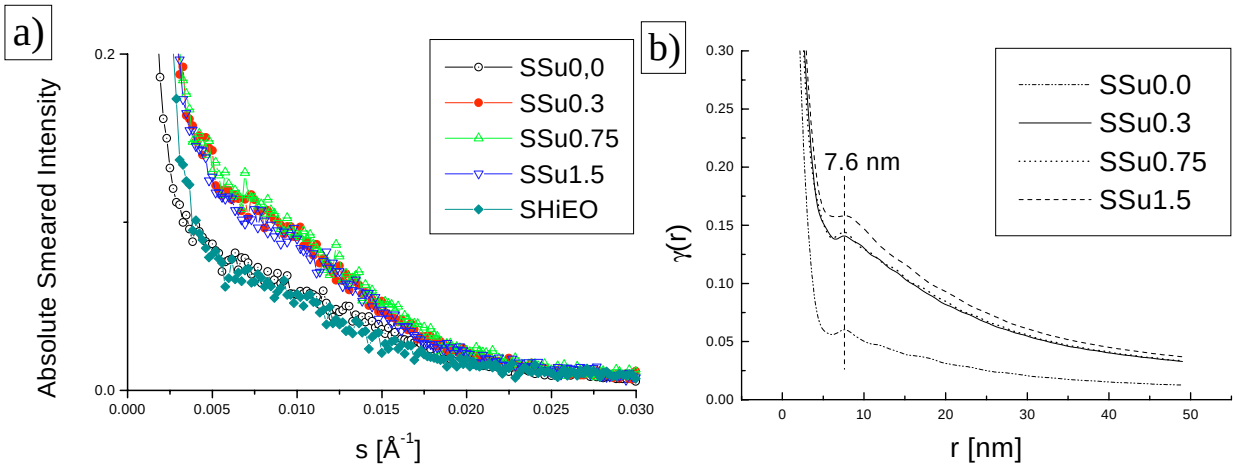

Figure 7.7 a) Small angles x-ray scattering data for foams of varying composition. 7 b) Three dimensional correlation functions for four slabstock foams of varying surfactant concentration.

On the other hand, Figure 7.8a shows the SAXS data for Q100-Su0.0 and Q120-Su0.0 wherein it can be seen that the patterns are clearly different although a definite shoulder position is difficult to place. Figure 7.8b shows the 3-D correlation functions for all of the quenched materials, where it can be seen that the foams with surfactant appear to have nearly identical distributions, both having most probable interdomain distances of 6.5 nm. Without surfactant, however, quenching at 100 seconds changes the microphase separation behavior significantly, developing an interdomain spacing of 7.6 nm. It is observed that the Q120-Su0.0, which had an additional twenty seconds in the high temperature reactive state, has a spacing of 6.9 nm,

seeming to approach the spacing of the surfactant-containing quenched materials. It is also noted that in Figure 7.8c the crushed materials are seen to both have interdomain distances of 7.5 nm. This confirms what is observed in the TEM data: adding reaction time alters the phase separation behavior of these foams.

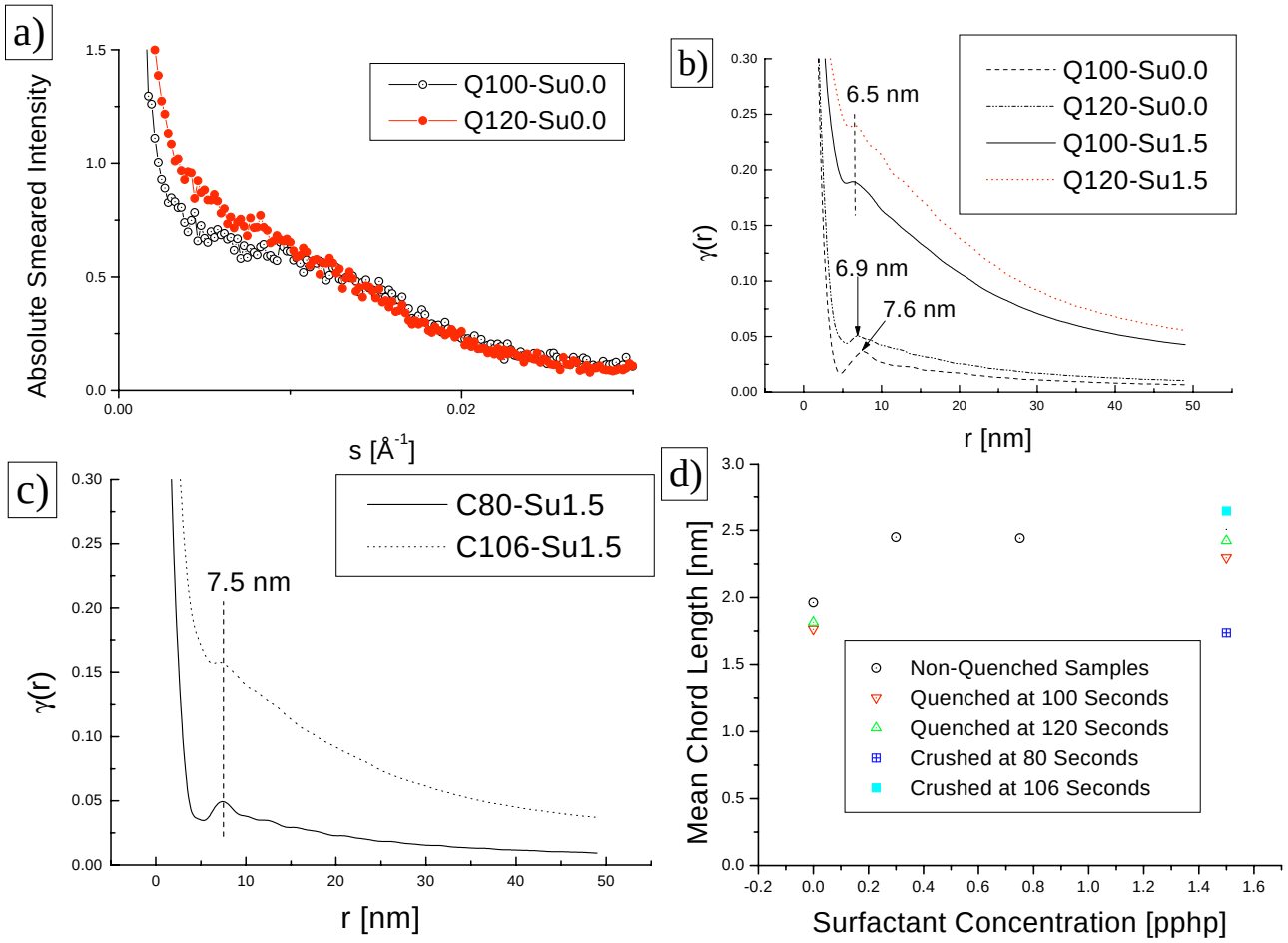

Figure 7.8a) Small angles x-ray scattering data for two foams quenched from reaction at different times. 8b) Three dimensional correlation functions for four quenched foams of varying surfactant concentration. 8c) Three dimensional correlation functions for two crushed foams of 1.5 surfactant pphp concentration. 8d) Comparison of the mean chord lengths for all the samples.

These results indicate that the most probable interdomain distance as revealed by SAXS is not strongly influenced by changes in surfactant concentration. However, another parameter that can be obtained from SAXS, the mean chord length, does exhibit some systematic changes. This parameter is interpreted to be the average size of the hard domains throughout the sample.[29] This interpretation applies to dispersed components, and it is strongly dependent on the shape of

each phase in the system.[29] For more lamellar-like or sponge-like structures, the mean chord length or inhomogeneity length characterizes the harmonic average of the chord lengths in each phase.[29] The results of this analysis performed on each sample are shown in Figure 7.8d. The clearest thing observed is the subtle yet consistent increase in the mean chord length of the non-quenched samples as the surfactant increases. It appears from Figure 7.8d that the mean chord length step jumps with the first increment of surfactant added and is fairly stable after that, varying only slightly (increasing from 1.96 nm in SSu0.0 to 2.50 nm in SSu0.3 to 2.51 nm in SSu1.5). This is significant since SSu0.3 had the lowest surfactant concentration of any sample which maintained a cellular structure. So it appears from Figure 7.8d that a mean chord length of ca. 2 nm may be expected in collapsed materials, and a length of ca. 2.5 nm may be expected in materials that have a cellular structure.

Another systematic trend is that the chord length increases steadily the longer the foam is left at the high temperature reactive condition. For instance, the 0.0 surfactant pphp samples exhibit a 1.76 nm chord length when quenched at 100 seconds, 1.81 nm if quenched at 120 seconds, and exhibit a chord length of 1.96 nm if not quenched at all. By comparing samples quenched at the same time, it also can be observed that in every case the sample with surfactant exhibits a longer chord length. For example, Q100-Su0.0 has a chord length of 1.76 nm whereas sample Q100-Su1.5 is spaced at 2.30 nm. This reveals a new pattern not observed in TEM: the presence of surfactant seems to facilitate either the growth of the hard segments themselves or the phase separation process as the hard domains become larger.

These results show progressing structural development in terms of increasing mean chord length with increasing time until quenched or crushed. It is not surprising that a foam quenched from reaction to liquid nitrogen temperatures would not achieve the same domain sizes that a fully developed foam has. However, it is especially interesting that a sample that was crushed and not quenched, C80-Su1.5, has a lower mean chord length (1.74 nm) than either C106-Su1.5 (2.64 nm) or SSu1.5 (2.51 nm). This indicates that being in the collapsed state prior to urea precipitation apparently does alter the microphase morphology of the foams. While this is additional evidence that the surfactant does not play a direct role in the development of hard domain structure, *it does further suggest that development of cellular structure has a strong influence on that process.*

These results have shown that the lack of large surface area of a gas-liquid interface at the time of urea precipitation has a large influence on solid state morphology in crushed and quenched materials. However, if high temperature is maintained in the collapsed state (as shown in the micrographs of SSu0.0) only a subtle change in micron-scale morphology is observed. These two apparently disparate results may indicate that, at the molecular level, a lack of surfactant has had an effect. Such an effect may only become readily observable at microscopic levels after the system is kinetically jarred by something like a quench in liquid nitrogen or by being mechanically crushed between two room temperature metal plates. If a molecular level effect does indeed exist, it should be detectable by FTIR, WAXS, and AFM.

The FTIR technique has been well established as a method for evaluating the level of hard segment hydrogen bonding in these materials. Although the WAXS studies on slabstock foams show that they are clearly not semi-crystalline materials, it has been widely observed that a distinct scattering or diffraction peak occurs in the patterns corresponding to ca. 4.7 Å spacing.[1,2] This peak has been widely attributed to ordering within the urea based hard domains or aggregates without exact knowledge of the exact source of its reflection. Figures 8a-8f show the correlation that exists between WAXS and FTIR for samples UPA, UPSu, and SHiEO. It can be observed that in Figure 7.9b, sample UPA, which is a pure polyurea powder based on TDI 80, has the many reflections expected of the highly-crystalline powder. These reflections have been reported by other workers,[2] and it is particularly noted that the strongest reflection is a doublet peak occurring at ca. 4.7 Å. The FTIR spectrum shown in Figure 7.9a reveals many absorbances, but one of particular strength occurs ca. 1640 cm^{-1}, corresponding to bidentate hydrogen bonding of the urea carbonyl group. Figure 7.9c shows that the FTIR of sample UPSu still exhibits a strong ca. 1640 cm^{-1} peak, indicating that the surfactant has not altered the bidentate hydrogen bonding of the urea. The WAXS pattern of UPSu (Figure 7.9d), however, shows that, even with only surfactant present, the only remaining periodic spacing in the sample is that which corresponds to the 4.7 Å ordering. This clearly indicates that not only does surfactant influence the way urea rich hard segments pack together, it only leaves one type of ordering at all, the 4.7 Å spacing. Comparison of these figures thus give strong evidence that the 4.7 Å spacing arises from the bidentate hydrogen bonding between urea linkages within the hard domains.

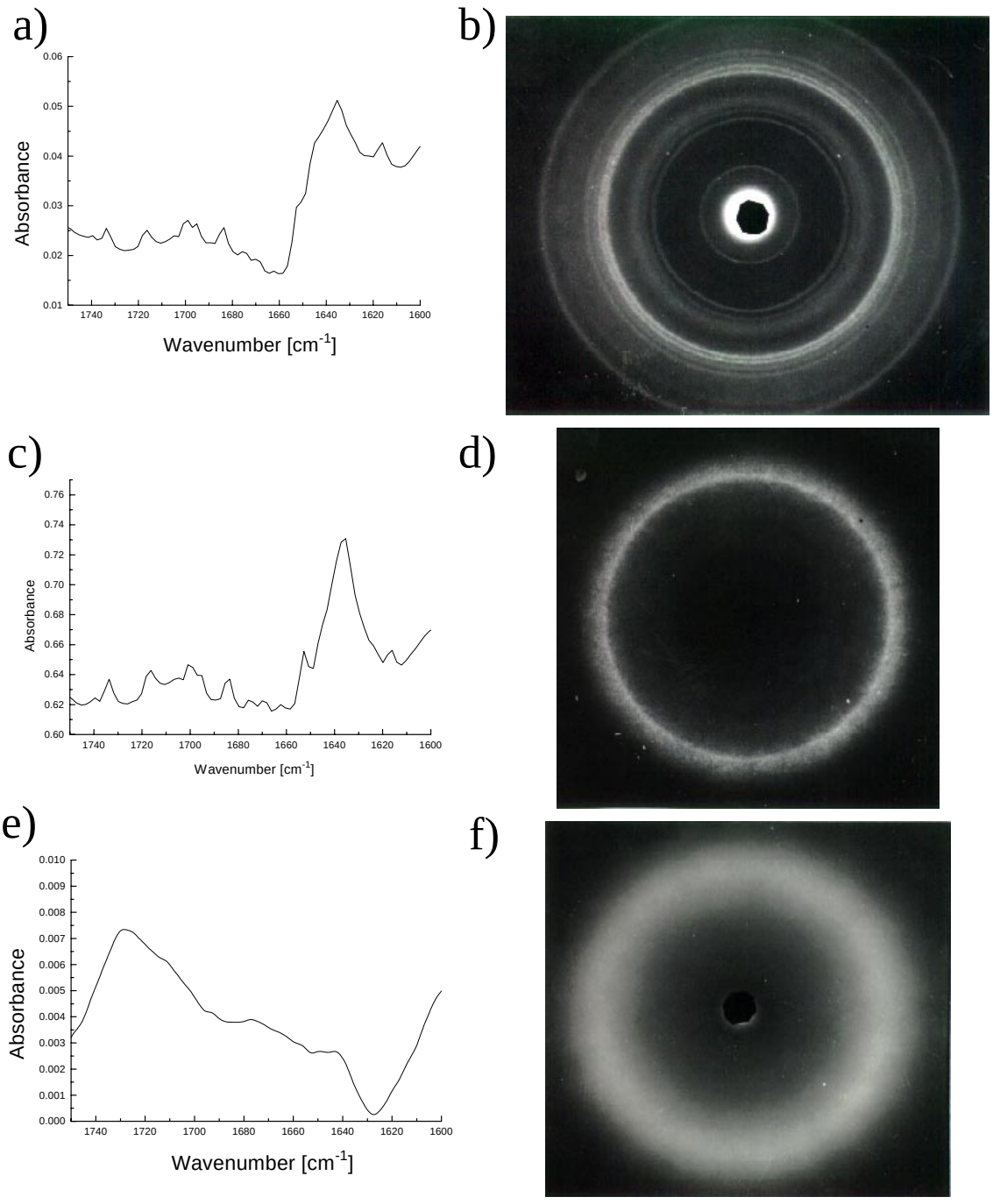

Figure 7.9 Correlation of Fourier transform infrared spectroscopy and wide-angle x-ray scattering for polyurethane foams: 9a) transmission mode FTIR spectrum of UPA, 9b) WAXS pattern of UPA, 9c) transmission mode FTIR spectrum of UPSu, 9d) WAXS pattern of UPSu, 9e) attentuated total reflectance mode FTIR spectrum of SHiEO, 9f) WAXS pattern of SHiEO

Final evidence of this attribution is given by sample SHiEO in Figures 7.9e and 7.9f. In the FTIR spectra of this high ethylene-oxide content foam, it is observed that the bidentate hydrogen bonding is highly disrupted or decreased relative to the free urea peak at 1710 cm^{-1}. Figure 7.10 shows an AFM phase image of SHiEO to confirm along with the SAXS data that SHiEO does have a two-phase morphology; however, as the FTIR shows the hard domains have nearly no internal ordering within them. Therefore, since it is observed in the corresponding WAXS pattern that the 4.7 Å reflection dissipated and only a diffuse amorphous halo remains, it becomes apparent that observing the WAXS peak is a way of confirming that bidentate hydrogen bonding is present in the system and that the hard segments are well ordered.

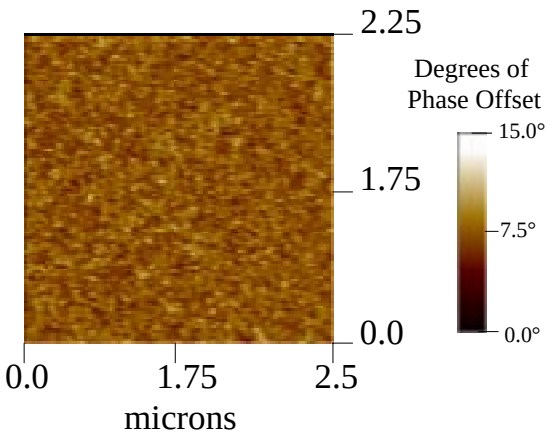

Figure 7.10 Atomic force microscopy phase image of SHiEO

The above knowledge is applied to the study of surfactants in Figure 7.11. As Figure 7.11a shows, removing all surfactant has a dramatic influence on the shape of the FTIR spectra in the carbonyl region. Three main differences are observed. Two of these are that the level of bidentate hydrogen bonding has decreased (the absorbance ca. 1640 cm^{-1}) and the level of free or dissolved urea particles has increased (higher absorbance at 1710 cm^{-1}). The other change is that the hydrogen bonding peak has actually shifted towards 1650 cm^{-1} indicating a increasing degree of monodentate hydrogen bonding. This indicates that the final solid polymer is without some of its strongest physical bonds. It is interesting to note that as shown in Figures 10b and 10c, the 4.7 Å reflection is still present in the WAXS. This indicates that within the hard domains themselves, there is still significant bidentate packing present. Therefore, this suggests that the higher level of free urea and monodentate hydrogen bonded urea stems from more urea still being out in the matrix and not fully precipitated.

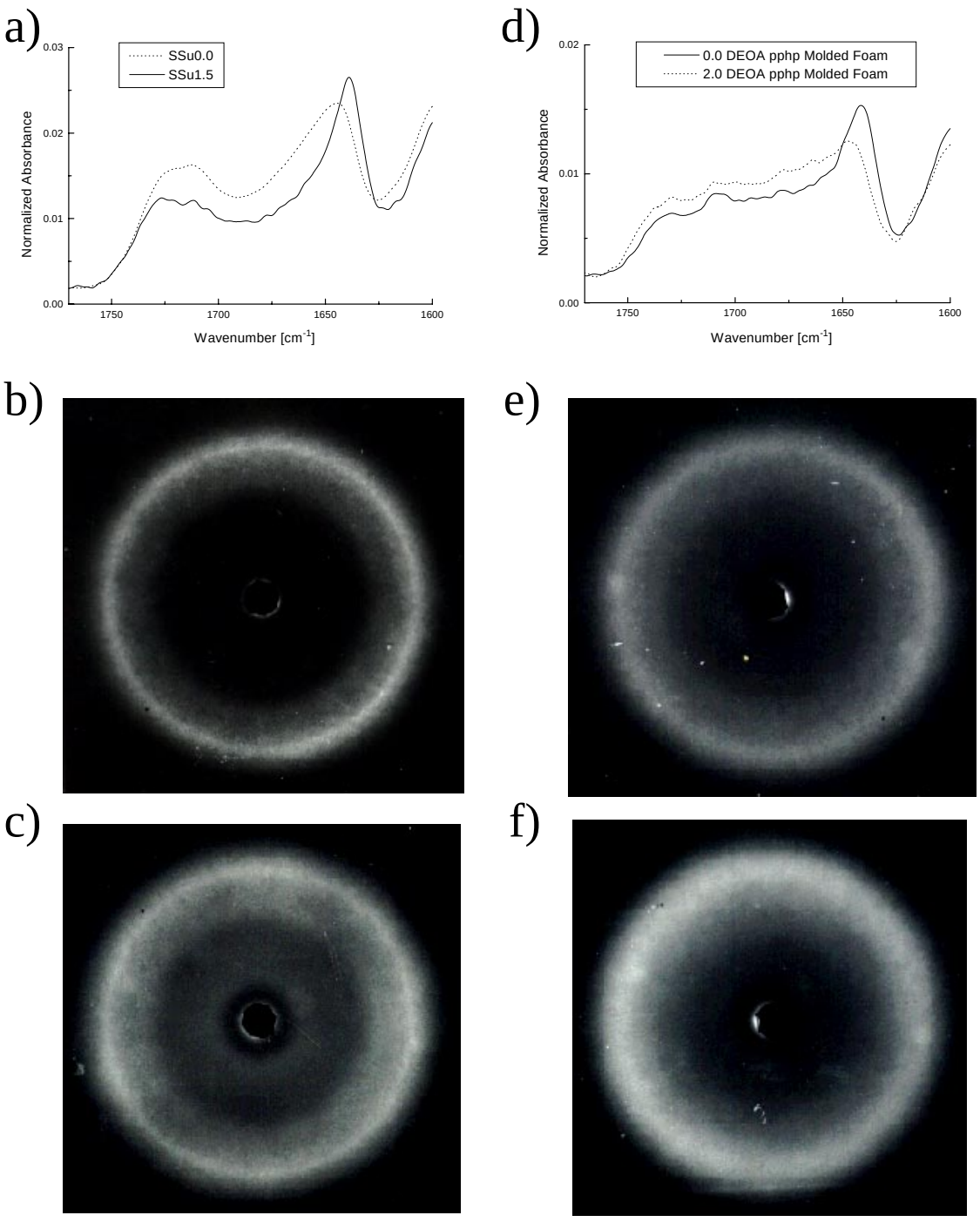

Figure 7.11 Fourier transform infrared spectroscopy and wide-angle x-ray scattering of polyurethane foams: 11a) attenuated total reflectance mode FTIR spectrum of SSu0.0 and SSu1.5, 11b) WAXS pattern of SSu1.5, 11c) WAXS pattern of SSu0.0, 11d) attenuated total reflectance mode FTIR spectrum of MD0.0 and MD2.0, 11e) WAXS pattern of MD0.0, and 11f) WAXS pattern of MD2.0

To clarify this argument, data from two molded flexible polyurethane foams have been added as shown in Table 7.1. By studying the tan delta peak from DMA, as will be done later for this study, it was shown that these two foams have similar degrees of phase separation or polyol matrix purity.[5] In Figure 7.11d it is shown that by adding the cross-linking agent diethanolamine (DEOA), the carbonyl region of the FTIR spectra transforms similarly to that of the no surfactant foam in Figure 7.11a: the peak at 1710 cm^{-1} rises, the absorbance at 1640 cm^{-1} falls, and the peak of hydrogen bonding shifts toward 1650 cm^{-1}. However, as can be seen in Figures 7.11e and 7.11f, the addition of DEOA completely disrupts the 4.7 Å reflection. This is in complete contrast to the effect of removing the surfactant and it points out the importance of using both of these techniques in studying the hard domains of polyurethane foams. Other work by the authors and others[5] has shown that DEOA resides within the hard domains and disrupts the ordering there as observed by WAXS. *Therefore observing hydrogen bonding via FTIR alone is not sufficient to conclude that ordering exists within the hard domains. Likewise observing a 4.7 Å reflection via WAXS indicates bidentate hydrogen bonding and good ordering within the hard domains or urea aggegrates but is not sufficient to conclude that the highest level of phase separation has occurred as shown by FTIR or by the polyol glass transition temperature.* These techniques thus complement one another in discerning the microphase separation behavior of polyurethane foams. The way that DEOA alters the composition of the hard segments precludes good packing in hard domains even in the presence of good phase separation. On the other hand, the slabstock foam without surfactant exhibits good hard domain ordering and its FTIR behavior can only be explained as a reduced degree of phase separation.

Another method for examining the phase separation behavior of these systems is with the phase images of AFM. It should be emphasized that, as described in the methodology section, a "phase image" is a 2-D plot of the phase lags or phase offsets recorded by the instrument as the tip interacts with the surface being studied. "Height images" are recorded simultaneously but because the surfaces studied here have been cryotomed smooth they are disregarded. Phase images of polymer systems can be used qualitatively to describe morphology, or they may be numerically examined to quantitatively characterize either periodically occurring structure in the surface or levels of phase offset induced by the tip-surface interactions. Figure 7.12 shows an AFM phase image of sample SSu1.5 wherein the scale is oriented so that harder material is shown by larger phase offsets. Figure 7.13 shows a Fourier transform analysis of the surface of

sample SSu1.5 called the power spectral density. The transform utilized and further details of this analysis with examples are available in reference 30. Basically, how often a phase offset occurs can be characterized in terms of a wavelength, and Figure 7.13 shows the distributions of the different wavelengths that occur throughout the image. Thus the most often recurring wavelengths are shown as peaks in the distribution and provide a way to find important structural parameters in the surface. It is worth pointing out that every slabstock sample examined with this technique exhibited peaks at two scale lengths in its distribution, a major one at ca. 1.0-0.5 μm and a much smaller one at ca. 8-10 nm. This signals that AFM may provide a systematic way to quantitatively characterize the micron scale aggregation behavior often observed in slabstock systems. Also, the smaller maximum appears to correlate with the interdomain distances typically observed in these materials via SAXS. A similar correspondence between SAXS and AFM was recently reported in other materials by McLean and Sauer.[26] For flexible polyurethane foams this suggests that AFM is probing the scale lengths of the hard domains; therefore, following phase offsets may be a way to characterize and detect alterations in the mechanical properties of the hard domains themselves.

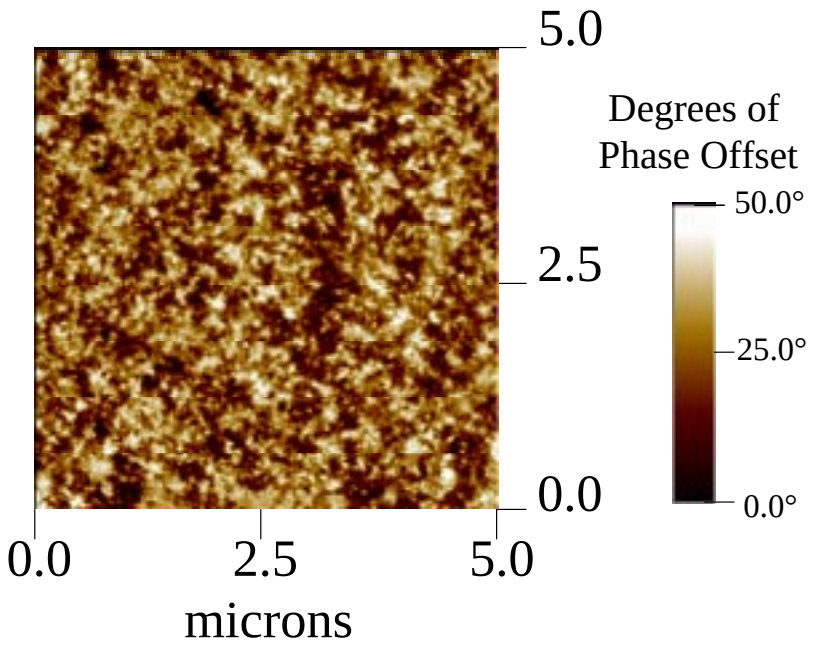

Figure 7.12 Atomic force microscopy phase image of SSu1.5, representative of a typical image from the polyurethane foams in this study

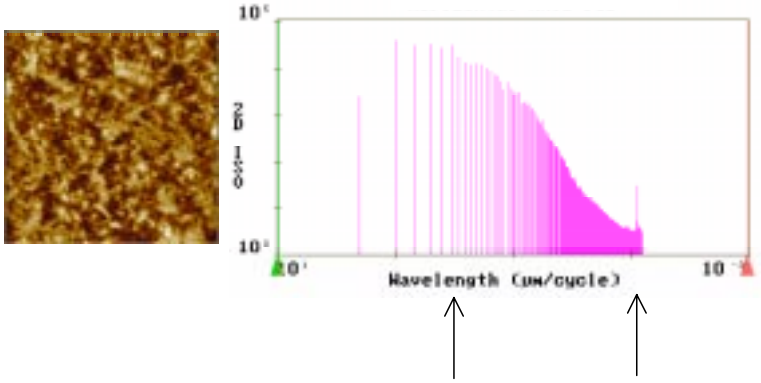

Wavelengths: 0.41 µm/cycle 8.6 nm/cycle

Figure 7.13 Power spectral density (a Fourier transform analysis) of SSu1.5 illustrating the two scale lengths (ca. 0.5 µm and ca 8 nm) in the distribution of wavelengths that characterize the distribution of domains with similar phase offsets in the surface.

Evaluation of the relative hardness of the urea-rich regions was accomplished by averaging the maximal phase offsets from several scans for every sample. Figure 7.14 shows a section analysis for the phase image of Figure 7.12, which shows how the hardness varies along a line drawn across the inserted figure. This provides a way to measure the maximal phase offset at many places on the surface. For the SSu series, as shown in Figure 7.15a, above surfactant concentrations of 1.5 pphp, the average relative hardness does not increase. This indicates that the surfactant helps the urea precipitates to achieve their hardest state, but the surfactant does not itself add hardness. Below 1.5 pphp, this relative hardness is seen to be dropping off with decreasing surfactant concentration. This region is examined in more detail in Figure 7.15b. Here it is observed that the increasing maximal phase offset matches the earlier trend of increasing the 1640 cm^{-1} normalized peak FTIR absorbance. This matches the increasing relative hardness to increasing the content of the strongest type of hydrogen bonding. It is also noted that the outlier from the trend of increasing the 1640 cm^{-1} absorbance, foam SSu0.75, is also an outlier form the trend of increasing phase offset. That helps to confirm the correlation between the two techniques that ordering in the hard domains or urea aggregates relates directly to their hardness which leads to the higher phase offset observed on the AFM. Finally, in Figure 7.15c, the results of the collapsed and quenched samples are added. Here it is seen that the same increase in relative hardness with surfactant addition is observed in the quenched samples. It is also noted that the additional twenty seconds of reaction time increases the relative hardness towards that of the completely reacted foams. It is also noted that the foam which was

mechanically compressed at 80 seconds has lower offset than the same surfactant level quenched at 100 seconds. Furthermore, it is observed that the foam crushed after urea precipitation has a relative domain hardness near the same level as that of the final foam.

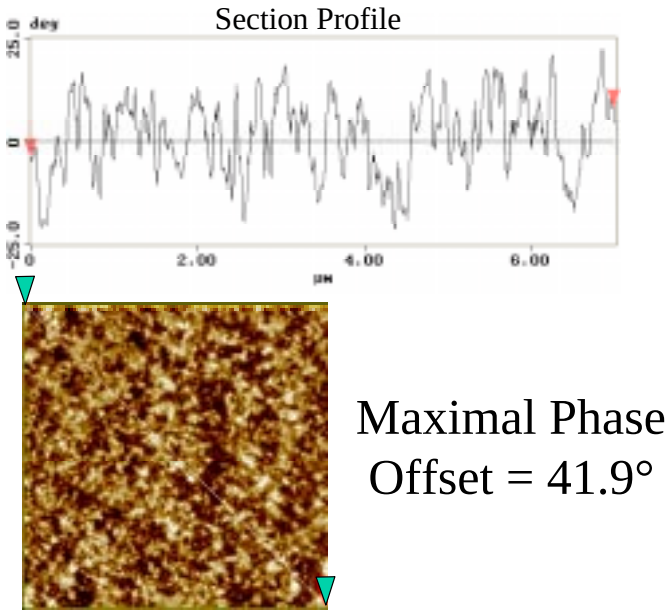

Figure 7.14 Representative section analysis of the phase image SSu1.5 shown in Figure 7.12

It is important to point out that the level of bidentate hydrogen bonding alone as shown by FTIR cannot completely explain the trends of maximal phase offsets. This is shown in Figure 7.15d. Within a given state (e.g. non-quenched, quenched, or crushed) increasing amounts of bidentate hydrogen bonding are observed as surfactant concentration increases. However, comparisons across the various states show opposite trends to those observed in Figure 7.15c. Q120-Su0.0 has more bidentate hydrogen bonding than SSu0.0, and Q100-Su0.0 has more than Q120-Su0.0. This demonstrates that while the increasing relative hardness shown by AFM is related to bidentate hydrogen bonding, these physical bonds cannot completely explain the behavior. Based on Figure 7.8d, it is thus hypothesized that the increased size (i.e. mean chord lengths) of the hard domains in addition to their increased level of hydrogen bonding leads to what is observed via AFM as higher relative hardness.

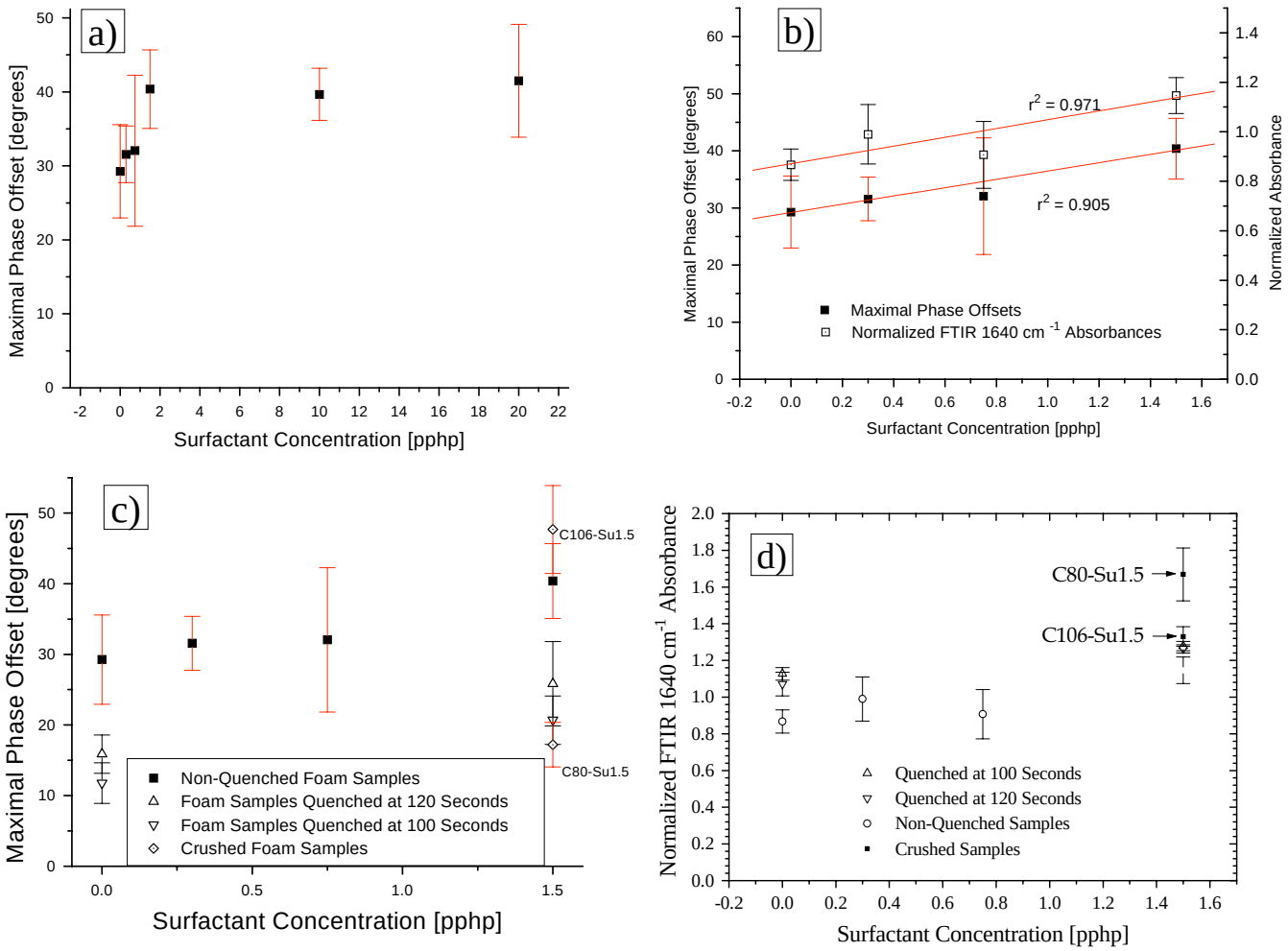

Figure 7.15a) Maximal phase offsets for foams of various surfactant concentration. 15b) Comparative trends between the 1640 cm^{-1} absorbance from FTIR and the maximal phase offsets of AFM tapping mode. 15c) Maximal phase offsets for foams in various states (fully developed, quenched, or crushed). 15d) Normalized 1640 cm^{-1} absorbances from FTIR for foams of various states. This demonstrates that the 1640 cm^{-1} absorbance is consistent for each level of cure but cannot be used to explain the behavior of samples at different states shown in Figure 7.15c.

These AFM results are consistent with themselves and are also well aligned with the data from the other structural analysis methods. Together, they indicate that the surfactant level has an effect on the development of the foam morphology at every level. Further evidence of this comes from thermal analysis via DSC and DMA. Figure 7.16a shows the tan delta plot from DMA. This shows that without surfactant, the polyol has a distinctly higher T_g, indicating much more dissolved polyurea in the polyol. With surfactant, however, the glass transition occurs a few degree lower, indicating a purer polyol and better phase separation. This is also shown in

that the tan delta peak height of SSu0.0 is significantly higher than the other peaks, which indicates that more "stiff" hard segment material is distributed throughout the polyol matrix.[19] Furthermore, as shown in Figure 7.16b, both quenching and mechanical crushing disrupts the process of phase separation. This is also exhibited in Figure 7.16c. These figures show that surfactant concentration does not directly control the degree of phase separation. The rise in the tan delta peak heights in moving from 100 to 120 seconds of quench shows that quenching the foam freezes some of the polyurea out in the polyol matrix and prevents less complete phase separation. These figures also show that mechanical collapse or spontaneous collapse has similar effects. These trends were confirmed by DSC, but that data is not presented here. This important data further indicates that the process of bubble growth or the presence of large gas-liquid interfacial area may well play an important role in the process of phase separation.

The tan delta behavior of these systems points out that for these flexible polyurethane foam systems, a difference in the location of the tan delta peak may not necessarily mean as much as the relative peak height. Every foam that was quenched or that collapsed has the same peak location has shown in Figure 7.16c. Even C106-Su1.5 has a glass transition at -46°C which is significantly higher than that of SSu1.5 (-51°C). This indicates that remaining at the high temperature of the reactive state (ca. 140°C) throughout the curing of the material while still in the presence of the cellular structure are important to the precipitation of the polyurea. The data also shows that comparing the relative heights of the tan delta peak may be a more effective way of evaluating mobility in the polyol phase. It is also worth pointing out that it is not assumed that the polyol is completely free of dissolved hard segments even in SSu1.5; since it is know that some low molecular weight hard segment material does form, some of that is probably still dissolved in the matrix. Thus a higher glass transition indicates a lower polyol purity relative to that which is achieved by the fully cured slabstock systems.

This study has so far shown that surfactant concentration has an influence on the degree of phase separation and phase ordering in the foams. This is thought to occur as a secondary effect. The presence of the surfactant primarily stabilizes gas bubbles and the nascent cellular structure, thus incorporating a large surface area of the high energy liquid-gas interface throughout the reactive mixture.

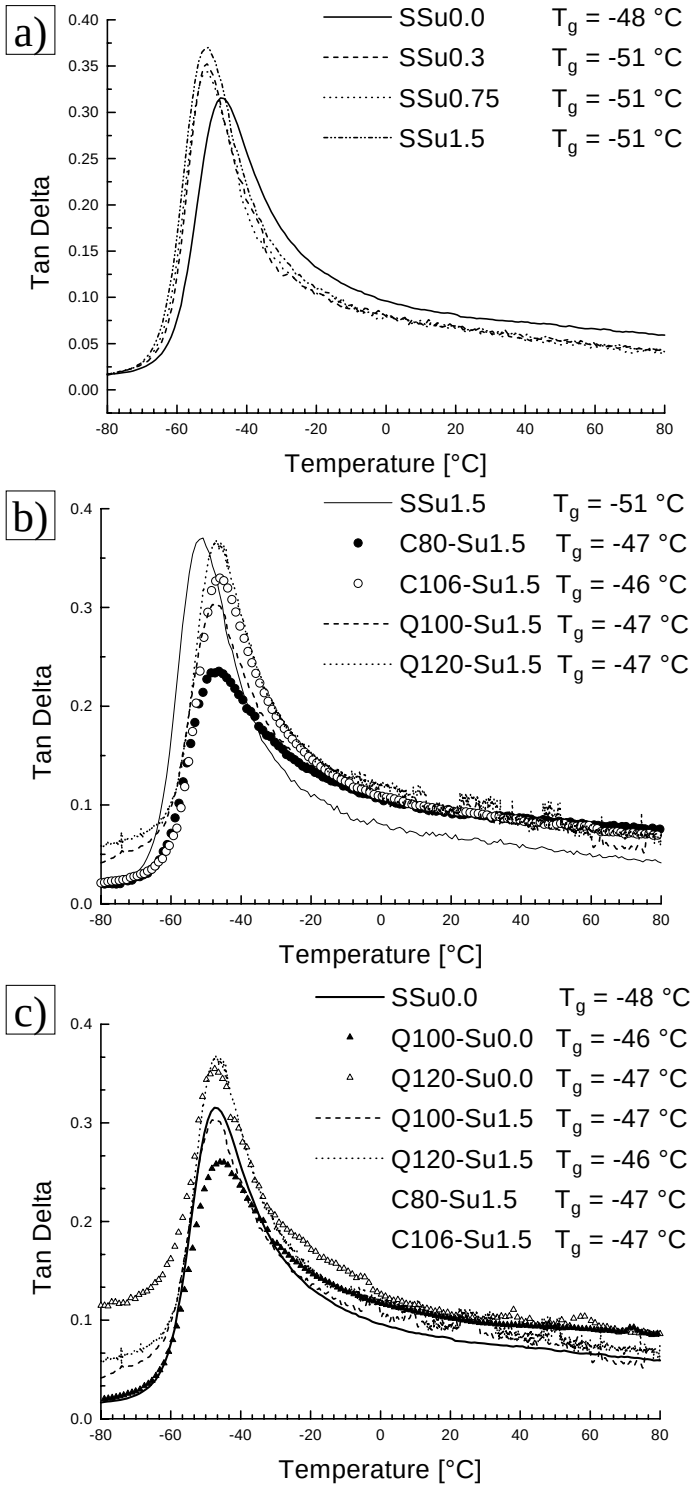

Figure 7.16 Tan delta from DMS for: 16a) samples of various surfactant concentrations, 16b) samples with 1.5 surfactant pphp concentration at different states, 16c) all samples that collapsed spontaneously, were quenched, or were crushed.

The secondary effect may arise from some combination of two sources. One source may be a preferential ordering at the interface of one component in the reactive mixture. The importance of that ordering would become of greater significance as the windows grow thinner, gaining surface area and losing material between interfaces. This ordering at the interface might thus enhance the process of phase separation during bubble growth. A corollary to this would simply be the presence of that large interfacial area at the time of urea precipitation. As the hard domains begin to organize, having the interface present may promote phase separation and the dispersion of the hard domains. It is known from other systems that amphiphilic particles form at oil/water interfaces, so a mechanism for this behavior suggests itself. If the surfactant molecules prefer to arrange themselves on the gas/liquid interface, their polyether block could, through hydrogen bonding, associate with the developing hard segments. These anisotropic particles might then serve as seeds for further polyurea precipitation. When that interface is unavailable (as in C80-Su1.5), surfactant molecules may associate into micelles in the fluid, inducing aggregation at their surfaces. Thus, without the presence of the gas/liquid interface, it is possible that the urea balls aggregate to sizes at which associations between them can occur, leading to the similarities in storage moduli for samples like SSu0.0 and C80-Su1.5 in Figure 7.17c. This might explain how the aggregation behavior observed in Figures 7.3-7.5 relates to the properties observed in the DMA.

A second source may be that the growth process of the bubbles in the mixture induces flow from the lamellae between bubbles (soon to be windows) into the plateau borders (becoming cell struts). The mixing that would occur during the draining fluid flow might assist in promoting the organization of hard domains or urea aggregates. Given the high viscosity of the liquid at this point in the gelation reaction, it is not suggested that the kind of mixing due to turbulent flow occurs at this point. However, the laminar flow that probably occurs would allow the polyurea in each layer further away from the gas-liquid interface to aggregate to developing precipitates. Without this additional flow, molecular diffusion may be too slow to allow the precipitates to completely form and it may slow the progress of the gelation reaction. This second hypothesis would explain the urea aggregation behavior observed earlier in Figures 7.4c, 7.4g, 7.5a, 7.5c, and 7.5e.

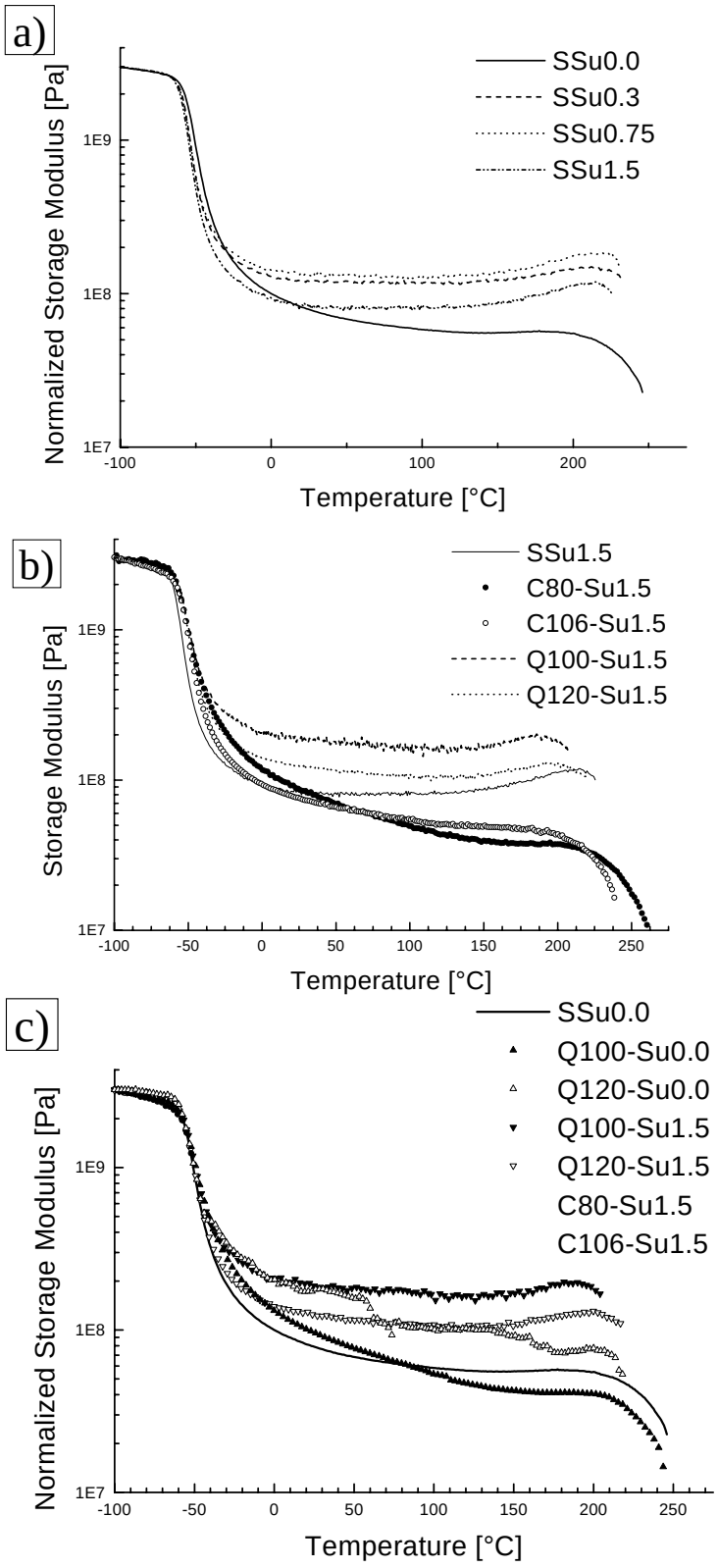

Figure 7.17 Storage modulus from DMS for: 17a) samples of various surfactant concentrations, 17b) samples with 1.5 surfactant pphp concentration at different states, 17c) all samples that collapsed spontaneously, were quenched, or were crushed.

DMA also provides a look at the stiffness behavior of these foams. By normalizing the storage modulus to 3 x 10^9 Pa in the glassy region, the density variations between samples due to cellular structure are removed.[14,19] The results of this are shown in Figure 7.17a, and it is seen that, without surfactant and without internal urea domain ordering, sample SSu0.0 has a much broader glass transition and a softer modulus in the rubbery region. These two observations support the hypothesis that lack of surfactant ultimately results in more dissolved urea and less internal organization within the hard domains. Figure 7.17b shows the storage moduli for all materials at 1.5 surfactant pphp. This shows that the crushed materials have very similar properties to the SSu0.0 material, indicating again the importance of maintaining a cellular structure to properties. This is further demonstrated by the quenched materials in that figure that show similar behavior to SSu1.5. Recalling that these foams were quenched in liquid nitrogen and then allowed to warm to room temperature, that is, they pass through the glass transition of the polyol, it is concluded that precipitation of the existing urea groups occurred in the presence of a cellular morphology. Bringing even more confirmation to this is Figure 7.17c, which shows that all of the materials which collapsed have similar properties in showing softer rubbery moduli and broader glass transitions than any material that maintained a cellular structure.

7.5 Conclusions

This study has shown that surfactant concentration has an influence on the degree of phase separation and hard domain ordering in flexible polyurethane foams. This is hypothesized to occur as a secondary effect, where the presence of the surfactant primarily stabilizes gas bubbles and the cellular structure during the urea precipitation. The secondary effect is suggested to be a combination of ordering at the gas-liquid interface and the influence of increased mixing due to cell growth, leading to the observed higher degrees of phase separation and higher concentrations of hard domains organized via hydrogen bonding. These hypotheses apply to foam and collapsed materials which experience typical thermal histories. When the cellular structure was not present at the time of urea precipitation, foams both with and without surfactant were observed to develop large urea aggregations. These exhibited no well defined structure via TEM, indicating that what connectivity exists may occur as associations between polyurea aggregates. The nature of those associations would be highly dependent on the geometry of the aggregations, whether more spherical or lamellar-like. The possibility of varying thermal history in collapsed materials to achieve properties similar to foams is a focal

point of current work. This study has presented the first experimental evidence that the surfactant plays a role in the organization of polyurea hard domains; however, it is emphasized that the nature of that influence is still hypothesis. The observation that the cellular structure was present at the time of polyurea precipitation in all samples with better organized hard domains may be coincidence and a more fundamental understanding of the precipitation and organization event is required before a causal relationship may definitely be concluded.

This work has illustrated the importance of organization within hard domains, and it has also brought together many different techniques in probing that organization. A high ethylene oxide content foam was used to show that phase separation, as shown by SAXS, does not imply urea precipitation as shown by either FTIR or WAXS. Furthermore, that high ethylene oxide content foam and two series of urea powders were used to document that the 4.7 Å WAXS reflection widely observed in polyurethane foams correlates to bidentate hydrogen bonded urea groups. AFM was also shown to be a valuable and quantitative tool for probing both phase separation morphology and relative urea domain hardness.

7.6 Acknowledgements

This work has been financially supported by Goldschmidt AG and their support is gratefully acknowledged. We also thank Helmut Schator for directing the slabstock foaming experiments at Goldschmidt AG. Molded foam samples were supplied by the Dow Chemical Company, and their generosity is greatly appreciated.

7.7 References

[1] Herrington R; Hock K; Flexible Polyurethane Foams, 2nd Ed.; The Dow Chem Co: (1998)
[2] Lidy WA; Rightor E; Thanh PH; Cadolle D; *Proc of the Polyurethanes Expo '96*: (1996) 119
[3] Armistead JP; Wilkes GL; Turner RB; *J Appl Polym Sci*: **35** (1988) 601
[4] Dounis DV; Wilkes GL; *Proc of the Polyurethanes 1995 Conf*: (1995) 353
[5] Lidy WA; Rightor E; Heaney M; Davis B; Latham L; Barnes G; *Proc. of the SPI/ISOPA Polyurethanes World Congress '97*: (1997) 95
[6] Neff R; Adedeji A; Macosko CW; Ryan AJ; *J Polym Sci: Part B: Polym Phys*: **36** (1998) 573
[7] Ade H; Smith AP; Cameron S; Cieslinski R; Mitchell G; Hsiao B; Rightor E; *Polymer*: **36** (1995) 1843
[8] Ade H; North Carolina State University, personal communication, March 30, 1998
[9] Moreland JC; Wilkes GL; Turner RB; *J Appl Polym Sci*: **43** (1991) 801
[10] Seymour RW; Allegrezza AE; Cooper SL; *Macromolecules*: **6** (1973) 896
[11] Moreland JC; Wilkes GL; Turner RB; *J Appl Polym Sci*: **52** (1994) 549
[12] Moreland JC; Wilkes GL; Turner RB; *J Appl Polym Sci*: **52** (1994) 569
[13] Dounis DV; Moreland JC; Wilkes GL; Dillard DA; Turner RB; *J Appl Polym Sci*: **50** (1993) 293

[14] Turner RB; Spell HL; Wilkes GL; *Proc of the SPI 28th Annual Technical/Marketing Conf*: (1984) 244
[15] Dounis DV; Wilkes GL; *J Appl Polym Sci*: **65** (1997) 525
[16] Moreland JC; Wilkes GL; Turner RB; Rightor EG; *J Appl Polym Sci*: **52** (1994) 1459
[17] Moreland JC; Wilkes GL; Moreland CG; Sankar SS; Stejskal EO; Turner RB; *J Appl Polym Sci*: **52** (1994) 1175
[18] Rossmy GR; Kollmeier HJ; Lidy W; Schator H; Wiemann M; *J Cell Plast*: **13** (1977) 26
[19] Rossmy GR; Lidy W; Schator H; Wiemann M; Kollmeier HJ; *J Cell Plast*: **15** (1979) 276
[20] Rossmy GR; Kollmeier HJ; Lidy W; Schator H; Wiemann M; *J Cell Plast*: **17** (1981) 319
[21] Elwell MJ; Ryan AJ; Grünbauer HJM; Van Lieshout HC; *Macromolecules*: **29** (1996) 2960
[22] Yasunaga K; Neff RA; Zhang XD; Macosko CW; *J CelL Plast*: **32** (1996) 427
[23] Weier, A., Goldschmidt AG, personal communication, January 7, 1999
[24] McClusky JV; Priester Jr RD; O'Neill RE; Willkomm WR; Heaney MD; Capel MA; *J Cell Plast*: **30** (1994) 338
[25] Magonov SN; Elings V; Whangbo M-H; *Surface Science*: **375** (1997) L385
[26] McLean RS; Sauer BB; *Macromolecules*: **30** (1997) 8314
[27] Rossmy GR; *Progr Colloid Polym Sci*: **111** (1998) 17
[28] Wilkes GL; Abouzahr A; Radovich D; *J Cell Plast*: July/August (1983) 250
[29] Tyagi D; McGrath JE; Wilkes GL; *Polym and Eng Sci*: **26** (1986) 1371
[30] Nanoscope III Command Reference Manual, Update Version 4.10, Digital Instruments Nanoscope Scanning Probe Microscopes, August 10, 1995, 12.52-60

8 Cure Temperature Influences on Structure-Property Relationships in Plaques Based on Molded Flexible Polyurethane Foam Formulations

8.1 Chapter Summary

Several voidless plaques were produced based on a typical molded flexible polyurethane foam formulation in which the cure temperature was varied from 70°C to 150°C. X-ray photoelectron spectroscopy (XPS), nitrogen analysis, solvent extraction, small angle x-ray scattering (SAXS), Fourier transform infrared spectroscopy (FTIR), and tensile-mode dynamic mechanical analysis (DMA) were used to evaluate their morphology and properties. It was found that cure temperature could be manipulated to predictably change the interdomain spacings and levels of hydrogen bonding which develop in the polymer. On the other hand, in these plaque samples where the polyurea precipitates without the cellular structure, SAXS and DMA indicated no temperature in the range studied which yielded comparable phase separation to their corresponding foams. It was found that varying the cure temperature, especially above 100°C, changes the amount of reactants vaporizing from the reactive mixture, thus altering the stoichiometry of the reaction. It was also observed that higher cure temperatures increase the degree of covalent cross-linking in the polymer. When comparing plaques of the same formulation, for example, polymerizing isothermally at 70°C resulted in higher polyurea hard segment content than plaques cured above 100°C, and the 70°C plaques exhibited correlating higher levels of hydrogen bonding and higher storage moduli. Foams were found to have higher hard segment contents than their corresponding plaques cured above 100°C and also to have much greater storage moduli stability with respect to temperature. This stability is suggested to be due to a more developed covalent network. Even annealing at 130°C for two hours did not significantly change the storage moduli of the plaques. It is therefore concluded that the lower level of phase separation in the plaques is significantly altering the thermal stability of the storage moduli. It is hypothesized the absence of the cellular structure in the plaques may be playing a role in the organization of hard domains as the polyurea precipitates.

8.2 Introduction

Flexible polyurethane foams are currently utilized in a broad range of applications in such areas as furniture, packaging, and transportation. Part of the great usefulness of these materials is due to the adaptability of their properties which enables them to meet many different performance criteria. This adaptability results from the dependence of their mechanical properties on the interaction of structure on two scale-lengths: the cellular structure and the microphase separated morphology of the solid state. The exact relation of structure to properties in cellular materials is complex, and it continues to be the subject of ongoing research.[1,2,3,4,5] Furthermore, the convolution of properties resulting from the cellular structure with those resulting from the solid-state morphology makes evaluating the effects of changes in the polymer more difficult.[6]

The wide use of flexible polyurethane foams and the continuing challenges to improve their performance provides the motivation to better understand the effects of altering the solid-state. Developing a way to evaluate changes in the polymer independently of the cellular structure would facilitate such research. However, producing a voidless plaque for mechanical testing that is morphologically equivalent to a flexible polyurethane foam of the same formulation is not straightforward. Removing the cellular structure during the reactions which produce flexible polyurethane foams has been recently shown by the authors[7] to result in altering both the mechanical properties and the solid morphology of the final material. These changes and their significance will be examined further below.

Polymer composition varies with each different polyurethane foam product, but this chemically complex family is united by utilizing a urethane linkage to covalently bond hard segments with soft segments. This linkage is typically formed from the reaction between the isocyanate functionality of one component with the hydroxyl group of another component. By controlling the composition of each component, two solid state phases are expected. This two-phase morphology provides the key to controlling performance of the final product and gives the manufacturer versatility in tuning properties as desired by varying the composition or content of one or the other phases.

One phase of typical water-blown foam systems is based upon the reaction of water with a diisocyanate such as toluene diisocyanate (TDI). This reaction initially produces a carbamic acid which then decomposes yielding heat, carbon dioxide, and an amine functionality. The heat

and carbon dioxide contribute to the expansion of the gas-liquid phase separation in the reactive mixture and so play important roles in the development of the foam's cellular structure. On the other hand, a disubstituted urea product results from the reaction of the amine with other isocyanate groups. A "hard segment" results from several isocyanate groups covalently bonding through the urea linkages, and solid-state phase separation in typical systems arises from the precipitation of these segments into "hard domains." The development of this microphase separated morphology is key to the properties of flexible polyurethane foams,[8,9] and more detailed discussion of it and the composition of these polyurea based hard domains may be found in references 7, 10, and 11.

The complex nature of the development of this phase separation is suggested by the role played by a non-reactive component, the surfactant.[7] This component is typically added to help produce the desired cellular structure. It initially compatiblizes the reactants into an emulsion, it stabilizes the swelling gas bubbles as the reactions proceed, and the surfactant prevents premature cell opening as the bubbles begin to impede each other's growth. Within the solid state, however, when the concentration of surfactant is varied from zero to typical feed levels (ca. 1.5 parts per hundred polyol parts), systematic changes may be observed in the final morphology.[7] The most dramatic differences were detected in samples which had collapsed prior to the precipitation of the polyurea into hard domains.[7] By comparison to samples which had enough surfactant to maintain their cellular structure, it was found that the collapsed specimens were less phase separated.[7] Because hard domain organization plays such a large role in the mechanical performance of polyurethane foam materials, this resulted in altering properties such as reduced storage moduli and broader polyol glass transitions.[7] On the other hand, it is important to note that these changes were observed without controlling thermal history, a variable which obviously must have significant impact on a phase separation process.

The use of the molded foam technique adds another complication. Molded production is more of a batchwise operation compared to the continuous technique used to produce slabstock foams. Therefore, higher productivity requires minimized demold times, and this demand has led to many formulation changes. Among these alterations is the addition of cross-linking agents such as diethanolamine (DEOA) for improved stability of the cellular structure. Increasing the rate of covalent cross-linking allows other changes to be made to the formulation which reduce the time that the foam requires to achieve enough dimensional stability for it to be removed from

the mold. These changes are enumerated in a recent publication by the authors.[6] The addition of DEOA has been shown to result in altering the composition of the hard segments, causing disorder in the packing within the hard domains.[6,12] Thus the introduction of this third competing reaction is already known to change the final morphology of the solid-state. It is not unexpected, therefore, that DEOA might also alter the phase behavior which leads to the development of the phase-separation.

This discussion has revealed some of the complexities involved in flexible polyurethane foam production. The wide application of these materials makes it clear that a better understanding of the morphological development during production would be beneficial. This research will therefore use variations in the cure temperature to further explore changes in properties and morphology due to the removal of the cellular structure. In typical molded systems, the molds are preheated to ca. 70°C, and the exotherm of the reactions heat the foam core temperature to ca. 130° within two minutes. Cure temperatures will therefore be selected to examine the range of 70°C to 150°C. Also, in order to provide the most insight into industrial foam products, this will be accomplished by analyzing and comparing plaque and foam samples that were based on a typical molded foam formulation.[13]

8.3 Experimental Materials and Methods

8.3.1 Materials

For use as a control, two foam samples of the same formulation were produced based on a typical molded flexible water-blown polyurethane foam. Following common commercial practices, these foam samples were made by workers using a Hi-Tech RCM 30 foam machine at Dow Chemical in Freeport, Texas. This operation consists of two hydraulic pistons to dispense the liquid components to the mixing head. The formulation components described below were prepared in two storage tanks, A and B. The A side consisted of the isocyanate. The B side consisted of the polyols, water, surfactants, and catalysts. An aluminum mold having dimensions of 15”x15”x4.5” was used which was heated to 68 °C prior to injection of the reactive mixture. After four minutes of curing in the mold, the foams were removed and mechanically crushed twice between two steel rollers set to have a 1” gap. One sample was then left to cool, and this sample will be called “MF.” The second foam was immediately placed in a 130°C oven for two hours and allowed to anneal. This second sample will be termed ”MFA.”

The foams were based on 62.86 parts of an experimental ethylene oxide endcapped polyether polyol produced by Dow Chemical which was based on a glycerine/sucrose mixed initiator and had a functionality ca. 2.4 and a molecular weight of 5000. The foam was also based on 37.14 parts of Voranol® 4935 (Dow Chemical), a copolymer polyol (CPP) containing 35 weight percent styrene/acrylonitrile random copolymer (60/40 styrene/acrylonitrile) particles. These particles were ca. 0.5-1.3 μm diameter. The cross-linking agent diethanolamine (DEOA) was used at 2.0 parts per hundred polyol (pphp). Total water in the foam was 3.82 pphp. Three catalysts were used: 0.15 pphp of Dabco® 33LV (Air Products and Chemicals) which is 33% triethylene diamine in dipropylene glycol; 0.08 pphp of Dabco® BL11 (Air Products and Chemicals) which is 70% bis(N,N dimethylaminoethyl) ether in dipropylene glycol; and 0.6 pphp of Niax® A4 (Union Carbide) which is a catalyst blend primarily promoting the gelation reaction but tends to increase the blow reaction rate as well. Two conventional foaming surfactants were utilized to obtain the desired cell structure: 0.5 pphp of DC5043 and 0.5 pphp of DC5169. The 80/20 2,4/2,6 isomeric blend of toluene diisocyanate was used at a stoichiometric feed of 46.45 pphp.

Using this same formulation, one set of plaques samples were produced using a technique developed by workers at Dow Chemical. *It should be noted that surfactant was not used in the plaque samples*, as using it invariably produced voids in the material. Due to concerns about softening of the CPP at higher temperatures, another set of plaques were produced with the same sample procedures but using no copolymer polyol. Formulated to have the same hard segment/soft segment ratio as the plaques with CPP, this second set used 72.25 pphp of the same experimental polyol and 27.75 pphp of Voranol 4703.

The B side components were well mixed in a beaker, and then the isocyanate was introduced. After stirring for ca. 10 seconds, the mixture was placed into a 5” dia. circular steel mold. The mold was closed at approximately 25 seconds from the time of isocyanate introduction. It was then pressurized in a hot press to ca. 30,000 lbs_f. After curing for one hour, the mold was opened and the sample was removed. This technique produced voidless plaques that were ca. 1-3 mm thick. Considering the thinness of the samples, the temperature of the mold was varied with the hot press thermal controller to moderate cure temperature. A hole bored in the mold base allowed monitoring of temperatures in the center of the mold base but not inside of the mold itself.

Three different heating procedures were examined. One method, which will be called "ramped," preheated the mold to ca. 68°C. After the reactive mixture is loaded and the mold is pressurized, the thermal control was set to ramp up to 130°C. Reaching that temperature was found to require ca. 60 minutes. A second method began with this same ramping procedure and it was followed by "annealing" the sample for two hours in the closed mold at 130°C. This method will be referred to as "ramped and annealed." In the third method, an "isothermal" cure was approximated by maintaining the mold at a constant temperature throughout the curing step. Monitoring of the core mold temperature for the 70°C plaque showed a ca. 5-10°C increase for 30-60 seconds after the mold was closed, but after ca. 15 minutes it returned to ca. 70°C. While this shows that tight control of the temperature was not maintained, this slight increase is well short of the ca. 130°C usually observed in foams. Therefore it was concluded that the mold did moderate the cure temperatures well enough to provide samples cured at approximately constant temperatures over the thermal range considered in this study. Three temperatures were studied with the "isothermal" method: 70°C, 110°C, and 150°C.

The plaque samples will have names beginning with "P." A second letter will be added to indicate whether or not copolymer polyol filler was used. "F" will indicate a sample with filler (i.e. CPP), and "N" will indicate no filler. The last letter (or letters) will designate what heating procedure was utilized: "R" for ramped, "RA" for ramped and annealed, and "I" for isothermal. Finally, a number will be added to the isothermal samples to indicate at what temperature they were cured. Thus "PNI-70" is a plaque without copolymer polyol filler which was cured isothermally at 70°C. All the samples used in this study are summarized in Table 8.1.

8.3.2 Methods

Dynamic mechanical analysis (DMA) was carried out using a Seiko model 210 in the tensile mode. The samples were heated from -120 °C to 350 °C at a rate of 0.5 °C/min. from which the storage modulus (E') and tan δ data were collected at a frequency of 1 Hz. Bar shaped samples were cut from the foams with die-punches and had dimensions of approximately 5 x 5 x 15 mm with a grip-to-grip distance of 10 mm. Well below the T_g of the soft segment (at ca. -100°C), the storage moduli were then normalized to 3×10^9 Pa to remove the effect of varying density which is only a function of cellular structure.[14] Plaques were not normalized, and were cut to ca. 5 x 15 mm with their thickness varying according from sample to sample.

Table 8.1 Thermal History of the Samples

Sample Name	Details and Thermal History
MF	Typical molded foam, removed and cooled ambiently after four minute cure
MFA	Typical molded foam, annealed for 2 hours at 130°C after curing
PFR	Plaque with filler, ramped from ca. 85°C to ca. 130°C, removed after 1 hour
PFRA	Plaque with filler, ramped as above and annealed for 2 hours at 130°C
PFI-70	Plaque with filler, held at 70°C for one hour
PFI-110	Plaque with filler, held at 110°C for one hour
PFI-150	Plaque with filler, held at 150°C for one hour
PNR	Plaque without filler, ramped from ca. 85°C to ca. 130°C, removed after 1 hour
PNRA	Plaque without filler, ramped as above and annealed for 2 hours at 130°C
PNI-70	Plaque with filler, held at 70°C for one hour
PNI-150	Plaque with filler, held at 150°C for one hour

Small angle X-ray scattering (SAXS) was utilized to provide quantitative characterization of the microphase separation of the monol based plaques. Nickel filtered CuKα radiation having a wavelength of 1.542 Å was produced with a Philips model PW1729 generator operating at 40 kV and 20 ma. A slit collimated (0.03 x 5 mm) Kratky camera was utilized for the scattering experiment using a Braun OED 50 position-sensitive platinum wire detector. Because apparent density varied, the beam path length for the foam samples were corrected based on density relative to the apparent density of the plaque samples (1.06 g/cc). The foam samples were cut approximately 8 mm thick and compressed to approximately 2 mm.

Fourier transform infrared (FTIR) was also used to evaluate hydrogen bonding (mono- and bi-dentate) in the hard domains.[8] FTIR Spectra were collected on a Nicolet 510 Spectrometer utilizing a Spectra-Tech ATR attachment model 0012-405 using a horizontal ZnSe crystal. Spectra were analyzed using Omnic 3.0 software, and all scans were normalized by the corrected peak height at 2970 cm^{-1} which corresponds to a CH_3 absorbance. For quantitative analysis, the ratio of the absorbance of the 1640-1650 cm^{-1} peak to the 1710 cm^{-1} peak was used. This provides a measure of the ratio of hydrogen bonded polyurea carbonyl groups to polyurea carbonyl groups which have not formed hydrogen bonds, and it serves as an internal calibration for each spectrum. Using this ratio allows the level of hydrogen bonding in one sample to be compared with another one with good precision (ca. 3% error).

X-ray photoelectron spectroscopy (XPS) was used to examine trends in the hard segment content of the various plaque and foam samples. A Perkin-Elmer model #5400 was used, operating at 14 kV, 25 mA, and 300 W. A Mg anode was used for x-ray generation with an Al filter. A take-off angle of 45° was used for all experiments, thus the composition of each sample was evaluated to approximately the same depth (ca 35 Å). Although the polyether component of these materials has been shown to be richer at the surface than in the bulk,[15] sampling at equal depth with samples of similar roughness should provide useful data for analyzing trends in composition. Thus to compare the plaques with the foam, a flat foam sample was necessary to ensure sampling at approximately equal depth. Therefore, foam sample MF was pressed between teflon sheets in a hot press at 130°C for two hours at ca. 20,000 lbs_f. Because the C-F binding energy is distinctly different from the C-O, C=O and C-H binding energies, it was possible to remove any effect from PTFE molecules which had transferred to the samples from either the mold release agents or the teflon sheets. The contribution to the C-O peak area of C 1s from the polyether block of the surfactant was subtracted by estimating the surfactant content based on the Si 1s peak. Previous workers on polyurethane materials utilized the ratio of carbon to nitrogen to estimate hard segment content;[15] however, the N 1s peak was found to be very weak and its area difficult to measure with confidence. The only possible source of the C-O part of the C 1s spectrum is the polyether component, and the only source for the C=O contribution occurs within the hard segments. Therefore, since the C 1s spectra were much stronger and since it was possible to deconvolute the contributions to the area of C 1s, the ratio of C=O/C-O will be used instead. Use of this ratio also eliminated possible contributions from the copolymer polyol particulate. One source of error for this technique is that residual isocyanate would contribute to both the N/C or C=O/C-O methods, and this will be discussed further in the results section.

Extraction experiments were carried out to compare the level of cross-linking (gel fraction). Samples were submerged in a succession of DMF solutions of LiCl. Lithium chloride solutions are used to increase the rate of extraction for these materials by disrupting the level of hydrogen bonding, thus facilitating the evaluation of the amount of extractable material in a given sample. The succession consisted of two submersions at 10 wt % LiCl, two at 6 wt %, two at 3 wt %, one at 1.5 wt%, followed by six submersions at 0 wt %. The period of each submersion was twelve hours, except for the last two pure DMF submersions which were 3 days. The samples were then repeatedly evacuated at 60°C for one week followed by one weeks at

100°C. Samples were weighed throughout the drying process until a stable weight was achieved. The level of weight lost via extraction provides an index of the sol fraction while the remaining extracted matrix represents the gel fraction.

Nitrogen analysis was performed by Alvetta Pryor at Dow Chemical by using a Hereaus CHN-Rapid Analyzer. Samples were decomposed through oxidative combustion in a stream of oxygen at temperatures between 950°C and 1050°C. During oxidative combustion, carbon, hydrogen, and nitrogen produce CO_2, H_2O, and various nitric oxides. A copper catalyst reduces the nitric oxides at approximately 550°C to nitrogen. By analyzing the gases produced, a weight percent of nitrogen in the original sample is calculated.

8.4 Results and Discussion

This study sought to examine the morphology and properties of polyurethane foam polymers that were produced at various cure temperatures. However, valid comparisons between phase separated materials demand that the hard segment content be similar in each. The procedure used for manufacturing the plaque samples required placing the reactive mixture onto a preheated metal plate which, for some samples, was as much as 50° above the boiling point of water and 30°C above that boiling point of TDI 80 (ca. 125°C). Since evaporating reactants from the mixture could alter the stoichiometry of the reactions and thus change the final hard segment content, the technique of XPS was applied to the sample surfaces to examine trends in the hard segment to soft segment ratios. FTIR spectroscopy was not used for this for two reasons. First, the N-H absorptions were outside of the detection range of the FTIR instrument utilized when using the ATR cell. Secondly, the carbonyl absorptions vary significantly depending on whether the hard segments have precipitated and whether they have associated with each other (i.e. hydrogen bonding). Thus, since these two major absorptions for the polyurea hard segment were prone to error, another technique was sought. The surface technique of XPS was selected for estimating the hard segment content because the binding energies depend only upon the state of the 1s orbital rather than several different factors such as hydrogen bonding and phase separation.

By deconvoluting the C 1s spectra,[15] it was possible to approximate the contributions from C-O groups and C=O groups. The ratio of C=O/C-O was therefore used to estimate the hard segment/soft segment ratio in the surface layer of the material, and these results are shown in Figure 8.1. Integrating the temperature data for the ramped samples indicate an average cure

temperature of ca. 107°C, and so the ramped samples are plotted at that point. It is noted that that the C≡N carbon of the acrylonitrile group has the same binding energy as C=O, thus the presence of copolymer polyol somewhat decreases the estimates of hard segment content. On the other hand, the similarities in the thermal dependence of the two sample types suggests some reliability in comparing samples of a given composition based on temperature. It may be seen that the materials cured at 70°C contained more hard segment material than any of the other samples, *including the foam MF*. *This suggests that water and TDI 80 vaporization did play a role in determining final hard segment content of polyurethane foams and plaques.*

It is thought that the difference in hard segment content between PFR and PFI-110 may be due to variation in the amount of time the mixture was stirred before placing it into to mold. If PFR was stirred only a few seconds longer, more water would have reacted and therefore less would have evaporated. Alternatively, if PFI-110 was stirred a few seconds less, more water would have been available to vaporize. Thus, variations in stirring times might alter the hard segment content of the material independently of mold temperature. On the other hand, it appears from the data that once the cure temperature passes 100°C no large changes in the hard segment content occur. Therefore, while the greater volume fraction of hard segment material in PNI-70 and PFI-70 can be expected to alter morphology and properties, any changes in the other samples are more likely to be due to other factors such as polyurea hard segment solubility in the polyol. It is unclear why the samples cured at 150°C have similar C=O/C-O ratios to the 110°C and ramped samples; however, one hypothesis is that the increased vaporization rate at the higher temperature is offset by increased reactivity, resulting in essentially the same amount of hard segment material.

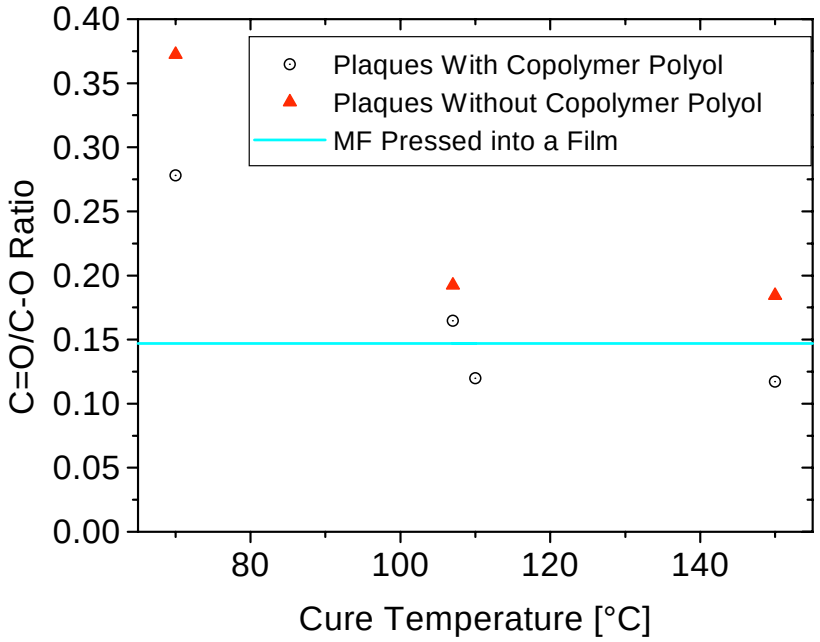

Figure 8.1 Estimate of hard segment content of the plaques showing variation due to cure temperature relative to that observed in the plaque pressed from a fully cured foam.

It is worth commenting on the observation that foam MF exhibits a lower C=O/C-O than plaque PNI-70. This indicates that significant amounts of reactants have vaporized from the foam rather than becoming entrapped in the foam cellular structure. This could have occurred in this sample as a result of three things. First, the rise of the foam typically begins at ca. 10 seconds after pour, when enough carbon dioxide has evolved to detect initiation of initial swelling the gas bubbles into the desired cellular structure. Thus, reactant vaporization might have occurred soon after pour when most of the available interfacial area was at the foam surface rather than in the cells. Small vent holes commonly exist in commercial foam molds to allow the escape of gases during foam expansion.[13] Secondly, the mold was preheated to ca. 70°C prior to pour, so the highly exothermic reactions only had to heat the mixture 30°C before reaching the boiling point of water. Slabstock systems are not preheated in this way, thus they would not reach the vaporization temperatures of the reactants until after the cells have begun to form. Finally, whereas slabstock foam buns are several feet thick, this molded bun was only four inches thick. Being much thinner from the time of pour onward means that vaporization effects would be more readily observed in molded systems than in slabstock foams.

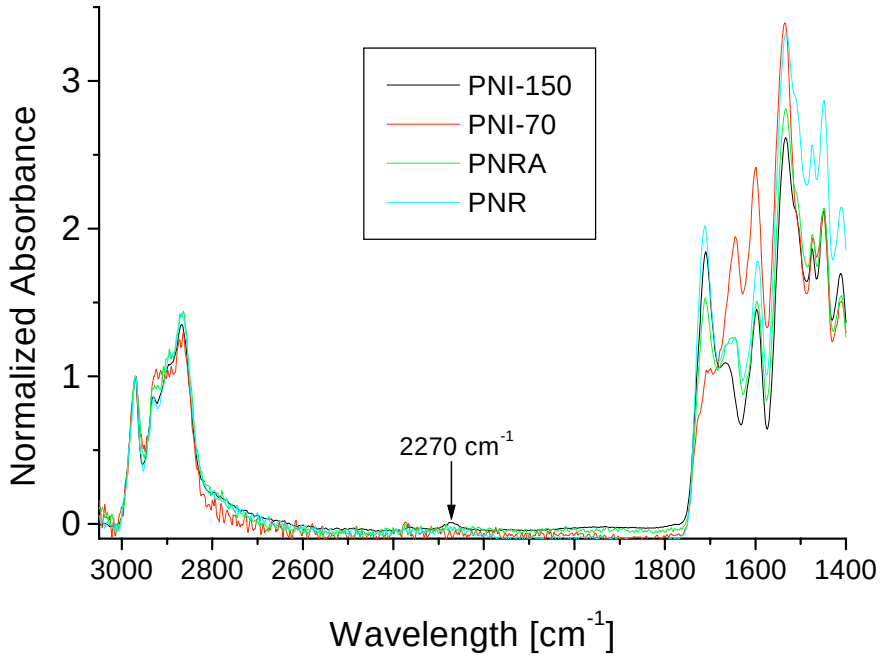

Figure 8.2 FTIR Spectra of Plaques without CPP

As discussed in the methods section, one source of error for the XPS technique is that residual isocyanate would contribute to the C=O portion of the C 1s spectrum thereby increasing the C=O/C-O ratio. FTIR spectra were therefore examined for the presence of the 2270 cm^{-1} vibration of the isocyanate group. As shown above in Figure 8.2, only a very minor absorbance was detected in the higher temperature samples (R, RA, I-110, and I-150). None of the plaques cured at ca. 70°C revealed any isocyanate absorption peak. This suggests that any overestimation of the hard segment content was minor and served to increase the C=O/C-O ratio of only the higher temperature plaques.

Another technique for evaluating the hard segment content is via the nitrogen analysis described in the experimental section. The results of this analysis may be seen in Figure 8.3, and it reveals many similar trends to the XPS technique. Because the SAN particles (CPP) contain nitrogen exclusive of that within the hard segments, an increase in the nitrogen content is observed for all samples containing CPP. Primarily it is observed that increased cure temperature generally decreased the nitrogen content of the plaque samples, for example from ca. 6 wt% in PFI-70 to ca. 5 wt% in PFI-150. This suggests a decrease in hard segment content possibly as a result of reactant vaporization. It is interesting to consider the increase in nitrogen content in the foams (from ca. 4.3 wt% in MF to ca. 5.5 wt% in MFA) as a function of annealing.

Following removal from the mold, the foam samples were placed in a fume hood to allow unreacted isocyanate to be drawn off. After two hours in the hood, one sample (MF) was left in the hood while the other (MFA) was removed and placed into a 130°C oven for the annealing treatment. It is therefore hypothesized that enough reactant remained in the foams following removal from the molds that sample MFA is observed to have a higher hard segment content compared to foam MF, the remaining reactants of which possibly evaporated. The outlier from the above described trends is PNI-70 which had a nitrogen content of 4.3 wt%. This sample may actually be atypical compared to the others due to the variation in mixing and mold closure times as described earlier. On the other hand, it may be that the small sample sizes used for the nitrogen analyses introduced some systematic error due to inhomogeneity in the plaque itself. Overall, by comparing the trends from this technique to what was observed via XPS, it appears that increasing cure temperature of the plaques generally decreased the final hard segment content of the sample. On the other hand, the variation seen in the foam samples with this technique and the low content observed via XPS does cause uncertainty in stating the hard segment content of the foams. While outside of the range of this study, it appears from this that a valuable contribution would be in determining how close the actual hard segment content is in typical flexible molded foams as compared to their formulations.

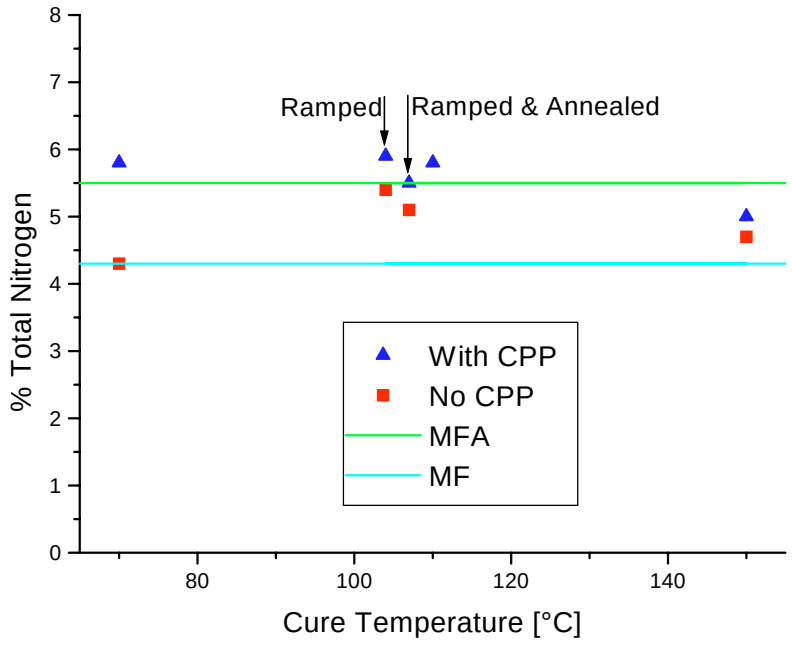

Figure 8.3 Nitrogen analysis of the various samples

Besides the hard segment content, the covalent network was examined through a solvent extraction study, and these results may be seen in Figure 8.4. It is pointed out that the much larger surface area of the foam sample would allow its soluble polymer fraction to dissolve faster than the plaques. It is possible, therefore, that the foam is closer to being completely extracted than the plaques are. However, when comparing samples of similar surface areas (i.e. the plaques), it is clear that higher cure temperatures have resulted in a more developed covalent network. As the solvent extraction work of Chapter 6 showed, the CPP particles are not completely bound and do contribute to the sol percent of a foam; therefore, the CPP containing samples were expected to be higher the unfilled samples.

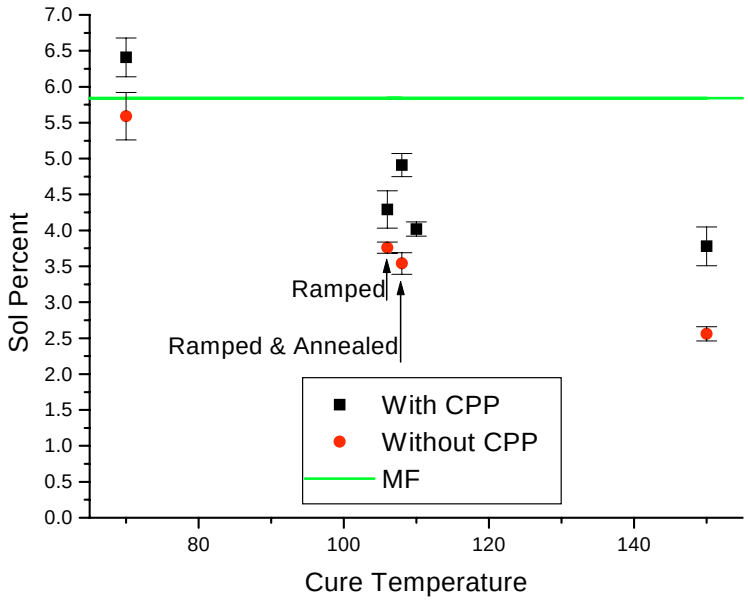

Figure 8.4 Solvent Extraction Results

Small angle x-ray scattering was used to characterize the morphology of the microphase separation. As Figure 8.5 shows, increasing the cure temperature *with* (Figure 8.5a) or *without* (Figure 8.5b) copolymer polyol resulted in systematically increasing the interdomain spacings. For example, PFI-70, PFI-110, and PFI-150 exhibited spacings of ca. 110 Å, ca. 200 Å , and above 250 Å, respectively. As discussed above, part of these thermal dependencies may be due to variation in the volume fraction of hard segments. Other workers have presented evidence that the precipitation of the polyurea hard segments may well occur in a spinodal decomposition.[9] If that hypothesis is correct, then these data may also suggest thermal variation

of the spinodal wavelength. It is noted that the observed trend of increasing wavelength with increasing temperature is consistent for the hypothesized UCST behavior of these systems.[9,16,17] Of these samples, PFI-110 had spacings most similar to the foam MF. However, as may be observed in Figure 8.5a, the scattering from the foam was approximately twice as intense as any of the plaques. This indicates much higher electron density difference between the two phases. It is hypothesized that this is due to much better phase separation in the foam than in any of the plaque materials, and this point will be strengthened further in this report.

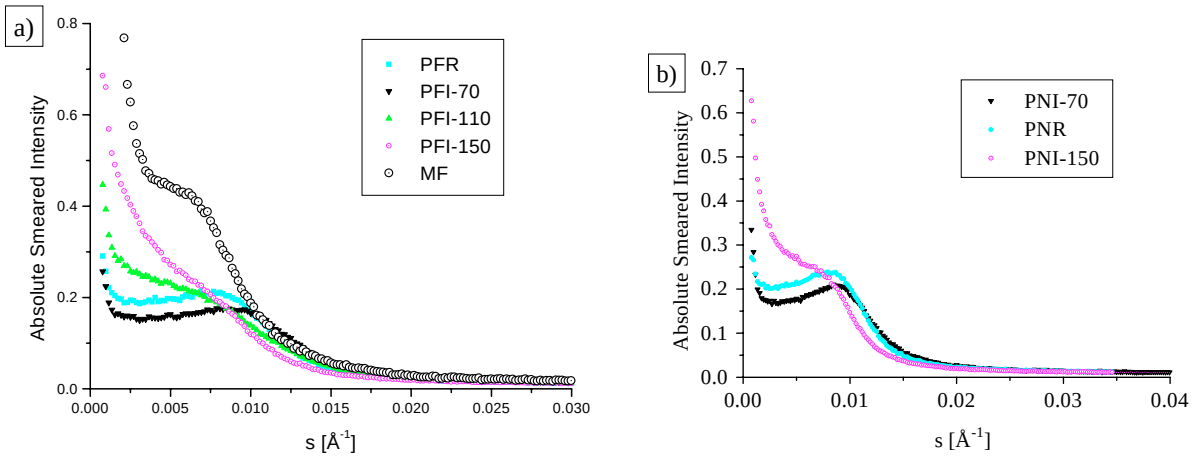

Figure 8.5 SAXS profiles of foams and plaques (a) with copolymer polyol and (b) without copolymer polyol

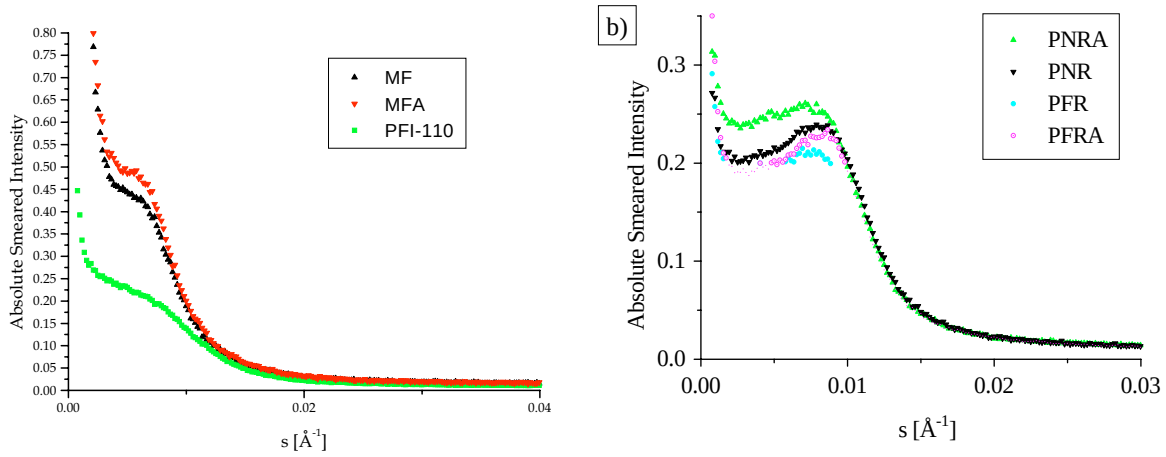

Figure 8.6 Influence of annealing treatment on the SAXS profiles of (a) foams and (b) plaques

Figure 8.6, above, compares the influence of annealing on the SAXS profiles of the plaques and foams. It may be seen in Figure 8.6a that, while the interdomain spacings of the foams were not altered by the annealing treatment, the electron density difference was apparently enhanced. These two observations indicate that the interdomain spacings are largely determined

by the conditions of the initial cure and that post-cure annealing may improve phase separation. Similar trends are also observed in the plaques in Figure 8.6b. It may again be seen there that the interdomain spacings were not greatly affected by the annealing, but the scattering intensity for each sample was increased.

Examining the carbonyl absorption region via FTIR spectroscopy offers another method for examining polyurethane foams. The carbonyl of the polyurea absorbs at ca. 1710 cm^{-1} when it is not associated via hydrogen bonding. Once it associates with the hydrogen of nearby molecules, this absorbance shifts to higher frequencies. Bidentate hydrogen bonding is the strongest such association and originates from the carbonyl oxygen and both hydrogens of another polyurea group. Carbonyl groups in this type of association absorb at ca. 1640 cm^{-1}. One common hypothesis is that unassociated polyurea hard segments largely reside in the soft matrix, and that hard segments precipitated into hard domains have probably undergone some form physical association. Thus, for a given composition, increasing absorption at ca. 1640 cm^{-1} may be interpreted to indicate increasing levels of phase separation.

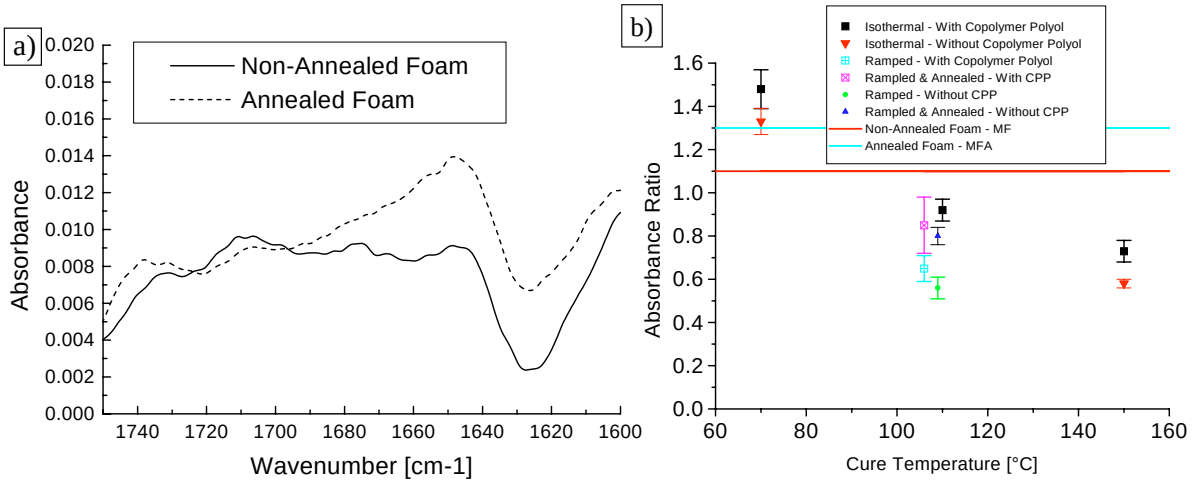

Figure 8.7 Analysis of carbonyl region of FTIR spectra of foams and plaques. (a) Shows influence of annealing upon spectra of foams, and (b) examines ratio of hydrogen bonded polyurea peak height (at ca. 1640cm^{-1}) to free polyurea peak height (at ca. 1710cm^{-1}).

Figure 8.7a above shows the influence of annealing upon the spectra of the molded *foam* samples. The character of the carbonyl spectrum of the non-annealed foam, MF, may be described as having absorbances at ca. 1710 cm^{-1} and at ca. 1640 cm^{-1} of approximately the same strength. As shown in the spectrum of MFA, this dramatically changes after annealing. The absorbance at ca. 1640 cm^{-1} becomes much more intense relative to that at ca. 1710 cm^{-1}. As

discussed above, this indicates that more polyurea hard segments have precipitated, correlating well with the observations from SAXS.

A more quantitative approach to this analysis is to examine the ratio of the peak heights of the absorbances at ca. 1640cm^{-1} and ca. 1710 cm^{-1}. The internal calibration allows direct comparison of samples to one another. As can be observed in Figure 8.7b, increasing cure temperature apparently reduces the level of hydrogen bonding in the material. This surprising result may indicate three combined effects. First, as the earlier XPS results showed, more hard segment material is in the 70°C plaques, and this might reasonably be considered to result in more precipitated polyurea material. Secondly, the reduced temperature alter the solubility of the hard segments in the polyol possibly resulting in more phase separation, and this might explain why the 150°C plaque had the lowest levels of precipitation as detected with this technique. Finally, it is possible that the water-isocyanate reaction might proceed faster than the diethanolamine reaction at 70°C. This last hypothesis has some support in that a similar ratio was observed in molded foams which contained no diethanolamine in their composition;[6] however, the introduction of diethanolamine alters the hard segment structure in a manner which prevents high levels of bidentate hydrogen bonding from being obtained. It can be seen in Figure 8.7b that curing at 110°C produced a plaque with the closest levels of hydrogen bonding to the molded foam MF (1.1). The pattern of increasing the hydrogen bonding ratio upon annealing is observed in both of the annealed plaques. However, it is interesting to note that all of the plaques cured above 100°C had a ratio much lower than the 1.25 observed after annealing as in MFA. It is hypothesized that this indicates that the plaques are less phase separated than the foams, resulting in lower observed levels of hydrogen bonding.

The impact that these changes have on the polymer properties were evaluated comparing thermomechanical spectra of these materials from DMA. It may be seen in Figure 8.8 that the storage moduli of the plaques with copolymer polyol exhibited two relaxations: the polyol glass transition at ca. -50°C and the copolymer polyol glass transition at ca. 125°C. It is noted that some annealing might occur during the heating at 2°C/min to 200°C; however, this will not influence the polyol glass transition behavior. Also, since any annealing effect would be equal for all of the samples, it is valid to examine any trends which are observed between them. Considering the variations in hard segment content suggested by Figure 8.1, the variations in storage moduli seen in Figure 8.8a are somewhat anticipated. This is seen in that PFI-70, with

the most hard segment material, exhibits the highest storage modulus, and PFI-150, with the least, has the lowest. Similar trends have been documented in foams where hard segment content was controlled by varying the feed composition.[14] PFI-110, PFR, and PFRA all exhibit very similar storage moduli, and this may be explained by their similar average cure temperatures. In Figure 8.8b, which shows the tanδ behavior for these plaques, it may be seen that the peak height for the polyol glass transition varies significantly. PFI-70 has a peak height of ca. 0.24, and PFI-150 has a height of ca. 0.67. These large differences are interpreted to indicate that the PFI-70 has much more hard segment material than PFI-150. It may also indicate that, although PFI-70 is more phase separated as shown via FTIR, more hard segment material resides in the polyol matrix as compared to PFI-150. This can be most clearly seen in that in the tanδ behavior on the high temperature side of the polyol glass transition. The tanδ curve for PNI-150 rapidly decreases to ca. 0.05, but PNI-70 remains at ca. 0.1 suggesting increased damping possibly resulting from a lower degree of phase separation. It is also observed that annealing has increased the magnitude of this tanδ peak from ca. 0.35 in PFR to ca. 0.4 in PFRA. This is a much smaller effect than was observed due to the composition difference (i.e. cure temperature).

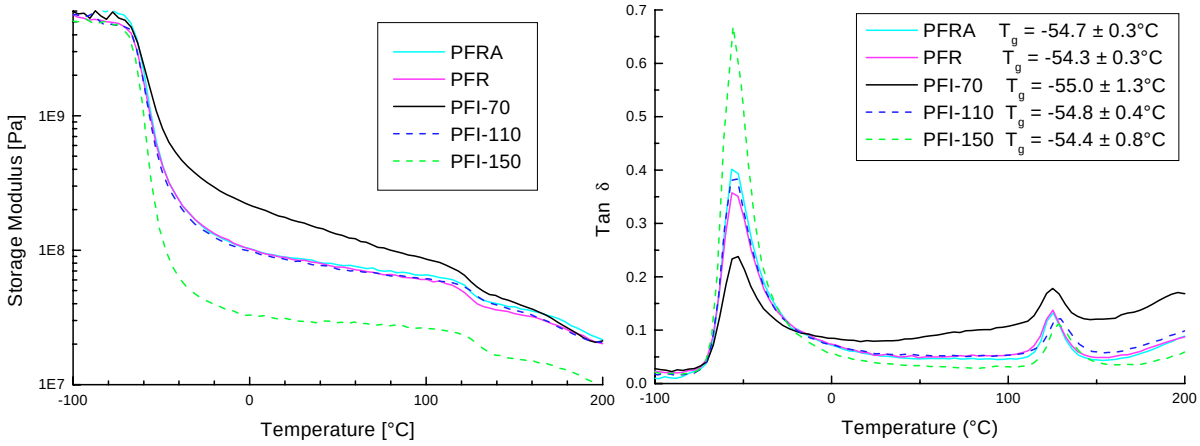

Figure 8.8 DMA data for plaques containing copolymer polyol (a) storage moduli and (b) tanδ

As Figure 8.9 shows, similar behaviors are observed in the plaques without the copolymer polyol, except that, as expected, no relaxation peak occurs at ca. 125°C. The data of Figure 8.9a again show that curing at the lower temperatures (PNI-70) result in higher storage modulus than curing at higher temperatures (PNI-150). This correlates well with all of the data

so far examined. The tanδ data of Figure 8.9b also show similar patterns. PNI-150 which has the least hard segment material exhibits the lowest peak height of the polyol glass transition, and PNI-70, with the most, exhibits the highest.

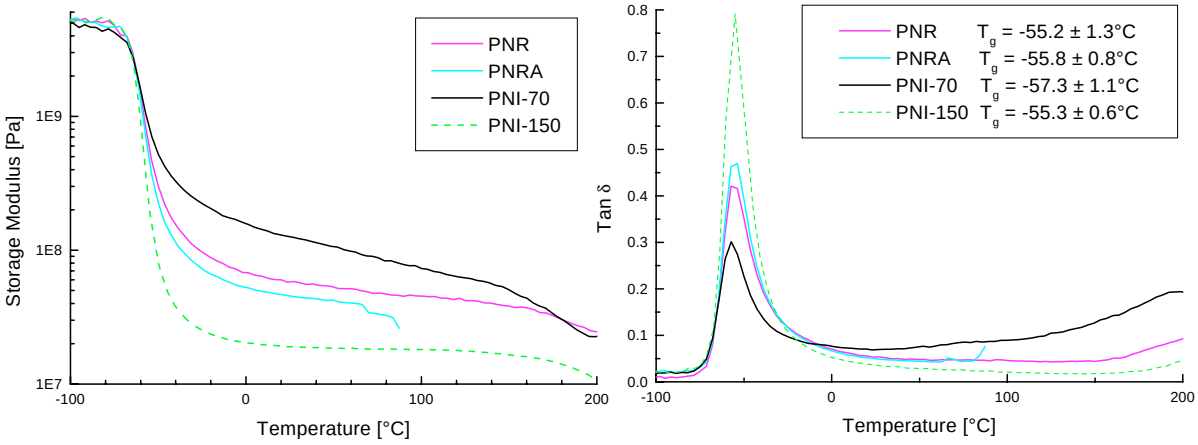

Figure 8.9 DMA data for plaques without copolymer polyol (a) storage moduli and (b) tanδ

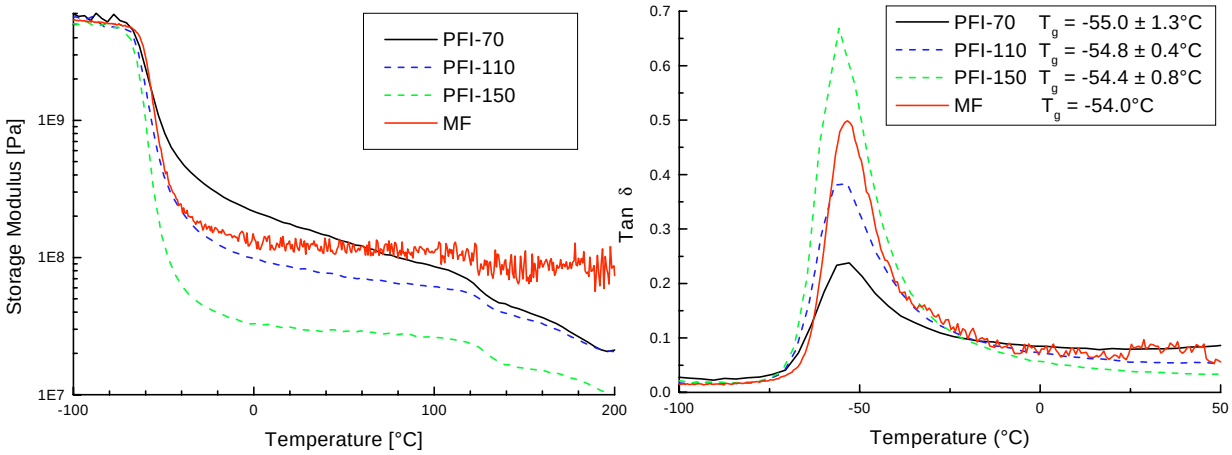

Figure 8.10 DMA data comparing plaques and foams: (a) storage moduli and (b) tanδ

The DMA data of the plaques are compared with foam MF in Figure 8.10 above. The storage modulus of foam MF, as shown in Figure 8.10a, varies from the plaques in two distinct ways. First, the polyol glass transition appears distinctly sharper than that of the plaques, and this may indicate a difference in its microphase separation. Second, a very flat rubbery plateau is observed in the foam which is much flatter than that of the plaques, remaining at ca. 200 MPa from -40°C through 125°C. At -40°C, the foam storage modulus is very similar to that of PFI-110, and at 60°C, it is similar to PFI-70. It is interesting to note that ambient foam storage

modulus between PFI-110 and PFI-70 correlates well with the hard segment content results from XPS in Figure 8.1. Above 60°C, the foam storage modulus remains reasonably stable through the highest temperatures tested. Although they exhibited much lower moduli, only the 150°C plaques exhibited a similar flatness over that range of temperatures. It is therefore hypothesized that this may result from a better developed covalent network; however, hard segment molecular weight and degree of phase separation may also be contributing to this flattening. Model studies in polyurethane urethane elastomers have shown that increasing the hard segment content or the degree of phase separation can also flatten storage modulus curves in the rubbery thermal region and increase the breadth of the rubbery plateau.[18]

It may be observed in the tanδ data in Figure 8.10b that foam MF has a slightly narrower polyol glass transition peak than the plaques, suggesting again differences in the microphase separation behavior of the foams compared to the plaques. It may be seen that the onset of the glass transition occurs at lower temperatures for all of the plaques as compared to the foam. This suggests that the plaques have some regions where the polyol is purer than is observed in the foam. On the other hand, since the glass transitions are all observed to end at approximately the same temperature, better overall phase separation can not be concluded to exist in the plaques. It is therefore hypothesized that the foam has a more even distribution of dissolved hard segment material throughout its polyol matrix than the plaques. Also, the magnitude of that peak is observed to be between PFI-110 and PFI-150. This pattern of higher storage modulus with higher peak heights is suggested to result from a polymer which contains more hard segment material but has better and more homogeneous phase separation than was observed in the plaques.

8.5 Conclusions

This study has shown that cure temperature is an important variable in the production of flexible polyurethane foam polymers. Curing at higher temperatures was shown via XPS and nitrogen analysis to reduce the hard segment content in the polymer and it was shown by solvent extraction to increase the degree of cross-linking in the system. Also, increasing the cure temperature was observed to influence the formation of hydrogen-bonded hard domains by decreasing the amount of bidentate hydrogen bonding observed. Larger interdomain spacings also resulted from higher cure temperatures. This was hypothesized to result of less hard segment volume contained within the polymer or possibly of thermal variation in the spinodal

wavelength. Finally, the dynamic mechanical properties of these polymers were observed to change significantly depending upon the cure temperature. It is hypothesized that the large reductions in storage modulus due to higher cure temperatures were a result of reduced hard segment content and of alterations in the microphase separated morphology.

By comparison to foams of the same formulations, it was shown that the foams were distinctly different from the plaques regardless of the cure temperature used. The foam developed more hard segment material than any plaque produced above 100°C. This may be the result of any vaporized reactants being entrapped within the cellular structure of the foam and eventually reacting rather than evaporating away as is hypothesized to occur with the plaques. The foam was also shown to have much higher levels of phase separation via SAXS. When compared to plaques with similar levels of hard segment content, the foams were shown to have developed higher levels of hydrogen bonding via FTIR. Finally, DMA testing suggested that a better phase separation and a more homogeneous distribution of dissolved hard segment material in the foam resulted in slightly narrower polyol glass transitions. It also showed that more hydrogen bonding yielded much higher storage moduli than plaques of similar hard segment content. Finally, the broad thermal range over which the rubbery plateau was stable in the foams may suggest a more developed covalent network than was obtained in the plaques; however, this may also be a result of the better overall microphase separation in the foam.

The differences observed here present some challenges for using plaques to determine the polymer properties that will be observed in corresponding foams. Considering that some polyurethane foam properties are dependent on the interconnectivity of the hard domains, the sensitivity of hard segment content on cure temperature might make direct correlation of the plaque properties to a foam difficult. The reduced phase separation in the plaques indicates that much more hard segment material is in the polyol phase, and this suggests that the polyol phase is somewhat stiffened by the dissolved hard segment material. Since physical associations of dissolved hard segments are much weaker than what is observed within the hard domains, it is anticipated that this might result in greater susceptibility of the plaques to thermal and humid plasticization. Finally, time dependent properties of the plaques such as creep and load relaxation may contain large amounts of deviation from foam behavior because the covalent network and microphase morphology are significantly different.

8.6 Acknowledgements

This work has been financially supported by the Dow Chemical Company, and their support is gratefully acknowledged. We acknowledge R.E.7 O'Neill for producing the molded foam samples used as a standard. Frank Cromer of the Dept. of Chemistry at V.P.I. & S.U. is thanked for his assistance in collecting the XPS data. We also recognize Dr. Werner Lidy and his coworkers for their development of the technique used for manufacturing the molded plaques. Ralph Priester is acknowledged for facilitating the nitrogen analysis of the plaques, and Alvetta Pryor is thanked for performing those tests.

8.7 References

[1] Gibson LJ; Ashby MF; Cellular Solids: Structure & Properties; Pergamon Press, Oxford: (1988)
[2] Kraynik AM; Reinelt DA; *J Coll Int Sci*: **181** (1996) 511-520
[3] Kraynik AM; Reinelt DA; *Chem Eng Comm*: **148-150** (1996) 409-420
[4] Weaire D; Fu T-L; *J Rheology*: **32** (1988) 271-283
[5] Ozkul MH; Mark JE; Aubert JH; *J Appl Polym Sci*: **48** (1993) 767-774
[6] Kaushiva BD; Wilkes GL; *J Appl Polym Sci*: in press
[7] Kaushiva BD; McCartney SR; Rossmy GR; Wilkes GL; *Polymer*: in press
[8] McClusky JV; Priester Jr RD; O'Neill RE; Willkomm WR; Heaney MD; Capel MA; *J Cell Plast*: **30** (1994) 338
[9] Elwell MJ; Ryan AJ; Grünbauer HJM; Van Lieshout HC; *Macromolecules*: **29** (1996) 2960
[10] Kaushiva BD; Wilkes GL; *Polym Comm*: in press
[11] Lidy WA; Rightor E; Heaney M; Davis B; Latham L; Barnes G; *Proc. of the SPI/ISOPA Polyurethanes World Congress '97*: (1997) 95
[12] Kaushiva BD; Wilkes GL; *Polymer*: in press
[13] Herrington R; Hock K; Flexible Polyurethane Foams, 2nd Ed.; The Dow Chem Co: (1998)
[14] Turner RB; Spell HL; Wilkes GL; *Proc of the SPI 28th Annual Technical/Marketing Conf*: (1984) 244
[15] Hearn MJ; Ratner BD; Briggs D; *Macromolecules*: **21** (1988) 2950-2959
[16] Hashimoto T; *Phase Transitions*: **12** (1988) 47-119
[17] Izumitani T; Hashimoto T; *J Chem Phys*: **83** (1985) 3694-3701
[18] Samuels SL; Wilkes GL;*J Polym Sci*: **Symp. 43** (1973) 149-178

9 Structure-Property Relationships of Polytetrafluoroethylene -- Poly(tetrafluoroethylene-co-vinylidene fluoride-co-hexafluoropropylene) Blends

9.1 Chapter Summary

The morphology and mechanical properties of blended samples of polytetrafluoroethylene (PTFE) and poly(tetrafluoroethylene-co-vinylidene fluoride-co-hexafluoropropylene) (FKM) were investigated. Samples with varying levels of PTFE content were produced by mixing the desired composition as aqueous dispersions and casting them onto a carrier film.[10] A thermally induced cross-linking reaction was used so that the FKM component could be cross-linked to various degrees by changing post-casting thermal treatments. Thus, greenleaf (not cured), cured, and post-cured samples were produced where the post-cured films were exposed for the longest times at the highest temperatures.

It was observed that below 50 wt% PTFE content, cross-linking the FKM can have a much larger influence on tensile modulus than changing the PTFE content. Above 50 wt% PTFE, however, the modulus showed a near exponential increase with respect to increasing PTFE content. Without cross-linking, the toughness of the cast blends was shown to systematically decrease as PTFE content was increased. However, when the FKM was cross-linked in films between 20-60 wt% PTFE, more stress was apparently transferred to the PTFE particulate leading to higher elongation-to-break and resulting in higher toughness. The thermal dependence of the tensile properties in greenleaf films were examined, showing that decreasing temperature dramatically increases the toughness. Without PTFE particles, the FKM was observed to have a peak toughness at ca. 13°C, but when PTFE was added to the system the peak occurred at ca. 19°C. This peak is hypothesized to result from increasing transfer of stress to the PTFE particles as temperature is reduced. DMA analyses showed a systematic increase of storage moduli with increasing PTFE content. A tanδ peak at ca. -10°C was observed which corresponds to the glass transition of the FKM, and the height of this peak was observed to decrease systematically with decreasing FKM content as more PTFE was added. Increasing the level of covalent cross-linking in the elastomer was also observed to decrease the tanδ peak height, suggesting a reduction in the molecular mobility in the FKM. However, for the levels of cross-linking tested, this change was not observed to be as

significant as increasing the PTFE content. Some variation in mechanical properties was also observed due to alterations within the PTFE or FKM components. A more systematic study is required to better understand the observed changes; however, two hypotheses for these variations is that FKM composition differences may alter the potential for the elastomer to undergo cross-linking and that significant differences in the FKM molecular weight distribution would effect the development of a three-dimensional covalent network.

The morphology of these systems was studied via solvent extraction, TEM, AFM, and WAXS. In a solvent extraction process which extracted nearly 100 wt% of the greenleaf (non-cured) films, ca. 80 wt% of the cured samples were extractable and ca. 40 wt% of the post-cured samples were removed. The solvent extraction results of the FKM thus confirmed the results of the DMA testing in that, while the FKM is cross-linked, even the post-curing does not cross-link it to a large extent. For all PTFE content levels studied, the TEM examination revealed a dispersed morphology for the PTFE particulate with the FKM forming a continuous matrix. The PTFE particulate was observed to generally be ca. 0.2 μm in size. In the 20 wt% PTFE films, the 0.2 μm PTFE particles were generally observed to form clusters with ca. 1 μm FKM domains that were relatively free of PTFE particles. As the PTFE content was increased, the size and frequency of the PTFE-poor domains was observed to decrease until they were not observed at all in the 60 wt% films. Tapping mode AFM was also shown to be a useful technique for imaging morphology that lies parallel to the plane of the film surface, with many observations correlating well with the TEM results.

WAXS was particularly useful for detecting the formation of oriented PTFE fibrils in the cast blends. Repeated calendering was shown to lead to high degrees of orientation via WAXS which corresponded to highly anisotropic mechanical properties. Parallel to the machine axis, the modulus was found to be ca. 33-35 MPa in the 40 and 60 wt% PTFE films. Perpendicular to the machine axis, it was observed to be ca. 5-10 MPa. The presence of oriented PTFE fibrillation was confirmed via AFM. Tensile drawing experiments also revealed that enough stress can be transferred to the PTFE particles by the flow of the FKM component alone. This was demonstrated by pressing films at various temperatures with as little surface shear as possible. It was shown that reducing the temperature of the film deformation results in an increased film modulus.

9.2 Introduction

The unusually high thermal stability, environmental resistance, and chemical inertness of fluoropolymers is well known, and makes the use of these materials desirable for many demanding applications.[1] However, matching mechanical properties to required performance specifications has presented many challenges. For example, polytetrafluoroethylene (PTFE) and other fluoroplastics have high modulus but are also prone to creep and are generally difficult to process.[2,3] Fluoroelastomers are ideal where the polymer must bear much deformation and absorb much mechanical energy, but they must be cross-linked to reduce creep and improve modulus. Reducing the glass transition temperature of the fluoroelastomers and improving the stability of their cross-links have been subjects of continuous research since the 1940's.[3] Rather than adding a common filler such as carbon black,[4] blending fluoroplastics with fluoroelastomers presents the opportunity to exploit the desirable properties of each. This research will thus seek to examine the utility of using PTFE to reinforce a fluoroelastomeric matrix. Fluoroelastomers are commonly produced by copolymerizing the various fluoromonomers which are available, and so this research used the terpolymer of the random copolymerization of tetrafluoroethylene, vinylidene fluoride, and hexafluoropropylene which will be referred to as FKM.[3]

The unique structure of polytetrafluoroethylene (PTFE) gives this polymer many unusual and useful characteristics. The high stability of the carbon-fluorine bonds make it chemically inert even at high temperatures, and the bulkiness of the pendant fluorine atoms, relative to hydrogen, provides an additional shielding effect for the carbon backbone of the molecule. PTFE also exhibits unusual toughness at temperatures as low as -273°C, yet it possesses a remarkably high nascent crystalline melt temperature of 342°C. High molecular weight PTFE (ca. 10^6-10^7 Daltons) has a very high melt viscosity of ca. 10^{11} Pa at 380°C.[1,2] Its outstanding thermal stability means that this polymer has useful properties over a 550°C range![1] PTFE also has a very low dielectric constant (ca. 2.1) and dissipation factor (<0.0004) that are both stable over a broad range of temperatures and frequencies (60-10^9 Hz).[1] The combination of these properties together with its well known low friction coefficient, excellent weatherability, and low surface free energy allow PTFE to perform well in many demanding environments, making it an ideal polymer uniquely suited for a variety of specialty applications.[3] Some of these applications include surface coatings, casting films, architectural

fabrics, acoustic membranes, expansion joint materials, flexible braided hose, conveyor belts, gaskets, electrical insulation, and fire-resistant thermal insulation.[1,5]

On the other hand, PTFE does have some properties which require special techniques to be applied for its analysis and application. It is insoluble in all common solvents below 300°C, limiting characterization by typical methods such as gel permeation chromatography or osmometry.[6] Therefore, PTFE molecular weight is usually classified by melt viscosity at 380°C or through correlations based on specific gravity or percent crystallinity.[2,6] Its typically very high melt viscosity generally precludes the use of conventional polymer processing techniques such as injection molding or melt extrusion.[1] Lower molecular weight PTFE (melt viscosity below ca. 10^9 poise at 380°C) is brittle and does not have a useful modulus, but because it retains its low coefficient of friction it is often applied as a dry lubricant.[6] More useful moduli are obtained at ca. 10^6-10^7 Daltons (10^{10}-10^{12} poise at 380°C); however, once the high molecular weight PTFE has been melted, regaining its high nascent crystallinity is not possible due to molecular constraints such as chain entanglement.[2,6] Because of these considerations, the most commonly utilized processing techniques all incorporate a "sintering" step after molding and pressing granular resins into the desired shape followed by heating above the melt temperature.[2] Cooling rate can be controlled to often achieve the desired level of crystallinity after the heat treatment, and this percent crystallinity largely determines the final mechanical properties of the polymer.[1] The other major type of operation used involves spinning fibers or coating materials using aqueous dispersions of PTFE, and these methods frequently also include a "sintering" step. [1]

PTFE is generally produced via a free radical polymerization typically performed under moderate pressure (100-1000 psi) and in warm water (ca. 60-95°C).[3] The most common initiator used for this polymerization is a mixture of potassium persulfate, hydrogen peroxide and oxygen.[3,7] Abstraction reactions are not thermodynamically favorable for fluorocarbons, thus there is minimal chain transfer or disproportionation.[3] Termination therefore occurs by combination, resulting in one PTFE molecule for each persulfate ion decomposed.[3] Two techniques are generally employed for the polymerization of PTFE. Suspension polymerization in an aqueous medium utilizes vigorous agitation and little or no dispersing agent.[2] The product from this method precipitates into granular resins which are produced in a wide variety of grades which are tailored to meet desired flow specifications

and end-use properties.[2] These granular resins are typically composed of high molecular weight, ca. one millimeter sized particles which have very high nascent crystallinity (ca. 95% or higher).[3] Emulsion polymerization is the other main technique, and it is also called "aqueous dispersion polymerization." This process utilizes mild agitation and adequate amounts of dispersing agents (such as perfluorocarboxylic acid) to yield a very different product.[2,3] Although still of high molecular weight and high nascent crystallinity, the product of this technique is a stable dispersion of small, colloidal particles ca. 0.2-0.3 microns in size.[6] Whereas the granular resin products can be molded into various shapes by pressing and sintering, the aqueous dispersions are generally used for dispersion coating or paste extrusion.[2]

It should be emphasized that both of these polymerization techniques are generally used to yield high molecular weight polymer. One substantial difference between high and low molecular weight is that high molecular weight PTFE readily fibrillates under shear.[6] This fibrillation can lead to the formation of a network of fibers which rapidly becomes unworkable.[6] Low molecular weight particles do elongate to some extent, but then disintegrate into the powder form that is useful as a dry lubricant. [2,6] The ease with which high molecular weight PTFE fibrillates, leading to dramatic changes in its properties, substantially limits the usefulness of this material, particularly in uses where much mechanical work will be borne by the polymer. On the other hand, many applications would greatly benefit from its unique combination of properties if it could be incorporated. This challenge has led to the development of a new class of materials which are based on reinforcing a fluoroelastomeric matrix with a high molecular weight fluoroplastic particulate.[8] The problems associated with blending PTFE have meant that earlier applications of this concept used milling to press PTFE microparticulate into the fluorinated elastomer which was subsequently cross-linked.[6] This milling process required micropowders of low molecular weight PTFE to be used in order to avoid the processing problems associated with fibrillation.[6] Also, such additions by milling were limited to ca. 25 wt% PTFE.[6]

Utilizing the product of the emulsion polymerization, the new processing technique blends aqueous dispersions of high molecular weight PTFE, fluoroelastomeric latexes, and curative agents.[6,8,9] These blends are then cast onto a carrier film and dried as described in references 6 and 10. The materials are then thermally cured which promotes the cross-linking

reactions in the elastomer.[6] This yields a very flexible product which can be produced with homogeneously dispersed filler particles of up to 70 wt% PTFE.[6] Moreover, the use of high molecular weight PTFE provides the later possibility of inducing fibrillation and providing additional reinforcement.[6]

Several factors can be varied in these systems to produce the desired properties. The PTFE content in the formulation can be adjusted to obtain higher modulus, while other fillers may also be added to the system. Different plastic and elastomeric components could also be used. To some extent, the degree of cross-linking can be controlled and the mechanism used for cross-linking could also be changed to improve the stability of the cross-links. Furthermore, the possibility of fibrillating the PTFE component suggests another possible way to increase modulus at a given PTFE content and degree of cross-linking. For example, fibrillation could possibly be induced by applying shear to the film surface, thus altering surface properties relative to the matrix. Given all of these various ways to control the properties of these new materials, it can be seen that a better understanding of how the variables relate to final properties would be of great importance to further optimizing the mechanical performance of these systems. Therefore, this research sought to focus on some compositions of industrial importance and explored the structure-property behavior based on three variables: the ratio of PTFE to fluoroelastomer, the degree of cross-linking, and the fibrillation of the PTFE component.

9.3 Experimental

9.3.1 Materials

The materials used in this study were produced by blending the components while still in an emulsified, microparticulate form. Particle sizes for the polymeric components generally ranged from 0.01 to 1.0 microns. In the components for this study, the average particle size in the aqueous state was determined to be 0.2 microns using a Leeds & Northrup Microtrac Ultrafine Particle Size Analyzer, which measures size via dynamic light scattering. Prior to blending with the other components in the formulations described later in this section, the aqueous latexes of fluoroelastomer were concentrated to facilitate the casting process. This concentration was performed by first adding Rhodofac RE-610 surfactant (Rhone-Poulenc) at 4 wt. % based on the weight of the polymer solids in the latex, followed by an addition of aqueous NaOH to reach a pH of 6.4-6.5. Aqueous ammonium alginate was then

mixed thoroughly into the blend at a level of 0.5-1% by weight of the polymer solids. The mixture was then allowed to settle at room temperature until the concentrated latex formed a stable separation. The supernatant water was then siphoned off and the remaining latex is blended with the other components and then used in the casting process described below.

Vertical casting of the blend utilized a carrier film[10] which was pulled through the latex. Each immersion in the latex was followed by a drying step at ca. 95°C.[10] Each pass resulted in a coating thickness of ca. 0.03 mm, and multiple passes were used to obtain a final thickness of ca. 0.13 mm.

Following casting, the film may be "cured" by heating it to promote the cross-linking of the elastomeric component. The curative used in these samples was N,N'-dicinnamylidene-1,6-hexane diamine (Diak #3, DuPont) which undergoes hydrolysis to form cinnamaldehyde and hexamethylene diamine. Above 100°C, the hexamethylene diamine reacts to form covalent cross-links in fluoroelastomers which incorporate vinylidene fluoride in their composition.[11,12] This curing step was performed by first layering uncured or "greenleaf" plies of the material until a desired thickness (typically 0.64-1.02 mm) was reached. Care was taken in stacking the films to minimize the formation of air voids between layers. Under pressure, the tackiness of the greenleaf film compounded the plies into a uniform sheet. Sections of the material were cut to fit the two presses (from Fred. S. Carver, Inc.) used for curing: a Model M press (22.9 cm x 22.9 cm) and a Model CMV50H-13-C press (45.7 cm x 45.7 cm). The curing step for these materials was performed by holding the films at 300 psi for 30 minutes at 177°C. An additional post-curing step was used for some samples which involved holding the films under atmospheric pressure for 20 hours at 204°C.

Prior to casting, the formulation components of Table 9.1 were blended together according to the following procedure. First, the curative agent (DIAK #3, Dupont) and the surfactants (non-ionic surfactant, Daxad 11, Hampshire Chemical; and ionic surfactant ammonium caseinate in a 10% dispersion, Technical Industries) were ball milled until well mixed and then de-aerated. The fluoroelastomer used in this study is a terpolymer of tetrafluoroethylene, vinylidene fluoride, and hexafluoropropylene; and this terpolymer will be called "FKM." The FKM used for most of this study will be referred to as "FKM A." Unpublished work by another laboratory at Virginia Tech determined that this FKM has a mole percent ratio of 12.4/63.9/23.6 TFE/VF_2/HFP.[13] Aqueous zinc oxide (60% solids,

Technical Industries, Inc.) was mixed into the concentrated FKM latex followed by the Diak mixture. Finally, the high molecular weight PTFE dispersion (ca. 60 wt% solids) was stirred in gently to minimize shear. Following the addition of these components, the blend was deaerated for one hour under a vacuum of 20 inches of mercury, whereupon it was then ready to be cast onto the carrier as described in reference 10.

Table 9.1 General Formulation for the Fluoroelastomer/Fluoroplastic Blends

	parts dry weight by dry weight of rubber
FKM	100
PTFE	varied
Zinc Oxide	10
Diak #3	5
Daxad 11 solution	1.5
Ammonium caseinate	1.5

The level of PTFE was varied to produce samples at 0, 20, 40, 60, and 70 wt% PTFE relative to the FKM, while keeping the ratio of all of the other components to the FKM constant. For each level of PTFE content, a greenleaf (i.e. not cured), cured, and post-cured sample was produced. Different supplies of FKM and PTFE were briefly examined in the evaluation of properties. The different FKM products tested will be referred to as FKM A, FKM B, FKM C, and FKM D. ***Unless otherwise specified, FKM will refer to FKM A.*** There is no standard composition of FKM, and each supplier uses different ratios of TFE, VF_2, and HFP. Those evaluated by the laboratory of Dr. McGrath via NMR are presented in Table 9.2.[13] Likewise, the different PTFE products tested will be referred to as PTFE 1, PTFE 2, and PTFE 3. Average particle sizes for the PTFE dispersions was found via light scattering to be 0.2 μm, but more detailed information on their composition was not available. ***Unless otherwise specified, PTFE will refer to PTFE 1.***

Table 9.2 - FKM Composition[13]

FKM Product	TFE [mol %]	VF_2 [mol %]	HFP [mol %]
FKM A	12.4	63.9	23.6
FKM B	15.1	62.6	22.2
FKM C	9.2	66.9	23.9
FKM D	not available	not available	not available

9.3.2 Methods

Dynamic mechanical analysis (DMA) was performed on a Seiko Model 210 in the tensile mode. The samples were heated from -110 °C to 400 °C at a rate of 2 °C/min. and the storage modulus (E') and tanδ data were collected at a frequency of 1 Hz. Bar shaped samples were cut from the films and had dimensions of approximately 0.1 x 5 x 15 mm^3 with a grip-to-grip distance of 10 mm.

Mechanical properties were also investigated at room temperature (ca. 22°C) through tensile testing based on ASTM D412 using an Instron 4400R equipped with a 1000 N load cell and Instron Series IX controller software. Dogbone shaped samples were cut having gauge sections 6.5 mm long by 2.8 mm wide. Thicknesses were typically ca. 0.15 mm. A 10 mm grip-to-grip distance was used, and the crosshead speed was 200 mm/min. To evaluate thermal dependence of mechanical properties, some tests were also performed in an environmental chamber produced by Russells Technical Products using a Watlow 922 microprocessor for environmental control. Samples were allowed to condition for fifteen minutes at the test temperature and humidity was not controlled. Tests were performed over the range from 5 to 55°C.

Small angle X-ray scattering (SAXS) was utilized to evaluate the presence of microphase separation or alterations in the crystalline lamellae spacings of the PTFE. This was performed with a Phillips model PW1729 generator operating at 40 kv and 20 ma and a slit collimated (0.03 x 5 mm) Kratky camera with nickel filtered CuKα radiation having a wavelength of 1.542 Å. The detector utilized was a Braun OED 50 position-sensitive platinum wire detector. Scattering data were corrected for parasitic scattering and normalized using a Lupolen standard.

Variation of the degree of covalent cross-linking between the greenleaf, cured, and post-cured samples was evaluated via solvent extraction using 2-butanone (methyl ethyl ketone). Elastomeric samples (0 wt% PTFE) were held in boiling solvent, and the solvent was drained and replaced six times at eight hour intervals. After removal from the solvent, all samples were dried at 100°C at 30 inches of mercury vacuum.

To explore the presence of oriented fibrillation, the technique of wide angle X-ray scattering (WAXS) was applied via a Phillips model PW1720 generator with a Warhus camera. Nickel filtered CuK radiation was used with a wavelength of 1.542 Å and pinhole collimation with a diameter of 0.020 inches. Film samples evaluated had thicknesses of ca. 0.15 mm. Sample to film distance was 7.7 cm and exposure times were ca. 3 hours.

The morphology of the solid state was investigated using transmission electron microscopy (TEM). From samples embedded in epoxy at 60°C, very thin sections were cryogenically microtomed using a diamond knife on a Reichert-Jung Ultracut-E ultramicrotome with the FC-4D cryo-attachment operating at -90 °C. Ethanol was used to collect the sections onto 600 mesh copper grids. Micrographs were taken using a Philips Model 420T scanning transmission electron microscope (STEM) operating at an accelerating voltage of 100 kv. At least three magnifications were taken for each sample. "High" magnification refers to 37,500 X on the negative, "medium" magnification refers to 10,500 X on the negative, and "low" refers to 3,300 X on the negative.

Atomic force microscopy (AFM) in tapping mode was also used to study nanoscopic level structure. Experiments were performed on a Digital Instruments Scanning Probe Microscope using Nanosensors TESP (Tapping Etched Silicon Probe) type single beam cantilevers. These cantilevers had nominal lengths of ca. 125 μm, force constants of approximately 35 ± 7 N/m, and were used at oscillation frequencies of ca. 290 kHz. All AFM micrographs presented here were of the film surfaces. However, cross sections of films could be imaged via AFM micrographs by examining the surfaces of samples mounted in epoxy for TEM after being smoothed by cryo-microtoming.

The mold shown in Fig. 9.1 was utilized to investigate the induction of orientation in the cast blends via planar deformation. Samples were cut to dimensions which forced planar deformation primarily along one axis when the mold was closed and pressed. Shearing the surface sample was not desired, therefore Kapton film was used to line the mold and the film

was heavily lubricated with a silicone mold release agent. Thus, any orientation developed in the sample would result from the FKM transferring shear to the PTFE particulate as it flowed in the mold. To evaluate the importance of molding temperature, the mold was conditioned at the desired pressing temperature overnight in an environmental chamber with the sample already loaded in it. The mold was then removed and placed under ca. 1500 psi for 9 or 11 minutes after which the pressure was released to ca. 5 psi for the remainder of the cure time. When the mold was pressurized, the hot press was set to heat to 177°C. It was found that ca. 30 minutes were required to heat the mold sufficiently for the film sample to reach the desired cure temperature. Therefore, to keep the films at 177°C for 30 minutes, the molds were removed from the hot press after 60 minutes and allowed to cool at ambient conditions.

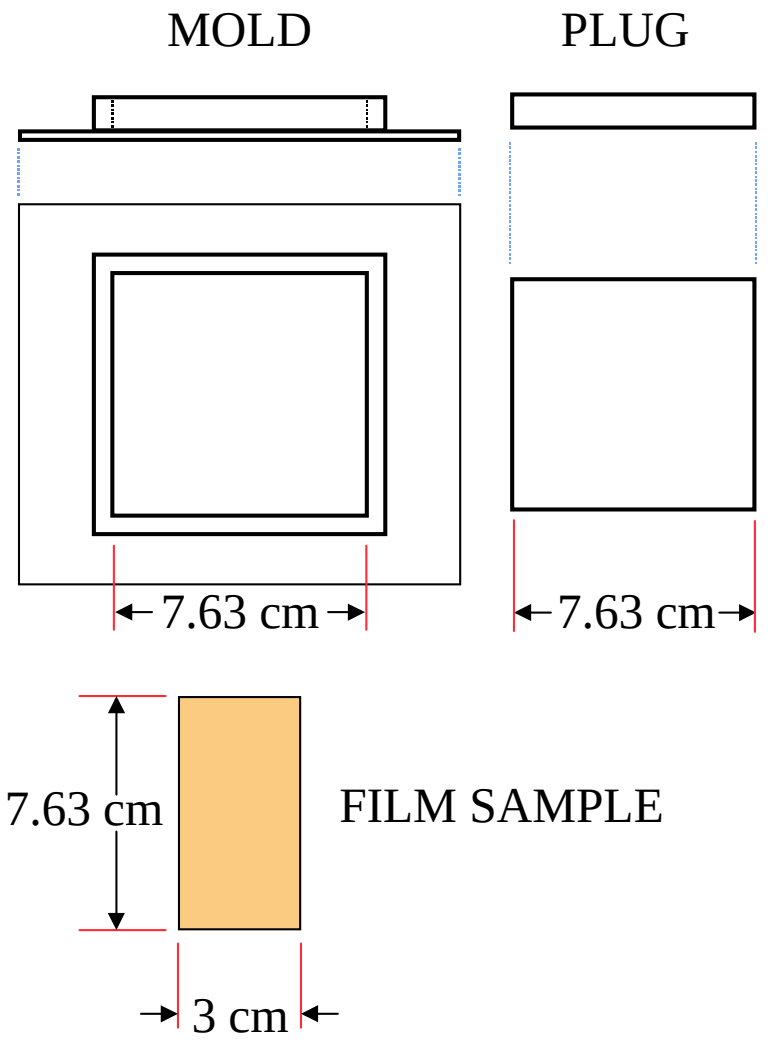

Figure 9.1 Schematic diagram of mold used to study film deformation at various temperatures

9.4 Results and Discussion

9.4.1 Mechanical and Viscoelastic Properties

The dependence of the mechanical and viscoelastic properties of these materials on the level of PTFE content and covalent cross-linking were investigated through tensile elongation testing and DMA. The modulus data presented in Fig. 9.2a suggests that the difference between greenleaf and cured materials is only detectable at higher PTFE content, but that post-curing provides enough cross-linking to increase the modulus significantly. For example, whereas the cured materials could only be distinguished from the greenleaf films above 50 wt% PTFE content, the post-curing increased the modulus at all PTFE levels by an average of ca. 120% over the modulus of the uncured samples. Figure 9.2a also suggests a dramatic increase in the modulus above fifty weight percent PTFE, which may indicate the development of connectivity between the PTFE particles. While some increase is observed as the PTFE content is increased from 0 to 40 wt%, it is a minor increase in comparison to the modulus improvement provided by the cross-linking. For example, the 20 wt% PTFE film after post-curing exhibited the same modulus as the 40 wt% PTFE greenleaf or cured films. On the other hand, as PTFE begins to form the majority of the matrix, the level of PTFE content can be seen to become more important to the final modulus of the film. That is, the modulus of the 60 wt% green leaf or cured films is higher than that of the post-cured 40 wt% film, indicating a greater increase based on the PTFE level. Figure 9.2a also shows that the increase in modulus due to cross-linking is multiplied by increasing the level of PTFE content particularly above 50 wt%.

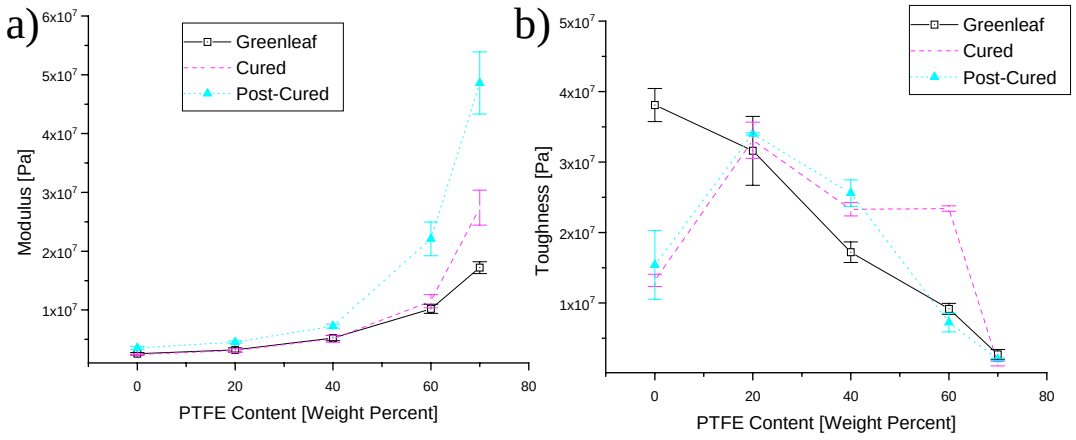

Figure 9.2 Summary of data from Instron tensile tests at room temperature: a) Young's modulus and b) toughness

In tensile testing, the "toughness" is calculated by numerically integrating the stress/strain curve, and this provides a measure of the energy absorbed by the material before it breaks. As Fig. 9.2b shows, the toughness of the films varies significantly relative to the PTFE content and the degree of cure. Prior to curing, it can be seen that the toughness systematically decreases with PTFE content from 38 MPa at 0.0 wt% PTFE to 3 MPa at 70 wt%. The convolution of the PTFE content with the degree of cure alters the behavior significantly. For example, the toughness of the cured and post-cured materials are ca. 14 MPa at 0 wt% PTFE, and they increase to ca. 33 MPa at 20 wt% before decreasing back to 2 MPa at 70 wt%. As compared to the greenleaf materials in the range of 20-60 wt%, curing or post-curing the films appears to reduce the rate of toughness loss as PTFE content is increased. To understand this behavior, a closer examination of the stress-strain curves is required.

Figure 9.3a shows representative stress-strain behavior of the greenleaf materials, revealing two systematic trends: the modulus increases and the strain-at-break decreases with increasing PTFE content. It is also interesting to note that the character of the curves shift from being very typical of elastomeric deformation behavior at 0 wt% PTFE to having a more plastic character at 70 wt% PTFE. This can be seen in that as the PTFE fraction is increased; the yield point of the stress-strain curve becomes much more distinct, and the draw region or the irrecoverable flow region becomes easier to distinguish. Similar alterations in the character of the stress response have been observed in elastomeric systems that have been reinforced with inorganic fillers such as rock salt and glass beads.[14] This behavior is considered to result from the close packing which occurs at higher filler contents. In other words, as the composite material is stretched, the close proximity of the filler particulate impedes any large deformations from occurring which results in much lower strain-at-break values.

The cured and post-cured materials exhibit behavior that is less straightforward. As the representative curves in Figs. 9.3b and 9.3c show, the moduli of the materials systematically increase with the PTFE content. Also like the greenleaf films, the yield point and draw regions become more distinct. Unlike the greenleaf materials, however, the strain-at-break behavior is significantly different. For the cured materials, the strain-at-break is relatively constant with respect to the PTFE content remaining in the 8-9 strain units region

between 20-60 wt% PTFE. This is 2 strain units higher than the point of break for the 0 wt% PTFE film. Likewise, the post-cured materials exhibit an increase in the strain at break up to 40 wt% PTFE before decreasing again. This is important to note, because after the initial yielding behavior (ca. 0.5 strain) the stress-strain curves of Figs. 9.3b and 9.3c are remarkably similar regardless of PTFE content. This suggests that the increased toughness does not come from higher stress bearing in the film, but rather it largely is due to a mechanism which increases the strain-at-break.

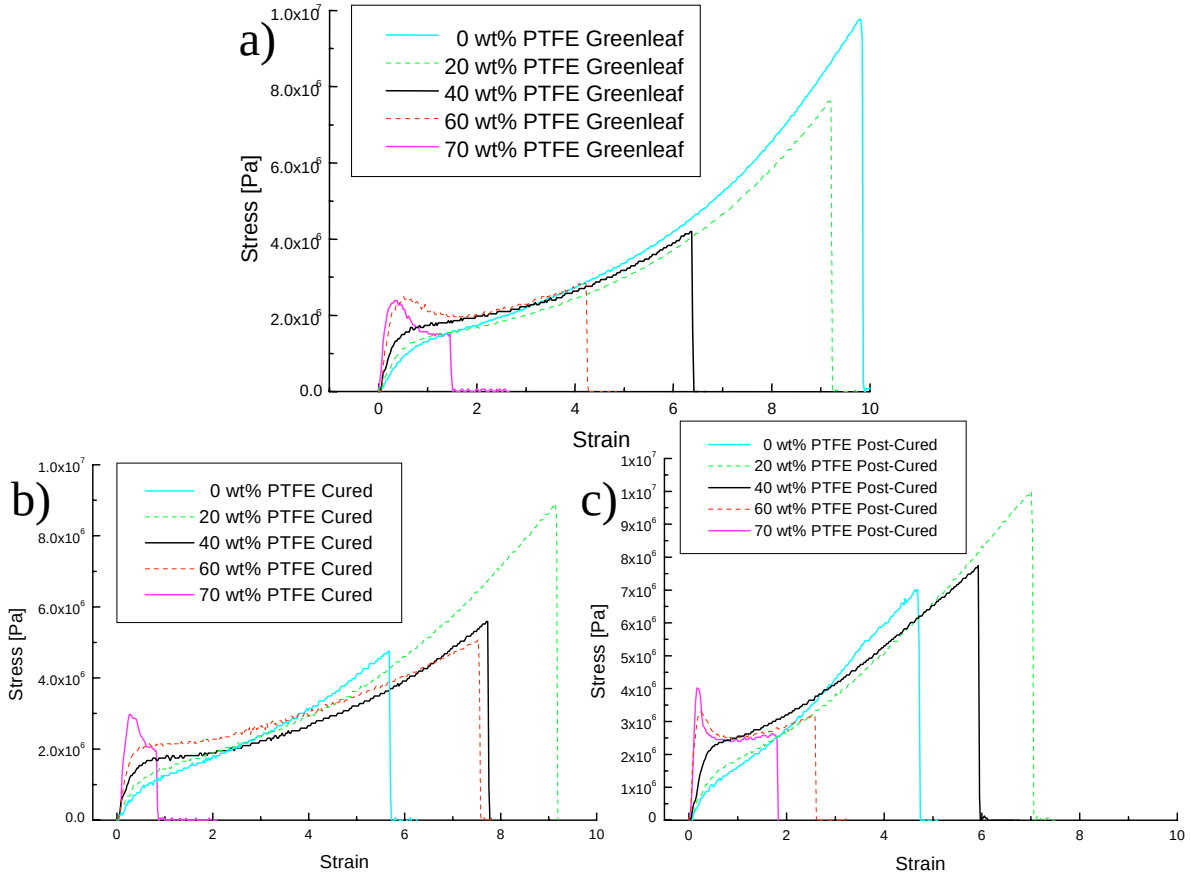

Figure 9.3 Room temperature stress-strain behavior comparing different levels of PTFE content for materials that are a) greenleaf, b) cured, and c) post-cured.

This mechanism appears to depend upon the interaction of the cross-linking with the level of PTFE content. Examining the variation of degree of cure at each level of PTFE content separately can facilitate discerning the nature of that mechanism. Figure 9.4a reveals that with no PTFE particulate present, the strain-at-break decreases systematically from 10 in the greenleaf film to 4.8 in the post-cured sample. Even with the lowest PTFE fraction studied, Fig. 9.4b suggests that adding 20 wt% PTFE has significantly altered the mechanical

behavior. Both the uncured and the cured films broke at the same strain (ca. 9.2), and the cured sample exhibited higher load bearing, breaking at a stress of 8.8 MPa compared to 7.5 MPa for the uncured film. The post-cured sample also exhibited higher load bearing at each strain, which must be a result of the higher level of cross-linking. Similar behavior can be observed in the 40 wt% PTFE material in Fig. 9.4c. *In summary, Figs. 9.4a-9.4c have shown that without PTFE particles, cross-linking results in breaking at lower strain levels; however, they have shown that adding PTFE particulate increases toughness by maintaining the strain-at-break while raising the load bearing.*

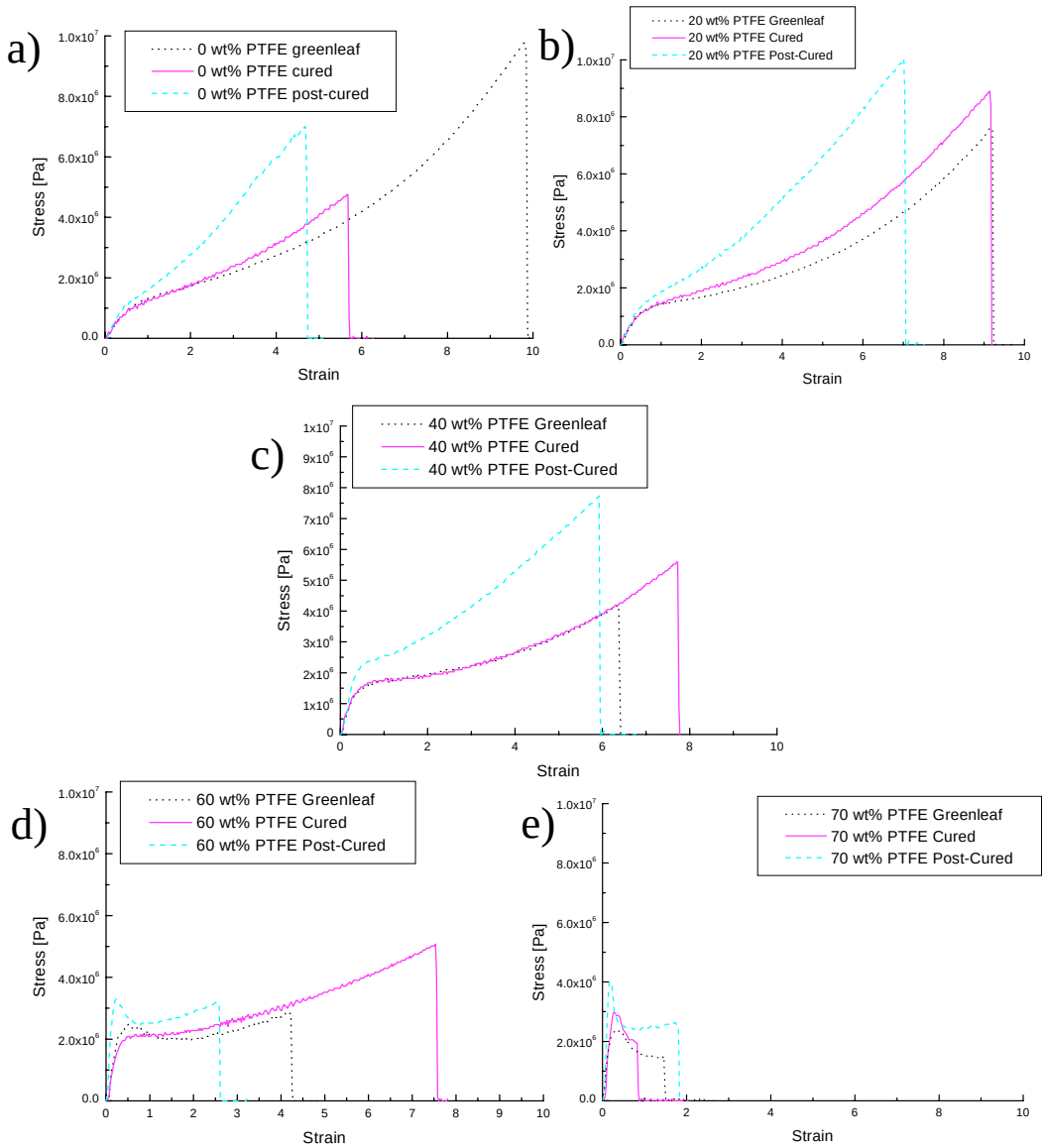

Figure 9.4 Room temp. stress-strain behavior comparing degree of cross-linking at each level of PTFE content: a) 0 wt%, b) 20 wt%, c) 40 wt%, d) 60 wt%, and e) 70 wt%.

The stress-strain behavior of the 40, 60, and 70 wt% PTFE cured and post-cured films demonstrate further that the draw or irrecoverable flow domain of the response curve, in addition to the subtle increase in load bearing, is substantially responsible for increases in toughness as the material is cross-linked. These data suggest two conclusions regarding the interaction of the PTFE content with the level of cross-linking. First, it suggests that, in the presence of cross-linking, enough stress is transferred to the PTFE particles to improve the toughness. This could occur either by distributing the stress more evenly throughout the material and/or by the PTFE undergoing a relaxation mechanism of its own. The other conclusion suggested by this stress-strain data is that without cross-linking, enough strain is not borne by the PTFE component to increase the toughness. In other words, it is hypothesized that, without cross-linking, the viscosity of the elastomer at room temperature is too low to transfer enough stress to the PTFE particles to increase the toughness.

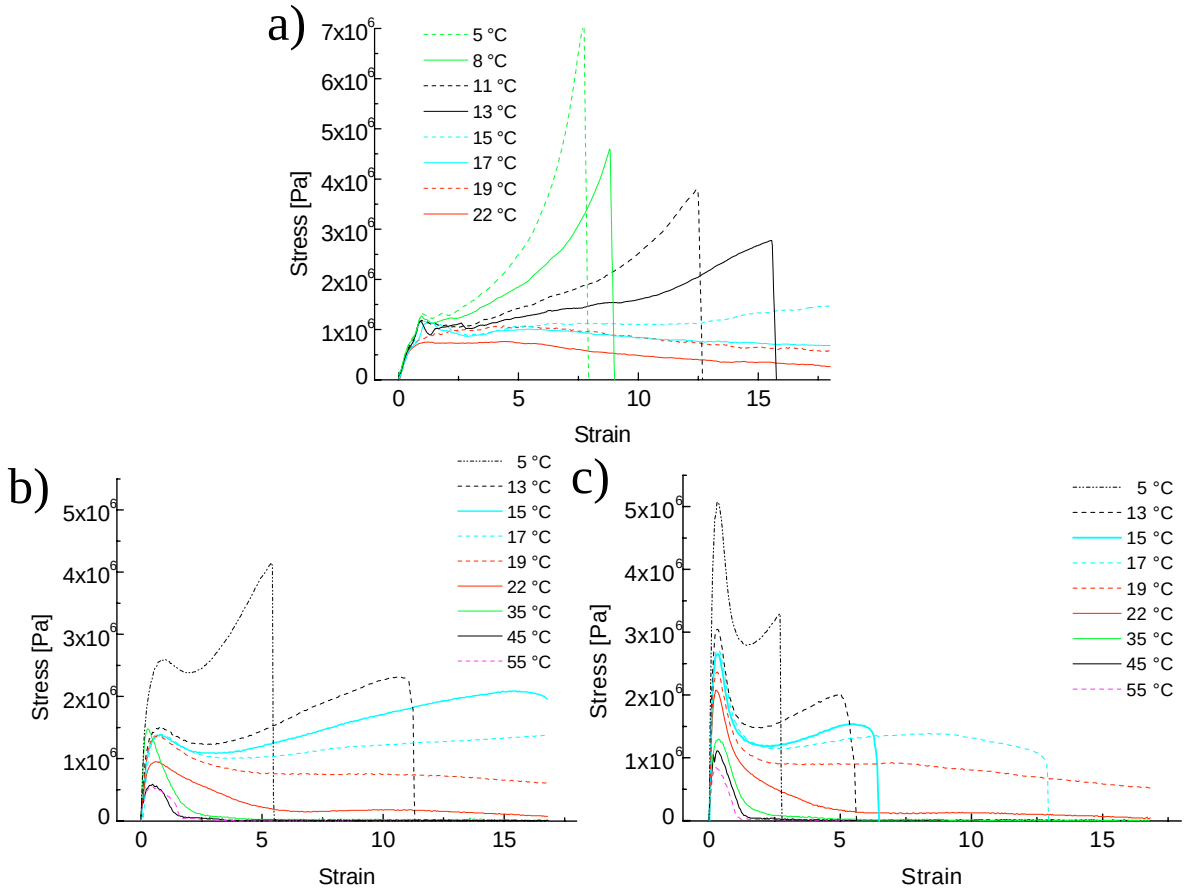

Figure 9.5 Thermal variation of the stress-strain behavior for the greenleaf materials. Stress-strain curves for a) 0 wt% PTFE, b) 40 wt% PTFE, and c) 60 wt% PTFE.

This hypothesis can be tested by examining the thermal dependence of the stress-strain behavior of greenleaf films. As can be seen above in the 0 wt% PTFE in Fig. 9.5a, the 40 wt% PTFE in Fig. 9.5b, and in the 60 wt% material in Fig. 9.5c, there is a strong influence of temperature on the response to deformation in the thermal range from 0-20°C. Because the glass transition of the FKM component occurs at ca. -10°C at 1 Hz in DMA testing, the viscosity of the FKM is understood to be changing rapidly in that range. At 5°C, the materials behave as ductile plastics, exhibiting distinct yield points and undergoing clear irrecoverable flow. As the temperature approaches 19°C, the materials are so extensible that the Instron could not extend far enough to stretch them to the breaking point. It is hypothesized that the high extensibility at these temperatures is augmented by the fact that the PTFE contained in the nascent crystals must have very few entanglements. Above 19°C, the FKM viscosity drops so much that the rapid stress relaxation in the films leads to breaking at systematically lower strain values.

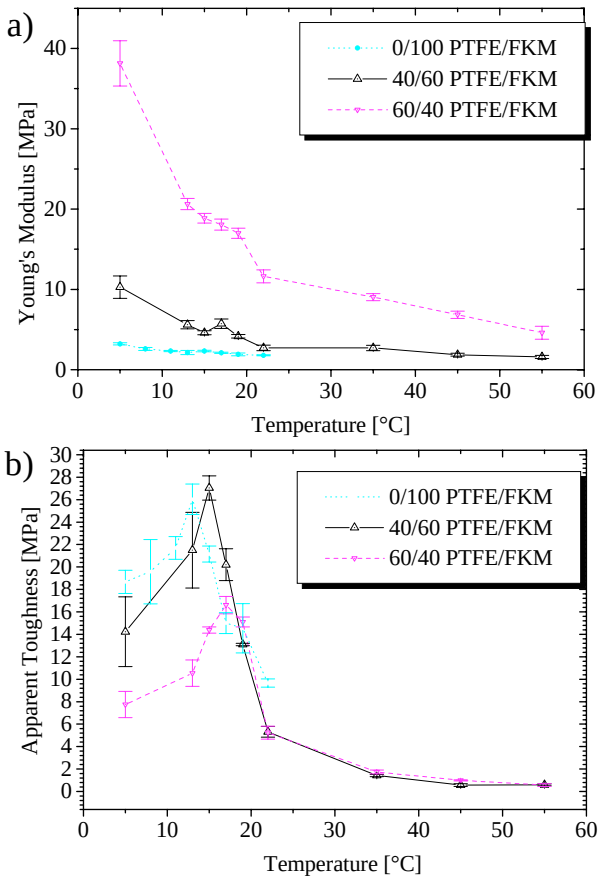

Figure 9.6 Summary of the thermal variation tensile tests: a) modulus and b) toughness.

The moduli data from these tests are summarized in Fig. 9.6a. This data again show the increase in modulus with increased PTFE content of the film, and it shows the clear increase in modulus as the temperature approaches the glass transition of the elastomeric matrix. For example, at 5°C the 60 wt% material has a modulus of ca. 38 MPa which is 3.6 times higher than the 10.5 MPa exhibited by the 40 wt% material. It is interesting that the increase in modulus due to PTFE content is somewhat dependent on the temperature. At 55°C, for example, the modulus of the 60 wt% material (ca. 4.5 MPa) is 3 times greater than that of the 40 wt% film (ca. 1.5 MPa). This may suggest improved transfer of stresses between the matrix and the PTFE at the lower temperatures. As the temperature is decreased, it also appears that the 60 wt% PTFE material undergoes a step jump in modulus at ca. 19°C, and it is hypothesized that this might occur as a result of the PTFE crystal transition which occurs at that temperature.[19] The toughness data from these experiments is exhibited in Fig. 9.6b, which shows, as Figs. 9.5a, 9.5b, and 9.5c suggested, that the materials have the greatest toughness in the thermal range of 13-19°C. The strong peak at 15°C in the 40 wt% PTFE films is suggested to be lower than the true peak as a result of the 17°C and 19°C materials not breaking in the Instron. The 60 wt% material indicates that the true peak in toughness occurs at ca. 19°C. Also, since the peak in toughness of the 0 wt% films occurs much lower, ca. 13°C, it appears that the peak occurs at 19°C due to the presence of the PTFE particulate and not the elastomer alone. Therefore, this toughness peak behavior is suggested to result from increasing the transfer of shearing forces from the elastomeric matrix to the PTFE particulate. *Furthermore, it is hypothesized that as the viscosity of the elastomer is modified by either cross-linking or thermal variation, more of the load is transferred to the PTFE component resulting in increased toughness.*

Although it is not a key part of this study, it was considered to be of interest to compare the modulus data for the greenleaf systems to the current theories of filled system behavior. Three approximations were applied: the Guth-Smallwood equation (Equation 9.1), the Kerner equation (Equation 9.2), and the Mooney equation (Equation 9.3).[15,16,17]

$$E = E_1\left[1 + k_E\phi_2 + 14.1\phi_2^2\right]$$ **[Equation 9.1 Guth-Smallwood Eqt.]**

$$E = E_1\left[1 + \frac{\phi_2}{\phi_1}\left(\frac{15(1-\nu_1)}{8-10\nu_1}\right)\right]$$ **[Equation 9.2 Kerner Eqt.]**

$$E = E_1 \exp\left[\frac{k_E\phi_2}{1-\frac{\phi_2}{\phi_M}}\right]$$ **[Equation 9.3 Mooney Eqt.]**

where E = observed modulus of the filled system
E_1= modulus of the matrix
k_E = Einstein's coefficient, 2.5 for well-dispersed, wetted spherical filler
ϕ_1, ϕ_2 = volume fractions of matrix and filler, respectively
ν_1 = Poisson's ratio of the matrix
ϕ_M = maximum filler vol. fraction: 1.0 is maximum, .714 fits most data

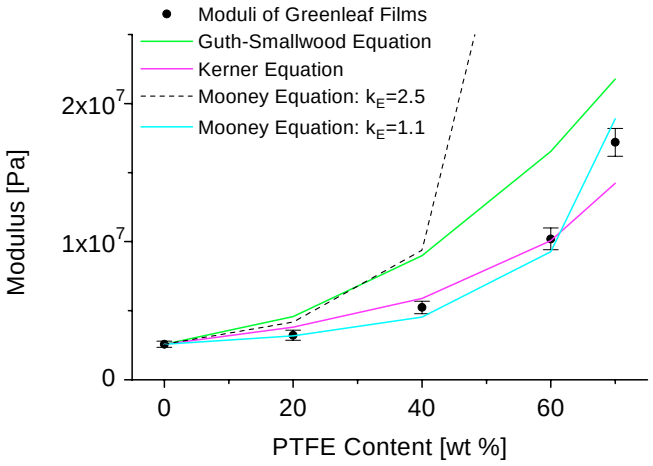

Figure 9.7 Comparison of the experimental data with various theories of filled materials

As shown in Fig. 9.7, the Kerner equation and the Mooney equation provided the best predictions for the action of the reinforcing PTFE. The quality of the fit of the Kerner equation suggests that its assumptions as applied here are valid. These assumptions are that Poisson's ratio of the matrix is 0.5 and that the PTFE particulate is much more rigid than the matrix. The Guth-Smallwood and the standard (i.e. k_E=2.5) Mooney equations show reasonable agreement below 20 wt%, as observed in many other systems,[15,17] but above that PTFE content, both over-predicted the moduli. This may indicate the limits of those

equations. It was found that the Mooney equation is not strongly dependent upon the value of ϕ_M used, but that it does vary significantly with k_E. The coefficient k_E in the Mooney equation is equal to 2.5 for well-dispersed particles; however, as shown in Fig. 9.7, when this is adjusted to 1.1 the equation fits very well. Since the assumption that k_E=2.5 is not valid, this may suggest that the PTFE is not functioning as a well-dispersed filler in the FKM matrix. An alternative hypothesis is that the PTFE does not have good adhesion to the matrix, thus voids may be developing as the film is deformed or the matrix may be flowing around the PTFE particles.

To further examine the thermal dependence of mechanical properties, these materials were tested using dynamic mechanical analysis (DMA). In Fig. 9.8a, the storage moduli of the greenleaf materials are compared at various levels of PTFE content. It can be seen that in the glassy state, below -25°C, the moduli are fairly close for the different samples, but even there it can be observed that the higher PTFE content films have higher storage moduli. It can also be seen in Fig. 9.8a that the onset of the glass transition, ca. -5°C, systematically occurs at somewhat higher temperatures for each higher level of PTFE content. However, no variation in the location of the tanδ peak was observed, as shown in Fig. 9.8b. As was observed with the tensile testing, the storage modulus systematically increases with each higher level of PTFE content above the FKM glass transition at ca. -5°C. Between 100 and 350°C, a reasonably flat, rubbery plateau is observed wherein the highest levels of PTFE content are easily distinguished as exhibiting the highest storage moduli. Between 50-100°C, a shoulder can be observed in the storage moduli curves of Fig. 9.8a, and this relaxation is hypothesized to result from the vaporization of water from the FKM component. This hypothesis is supported by the observation that the shoulder does not occur in the cured or the post-cured materials, as shown in Figs. 9.8c and 9.8e.

This hypothesis is also supported by the tanδ behavior shown in Figs. 9.8b, 9.8d, and 9.8f. These show that the broad transition that begins at 50°C reaches its maximum at 100°C. It may also be observed that the transition does not occur in the tanδ plots of the cured and post-cured materials. Although the softness of the low PTFE content films resulted in “noisy” high temperature tanδ data, the 60 and 70 wt% PTFE are smooth enough to show clearly the reality of this broad transition. Figure 9.8b also shows more clearly than Fig. 9.8a that the glass transition region steadily becomes broader as PTFE particulate is added. This suggests

that adding the filler widens the range of molecular mobilities in the material. These figures reveal, however, that the shift to higher temperatures of the FKM glass transition is minor compared to the dramatic change in the magnitude of the tanδ peak. As PTFE is added, the peak is systematically reduced from 1.4 at 0 wt% PTFE to 0.4 at 70 wt% PTFE. This behavior correlates well with the reduction in material in the film that is undergoing its glass transition at that temperature.

The cured and post-cured materials show many similar trends observed in the greenleaf films. The storage moduli are presented in Figs. 9.8c and 9.8e, and the tanδ curves are presented in Figs. 9.8d and 9.8f. One difference between these and the greenleaf films is the narrowness of the FKM glass transition in the 0 wt% PTFE cured and post-cured materials observed in Figs. 9.8c and 9.8e. It can be observed there that the flat rubbery plateau is reached at ca. 0°C, instead of 150°C as in the greenleaf film. It is hypothesized that the greenleaf materials would have a similar distinctness to their glass transitions if they could be adequately dried without cross-linking. Similar to the greenleaf films, Figs. 9.8c and 9.8e show that increasing the PTFE content systematically increases the storage moduli in the rubbery region. For example, increasing the PTFE content from 0 to 70 wt% at ca. 100°C increases the storage modulus from ca. 5 MPa to ca. 20 MPa in the post-cured films. In terms of altering the character of the thermal spectrum of the storage modulus, however, the most significant effect of adding the PTFE is the broadening of the glass transition at ca. -5°C. The relaxation becomes consistently more indistinct as the PTFE component is increased until a truly flat rubbery plateau can not even be identified in the 60 and 70 wt% PTFE post-cured films, as compared to the 0 wt% PTFE films. Also, in comparing Figs. 9.8c and 9.8e, it may be observed that in the 200-350°C range the level of PTFE content only increases the storage modulus in the post-cured materials. Finally, it can be noticed in all of the storage moduli data that as the PTFE fraction of the composition is increased a distinct relaxation occurs at ca. 350°C, and this corresponds to the melt temperature of the PTFE. This is an important observation, because it is one strong piece of evidence which shows that the PTFE particulate contributes in a significant way to the properties of the film.

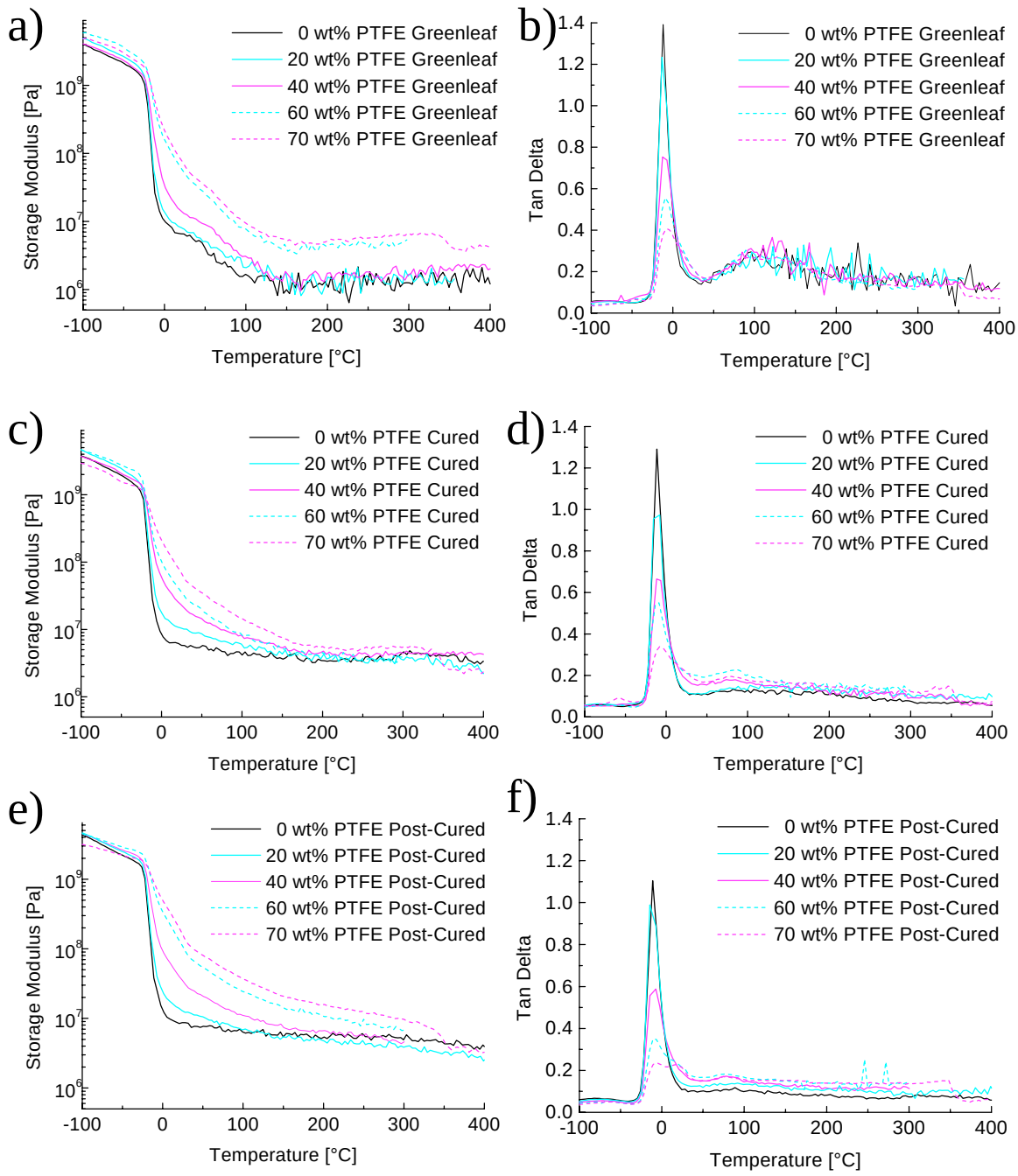

Figure 9.8 Influence of PTFE wt% on the Dynamic Mechanical Analysis results: a) storage moduli and b) tanδ curves of greenleaf materials; a) storage moduli and b) tanδ curves of cured materials; and a) storage moduli and b) tanδ curves of post-cured materials

The tanδ behavior of the cured and post-cured films, as a function of PTFE content, was similar to that of the greenleaf materials except for the lack of the 100°C peak. As PTFE content is increased, the systematic decrease in the magnitude of the glass transition peak can be observed in both the cured and post-cured materials. The broadening of the glass transition is also clear. Adding cross-linking apparently increases the modulus enough that the more cured materials exhibit much less "noise" at high temperature than the greenleaf films do. Comparing the 60 or 70 wt % PTFE greenleaf films to any of the cured or postcured films makes it clear that the ca. 100°C peak only occurs in the greenleaf materials. An interesting observation is that a minor peak appears in the tanδ curves of the 60 and 70 wt% PTFE films at ca. 80°C. It is especially clear in the post-cured films of Fig. 9.8f that this peak only occurs at high PTFE content, suggesting that, just as with the PTFE melting peak at 350°C, this relaxation is occurring only in the PTFE phase of the film. This is corroborated by studies on pure PTFE which have shown that a beta relaxation peak occurs at ca. 100°C for highly crystalline PTFE materials.[18]

One other interesting observation from the tanδ behavior occurs in the post-cured 70 wt% sample (Fig. 9.8f), which shows that the glass transition peak has broadened so much that it has formed two distinct peaks, one located at ca. -5°C and one at ca. 17°C. This bimodal behavior is hypothesized to be observed as a result of cross-linking at higher PTFE content. It is hypothesized that the -5°C peak occurs because of relaxation in the fluoroelastomer and that the 17°C peak occurs due to the first-order crystalline transition in the PTFE which is widely known to occur at 19°C.[1,2,3,7,11,12,19] This can also be corroborated by a beta transition peak observed at ca. 20°C in pure PTFE by other workers.[18] That there are two distinct peaks becomes evident due to the interaction of the cross-linking and the increased PTFE content. As the cross-linking is increased, FKM molecular mobility is decreased which leads to reductions in the magnitude of the glass transitions peaks. As the PTFE content is increased, the magnitude of the peak resulting from its crystalline transition becomes stronger. These two opposing trends act to make clear that what appears in the greenleaf materials to be only a broadening is actually the convolution of two discrete relaxations.

PTFE content effects on the influence of cross-linking on the mechanical properties can be more clearly seen in Figure 9.9. Figures 9.9a and 9.9b are the storage moduli and tanδ curves for the 0 wt% PTFE films, Figures 9.9c and 9.9d are the results for the 40 wt% PTFE films, and data from the 70 wt% films are shown in Figures 9.9e and 9.9f. The data for the 20 and 60 wt% films are not presented because they exhibited the same trends shown by the other compositions. It can be clearly observed in the storage modulus graphs of Figure 9.9 that all the greenleaf films exhibit a distinct shoulder beginning at ca. 25-50°C which, as discussed earlier, correlates well with the broad transition observed in the tanδ plots at ca. 50-150°C and is thought to originate in the vaporization of water which remains from casting the film.

As shown earlier with the tensile testing, the storage moduli plots also show that the cross-linking increases the storage modulus. When compared at 150°C to avoid the peak caused by the vaporization of water, it is clear that cross-linking leads to higher modulus. For example, heating a 0 wt% PTFE film from greenleaf to the post-cured state increases its storage modulus from ca. 1 MPa to ca. 6 MPa. Heating a 70 wt% PTFE film from greenleaf to the post-cured state increases its storage modulus from ca. 6 MPa to ca. 20 MPa. While these increases in modulus are clearly due to decreasing molecular weight between cross-links, except for the 100°C peak shoulder due to water vaporization, it does not appear that curing significantly alters molecular mobility as observed in the width of the FKM glass transition. The tanδ behavior in Figs. 9.9b, 9.9d, and 9.9f all show that for a given level of PTFE content, the width of the FKM glass transition tanδ peak is constant over these levels of cross-linking. Also the peak height observed in Fig. 9.9b does not vary greatly when compared to the effect of adding filler. This indicates that the cross-linking has not greatly altered the molecular mobility in these films, suggesting that they are not highly cross-linked even after post-curing. This indicates that the much of the broadening of the glass transition observed in Figs. 9.9c and 9.9e are due to the PTFE component and not the cross-linking alone. Thus, at 70 wt% in Fig. 9.9e, it can be observed even in the greenleaf films the FKM glass transition is so broad that the rubbery plateau does not become truly flat until ca. 200°C. Figure 9.9f further clarifies the interaction of the -5 and 17°C transitions. In the greenleaf film, it appears to be a single relaxation. However, as the -5°C peak height is reduced by restricting molecular mobility through cross-linking, the 17°C peak height does not change at

all and so becomes distinguishable. It is hypothesized that the 17°C and 80°C peaks of the PTFE component[3] result in the broadening of the glass transition as observed by the storage moduli curves.

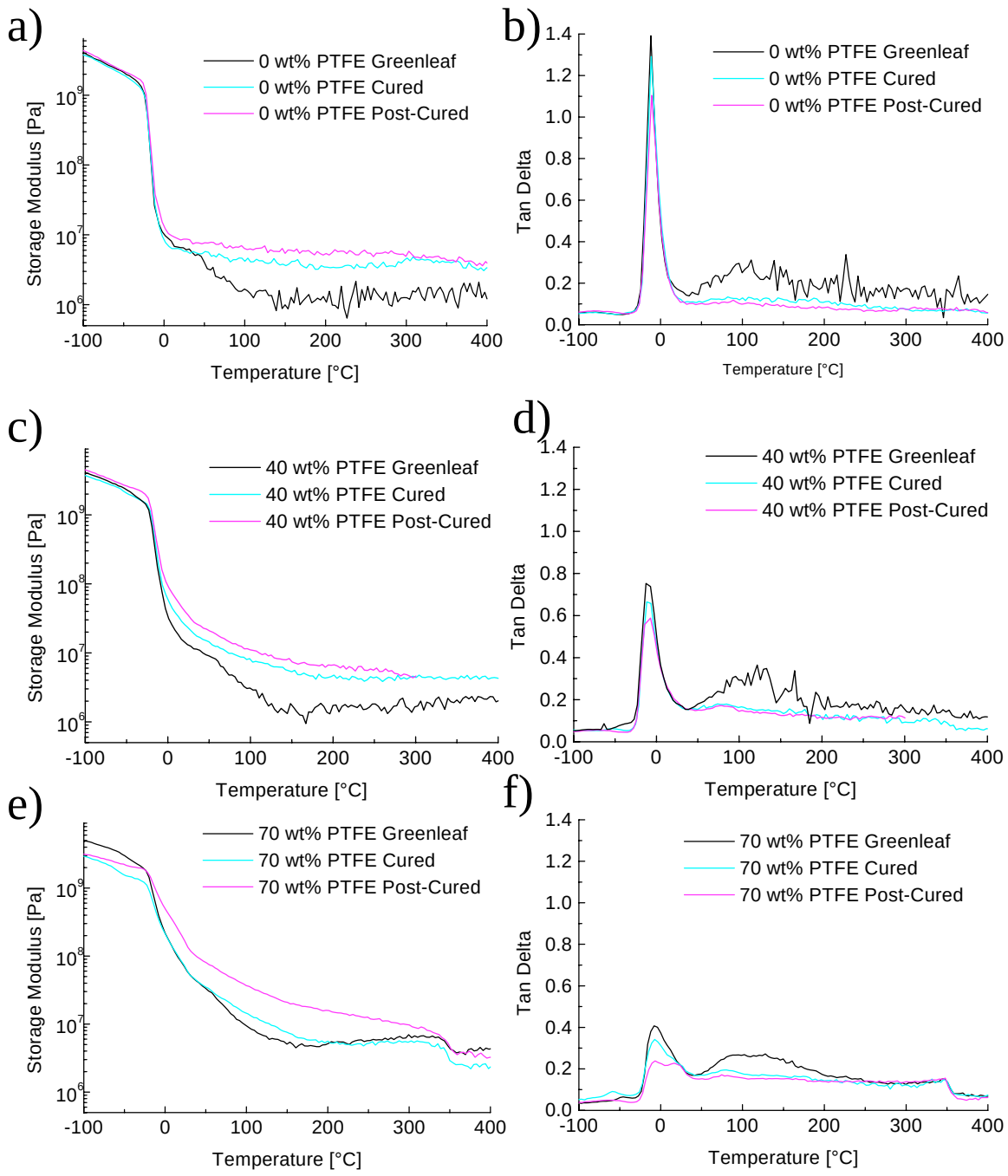

Figure 9.9 Influence of cross-linking on the Dynamic Mechanical Analysis results: a) storage moduli and b) tanδ curves of 0 wt% PTFE films; a) storage moduli and b) tanδ curves of 40 wt% PTFE films; and a) storage moduli and b) tanδ curves of 70 wt% PTFE films.

9.4.2 Property Dependence on Raw Material Sources

Because different manufactures use different formulations and processing techniques, variation of supplier does lead to significant property changes.[6] For example, as shown in Figure 9.10a, the FKM B has a consistently higher storage modulus than the FKM A for every state of cure tested. This corresponds well with the results of other workers[6] who observed that the pure FKM B exhibited higher tensile strength and modulus than the pure FKM A. Also, as shown in Figure 9.10b, the tanδ peaks for the FKM B material are also systematically lower than those of the FKM A. This suggests lower molecular mobility in the FKM B elastomer which must be a result of altering the composition of the terpolymer as shown in Table 9.2. However, lacking a systematic study based on terpolymer composition variation, it is impossible to conclude whether the higher storage moduli of the FKM B results mainly from increasing the TFE component, decreasing the VF_2, reducing the HFP, or variation in molecular weight distribution.

Since the FKM forms the continuous matrix, it is possible that the differences observed in Figs. 9.10c-9.10h are mainly due to changes in the elastomer. Thus, as shown in Fig. 9.10c, the higher storage moduli of the PTFE 2 / FKM B films might be due to the FKM B component. This suggests that the higher dynamic moduli of the PTFE 3 / FKM C and PTFE 3 / FKM D could result from the composition differences between FKM A, FKM C, and FKM D elastomers. However, as shown in Table 9.2, FKM C has the lowest TFE content of the known FKM materials.

These results do not include the possibility of variation in the PTFE dispersions. Differences in the particle sizes of filler components could result in significant variation in the mechanical properties of the cast blends. Also, variation in particle size and PTFE molecular weight might change the mechanical treatments required to induce PTFE fibrillation. It should be clear from this discussion that a more systematic approach is needed to characterize the significant effects of alterations in the PTFE and FKM components.

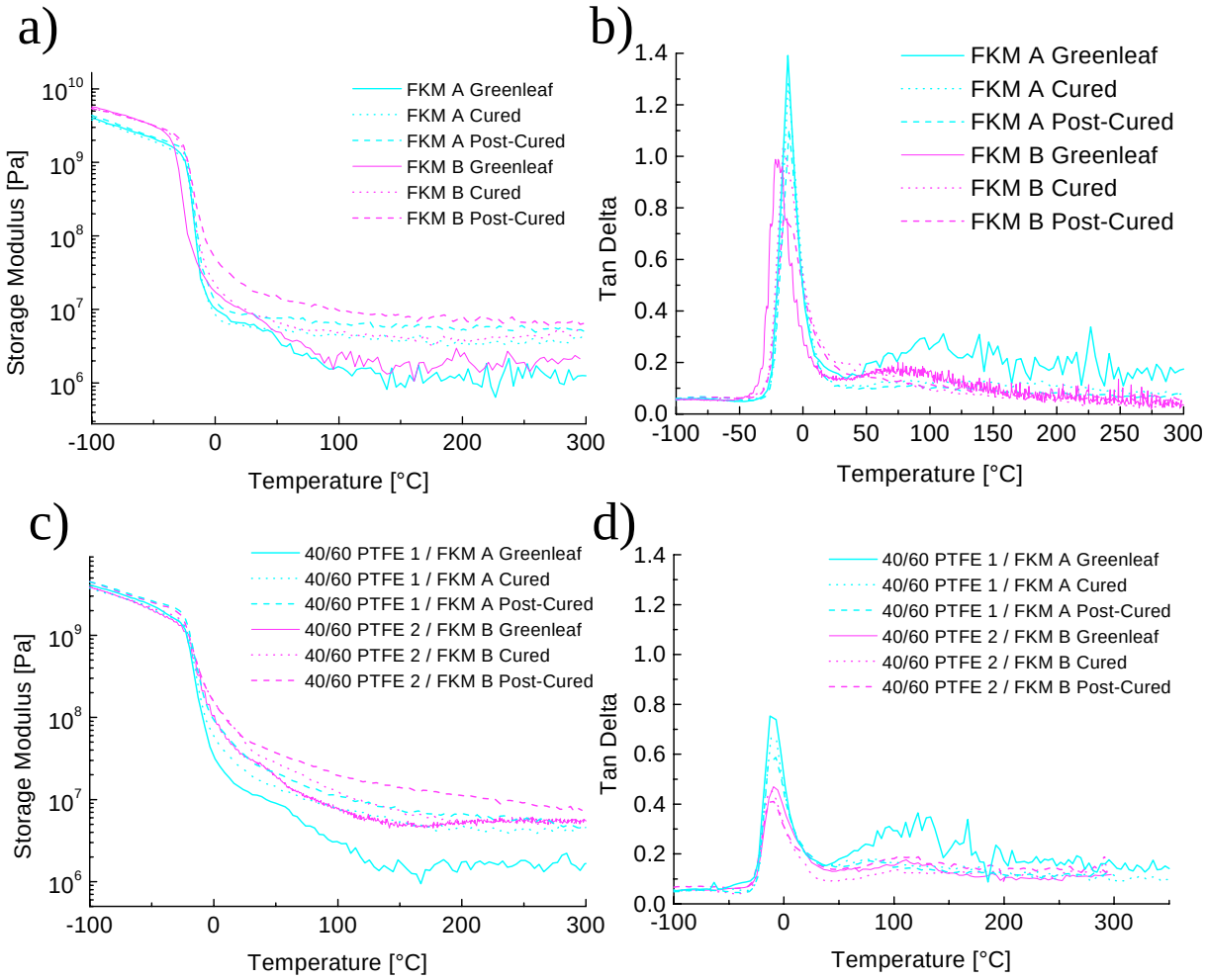

Figure 9.10 Mechanical property variation due to changes in altering FKM or PTFE component. Comparison of:
a) storage moduli and b) tanδ curves of 0 wt% PTFE films of FKM A and FKM B;
c) storage moduli and d) tanδ curves of 40 wt% PTFE films based on PTFE 1 / FKM A and PTFE 2 / FKM B;

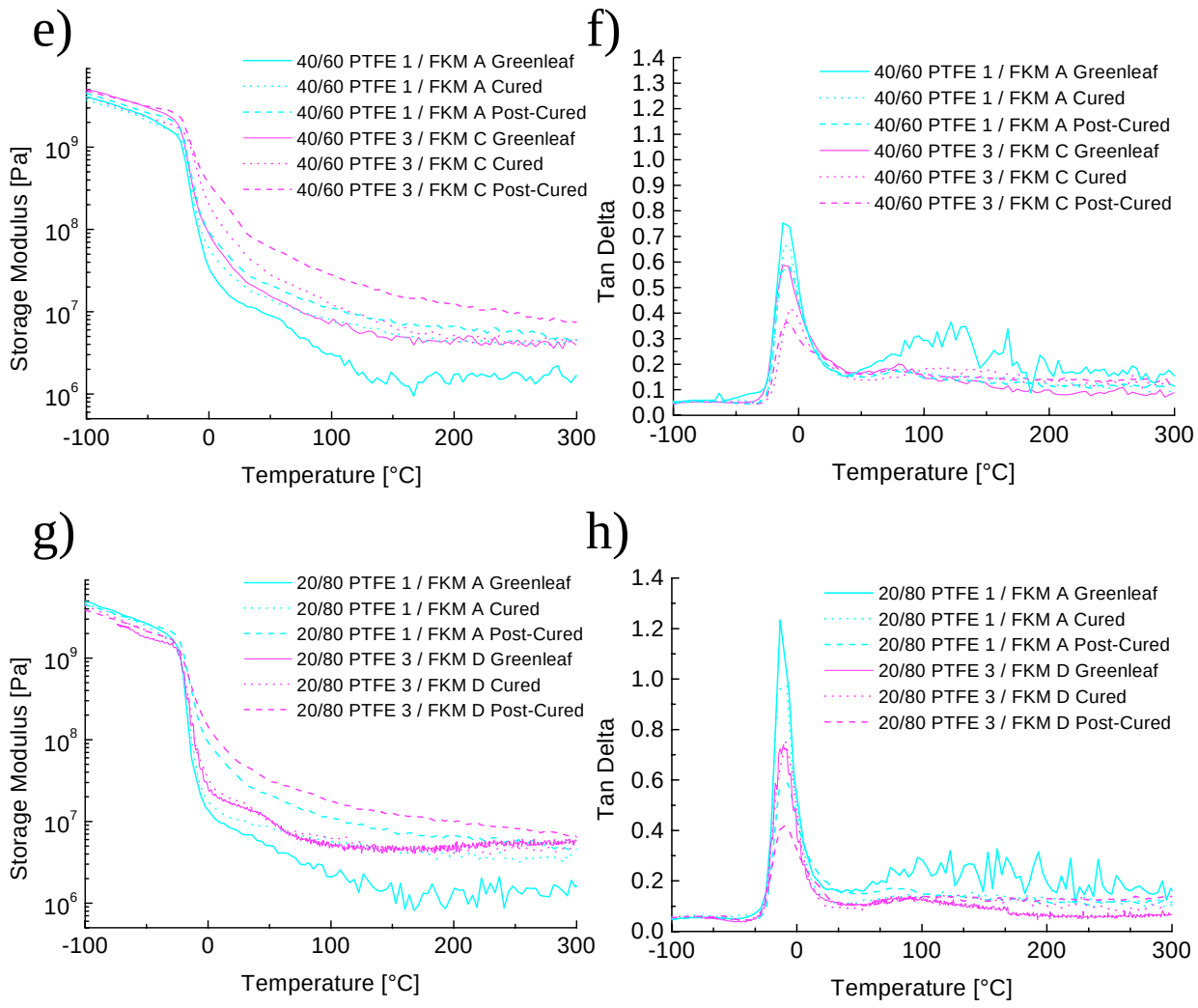

Figure 9.10 Mechanical property variation due to changes in altering FKM or PTFE component. Comparison of:
d) storage moduli and e) tanδ curves of 40 wt% PTFE films based on PTFE 1 / FKM A and PTFE 3 / FKM C; and
g) storage moduli and h) tanδ curves of 20 wt% PTFE films based on PTFE 1 / FKM A and PTFE 3 / FKM D.

9.4.3 Polymer Morphology

Characterization of the solid state was performed with solvent extraction, atomic force microscopy (AFM), transmission electron microscopy (TEM), and wide angle x-ray scattering (WAXS). Small angle x-ray scattering (SAXS) was attempted, however, no peaks were observed even in the 70 wt% PTFE materials. It is hypothesized that the nascent crystallinity of the PTFE in these materials may be in a form which does not induce x-ray scatter in the small angle region.[18,20]

Solvent extraction was performed to characterize the formation of covalent cross-links during the curing and post-curing steps. The samples were kept in boiling solvent until the greenleaf materials were as dissolved as possible; however, none of the greenleaf films tested was completely soluble. As shown in the data of Fig. 9.11, ca. 95% of the greenleaf material was extractable indicating that a three dimensional covalent network has not formed due to heating in the drying steps of the film production. After curing, ca. 79% of the films were extractable. This is a relatively small change and it suggests little of the material is bound into a covalent network. The post-curing steps resulted in substantially more cross-linking, as only ca. 42% of the material was extractable. These results correspond well with the mechanical behavior, in that little change occurs as a result of the curing step but that the post-cure induces significant levels of cross-linking.

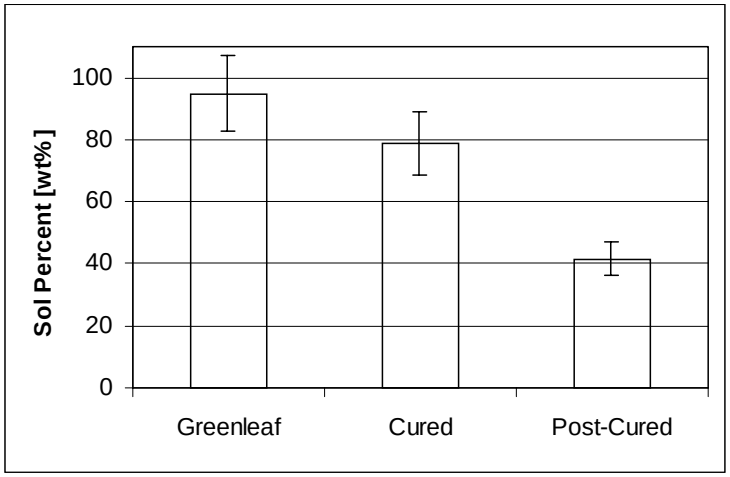

Figure 9.11 Degree of covalent cross-linking characterized by solvent extraction where sol percent represents the weight percent of extractable material.

TEM provides a 2-D projection of a ca. 70-110 nm thick cross-section of the film. Using TEM to characterize these materials presented one large difficulty in that the PTFE

particulate rapidly undergo a reaction upon exposure to the electron beam. As can be seen in Fig. 9.12a, upon initial viewing the 0.2 μm PTFE particulate appear darker than the elastomer indicating higher electron density than the matrix, which is expected given the high crystallinity of the PTFE. Within 5-15 seconds, however, all of the particulate in the matrix turn white indicating some interaction with the electron beam. It is hypothesized that this change may be due to chain scission and degradation caused by the electron beam, as has been noted in PTFE by other workers.[21,22] Because this interaction could lead to changes in morphology and size, it is worthwhile to compare the 40 wt% film of Fig. 9.12a with Fig. 9.12b which was taken after allowing the cross-section to stabilize in the beam. The PTFE particulate in Fig. 9.12b are white and the elastomer is gray. In both images, the smallest particulate appear to be ca. 0.2 μm, but they both contain some larger particles of ca. 1 μm in size. These white micron-sized particles that can be observed in Figs. 9.12a and 9.12b will be further discussed below. The beam damage occurred too quickly to collect micrographs at higher (at or above ca. 10,500 X) magnification. However, by focusing on one place and then moving to an adjacent area another and collecting immediately, it was possible to observe the morphology at ca. 3,300 X before it changed. Magnifying from the negative provides the closer views shown of a 60 wt% calendered film in Fig. 9.12c and 9.12d. Fig. 9.12c is the micrograph collected initially, and it may be seen that the black PTFE particles have a much higher electron density than the white FKM matrix. Also it may be noted that, prior to the onset of beam damage, the particles appear to be aggregated and to exhibit some connectivity. This correlates well with the stress-strain behavior of Fig. 9.2. Fig. 9.12d was collected ca. 15 seconds later, and it may be seen that the beam damage has significantly altered the morphology. The FKM appears darker, and the PTFE particles appear smaller and whiter. This indicates that the PTFE has lost electron density. Also, even in this incompletely damaged sample, the particles appear less aggregated and interconnected. These changes suggest that detecting alteration in polymer morphology requires collection and analysis of micrographs of the cross-sections prior to the onset of beam damage.

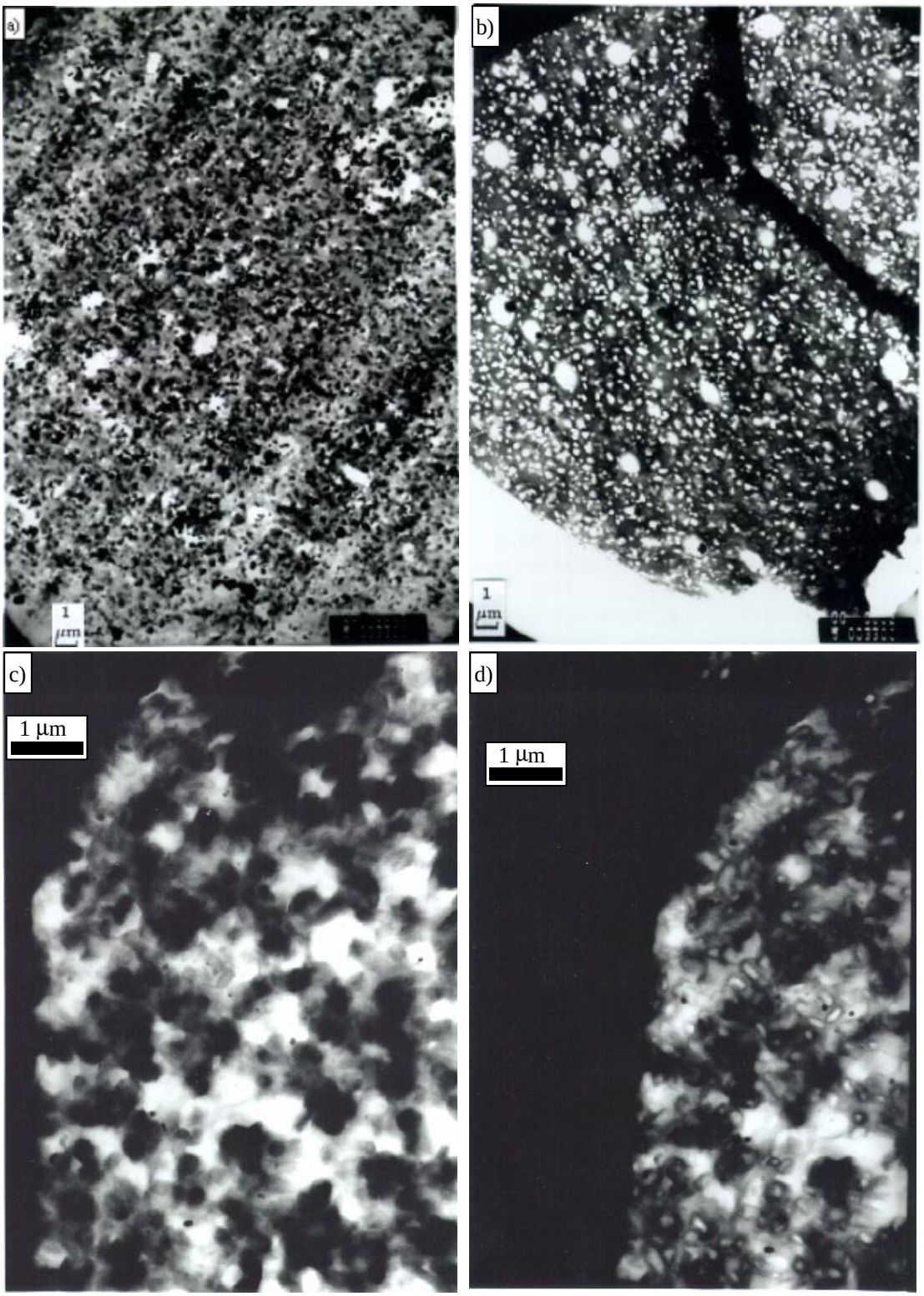

Figure 9.12 TEM micrgraphs showing the development of beam damage: a) and b) in as-cast greenleaf films containing 40 wt% PTFE; and c) and d) showing the same area of a 60 wt% PTFE calendered film.

As Fig. 9.12b has shown, the 40 wt% PTFE material can be generally characterized as an elastomeric matrix containing evenly dispersed sub-micron particulate (ca. 0.2 μm). However, some irregularly shaped, 0.1-0.5 μm sized, black particles can be seen in that micrograph, and these were found to probably be inorganic materials by their electron diffraction patterns. Finding an exact source for these particles was not pursued as they appeared to be a relatively minor part of the composition. Therefore, although these irregularly shaped particles occurred in all of the samples examined, they will not be discussed in the many subsequent micrographs in which they appear. Another occasionally occurring structure in the polymer are larger ca. 1 μm particles. As shown in Fig. 9.12b, they are frequently spheroidal; however, as can be observed in Fig. 9.12a, they can also be somewhat irregular in shape. Whenever these large particles appear, it is worth noting that they were always observed to be white prior to the onset of beam damage (as in Fig. 9.12a). This indicates low initial electron density. Two hypotheses might explain these larger particles. Either they are PTFE particles of low crystallinity, or they are some non-PTFE material. They were not observed in every sample, and they occurred with varying frequency. One possibility is that these particles are epoxy which as filled voids in the sample as has been observed in other materials. This hypothesis finds some support in Fig. 9.12b which shows that they have the same contrast as the epoxy seen in the lower left corner of the micrograph. Small voids do exist in these films as may be shown by their dramatic expansion under vacuum. Because of their irregular occurrence and their unknown origin, the remaining TEM analysis will focus on the dispersion of ca. 0.2 μm PTFE particulate.

Since TEM will be used to investigate morphological changes after calendering and otherwise deforming the films, it is important to fully characterize the structure near the surface. Fig. 9.13 is a high magnification view of the epoxy/film interface of the non-deformed 40 wt% PTFE film. It can be observed in this micrograph that there are some smaller, ca. 100 nm PTFE particulate also in the elastomeric matrix which were difficult to distinguish in the lower magnifications views. It is also interesting to see that even at this high magnification some association of the smaller particulate can be observed as indicated by the arrow in Fig. 9.13. The most important thing to note from Fig. 9.13 are the PTFE particulate which are in the epoxy near the interface. Apparently, when encased in epoxy, the PTFE is sufficiently shielded from the electron beam that it undergoes little if any change,

and, even after the rest of the PTFE particulate have interacted with the electron beam, they continue to appear as dark particulate in the epoxy. This observation will greatly aid in the characterization of the deformed films in a later section.

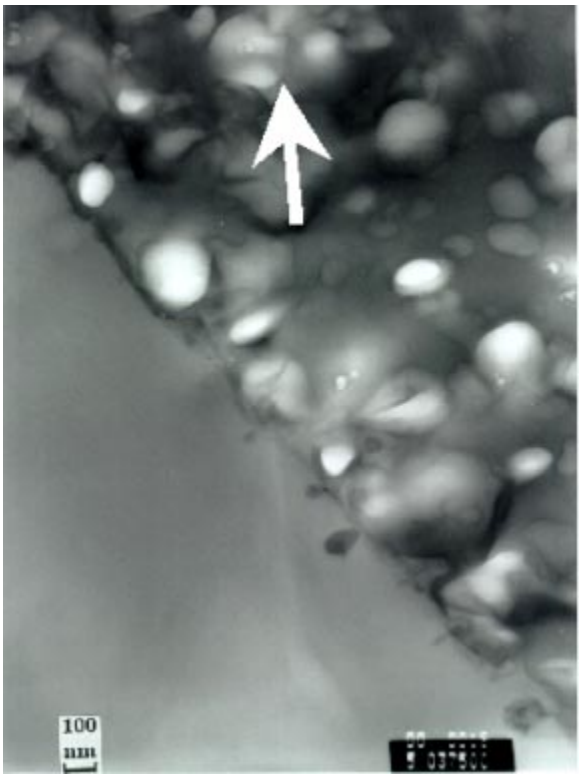

Figure 9.13 High magnification view of epoxy/film interface for the 40 wt% film. Arrow indicates aggregate of ca. 0.2 μm PTFE particles.

The four micrographs of Fig. 9.14 examine the morphology of as-cast films as a function of PTFE content. Figures 9.14a and 9.14b show that at 20 wt% PTFE, the particulate are not evenly dispersed but show some ca. 1-2 μm clusters of discrete particles that are separated by ca. 1 μm relatively PTFE poor regions. Also, Figs. 9.14 a and 9.14b are the first micrographs in which particle "pull-out" may be observed as indicated by the arrows. This is an artifact which occurs when the knife comes to a particle much thicker than the ca. 70-100 nm thick section it is cutting. Rather than cut, the particle merely pulls out of the section leaving a hole. This frequently occurs in composite materials where there is no significant bonding between the matrix and the filler.

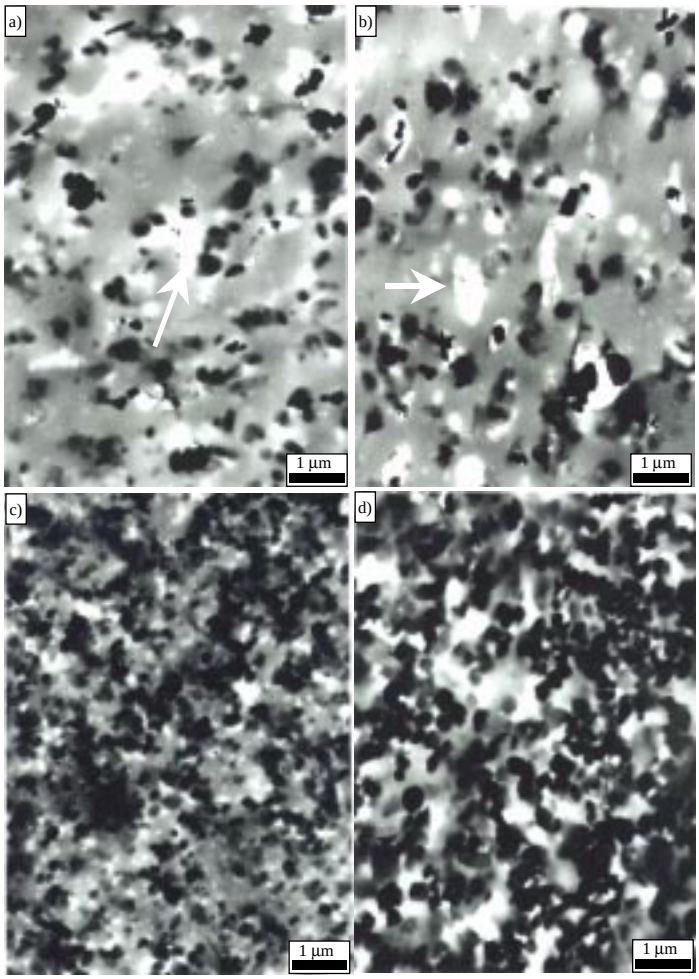

Figure 9.14 TEM micrographs of as-cast greenleaf films containing a) and b) 20 wt% PTFE; c) 40 wt% PTFE; and d) 60 wt% PTFE. White arrows indicate pull-out artifacts.

Figures 9.14c and 9.14d show the morphology of films with 40 wt% and 60 wt% PTFE, respectively. It should be noted that the section is somewhat thicker in Fig. 9.14c resulting in the appearance of more PTFE particles. The tendency of the PTFE particles to form clusters may be observed in all of the micrographs. The difference between the samples appears to be the frequency of the PTFE poor domains. As the weight percent of PTFE is increased, space filling considerations reduce the distance between PTFE particle clusters. Thus, the 60 wt% PTFE film of Fig. 9.14d exhibits the most even distribution of PTFE particles.

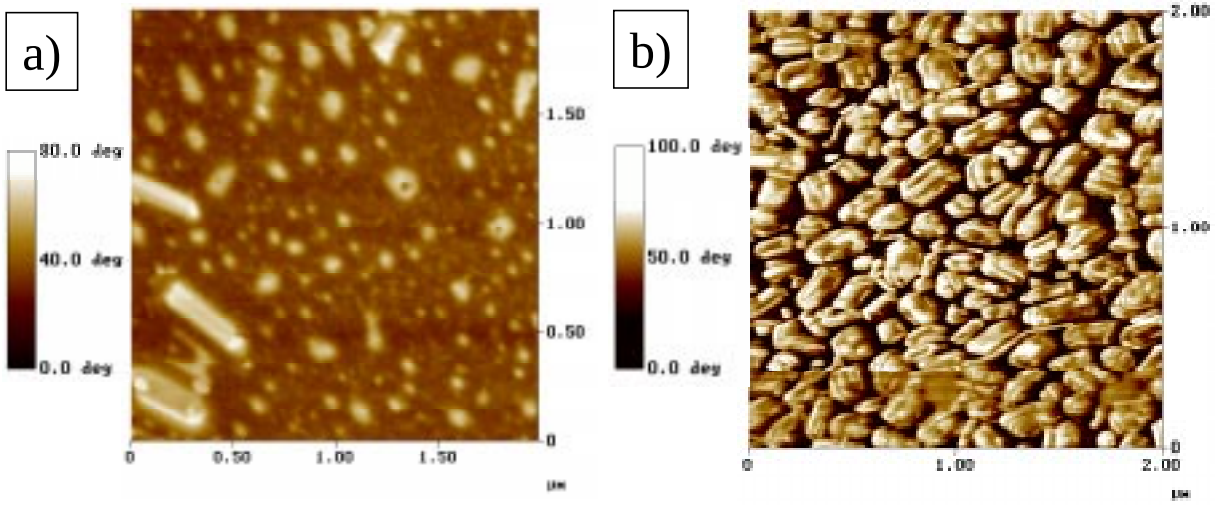

Figure 9.15 Phase images from atomic force microscopy: a) of the carrier film side of a 20 wt% PTFE film; and b) of the carrier side of an 80 wt% PTFE film.

When compared to the experimental challenges of TEM, tapping-mode AFM is a technique that is ideal for studying the morphology of thin films that lays in the plane of the film surface. Therefore, in order to utilize AFM in the later section on PTFE fibrillation, it is useful to document the morphology observed in non-deformed or as-cast films. Phase imaging with AFM is based on tracking phase offsets or differences between the drive oscillation to the cantilever probe and the actual oscillation of the cantilever tip as it interacts with the surface of the sample. At typical drive amplitudes, harder material induces higher phase offsets which are shown as white in the phase images. Thus, as shown in Fig. 9.15a, PTFE particulate are shown as white corresponding to high phase offsets, and the elastomer appears as a moderate phase offset. In the non-deformed samples, these micrographs showed great similarity to the results from TEM. As can be seen in Fig. 9.15a, at 20 wt% PTFE, particulate be seen to be dispersed in the FKM matrix. Unlike the TEM micrographs, Fig. 9.15a does not reveal structure larger than ca. 0.3 microns. However, because AFM only reveals structure to a depth of ca. 10 nm, it is not expected that large particles would be fully visible unless they are oriented near to parallel with the film surface. Fig. 9.15b is a phase image of an 80 wt% PTFE film, and it provides further confidence in this technique in that the same type and size of particulate are observed as in Fig. 9.15a. Also occasionally observed are some fibril structures ca. 0.05 microns across and ca. 0.1-0.6 microns long. As this was representative of the film surface, it is unclear whether small amounts of fibrillation occur at

high PTFE content during the normal casting process or whether this was induced by the handling which occurred as the film was removed from the carrier.

Another technique which will prove useful in studying PTFE fibrillation is wide angle x-ray scattering (WAXS). Because well defined reflections in wide angle x-ray scattering result solely from crystalline domains, the distinct rings in the WAXS patterns observed in these films must result from the PTFE component. This means that the integrated scattering intensity as measured with a diffractometer could be used to exactly characterize the PTFE weight fraction in a film sample. Or, as will be used in this study, WAXS can be utilized to provide information regarding the orientation behavior of the PTFE crystals. These measurements may be made by either using data collected from the film of a Warhus camera or from carefully performed diffractometer experiments.[23]

In the crystalline domains at room temperature and ambient pressure, PTFE molecules arrange in a hexagonal unit cell which is frequently referred to as Phase IV.[24] In this phase, the chain exists in a 15/7 helix with a repeat distance of 19.5 Å, and the chain axes are 5.66 Å.[3,7,25] As has been well documented in the literature, a first-order crystalline transition at 19°C transforms the PTFE unit cell into the triclinic unit cell as the molecule rearranges into a 13/6 helix.[7,25,26] This low temperature state is often termed Phase II. Another transition at ca. 30°C occurs and the PTFE crystal forms what is usually referred to as Phase I. The molecules in this high temperature phase are still arranged in a hexagonal packing; however, reflections of true hexagonal unit cells which are observed between 19 and 30°C disappear at higher temperatures.[7] Workers have suggested that this is due to irregular twists in the molecule.[2,7] Ambient conditions are convenient for using WAXS to estimate crystalline orientation because the symmetry of the hexagonal structure only requires the measurement of a single azimuthal angle.

For example, the WAXS pattern observed in Fig. 9.16a is of an non-oriented 70 wt% PTFE greenleaf film, and it shows one intense ring which is isotropic in intensity with respect to the azimuthal angle. This lack of azimuthal dependence indicates no crystalline orientation as detectable via WAXS. The (100) plane of the PTFE hexagonal unit cell has a “d” spacing of 4.9 Å and this corresponds to the first major reflection from the center of the pattern. Fig. 9.16b, on the other hand, shows the WAXS pattern of that film after it has been drawn to 103% elongation where the elongation axis is vertical. The same reflection in this pattern

exhibits an intensity which has azimuthal angular dependence. For qualitative purposes, the stronger azimuthal dependence of Fig. 9.16b is sufficient for concluding the presence of PTFE crystalline orientation. More quantitative analysis requires estimation of the average azimuthal dependence for the reflections. For example, using the half-arc-width method indicates an estimate for $\overline{\sin^2 \psi_{100}} = 0.23$ where ψ_{100} is the azimuthal angle measured from an equatorial line. To relate this to the orientation of the PTFE molecule in the crystalline domains, the method of Wilchinsky[23,27] was utilized to relate the azimuthal dependence of the (100) plane to the Hermans orientation function[28] based on the hexagonal unit cell under uniaxial orientation. This function is shown in Equation 1, and it indicates that $f_{c,z} = 0.33$ for the elongated film.

$$f_{c,Z} = 1 - 3\left\langle \cos^2 \phi_{100,Z} \right\rangle \qquad \text{[Equation 9.4]}$$

where f_c = Hermans orientation function[28] for the PTFE chain (c axis of the unit cell) in which 1 = perfect parallel orientation, -0.5 = perfect perpendicular orientation, and 0 = no preferred direction of orientation

$\phi_{100,Z}$ = angle between the (100) plane normal and the fiber axis, "z," as calculated from Equation 9.5

$$\cos^2 \phi_{100,Z} = \left(\cos^2 \vartheta_{100}\right)\left(\overline{\sin^2 \psi_{100}}\right) \qquad \text{[Equation 9.5]}$$

where θ_{100} = Bragg scattering angle for the (100) plane calculated from Equation 9.6

$$\theta_{100} = \arcsin \frac{\lambda}{2d} = \frac{1}{2} \arctan \frac{R}{F} \qquad \text{[Equation 9.6]}$$

where d = spacing between crystallographic planes, for PTFE d_{100}= 4.9 Å[23,26]

R = distance on the film from center to the observed ring (varies with F)

F = film distance from the sample (varies according to film placement)

Figure 9.16c provides a further comparison by exhibiting the WAXS pattern of a drawn, paste-extruded, 100% PTFE fiber, where the fiber axis is vertical. Using the same method for estimating the azimuthal angle, it was estimated that, for the PTFE crystalline orientation, $f_{c,z}$ = 0.87. Thus either qualitative comparisons or quantitative estimates of azimuthal dependence may be used in these materials to determine that compared with the drawn PTFE fiber, much less orientation is observed in Fig. 9.16b and it is nonexistent in Fig. 9.16a. The largest weakness in using the quantitative technique is the great difficulty in

measuring with confidence an azimuthal angle for low degrees of orientation using the half-arc-width method. More accurate and precise measurements could be made using the diffractometer technique suggested in reference 23. Despite this weakness, this method can be used qualitatively to differentiate between samples so long as the exposure time and sample thicknesses are maintained constant. Such comparisons have been used in these materials previously to show that drawing them into fibers at higher rates does lead to higher PTFE crystalline orientation.[6] The weakness in using qualitative comparisons is that they fail to provide quantitative information regarding how much more oriented one sample is than another.

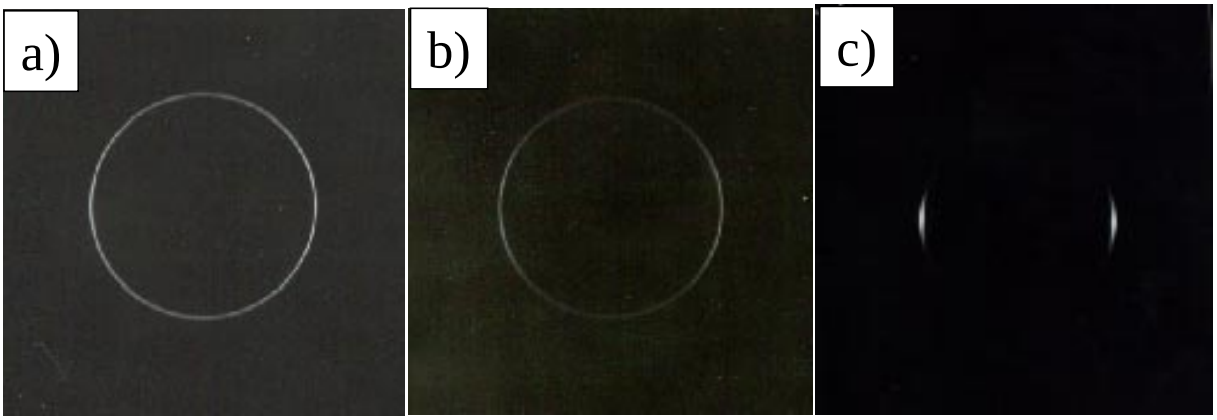

Figure 9.16 WAXS patterns of a) an as-cast 70 wt% PTFE film, b) the 70 wt% film at 103% elongation, and c) paste-extruded and drawn 100% PTFE fiber

A final weakness to the WAXS approach presented here is that it assumes uniaxial orientation. Planar orientation or biaxial orientation can have dramatic effects on the azimuthal dependence of the WAXS pattern,[29] invalidating the equations and requiring alternative interpretations for the qualitative method. Biaxial or planar orientation could occur in these films during calendering or deformation under pressure. Such orientation could be detected by examining WAXS patterns collected along each axis.[29] Deviation from true uniaxial orientation could possibly also result if the film is deformed uniaxially and relaxes due to the elastomeric retractive forces. Thus, a film with large amounts of fibrillation could, after the elastomer relaxes, exhibit a WAXS pattern that shows no or little orientation.

9.4.4 Fibrillation Reinforcement of the Polymer Film

Inducing fibrillation of the high molecular weight PTFE could enhance the reinforcement of the PTFE filler in the elastomeric matrix. If enough interconnectivity between PTFE particles is induced, this could lead to the formation of a network of the semicrystalline polymer that would be essentially co-continuous with the covalent network in the elastomeric matrix. The high dependence of modulus on the level of PTFE content was shown in Fig. 9.2a, but fibrillation presents the possibility of increasing the modulus without increasing the weight percent of PTFE in the composition. PTFE fibrillation has been shown to occur under shearing of PTFE pastes as induced in paste extrusion and by milling (calendering) of the cast blends;[6] however, these methods induced fibrillation mainly at the surface of the material where the greatest shearing forces occurred. Therefore, three mechanisms for inducing shear in the matrix of the polymer blends were examined: milling (i.e. calendering), tensile drawing, and compression molding.

Milling experiments were performed at the Chemfab Corporation on 40 and 60 weight percent materials. Samples were calendered at 100°C through a 0.03 mm gap, folded while keeping the machine axis constant, and passed through the calender again. Each sample was cycled through the calender several times. As Fig. 9.17a shows, these films exhibit behavior similar to that of highly oriented semicrystalline polymers. Parallel to machine axis, the 40 and 60 wt% calendered films exhibit much higher stress at yield than is observed either along the transverse axis or in the non-calendered films. This suggests that the load is being borne by the PTFE which has been made continuous parallel to the machine axis. Also, rather than extensive drawing, the films broke similar to the as-cast films. Perpendicular to the machine direction, low stress and high drawability was observed, and this is consistent with behavior transverse to highly oriented PTFE domains. It was unexpected, however, that the 40 wt% films would exhibit higher yield stresses than was observed in the 60 wt% films. As Fig. 9.17b shows, these calendered films exhibit machine axis moduli that are twice that observed in the 70 wt% as-cast films. Without PTFE connectivity, however, the transverse moduli are shown to be very similar to their corresponding as-cast films. As can be observed in Fig. 9.17c, the toughness along both axes in the calendered films was higher than that observed without milling. As Fig. 9.17a shows, however, this occurs by two different mechanisms. Along the machine axis, the calendered films break at approximately the same elongations as

the as-cast films; therefore, the increase in toughness must be due to the dramatically higher stress response for each strain input. Conversely, no increase in stress is observed along the transverse axis relative to the as-cast films, and thus the toughness is increased by the films drawing three times further than the as-cast films.

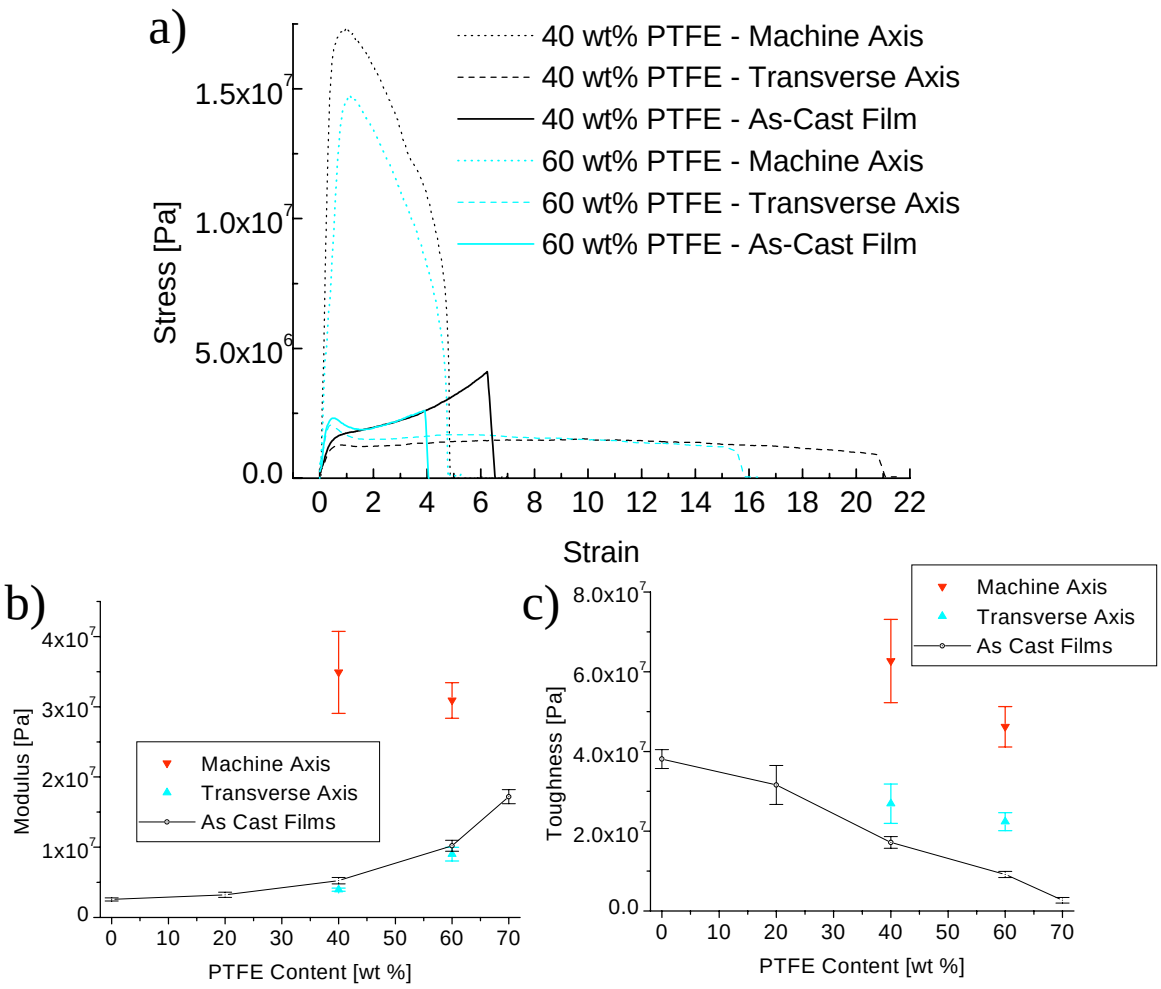

Figure 9.17 Mechanical properties from tensile testing of the calendered films: a) stress-strain data for the 40 and 60 wt% films comparing machine axis properties to those of the transverse axis and of as-cast films; b) modulus data; and c) toughness data from the tensile experiments.

This highly anisotropic mechanical behavior correlates well with the WAXS of the calendered films. As shown in Fig. 9.18a and 9.18b, both the 40 and 60 wt% films, respectively, appear to have an azimuthal dependence similar to the PTFE drawn fiber of Fig. 9.16c. This is supported by the quantitative estimate which shows for the 40 wt% film $f_{c,z}$ = 0.86 and for the 60 wt% film $f_{c,z}$ = 0.81.

Figure 9.19a and 9.19b show the AFM phase images for the 40 wt% and the 60 wt% calendered films, respectively. It may be observed in these micrographs that nearly all of the PTFE observed has taken the fibrillated form. The machine axis is vertical in these phase images, and, therefore, these phase images of the calendered film surfaces provide further support for the high levels of PTFE orientation in the films. Furthermore, these micrographs suggest that the much higher stress response observed in Fig. 16a is due to the near continuous nature of the PTFE domains formed as a result of the calendering.

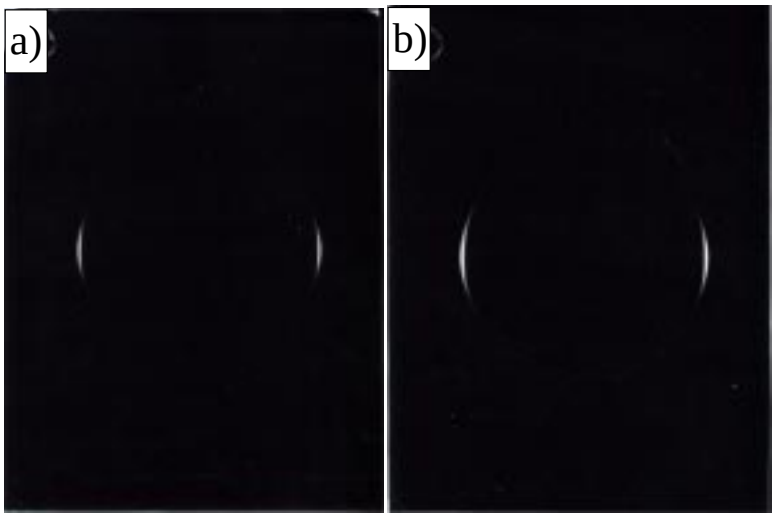

Figure 9.18 WAXS patterns of the calendered films: a) the 40 wt% PTFE film and b) the 60 wt% PTFE film where the machine axis is shown as vertical.

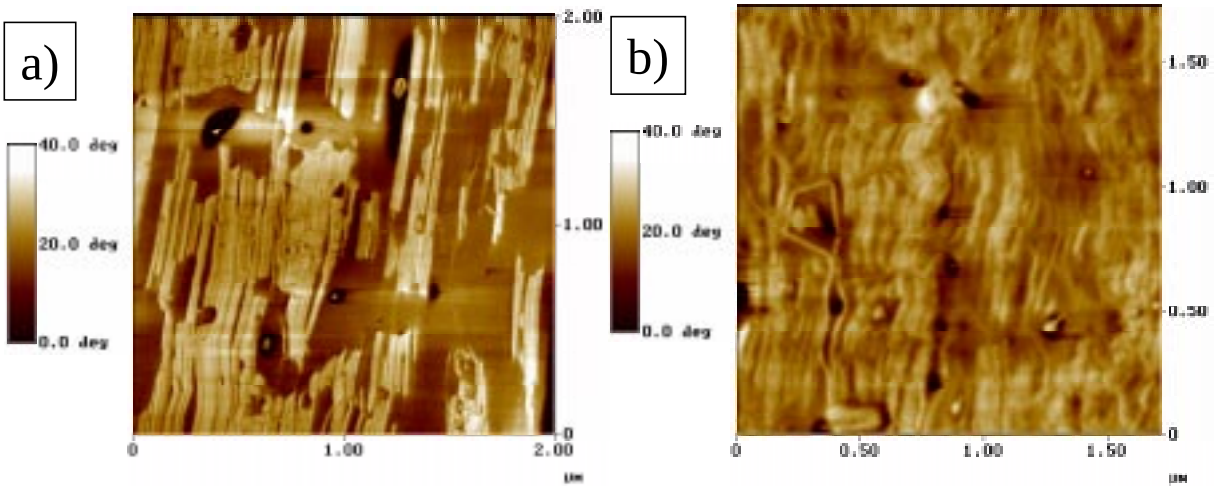

Figure 9.19 Phase images from atomic force microscopy of: a) the 40 wt% PTFE calendered film and b) the 60 wt% PTFE film where the machine axes in the images are vertical.

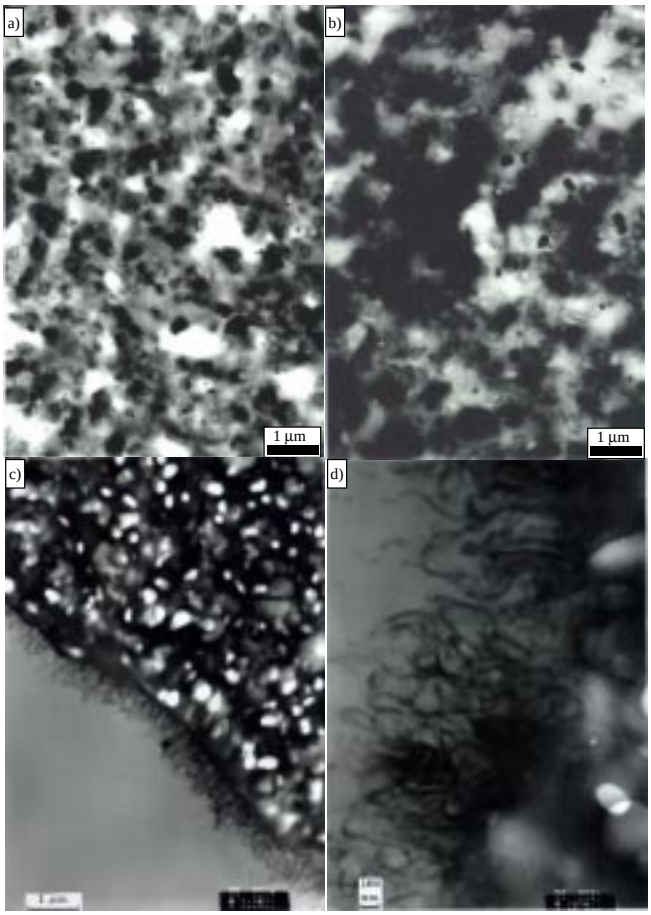

Figure 9.20 TEM micrographs of the calendered 40 wt% PTFE films a) parallel to the machine axis, b) perpendicular to the machine axis, and the film/epoxy interface after beam damage has stabilized at c) low mag. parallel to the machine axis and d) at high mag perpendicular to the machine axis.

To attempt to examine alterations in the matrix of the polymer, TEM was applied to these calendered films. The 40 wt% and 60 wt% films are shown in Fig. 9.20 above and in Fig. 9.21, respectively. The electron beam damage discussed earlier occurred during the micrograph collection for the 40 wt % films but is less evident in the 60 wt% films. These images suggest that the calendering process has not significantly altered the morphology of the PTFE particles in the bulk. That is, no extensive fibrillation can be seen, and no greater interconnectivity between PTFE particles is observed when compared to Fig. 9.14. It is possible that the electron beam damage has altered the morphology of the bulk. Another possibility is that the fibrillation is at too low a scale to be observed at these low magnifications. Figure 9.20c shows that at the milled surface, a significant change appears to have occurred. This is not the same particulate morphology that has been noted at and near the film/epoxy interface in the as-cast films. While some spherical particles can still be observed in the epoxy in Figs. 9.20c and 9.20d, they are now surrounded with fibrils

extending outwards from the film. No difference in the structure was observed whether viewed parallel to the machine axis as in Fig. 9.20c or perpendicular to it (Fig.9.20d). This lack of directionality is suggested to result from two causes. Primarily, penetration into the film surface by the epoxy has obviously occurred, and this might have resulted in some loss of orientation of the fibrillation near the surface observed in Fig. 9.19. Secondly, the entangled nature of the fibrils in the epoxy interface makes it difficult to discern directionality. Based on the highly anisotropic mechanical properties observed in Fig. 9.17, it is hypothesized that this fibrillated structure may exist within the matrix as well, but that it can only be observed via TEM once it is stabilized by the epoxy. It is noted that Fig 9.20d shows much more PTFE particulate in the epoxy than was observed without calendering (see Fig. 9.22c); however, it exhibits less of the fibrillation at the surface than was observed in the 40 wt% films as in Figs. 9.20c and 9.20d. This may indicate that epoxy penetration has been reduced in the 60 wt% film as a result of the more continuous PTFE surface suggested by Fig. 9.19b.

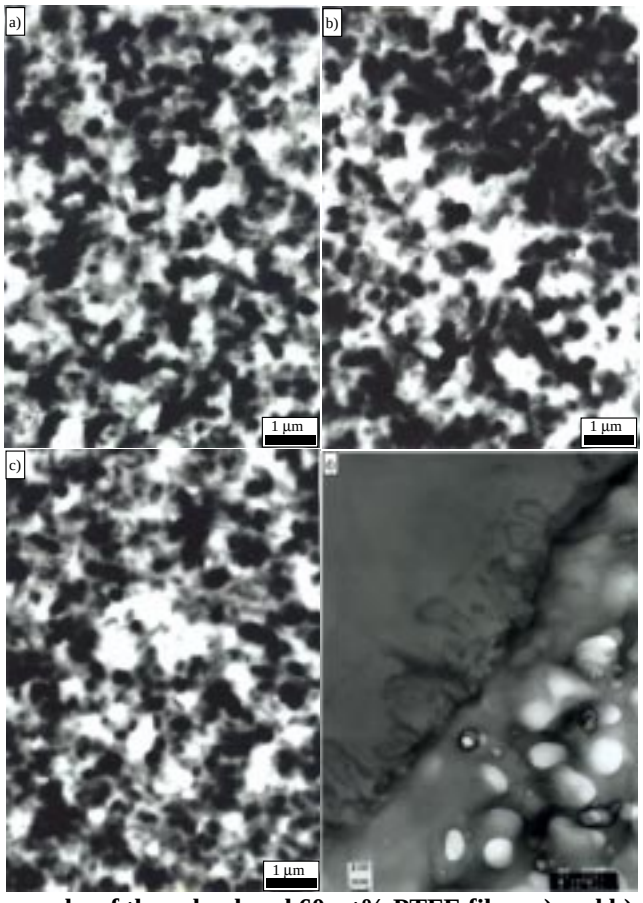

Figure 9.21 TEM micrographs of the calendered 60 wt% PTFE films a) and b) parallel to the machine axis, c) perpendicular to the machine axis, and d) the film/epoxy interface after beam damage has stabilized viewed parallel to the machine

Examination of the calendered materials has demonstrated that shearing the film surfaces can be exploited to induce adequate fibrillation to significantly alter mechanical properties. Since repeating folding and calendering steps to achieve these modulus increases are not necessarily ideal from a processing standpoint, it was of interest to investigate whether fibrillation may be induced through shear transferred to the PTFE particles by the flow of the elastomeric component. To examine this question, the effect of two types of deformation were examined: cycling at low extension and drawing to high extension. Cyclic tensile deformation of 40 and 60 weight percent materials to induce fibrillation was not successful. After one to two cycles, even at less than 3% elongation, the 60 wt% films formed necks. The 40 wt% films generally did not form necks when cycled below 3% elongation, however, the WAXS patterns of these materials revealed no signs of orientation even in the necked regions.

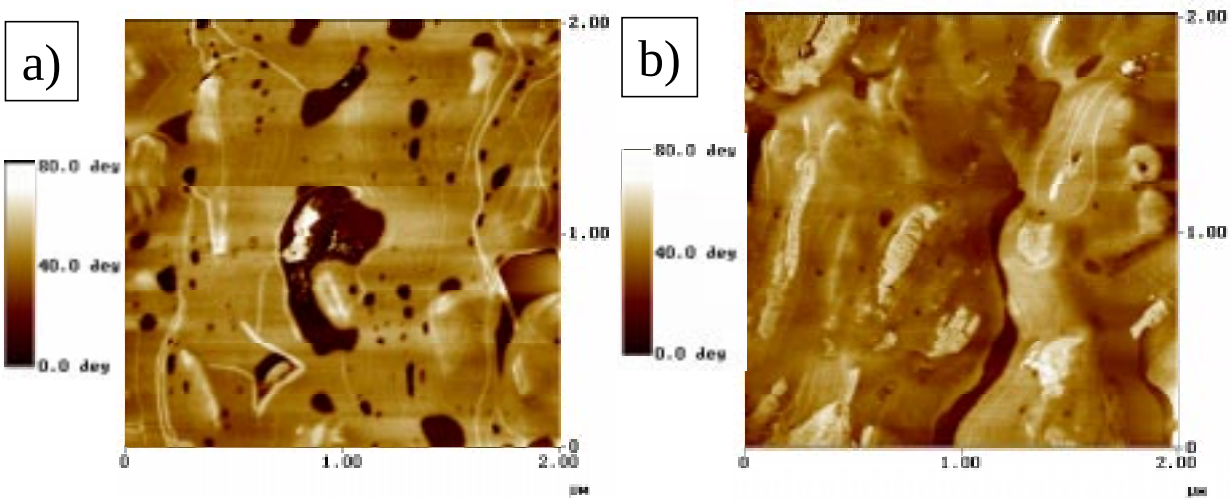

Figure 9.22 Phase images from AFM of: a) the 40 wt% PTFE film and b) the 60 wt% PTFE film drawn to ca. 3,130% elongation where the deformation axes are oriented vertically in the images.

Because of the failure of cycling to induce fibrillation detectable via WAXS, cold drawing the films to high elongations was attempted. The 40 and 60 wt% films were drawn at room temperature to ca. 3,130% elongation and held for fifteen minutes. This did result in orientation of the PTFE crystalline domains as detected by WAXS. Estimations of the half-arc width in WAXS suggest that $f_{c,z}$ = 0.4 for both the 40 and 60 wt% materials. This result was confirmed via AFM, as shown above in Fig. 9.22, were the draw axis is oriented vertically in the micrographs. Fibrillation can be observed to have occurred in both the 40 and 60 wt% materials. It is also interesting to note that the fibrils appear to have curled somewhat due perhaps to the substantial relaxation which occurred after the drawn films were released from the Instron grips. This loss of fibril orientation due to the retraction of the elastomer

suggests that the initial orientation actually achieved was probably much higher than the molecular orientation as shown via WAXS in the relaxed samples.

These drawn materials were also examined via TEM, and micrographs viewing them parallel to the stretch direction can be seen in Fig. 9.23. Similar to what was observed in the calendered materials, little change in the morphology of the matrix can be detected. Some pull-out artifacts may also be observed in the micrographs. Examining the film/epoxy interfaces also reveals some parallels to the calendered materials. Figure 9.24a shows many fibrils extending out into the epoxy away from the 40 wt% PTFE film surface, and this indicates that the interaction with the epoxy is a function of the wt% PTFE in the film and not of the mechanical treatment used to induce fibrillation. Further support for this hypothesis comes from Fig. 9.24b which shows fewer PTFE particles in the epoxy than in Fig. 9.24a, but many more than were observed in the non-deformed 60 wt% film in Fig. 9.24c.

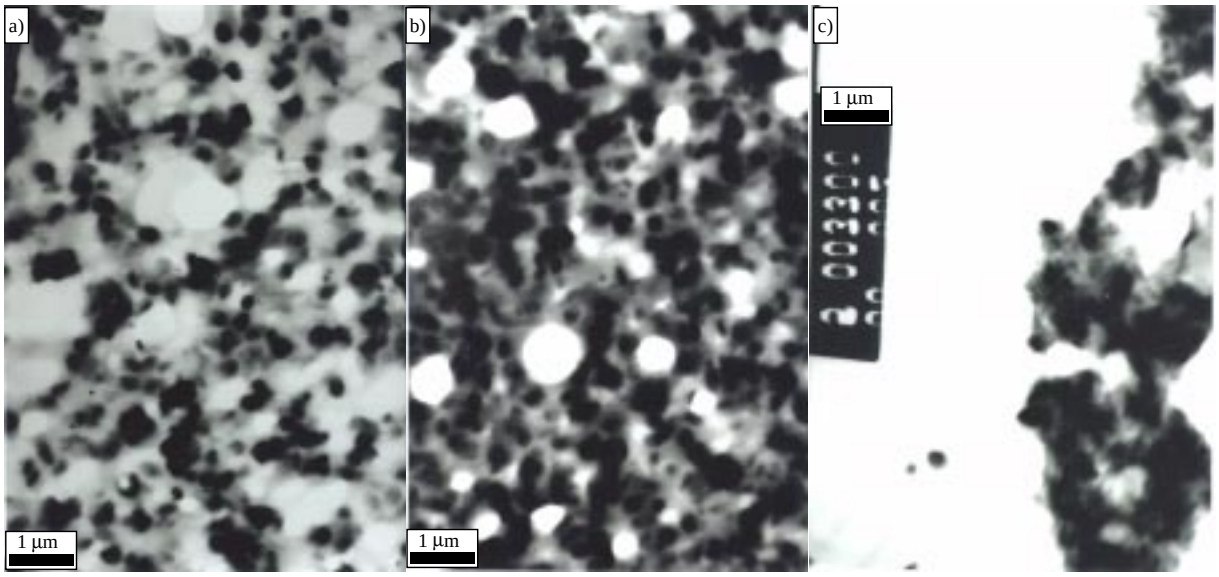

Figure 9.23 TEM micrographs of the drawn PTFE films parallel to the machine axis: a) and b) the 40 wt% film, and c) the 60 wt% film.

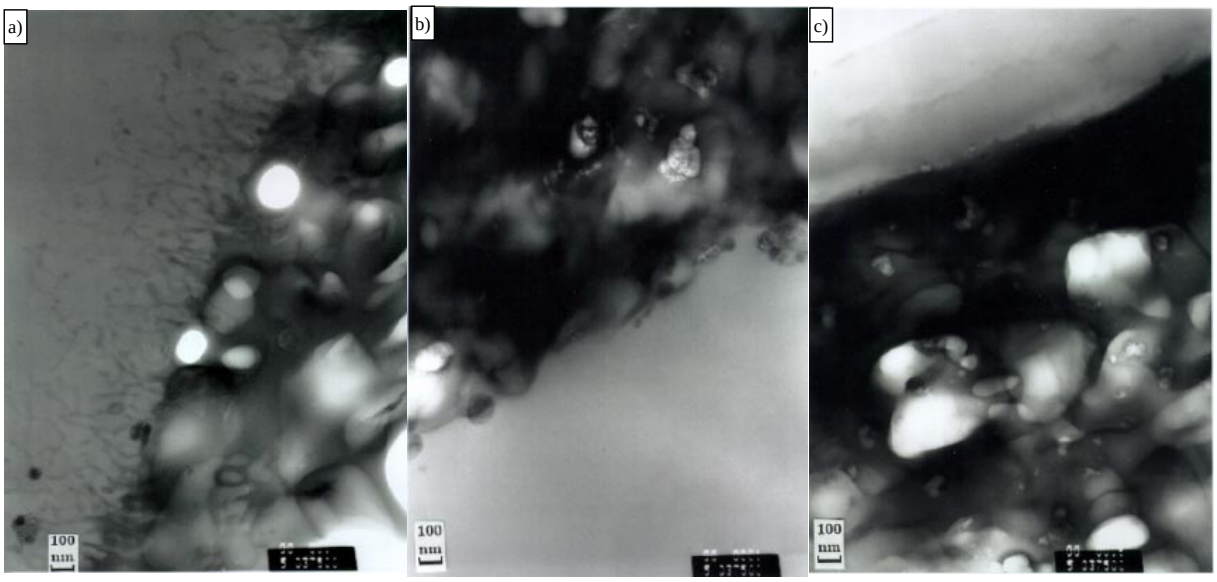

Figure 9.24 TEM micrographs of the drawn PTFE films parallel to the machine axis after beam damage has stabilized: a) the 40 wt% film and b) the 60 wt% film. The as-cast 60 wt% film/epoxy interface is shown in c).

Drawing the films to high extension has thus shown that shear applied to the PTFE particles by the flow of the elastomer is sufficient for inducing fibrillation. To manipulate this for the production of films, samples were deformed along a single axis in the mold described in the experimental section (Fig. 9.1). To induce deformation that was shear-free relative to the film surface, liberal amounts of silicone mold release were used on the Kapton sheets which cover the mold. Furthermore, by varying the mold temperature at the time of compression, it was possible to examine the dependence of fibrillation on temperature. Releasing the pressure on the mold at 9 minutes resulted in samples which were elongated to ca. 0.8 true strain, and releasing at 11 minutes resulted in samples which were elongated to ca. 0.9 true strain. Because the films treated in the mold had a thermal history which was different from the films in the rest of this study, a sample was prepared for comparisons which was not pressurized during the heating cycle. Also, these experiments were performed using PTFE 2 and FKM B, rather than PTFE 1 and FKM A as used in the rest of this work. The PTFE 2 / FKM B films were observed in Fig. 9.10 to exhibit higher storage moduli, and, in data not presented, were found via TEM to have a similar morphology to the PTFE 1 / FKM A films. Using this other combination of components will broaden insight on the general behavior of PTFE/FKM blends rather than of materials from specific suppliers. It should be noted that some material squeezed out of all sides of the mold, making the assumption of

uniaxial deformation rather dubious. This implies that the flow field varied in different parts of the mold which probably resulted in biaxial or planar orientation of the PTFE fibrils. Effects of variance from uniaxial deformation were attempted to be minimized by varying where samples were cut from the molded piece and by not sampling near the edges.

It may be seen in Fig. 9.25 that deforming the films in this manner did result in modulus increases. Even at room temperature, if the film was elongated enough, the sample achieved higher modulus compared to that of the non-deformed piece. Although it is not shown, it should be noted that the properties of the non-deformed sample were determined to 8% error. That the transverse axis moduli are generally lower than those in the flow axis does provide some evidence that uniaxial deformation was approximated. A highly significant result is that the reducing the temperature systematically increases the modulus improvement of the molded samples. This corresponds well with the thermal variation shown in Fig. 9.5, and it suggests that increasing the viscosity of the elastomer has resulted in increased fibrillation of the PTFE as the film is deformed. Fig. 9.25b shows that the deformed samples all had lower toughness than the non-deformed sample, and this occurred due to lower strain-at-break values.

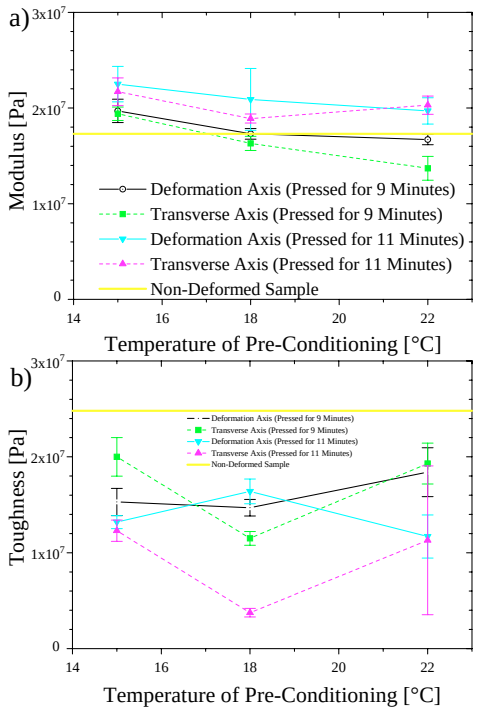

Figure 9.25 Results of the mechanical testing of the deformed 40 wt% PTFE 2 / FKM B films: a) moduli and b) toughness data.

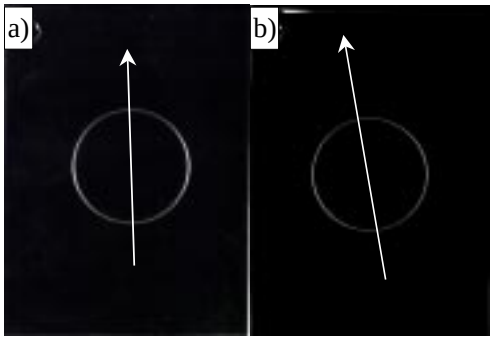

Figure 9.26 WAXS patterns of the 40 wt% PTFE 2 / FKM B films deformed for 11 minutes at a) 15°C and b) at 22°C. Direction of "c" axis orientation indicated by white arrows.

The WAXS behavior for the 40 wt% PTFE materials deformed at 15°C and 22°C is shown in Figs. 9.26a and 9.26b, respectively. These patterns support the hypothesis of oriented fibrillation. The azimuthal dependence of the (100) reflection observed in Figs. 9.26a and 9.26b, has been consistently observed in this study to correspond to oriented fibrillation in these materials. Because the film thicknesses varied after the deformation, direct comparison with each other and to the other WAXS analyses in this study could not be made. The development of oriented PTFE fibrillation can be concluded to have occurred to some extent, however, and this is supported by the phase images shown in Fig. 9.27. Figure 9.27a shows that prior to deformation the film is composed of evenly dispersed PTFE particles of a consistent submicron size. After 11 minutes of deformation at 15°C, Fig. 9.27b shows that fibrillation has occurred and it has led to interconnectivity of the PTFE domains. The flow axis is oriented vertically in the image, but this sample came from near an edge of the deformed film where the flow field may have deviated from being perfectly uniaxial.

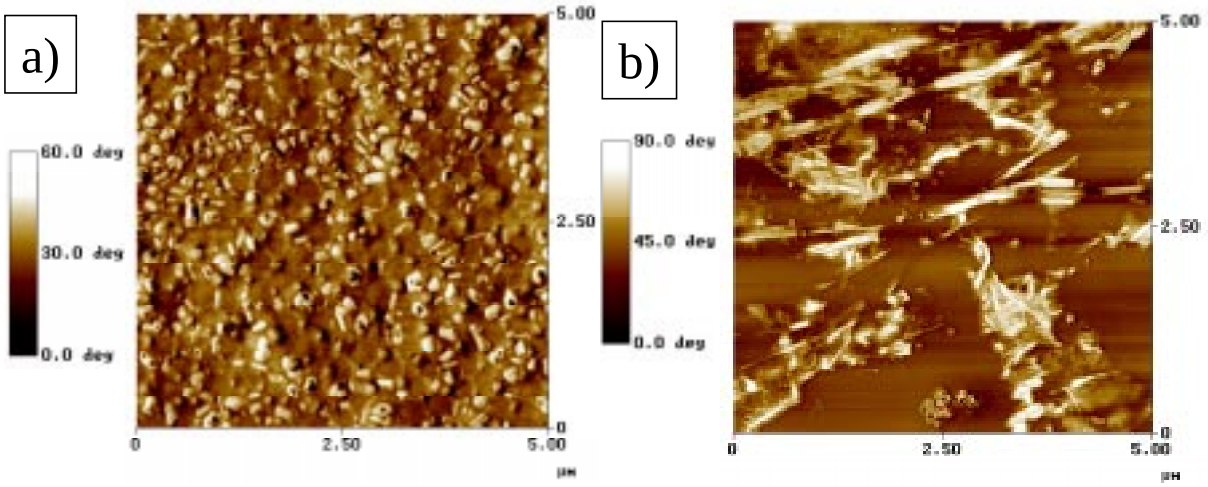

Figure 9.27 Phase images from AFM of the 40 wt% PTFE 2 / FKM B film a) prior to deformation and b) after 11 minute deformation at 15°C

9.5 Conclusions

This study has elucidated the structure-property relationships of polytetrafluoroethylene — poly(tetrafluoroethylene-co-vinylidene fluoride-co-hexafluoropropylene) (PTFE/FKM) cast blends. It has been shown that increasing the PTFE content of the blend or cross-linking of the FKM leads to systematically higher modulus and generally reduced toughness. In dynamic mechanical analysis, these two factors were also shown to increase the rubbery moduli of the films and to reduce the magnitude of the tanδ peak corresponding to the FKM glass transition. Temperature was also shown to have significant effects on the deformation behavior of the greenleaf (non-cross-linked) films. It was shown that maximal transfer of shear to the PTFE particulate occurs at ca. 17-19°C. Corresponding well with the mechanical behavior of the films, it was also demonstrated via solvent extraction that the curing step only marginally cross-links the FKM, but that the post-curing treatment leads to dramatically higher degrees of cross-linking.

TEM was used to examine the morphology of films. Some aggregation of the 0.2 micron PTFE particles was observed to occur at all levels of PTFE content studied, from 20 wt% PTFE to 60 wt% PTFE. The main morphological difference observed to be dependent on PTFE content appears to be the formation of micron sized domains which are relatively poor in PTFE particles. At higher PTFE contents, these domains were not observed. It is worth noting that even at 80 wt% PTFE, as studied via AFM, the FKM always forms a continuous elastomeric matrix.

Inducing interconnectivity via fibrillation of the PTFE was found to greatly enhance the modulus and the toughness of the films parallel to the axis of orientation. For example, by shearing the surface of the films via calendering, the machine axis modulus of the non-cross-linked films was found to be 4-7 times higher than that of the non-calendered films. The calendering was shown via AFM and WAXS to lead to high degrees of PTFE orientation. Inducing fibrillation without shearing the surfaces either by drawing or uniaxially pressing the films was also shown to induce fibrillation and lead to higher moduli. It was observed, however, that shear transfer from the FKM to the PTFE during deformation is increased at lower temperatures resulting in consistently higher moduli values.

9.6 Acknowledgements

The financial support of the Chemfab Corporation is gratefully acknowledged. Christopher Comeaux is particularly acknowledged for his close work with this characterization effort, and Richard Stone is thanked for producing so many of the samples studied. Dr. Baird's laboratory here at VPI&SU is acknowledged for lending us the mold used in the deformation analysis, and Dr. Robert Young is specifically thanked for his many insightful discussions. Finally, Steven McCartney is acknowledged for his help in the TEM examination of these materials.

9.7 References

[1] Blair JA; "Fluorocarbons, Polymers," Enc of Ind Chem Anal: **13** (1971) 73-93
[2] Grot W; "Tetrafluoroethylene Polymers," Enc of Polym Sci and Eng: **16** (1989) 577-599
[3] England DC; Uschold RE; Starkweather H; Pariser R; *Proc of the Robert. A. Welch Foundation Conf on Chem Res*: **XXVI Synthetic Polymers** (1983) 193-232
[4] Righetti MC; Ajroldi G; Vitali M; Pezzin G; *J Appl Polym Sci*: **73** (1999) 377-384
[5] Powers J; *Chemical Processing*: **Mid-November** (1984) 145
[6] Effenberger, JA, et al, U.S. Patent Application #09/096,700, June 12, 1998, Chemfab Corp.
[7] Sperati CA; Starkweather Jr HW; *Fortshr Hochpolym-Forsch*: **Bd. 2, S.** (1961) 465-495
[8] Effenberger JA; Keese FM; **US Pat 4,555,543**: Nov. 26, 1985
[9] Effenberger JA; Keese FM; **US Pat 5,194,335**: Mar. 16, 1993
[10] Effenberger JA; Koerber KG; Latorra MN; Petriello JV; **US Pat 4,883,716**: Nov. 28, 1989
[11] Logothetis AL; *Prog Polym Sci*: **14** (1989) 251-296
[12] Pelosi LF; *Rubber Chem Technol*: **49** (1976) 367-374
[13] Bhattacharjee S; McGrath JE; presentation at ChemFab Corp: July 18, 1998
[14] Nielsen LE; Mech. Prop. of Polym. and Composites, Vol 2; Marcel Dekker, Inc; New York: (1974) 405-408
[15] Nielsen LE; *J Comp Mat*: **1** (1967) 100-119
[16] Nielsen LE: *J Comp Mat*: **2** (1968) 120-123
[17] Smallwood HM; *J Appl Phys*: **15** (1944) 758-767
[18] McCrum NG; Read BE; Williams G; Anelastic and Dielectric Effects in Polymeric Solids; Dover ed, J Wiley & Sons, Inc; New York: (1967) 452-454
[19] Clark ES; *Polymer*: **40** (1999) 4659-4665
[20] Davidson T; Gounder RN; Adhesion and Adsorption of Polymers, Vol 12B; Plenum Press; New York: (1980) 775-790
[21] Clough RL; Shalaby SW; Irradiation of Polymers, Fundamentals and Technological Applicaitons; American Chemical Society; Washington, DC: (1996) 4-256
[22] Ribeiro CA; Vargas H; Galembeck F; *J Electron Microsc*: **30** (1981) 148-149
[23] Alexander LE; X-Ray Diffraction Methods in Polymer Science; J Wiley & Sons, Inc; London: (1969) 245
[24] Kimmig M; Strobl G; Stuhn B; *Macromolecules*: **27** (1997) 2481-2495
[25] Clark ES; Weeks JJ; Eby RK; *ACS Symposium Series*: **141** (1980) 183-192
[26] Bunn CW; Howells ER; *Nature*: **174** (1954) 549-551
[27] Stein R; *J Polym Sci*: **31** (1958) 327-334
[28] Hermans JJ; Hermans P; Vermaas D; Weidinger A; *Rec trav chim*: **65** (1946) 427
[29] Ward IM; Structure and Properties of Oriented Polymers, 2nd Ed., Chapman & Hall, London: 1997, 44-141

10 Summary Chapter

This study examined several structure-property features of flexible polyurethane foams that are important aspects of foam production. Diethanolamine is widely used as a cross-linking agent in molded foam systems, but its impact upon solid-state morphology and viscoelastic properties is not well understood. Copolymer polyol is frequently applied as reinforcing filler in both slabstock and molded systems, but its properties and influences also need further elucidation. Even more fundamental than these aspects, many studies have demonstrated the importance of the polyurea hard domains to polyurethane foam performance, yet the morphology of these solid-state features is incompletely understood. Furthermore, many factors have not been examined which influence the precipitation of the polyurea into hard domains, such as cure temperature and surfactant concentration. The insights provided by this investigation into these areas are summarized below.

The viscoelastic and morphological properties of molded foams were investigated to determine the influence of varying the concentration of diethanolamine (DEOA). It was shown via Fourier transform infrared (FTIR) spectroscopy and wide angle x-ray scattering (WAXS) analyses that the DEOA had a disrupting affect on the bidentate hydrogen bonding within the hard domains of the polymer. Dynamic mechanical analysis (DMA) revealed that DEOA softens the foam above the T_g of the soft segment, but it only causes minor changes in the degree of microphase separation. Annealing treatments were shown to remove the DEOA influence on microphase separation as well as some of the softening effect. FTIR was used to show that bidentate hydrogen bonding is enhanced through the annealing of DEOA foams. Structural studies via tapping mode atomic force microscopy (AFM) revealed that DEOA greatly disrupts the interconnectivity of the hard domains leading to a more dispersed morphology.

Another set of molded foams were investigated to determine the influence of the presence or absence of reinforcing particulate copolymer polyols (CPP). Two series of foams were studied. In Series 1, as CPP is added to the formulation, the amount of TDI fed is kept constant. This results in a constant amount of hard segment content as the filler in the system displaces, by weight, the polyether polyol in the foam, and it increases the hard segment to soft segment ratio (HS/SS). In Series 2, the amount of hard segment material is proportionally decreased as CPP is

added resulting in a constant HS/SS ratio. It was also found that the copolymer polyol particles, as added to the molded foams of Series 1, increased load bearing capabilities but had a negative effect on the stress relaxation, creep and compression set properties. In particular the viscoelastic properties of the CPP containing foam were distinctly more time-dependent than those of the foam lacking these particles. However, the Series 2 foams show that most of these effects are a result of the increased HS/SS ratio and not a result of the CPP particulate. It was shown that adding CPP while maintaining a constant HS/SS ratio improves percent load loss and load bearing under high humidity conditions, two important properties in flexible polyurethane foams. Finally, it was shown that at high temperatures (ca. 100°C) an additional relaxation mechanism occurs which cannot be attributed to changes in the HS/SS ratio, but must be a result of the CPP components themselves. This additional mechanism results in higher rates of load relaxation and creep in foams containing CPP at high temperatures for foams of both series.

Surfactants are an important but non-reactive component in foam manufacturing. Their influence on the development of polyurea hard domains were examined by varying the surfactant concentration in a series of slabstock foam samples. This made it possible to examine the influence of the presence and absence of the cellular structure at the time of polyurea precipitation. It was shown in this study that collapse of the cellular structure of a foam prior to the point of urea precipitation alters the aggregation behavior of the hard domains and alters solid-state properties. Samples without surfactant that were quenched in liquid nitrogen exhibited urea-rich aggregations on the order of 2-4 microns with similarly sized urea-poor regions. Equivalent samples with surfactant showed no such aggregations, suggesting that surfactant does play a principal role in the way that urea precipitates in these materials. DMA and dynamic scanning calorimetry (DSC) revealed that all samples of any surfactant concentration which spontaneously collapsed or were quenched or crushed prior to completely curing had a polyol glass transition 3-5 degrees higher and somewhat broader than any foam sample which maintained its cellular structure until cured. This is interpreted to mean that the polyol matrix of the collapsed, crushed, or quenched materials is not as pure as the cellular samples, indicating that the presence of the cellular morphology plays a significant role in the microphase separation behavior of the solid-state at the molecular level. This hypothesis is supported by the results of WAXS, FTIR, AFM, and small angle x-ray scattering (SAXS). The WAXS results demonstrate that at no surfactant concentration is the ordering, or hydrogen

bonding, within the hard domains being significantly altered; however, in the lower range of the concentrations studied here, the FTIR results show that the surfactant level in the formulation does play a significant role on the amount of bidentate hydrogen bonded hard domains that locally organize. Furthermore, as shown by SAXS, the surfactant concentration influences the mean chord length across the hard domains. These changes in structure and domain size distribution lead to the properties investigated via AFM, where the relative hardness of the hard domains was noted to initially increase as the surfactant concentration increases and then levels off above a certain concentration. The surfactant is thus suggested to play a secondary role in the development of the hard domains by maintaining the cellular structure in the foam as the phase separation occurs and at least until the polyurethane foam has more fully organized hard segment domains.

AFM and WAXS were used to further examine the morphology of hard domains in flexible polyurethane foams and plaques based on typical slabstock formulations. In plaque samples that were uniaxially deformed to 50% elongation, WAXS was utilized to demonstrate transverse hard segment orientation relative to the axis of deformation. AFM was utilized to directly observe the morphology of the foams and plaques. Micrographs from this technique present, for the first time in polyurethane foam systems, lamellae-like structures ca. 0.2 μm long and ca 10 nm across. These structures are believed to be precipitates of polyurea hard segments and are considered to be responsible for the orientation behavior presented. Furthermore, it is suggested that aggregations of these lamellae-like hard domains are the polyurea balls typically observed via TEM.

Thermal dependence of the development of solid-state morphology and properties were investigated further by studying several voidless plaques. These samples were produced based on a typical molded flexible polyurethane foam formulation and by varying the cure temperature from 70°C to 150°C. X-ray photoelectron spectroscopy (XPS), SAXS), FTIR, and DMA were used to evaluate their morphology and properties. It was found that cure temperature could be manipulated to predictably change the interdomain spacings and levels of hydrogen bonding which develop in the polymer. On the other hand, in these plaque samples where the polyurea precipitates without the cellular structure, SAXS and DMA indicated no temperature in the range studied which yielded comparable phase separation to their corresponding foams. It was found that varying the cure temperature, especially above 100°C, changes the amount of water

vaporizing from the reactive mixture, thus altering the stoichiometry of the reaction. For example, compared to plaques cured above 100°C, polymerizing at 70°C using the same formulation resulted in much higher hard segment content with correlating higher levels of hydrogen bonding and higher storage moduli. Foams were found to have higher hard segment contents than plaques cured above 100°C and also to have much greater storage moduli stability with respect to temperature. This stability is suggested to be due to a more developed covalent network. However, even annealing at 130°C for two hours did not significantly change the storage moduli of the plaques. It is therefore concluded that the lower level of phase separation in the plaques is significantly altering the thermal stability of the storage moduli. It is hypothesized that the absence of the cellular structure may be playing a role in the organization of hard domains as the polyurea precipitates.

As a departure from polyurethane materials, the morphology and properties were evaluated of cast blends based on polytetrafluoroethylene (PTFE) and the terpolymer poly(tetrafluoroethylene-co-vinylidene fluoride-co-hexafluoropropylene) (FKM). FKM formed an elastomeric matrix at all compositions studied (from 0 to 70 wt% PTFE), and the 0.2 μm PTFE particles behaved as a reinforcing filler. It was observed that below 50 wt% PTFE content, cross-linking the FKM can have a much larger influence on tensile modulus than changing the PTFE fraction. Above 50 wt% PTFE, however, the modulus increased exponentially respect to increasing PTFE content. When the PTFE is cross-linked, more stress is apparently transferred to the PTFE particulate leading to higher elongations-to-break and resulting in higher toughness. Increasing PTFE content or degree of cross-linking were also observed to systematically increase the storage moduli in the rubbery region. Inducing fibrillation via calendering the films repeatedly was found to lead to oriented fibrillation of the PTFE component, leading to highly anisotropic mechanical properties. Modulus of the calendered 40 wt% PTFE films was found to be ca. 33 MPa parallel to the machine axis and ca. 5 MPa perpendicular to it. When deforming the films under pressure, it was also found that higher levels of fibrillation could be obtained by reducing the deformation temperature, resulting in higher modulus.

A. Appendix - Tapping Mode Atomic Force Microscopy

Atomic Force Microscopy (AFM) or Scanning Probe Microscopy (SPM) is based on surface interactions with probes that have been specially fabricated to have near atomic sharpness. These techniques may be utilized in either of two modes: contact mode and tapping mode. Contact mode involves bringing a tip into contact with a surface, pushing with a selected force. This mode can provide information regarding the necessary force required to indent a surface. Special probes are manufactured for this techique which have sturdier cantilevers (i.e. higher force constants) than those utilized for tappling mode, and they may also use special tips such as diamond rather than silicon.

Tapping mode AFM has been the subject a great deal of research recently. This technique applies an oscillating voltage to a piezocrystal, resulting in proportional and oscillating dimensional changes in the piezocrystal. This oscillation induces an oscillation at the tip of the probe. A typical frequency for these instrements is ca. 290 kHz. By reflecting a laser off the end of the probe cantilever, deflection of the tip can be measured. In the free air where no surface can effect the tip, the oscillation of the probe is perfectly in phase with the drive oscillation. However, interaction between the tip and sample induce phase offsets (or phase lags) between the drive oscillation and oscillation of the tip. This process is illustrated in Figure A.1.

These phase offsets provide a useful parameter for learning about the properties of a surface. By scanning across a surface, phase offsets all across a sample may be tracked. This data is then presented in a “phase image” where the x and y axes are the dimensions of the sample, and the z axis is the phase offset of each point in the scan.

Another important parameter is the amplitude of the tip oscillation. When tuning the instrument in the free air, an amplitude may be selected for that oscillation where there is no impedement from the surface. As interaction begins with the surface, the tip oscillation will have an amplitude that is some fraction of the free air amplitude. This fraction is termed the “setpoint,” and it can be selected by the experimentalist. Once this setpoint is selected, the instrument maintains it throughout that scan. It accomplishes this by moving the whole assembly up and down with the surface features, and this provides a way for the instrument to also map out height variation. Thus tapping mode AFM provides two images: a height image and a phase image.

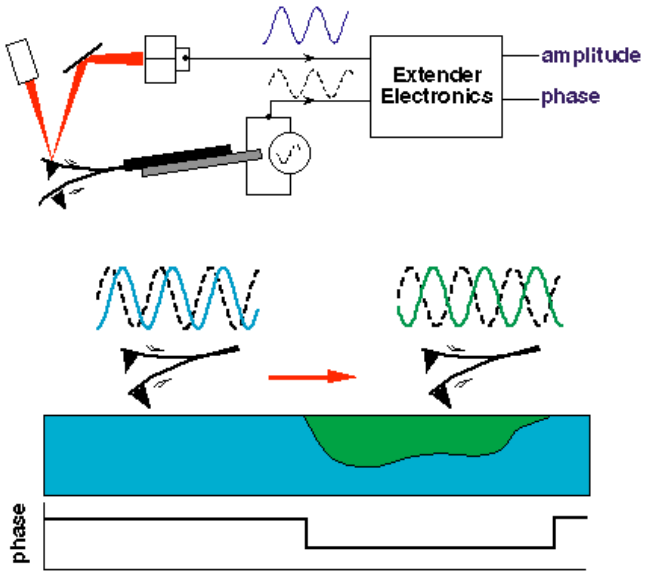

Figure A.1 Surface Interaction in Tapping Mode AFM[1]

For qualitative evaluation of a morphology, AFM provides a relatively easy technique for examining many different length scales. However, if the data is to used for quantitative work, such as for analyzing trends, it becomes important to carefully control the forces applied to the surface. The setpoint effectively determines how hard the tip is hitting the surface; therefore, it is necessary to maintain a constant setpoint for every scan in the compairson. Another important item to control is the quality of the tip. For soft materials like polyurethanes, little tip damage generally occurs and a tip may be useful for many scans. However, sometimes the tips become contaminated through adhering of particles from the surface, leading to higher than normal phase offsets. Some work has been done to develop ways of monitoring tip quality, but these techniques are not straightforward and usually result in ruining that tip.[2] Therefore, for the pursposes of this research, tip quality is assured by having a benchmark sample which was used to check if the same phase offsets are still being observed. Also, using this benchmark, it was found that tips all have similar tip dimensions, so that data collected with a new tip could used for the comparative analyses. Finding better ways to more tightly control tip quality may be a way to improved the percent error in these type of measurements.

For this research, quantitative work will focus on two main treatments of the phase image: the section analysis and the power spectral density analysis. The basis for using a section analysis on a phase image rests in the complicated relation between the phase offsets observed in AFM scanning and the stiffness of the surfaces being scanned. These relationships

were recently examined in detail by Maganov and coworkers.[3] The result of the derivation contained in that work is the relationship shown in Equation 4.1.

$$\Delta\phi_o = \varepsilon\langle a\rangle E^* \left(\frac{Q}{K}\right) \qquad \textbf{[Equation A-1]}$$

where: $\Delta\phi_0$ is the phase shift relative to the phase of the cantilever when oscillating in free air and at its natural frequency

ε is a factor from the Hertz theory[4] between 1.9 and 2.4[5]

$\langle a\rangle$ is the contact radius of the tip with the surface

E* is the effective modulus of the surface when the modulus of the tip is much higher than that of the surface

Q is the quality factor of the tip

K is the force constant of the cantilever

This relation may, in some future research, lead to the evaluation of the modulus of microdomains. This work, however, will simplify this relationship by excluding all constants from the equation. This leads to Equation 4.2:

$$\Delta\phi_o \propto E^* \qquad \textbf{[Equation A-2]}$$

Again, it is assumed by maintaining tip quality that <a> is in fact a constant; however, this may be adding systematic error to the work. By following trends in E*, it is hoped that the proposed research will be able to find confirming trends with other techniques.

Some qualitative confirmation has been already provided by McLean and coworkers.[6] This work demonstrated in two different materials (poly(styrene-*block*-ethylene/butylene-*block*-styrene) and polyurethane elastomer) that with normal tapping conditions, harder material does induce higher phase offsets. They also showed that the power spectral density analyses of phase images can be used to provide interdomain spacing information that correlates well with the spacings shown via SAXS. One feature of tapping mode AFM that must be used with caution is the possibility of inducing phase inversions. This can occur when tapping at high amplitudes and low setpoints, and it is seen on the instrument when harder phases have lower phase offsets than softer domains.

Therefore, this research proposes to handle a data set in a consistent manner to allow quantitative comparative analyses. The section analysis is performed on a collected image by choosing a line of the image to cross section, as shown in Figure A.2. The cross section then shows how the z axis varies along the line selected by the user, and this cross section is used to make direct measurements of surfaces features. For example, the maximal phase offset is measured by taking the difference between the highest and lowest z axis values along the line.[7] For this research, the section analyses will only be used to evaluate the maximal phase offset, but other parameters can be gleaned as well such as mean roughness and RMS deviation of values from the mean. The procedure for evaluation was to take ten cross sections of every phase image collected, and to collect between six and ten images of every sample.

Another analysis of the collected image is the power spectral density. The reason that this is necessary may be seen in the following illustration. Both of the surfaces presented in Figure A.3 would have the same roughness as measured by the section analysis. That is, both would have equal average offsets from the mean surface centerline. Yet clearly, these surfaces differ in the frequency that a feature appears on the surface. It can be imagined that different structures can be added to a surface making it more complex, and so it is helpful to be able to also determine which frequency on a surface occurs most often. Or, in other words, which of the features exerts the greatest "power" in determining the character of that surface. This is the purpose of the power spectral density analysis.

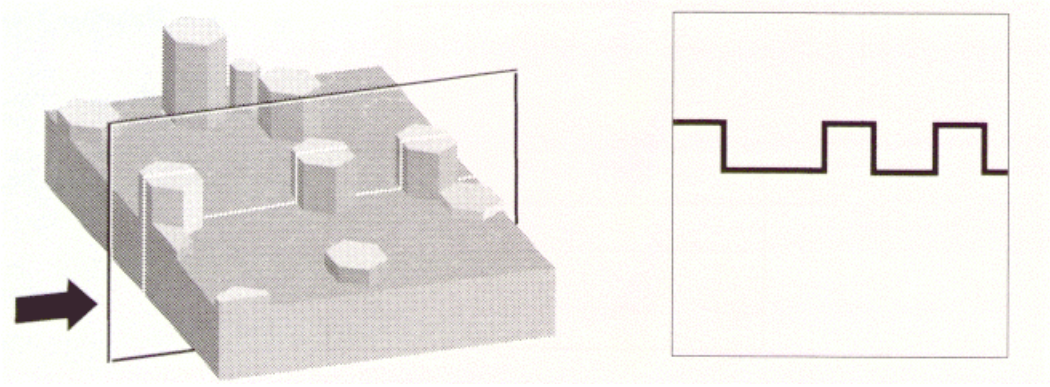

Figure A.2 Taking a Cross-section of an Image[7]

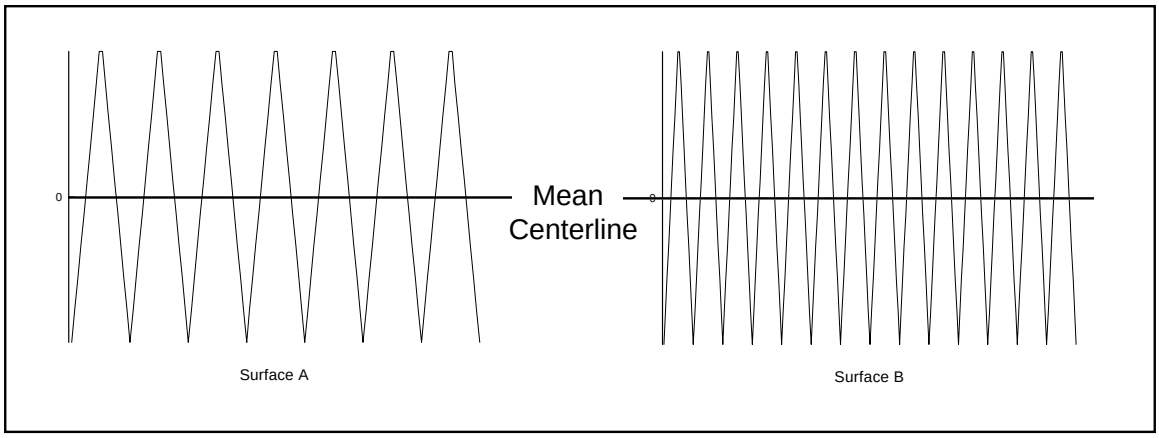

Figure A.3 Two Surfaces with Equal Roughnesses[7]

One example of a surface composed of two periodic structures is shown in Figure A.4. It is obvious that this surface has two dominant waveforms. The two dimensional power spectral density plot for such a structure would show two spikes, each corresponding to one of the wavelengths.

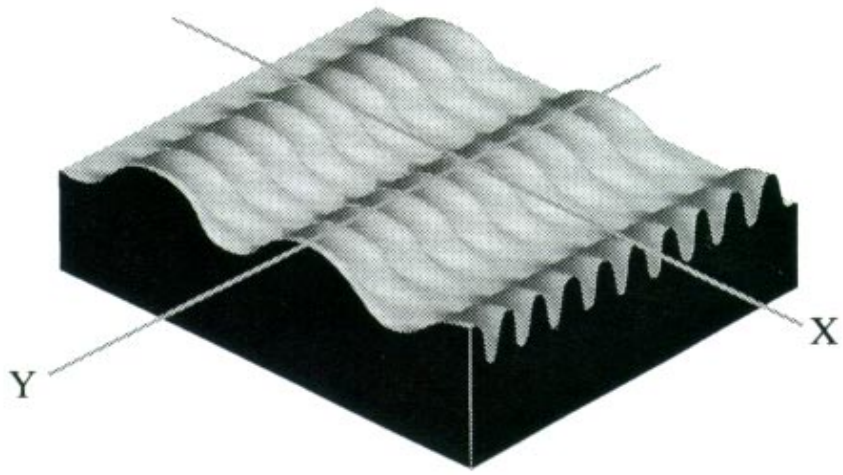

Figure A.4 A Surface Comprised of Two Waveforms[7]

Rarely do such nicely ordered surfaces actually occur in nature, where it is clear from a glance that a periodic structure indeed exists. More frequently, in fact, structure is observed which appears to be essentially random, but the PSD analysis provides a way to discern the truly random from those structures which contain underlying periodicity. For example, a height image of epitaxial gallium arsenide is presented in Figure A.5. The surface presented is comprised of "terraces" natural to the materials lattice structure, each is one atomic monolayer thick. Despite this flatness, the PSD analysis shown in Figure A.6 reveals that there is a periodicity to the width

of each terrace—observed in the spike in the plot. The tapering off of the rest of this PSD plot is characteristic for flat, isotropic surfaces.[7]

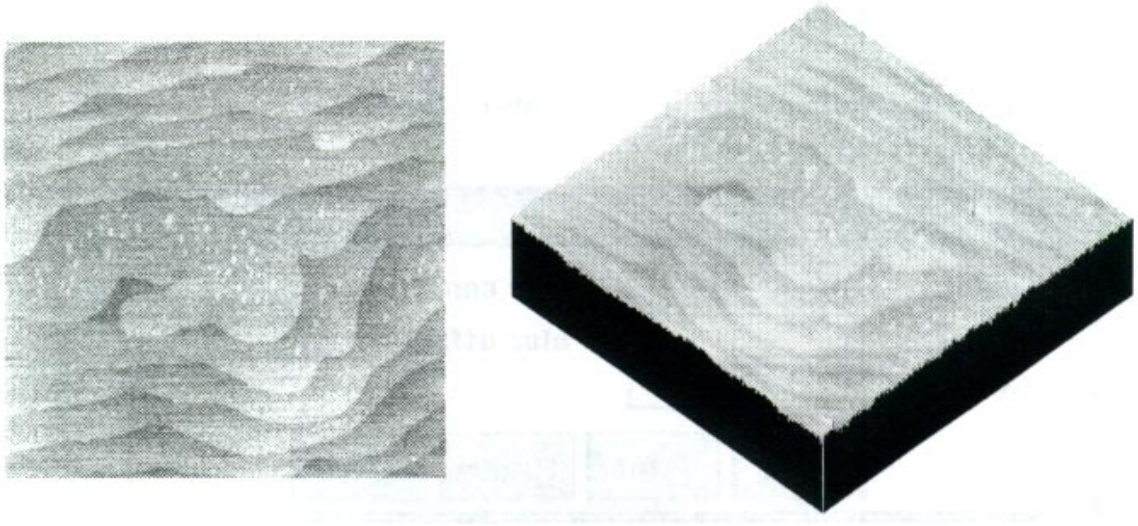

Figure A.5 Height Image of Epitaxial Gallium Arsenide[7]

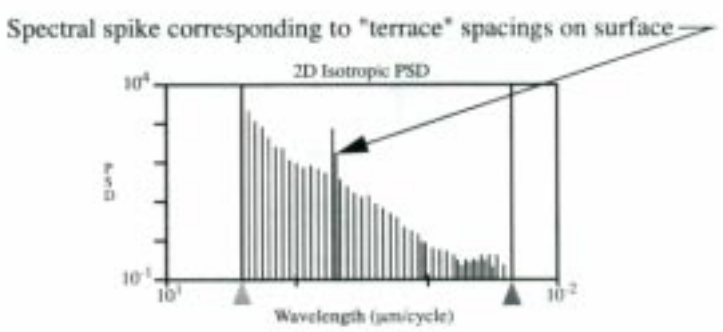

Figure A.6 Power Spectral Density Plot for Epitaxial Gallium Arsenide[7]

A clearer example of the details of PSD analysis can be obtained by examining an ideal structure like that shown in Figure A.7 and its PSD is plotted on a vertical log scale in Figure A.8. It is important to notice that the PSD is not a smooth Gaussian shape, but it does contain several minor maxima. This indicates that the image is composed of multiple waveforms, but that there is one major one corresponding to the ring spacing of 100 nm. However, the actual peak in Figure A.8 corresponds to 91.4 nm, and this is because the square shape of the image clips off the outermost waves reducing the overall average. This emphasizes that everything in an image will end up in the PSD analysis and not just what may be of particular interest.

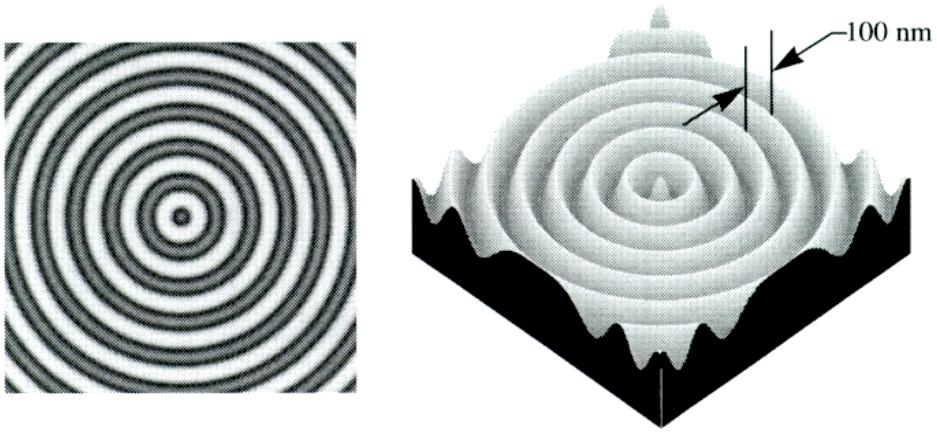

Figure A.7 A Synthetic Waveform Having a Wavelength of 100 Nanometers[7]

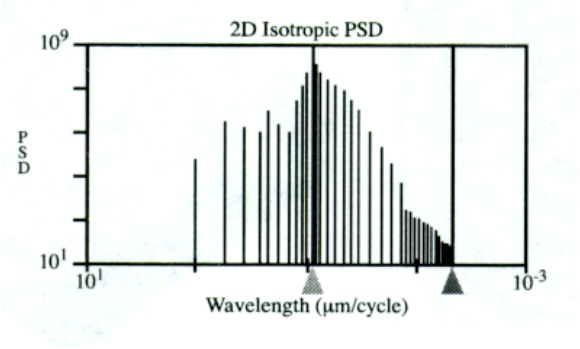

Figure A.8 Power Spectral Density Plot for the Synthetic Waveform[7]

Some other parameters are measureable with the software while performing a PSD analysis. On screen, the "wavelength" (in μm/cycle) and "frequency" (in cycles/μm) are shown for the current position of the cursor; this allows the user to find the frequency for any peak in the PSD plot. If a 2D PSD is being performed, the computer also automatically calculates values for the 1D PSD, 1D isotropic PSD, 2D isotropic PSD, and the total power for the spectrum. The precise equations for each of these are listed in the reference 7.

The one parameter in need of further explanation is the equivalent RMS. This is not a parameter characterizing the distribution of features on the image. Rather, it is the root mean square roughness of the entire surface of the sample. Whereas the section analyses calculate an RMS roughness along a single profile, this accounts for deviations on the Z axis from the the Z axis average along X and Y across the whole image.

A.1 References

1. taken from “Applications” section of Digital website (www.di.com), image used with permission
2. Rao, S.S., Mechancial Vibrations, 3rd Ed., Addison-Wesley, New York, 1995
3. Maganov, S.N., Elings, V., and Whangbo, M.-H., *Surface Science*, **375** (1997), pp. L385-L391
4. Hertz, H. and Reine Agnew, J., *Math*., **92** (1882), p. 156
5. Kendall, K. and Tabor, D., *Proc. R. Soc. A*, **323** (1971), p. 321
6. McLean, R.S. and B.B. Sauer, *Macromolecules*, **30** (1997), pp. 8314-8317
7. *Nanoscope® Command Reference Manual, pp.12-3 through 12-81*

VITA

Bryan Dinesh Kaushiva was born on March 25, 1972 to Dinesh and Shirley Kaushiva in Meadville, Pennsylvania. He grew up in Harrison, Ohio where he attended William Henry Harrison High School and graduated in 1990. He obtained a Bachelor of Science degree in chemical engineering from the University of Cincinnati in 1995. While enrolled at the Univ. of Cincinnati, he spent two years in the co-operative education program. One year was spent with the Westinghouse Environmental Management Company of Ohio (formerly Westinghouse Materials Company of Ohio, a D.O.E. contractor) in Fernald, Ohio; and one year was spent working at Mead Fine Papers in Chillicothe, Ohio. In the fall of 1995, Bryan entered the chemical engineering graduate program of Virginia Polytechnic Institute and State University, and he joined the research group of Professor Garth L. Wilkes in 1996. In December of 1998, he received his Masters of Engineering degree, and in August of 1999 he completed his Doctorate in chemical engineering. Bryan will be continuing in the area of polyurethane foams as he joins the Molded Applications group of Lyondell Chemical Company in Charleston, West Virginia.